Characterising extracellular α-synuclein and its associated release mechanisms in hiPSC-derived dopamine neurons

Iona Thomas-Wright
Merton College
University of Oxford

A thesis submitted for the degree of
Doctor of Philosophy

Michaelmas 2025

For the Venda boys

per ardua

Word Count: ~ 49,750

Abstract

Parkinson's disease is neuropathologically characterised by the accumulation of aggregated α-synuclein, a small synaptic protein which is capable of prion-like propagation in its misfolded state. The extracellular release of α-synuclein enables inter-neuronal spread of toxic α-synuclein conformers which precipitates neuronal dysfunction, degeneration and Parkinsonian symptoms. In this work I employ induced pluripotent stem cell-derived dopaminergic neurons to investigate α-synuclein secretion *in vitro*.

By integrating techniques from cell biology, classical biochemistry and biophysics I have investigated the variability in α-synuclein primary sequence, post-translational modifications and aggregation state in mature neurons from PD patients with SNCA mutations and healthy controls. I show that most α-synuclein transcripts encode the full length 140-amino acid protein however this is truncated to remove the N-terminus in a maturation-dependent manner. By studying stem-cell derived α-synuclein in its native conformation I provide evidence for the presence of high molecular weight α-synuclein conformers in dopaminergic neurons as well as heat labile products of C-terminal truncation of the primary sequence.

Funded by ARUK, I optimised an assay for the amplification of prion-like α-synuclein seeds from conditioned media. This demonstrate that *SNCA*-triplication and *SNCA-A53T* mutations increase the release of seeding-competent α-synuclein conformers, a population which may include secreted truncation products. In collaboration with other research groups in Oxford and Cambridge I pilot various single-molecule approaches to study these secreted α-synuclein seeds.

Using CRISPR interference knockdown technology and pharmacological modulators I then interrogate the release mechanisms for α-synuclein in dopaminergic neurons. Through identification of four possible genetic regulators of secretion, I provide the first evidence that SNARE-mediated fusion of autophagic vesicles is essential to α-synuclein secretion from dopaminergic neurons.

Together the data presented in this thesis highlight the value of iPSC-derived neuronal models for the study of α-synuclein biology and pathobiology in the quest for a α-synuclein-direct disease-modifying therapeutic.

Acknowledgements

This thesis would not have been possible without the endless support of my family, friends and colleagues.

I am indebted to my supervisors Prof Richard Wade-Martins and Dr Benjamin Vallin for their support and encouragement throughout this PhD. Thank you for giving creative freedom to explore my scientific interests in this project and for enabling me to grow as a scientist and independent thinker. I am very grateful for all the collaboration and publication opportunities I have received while in the lab and will look back on these years with fond memories. I would also like to extend my thanks to Associate Prof. Becky Carlyle for her patience and generosity of time and resources, and to my former supervisor Dr Margarida Rodrigues for providing me the grounding in single-molecule biophysics which enabled this project. To my many wonderful collaborators Dr Neha Kalmankar, Dr Livia Civitelli, Raman van Wee, Dr Barney Williams, Dr Fran Donnellan and Florence Layburn, thank you for welcoming me into your labs and for sharing your knowledge, skills and passion for science.

This project would not have been possible without the support, friendship and scientific guidance of friends in the lab and wider department. In particular, I would like to thank Dr Sandor Szunyough, Dr Kaitlyn Cramb, Dr Ajantha Abey, Dr Kalina Naidoo, Dr Rodrigo Gaspar, Dr Rachel Heon-Roberts, Dr Johanna Hoffman, Féodora Bertherat, Aishwarya Vedula and Marissa Mueller, who have motivated me, challenged me and problem solved with me more times than I can count.

Finally, I am endlessly grateful for the love and patience of my friends and family, who now know far more about α-synuclein than they would ever have imagined. To Dr Antonia Anstatt, Dr Francesca Lovell-Read, Dr Rachel Macleod, Laura Pearson, Jonah Schreier, Svenja Vorthmann and Matila Houston-Brown thank you for keeping me sane and forgiving me every time I was late to plans because of problems in the lab. To my dear friends and colleagues at Asylum Welcome, and in particular to Dr Fareed Fakhoury, thank you for providing me much needed perspective, reminding me who I am and always making me smile. Lastly, I would like to thank my parents Libby Thomas and David Wright for their support, encouragement and confidence since the beginning. You always believed I could do anything and without your faith I wouldn't be the scientist or person I am today.

In loving memory of Nancy Wright, biologist, and Sir David Knox, Parkinson's UK funder.

Statement of collaborative working

Several experiments presented in this thesis were undertaken in collaboration with investigators. I have endeavoured to make this clear in the relevant section of text and have additionally summarised these collaborations below:

Prof Randy Schekman (Principal Investigator & Nobel Laureate, Department of Molecular and Cell Biology, University of California Berkeley): DNAJC5 palmitoylation and inhibition – Theoretical input

Dr Neha Kalmankar (Robinson Group, Department of Chemistry, University of Oxford): Intact mass spectrometry and gel band digests – Theoretical and experimental input

Dr Livia Civitelli (Parkkinen Group, Nuffield Department of Clinical Neurosciences, University of Oxford): RT-QuIC for conditioned media - Theoretical and experimental input

Dr Barnabas Williams and Dr Francesca Donnellan (Draper Group, Department of Biochemistry, University of Oxford): Size-exclusion chromatography, Blue-native PAGE, C-Tag Affinity purification - Experimental Input

Dr Marjorie Fournier and Vaishnavi Ravikumar (Advance Proteomics Facility, Department of Biochemistry, University of Oxford) – Mass spectrometry for additive PTMs

Dr Razan Sheta (Oueslati Group, Department of Molecular Medicine, Laval University): establishment of NGN2 dopaminergic differentiation protocol - Theoretical input

Raman van Wee (Kukura Group, Department of Chemistry, University of Oxford): Mass Photometry - Theoretical and experimental input

Florence Layburn (Klenerman Group, Department of Chemistry, University of Cambridge): Single-molecule pull down of α-synuclein - Theoretical and experimental input

Table of contents

Chapter 2 - Materials and Methods

Chapter 1 – Introduction

1.1 Parkinson's Disease

1.1.1 Clinical Presentation and Symptomology

Parkinson's Disease (PD), first described as the 'Shaking Palsy' by Dr James Parkinson in 1817, is an age-related progressive motor disorder characterised by a triad of cardinal symptoms: bradykinesia, rigidity and resting tremor (Bloem, Okun and Klein, 2021). Motor symptoms tend to initially present asymmetrically but progress to bilateral impairment which hinders ambulation, balance and independent living. It is now recognised that most patients also experience a range of non-motor symptoms including sleep disturbances, autonomic and gastrointestinal dysfunction, mood changes and cognitive impairment (Tanner and Ostrem, 2024). These often predate the onset of motor symptoms and are less effectively treated by current therapies (Heinzel *et al.*, 2019).

200 years on from James Parkinson's original description there is still a lack of disease modifying therapies for PD. The search for a cure is complicated by the heterogeneity of clinical presentation. Not only does age of symptom onset and rate of disease progression vary dramatically between patients but the prominence of motor vs non-motor symptoms also differs (Pagano *et al.*, 2016). Data-driven clustering using the Oxford Parkinson's Disease Centre Discovery Cohort has allowed the identification of four possible PD subtypes classified by motor and non-motor progression as well as drug responsiveness (Lawton *et al.*, 2018). Disease stratifying studies such as this are essential both to better select patients for future clinical trials and to gain a clearer understanding of the (potentially divergent) underlying biology, in order to identify novel biomarkers and targets for drug development.

1.1.2 PD Prevalence

PD is the second most common neurodegenerative disorder after Alzheimer's disease affecting ~0.4% of the global population, a figure which rises to 1.5% in those over the age of 70 (Pringsheim *et al.*, 2014). It is significantly more common in men than women although the reasons for this are unknown (Van Den Eeden, 2003; Wooten, 2004). PD prevalence is higher among people of European descent and there are currently over 160,000 people living with Parkinson's in the UK alone (Van Den Eeden, 2003; Wright Willis *et al.*, 2010, Parkinson's UK, 2025).

1.1.3 Genetic and environmental causes of PD

A prevalence which varies with ethnicity indicates a role for genetic risk factors in PD. Approximately 10% of cases exhibit a positive family history (familial PD) whereas there is no clear heritability for the remaining 90% of patients (sporadic PD) (Klein and Westenberger, 2012). Numerous familial PD genes have now been identified (Table 1.1), providing valuable insight into the cellular pathophysiology in both familial and sporadic disease. Several of these genes such as *PRKN, PINK1, DJ1* and *CHCHD2* cluster in pathways regulating mitochondrial energy production and quality control, while others such as *LRRK2, VPS35* and *ATP13A2* are implicated in lysosome function and response to lysosomal stress (Blauwendraat, Nalls and Singleton, 2020; Bentley-DeSousa, Clegg and Ferguson, 2025). In accordance with these findings, *in vitro* studies have observed both mitochondrial and lysosomal dysfunction in cells from familial and sporadic PD patients (Carling *et al.*, 2020; Arena *et al.*, 2024).

Table 1.1 – Genes mutations linked to familial monogenic PD

Gene	Inheritance Pattern	Types of Mutation
SNCA	Dominant	Missense or Multiplication
PRKN	Recessive	Missense or loss of function
PINK1	Recessive	Missense or loss of function
DJ1	Recessive	Missense
GBA1	Dominant	Missense or loss of function
LRRK2	Dominant	Missense
VPS35	Dominant	Missense
CHCHD2	Dominant	Missense
PSAP	Dominant	Missense
POLG	Dominant	Missense or loss of function
ATP13A2	Recessive	Missense or loss of function
FBX07	Recessive	Missense
PLA2G6	Recessive	Missense or loss of function
DNAJC6	Recessive	Missense or loss of function
SYNJ1	Recessive	Missense or loss of function
VPS13C	Recessive	Missense or loss of function

Adapted from (Blauwendraat, Nalls and Singleton, 2020)

The process of identifying PD-linked genes is complicated by the fact that many exhibit incomplete penetrance, increasing disease risk but not causing symptoms for all carriers. For example, despite being the most common genetic risk factor, heterozygous mutations in *GBA1* which encodes the lysosomal hydrolase β-glucocerebrosidase, only have a penetrance of ~30% by the age of 80 (Anheim *et al.*, 2012). Interestingly, homozygous mutations of the same gene cause the lysosomal storage disorder Gaucher's disease which has a much earlier age of onset (Huh *et al.*, 2023). This suggests that a single functional copy of *GBA1* can compensate for most of the carrier's lifetime, only failing when compounded with aging-related cellular dysfunction.

In recent years, genome-wide associations studies (GWAS) have enabled interrogation of the genetics of sporadic PD. These studies have identified 90 risk loci in patients with no clear family history of PD, from which polygenic risk scores (PRS) can be calculated that provide significant predictive power for lifetime PD incidence (Nalls *et al.*, 2019).

Several genes implicated in monogenic PD such as *SNCA, LRRK2, GBA* and *VPS13C* have also had risk variants identified through GWAS, lending further support to the concept of shared mechanisms in familial and sporadic disease (Bandres-Ciga *et al.*, 2020). Additionally, the understanding of genetic background and polygenic risk provided by GWAS is important in familial PD. A recent study demonstrated that PRS modulates the PD risk conferred by *GBA1* pathogenic variants as well as influencing the age of disease onset (Hassanin *et al.*, 2025).

Beyond genetics, various environmental factors contribute to PD risk. In particular, exposure to certain chemicals including pesticides such as paraquat and rotenone, and industrial solvents like trichloroethylene, is positively correlated with developing PD (Tanner *et al.*, 2011; Dorsey and Bloem, 2024). These findings also provide insight to underlying disease mechanisms since many of these chemicals are mitochondrial toxins, highlighting the role of mitochondrial dysfunction in PD pathogenesis. Finally, PD risk is increased by lifetime exposure to head injuries, certain infections and comorbidities including type 2 diabetes (Periñán *et al.*, 2022). Emerging evidence is beginning to unpick the interactions of these, potentially modifiable, risk factors with patients underlying genetics, for example showing interaction between head injury and *GBA1-N370S* status to lower age of PD onset (Yahlom *et al.*, 2020).

1.1.4 Preferential vulnerability of dopaminergic neurons

The characteristic motor symptoms of PD are caused by the loss of A9 neurons in the substantia nigra pars compacta (SNpc) which provide the dopamine tone to striatal motor circuits. At autopsy this is evident as profound loss of pigmented nigral neurons, with most patients loosing 50-60% of neurons and ~80% of striatal projection fibres before the onset of PD symptoms (Rinne, 1993). Progressive functional deficits in dopamine

secretion can also be detected in living patients using positron emission tomography (PET) with radiotracers that bind the dopamine transport (DAT) (Ikeda *et al.*, 2019). Rodent models of PD overexpressing pathogenic variants of familial PD genes *SNCA* and *LRRK2* demonstrate nigral dopaminergic degeneration, while deficiency of other PD-linked genes e.g. *PRKN* amplifies dopaminergic vulnerability in response to environmental triggers (Frank-Cannon *et al.*, 2008; Dusonchet *et al.*, 2011; Janezic *et al.*, 2013). Single cell transcriptomic analysis has also demonstrated that expression of PD risk genes is enriched in SNpc dopaminergic neurons (Agarwal *et al.*, 2020; Kamath *et al.*, 2022; Kilfeather *et al.*, 2024). However, given both the prevalence of sporadic PD and expression of PD-linked genes in other cell types (albeit at lower levels in some cases), genetics alone is clearly insufficient to confer dopaminergic neurons their preferential vulnerability.

A9 dopamine neurons have vast axonal arbours which project from the SNpc to the striatum, where a single axon can cover over 5% of the striatal volume (Matsuda *et al.*, 2009). Dopamine is released both from terminal synapses and through en passant transmission from axonal varicosities (Freund, Powell and Smith, 1984). Dopamine itself is an unstable molecule whose metabolism generates various aldehydes and quinones which damage cellular proteins, nucleic acid and lipids (Bisaglia *et al.*, 2014) – Fig. 1.1. However, SNpc neurons are considerably more vulnerable than their ventral tegmental area (VTA) counterparts which also project dopaminergic terminals to the striatum. SNpc dopamine neurons exhibit slow pace-making activity which favours Ca^{2+} entry through L-type channels, necessitating ATP-dependent extrusion and placing additional strain on mitochondria on top of the energetic demand of high levels of neurotransmitter release (Guzman *et al.*, 2010). This is particularly pronounced in the most vulnerable

population of nigral dopamine neurons which have limited Ca^{2+} buffering capacity due to low endogenous expression of calbindin (Del Rey *et al.*, 2024). As such the L-type channel blocker isradipine has shown efficacy in preclinical work and may delay the need for symptomatic medication in PD patients (Chan, Gertler and Surmeier, 2010; Surmeier *et al.*, 2022). To support their high metabolic demands substantia nigra dopamine neurons have more axonal mitochondria than their counterparts in the VTA but still have a lower respiratory reserve capacity and are more vulnerable to oxidative stress (Pacelli *et al.*, 2015).

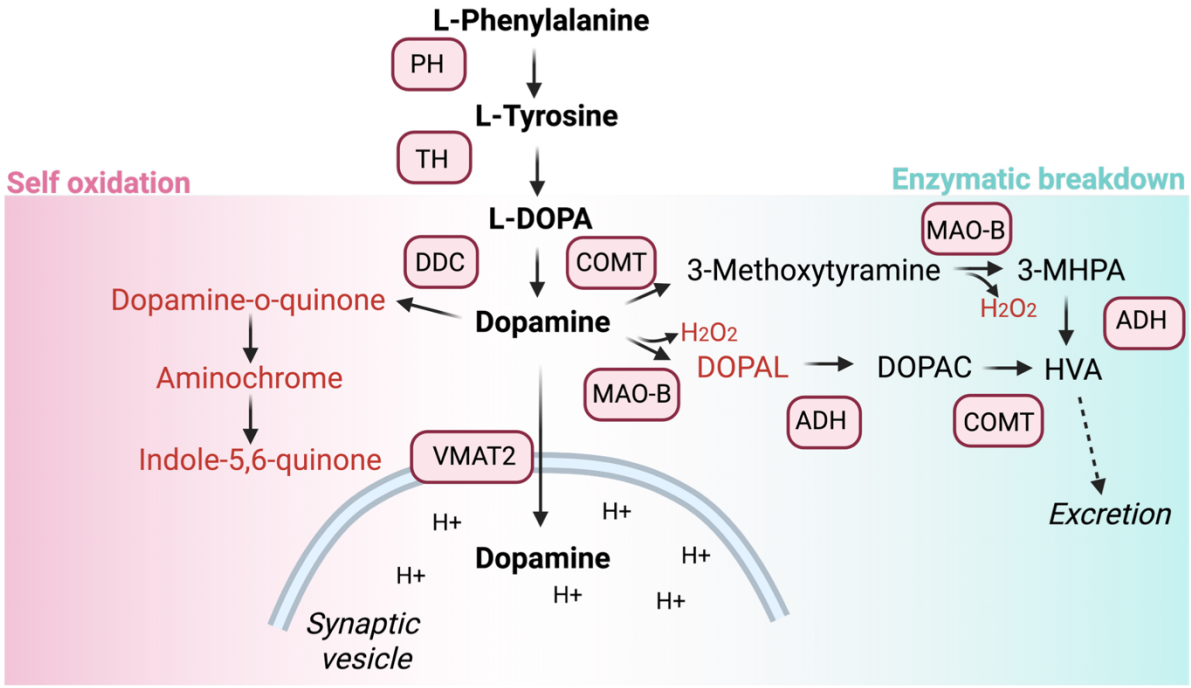

Fig. 1.1 Dopamine synthesis and metabolism generates toxic electrophiles
Schematic representation of the metabolic pathways for dopamine synthesis, catabolism and loading into synaptic vesicles where it is stabilised against oxidation by the acidic environment. PH = phenylalanine hydroxylase, TH = tyrosine hydroxylase, DDC = dopa decarboxylase, VMAT2 = vesicular monoamine transporter-2, MAO-B = monoamine oxidase B, COMT = catechol-O-methyltransferase, ADH = aldehyde dehydrogenase. Cytotoxic molecules including electrophiles which form covalent adducts with proteins and DNA are shown in red. Figure based on data presented in Bisaglia et al. (2014)

Dopamine quinones produced by cytosolic oxidation (Fig. 1.1) also cause lysosomal dysfunction, for example through electrophilic attack on cysteine residues in β-glucocerebrosidase (encoded by the PD risk gene *GBA1*) which reduces its activity (Burbulla *et al.*, 2017). There is also emerging evidence that autophagy-lysosome dysfunction increases dopamine-mediated toxicity through failure of DAT degradation, which increases dopamine reuptake precipitating a toxic cycle (Harraz *et al.*, 2021).

While many features contributing to SNpc dopaminergic preferential vulnerability have been elucidated, it is important to note that other neuron types, including VTA dopamine neurons and even peripheral catecholaminergic sensory neurons share several of these features including long unmyelinated axons and dopamine metabolism (Katz *et al.*, 1983). This highlights that it is not a single feature of SNpc dopamine neuron physiology which contributes to their preferential vulnerability, but rather combination of the above factors and those yet to be identified, which creates a 'perfect storm' and tips the scales from cell survival to degeneration on a faster timeline than for surrounding cell types.

1.2 α-synuclein: a synaptic protein at the heart of PD

SNCA, located on chromosome 4, is one of the familial PD genes highly expressed in vulnerable SNpc dopamine neurons (Agarwal *et al.*, 2020). This gene encodes α-synuclein, a small (140 amino acid, 14.5 kDa) protein which is enriched in synaptic terminals (Calabresi *et al.*, 2023). As well as being linked to PD through GWAS, duplication or triplication of the *SNCA* locus as well as various point mutations cause autosomal dominant PD (Polymeropoulos *et al.*, 1997; Krüger *et al.*, 1998; Singleton *et al.*, 2003; Chartier-Harlin *et al.*, 2004; Zarranz *et al.*, 2004; Lesage *et al.*, 2013; Proukakis *et al.*, 2013) – Fig. 1.2.

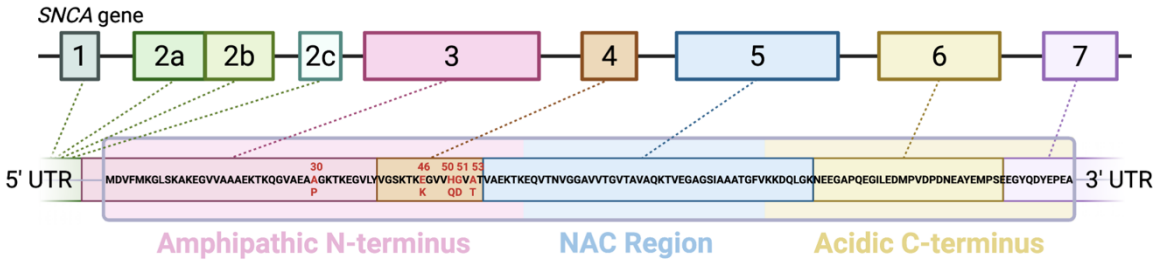

Fig. 1.2 Structure of the α-synuclein transcript and protein coding sequence
Schematic representation of the 9 possible exons (1, 2a-c, 3, 4, 5, 6 & 7) which are spliced together to encode 140 amino acid α-synuclein. The protein coding region is marked inside a grey box with the amino acid sequence encoded by the exon triplet code highlighted. The three domains of the protein sequence are indicated. Point mutations which cause autosomal dominant PD (A30P, E46K, H50Q, G51D and A53T) are highlighted in red on the protein sequence.

Full length α-synuclein mRNA transcripts are formed from the in frame splicing of 6 exons from a total of 9 possibilities, generating variability in the 5′ untranslated region (UTR) (Beyer and Ariza, 2013) – Fig. 1.2. Use of exon 2a is most common giving rise to SNCA_205/NM_000345 when all protein-coding exons are included (Gámez-Valero and Beyer, 2018). Skipping of exons 4, 6 or both generates 126-, 112- or 98-amino acid α-synuclein which differ in their chemical properties due to loss of a large proportion of

the negatively charged C-terminal residues (Röntgen *et al.*, 2025). Additionally, replacement of exons 6 & 7 with a small portion of intron 4 has been reported to generate a 115-amino acid isoform in the cortex (Janeczek *et al.*, 2015).

The native conformation of α-synuclein protein is largely unstructured though the N-terminus can adopt a helical conformation which is stabilised by interaction with phospholipid membranes (Bartels *et al.*, 2010; Burré *et al.*, 2013; Theillet *et al.*, 2016; Rovere *et al.*, 2018). α-helix formation is driven by imperfect 11-mer repeats containing the KTKEGV sequence and results in either two antiparallel helices connected by a linker or a single long curved helix (Bussell and Eliezer, 2003; Ulmer *et al.*, 2005; Lokappa and Ulmer, 2011). The affinity of α-synuclein for lipid membranes is modulated by the conformation of the non-amyloid β-component (NAC) region with only weak (Ca^{2+}-induced) membrane binding of the C-terminus membranes (Fusco *et al.*, 2014; Lautenschläger *et al.*, 2018). The affinity of α-synuclein-membrane interactions is highest for small highly curved vesicles containing anionic lipids, similar in composition to synaptic vesicles (Sarchione *et al.*, 2021).

Although the exact function of α-synuclein is unclear, in neurons it appears to interact with and chaperone synaptic SNARE proteins to promote vesicle clustering and fusion with the plasma membrane on (Burré *et al.*, 2010; Diao *et al.*, 2013). The C-terminus of α-synuclein binds VAMP2 on the synaptic vesicle while the amphipathic N-terminus interacts with negatively charged phospholipids on the plasma membrane, forming dense condensates (Lou *et al.*, 2017; Agarwal *et al.*, 2024). While this interaction is not essential for neurotransmitter release it alters synaptic physiology through a bidirectional plasticity mechanism that potentiates release, including release of dopamine from SNpc

dopaminergic boutons over short timescales, but depresses exocytosis with longer inter-stimulus intervals (Liu *et al.*, 2004; Somayaji *et al.*, 2020). Despite the altered dopamine plasticity *Snca* -/- mice do not show a behavioural phenotype or impaired viability (Abeliovich *et al.*, 2000). However, if homologues β- and γ-synuclein are also deleted mice exhibit elevated baseline dopamine release (in the absence of paired-pulse stimuli), altered synaptic ultrastructure and hyperactivity in novel environments (Greten-Harrison *et al.*, 2010; Anwar *et al.*, 2011). This more severe phenotype of the triple-knockouts suggests a degree of epistasis between the members of the synuclein family, which share considerable sequence homology particularly in the N-terminus.

However, α-synuclein is not only found in neuronal synapses. α-synuclein has been identified in the nucleus of neurons and non-neuronal cells where it is thought to play a role in nucleocytoplasmic transport (Yuan *et al.*, 2008; Chen *et al.*, 2020; Outeiro and Koss, 2025). Moreover, α-synuclein is abundant in some peripheral tissues, particularly those of the erythroid lineage including red blood cells (Nakai *et al.*, 2007; Barbour *et al.*, 2008). Lipid interactions also appear to be important in red blood cells where the α-synuclein N-terminus interacts with the plasma membrane and may facilitate enucleation during erythroblast to erythrocyte maturation (Araki *et al.*, 2018). Consistent with this *Snca* -/- mice demonstrate mild anemia despite the absence of cognitive impairment (Xiao *et al.*, 2014)

In 1997, Spillantini and colleagues identified α-synuclein as the major component of the proteinaceous aggregates, so called Lewy bodies, which are abundant in the brains of ~90% of clinically defined PD cases and are the dominant feature of post-mortem histopathology (Spillantini *et al.*, 1997). This key breakthrough not only provided a

crucial link between α-synuclein and sporadic PD but also demonstrated that α-synuclein was capable of forming β-sheet rich aggregates. In the last 25 years a vast literature has been amassed with the goal of determining whether α-synuclein aggregation and deposition is a cause or a consequence of neuronal degeneration in PD. Strong evidence of causal involvement is provided by *in vivo* experiments in rodents and primates in which both overexpression of *SNCA* and injection of pre-aggregated fibrillar α-synuclein induce SNpc degeneration, parkinsonian-like motor symptoms and, to varying extents, the formation of α-synuclein inclusions (Kirik *et al.*, 2002; Eslamboli *et al.*, 2007; Luk *et al.*, 2012; Janezic *et al.*, 2013; Chu *et al.*, 2019; Bengoa-Vergniory *et al.*, 2020; Aniszewska *et al.*, 2022).

1.3 Pathological α-synuclein: a story of aggregation

1.3.1 Misfolding and structural conversion

The key transition from a physiological protein involved in vesicle release and synaptic plasticity to a toxic mediator of disease lies in the structural conversion of intrinsically disordered or helical α-synuclein to a β-strand conformer. Amino acids 71-82 in the hydrophobic NAC region are both necessary and sufficient for misfolding (Giasson *et al.*, 2001). α-synuclein spontaneously aggregates to oligomers through a process of primary nucleation although this process is slow under physiological conditions (Buell *et al.*, 2014; Iljina *et al.*, 2016). The formation of liquid condensates through phase separation increases the rate of primary nucleation and interestingly is regulated by synaptic interaction partner VMAP2 (Ray *et al.*, 2020; Dada *et al.*, 2023; Agarwal *et al.*, 2024) Föster Resonance Energy Transfer (FRET) suggests that oligomers (generated *in vitro*) are initially more disordered and undergo a compaction step, which increases FRET signal, prior to the fibrillar transition resulting in a three step kinetic model for the aggregation reaction (Iljina *et al.*, 2016). Only the more compact oligomers are detectable with β-sheet-binding dye Thioflavin-T, which super-resolution microscopy shows to be accompanied by a change from a globular to more elongated conformation (Lee *et al.*, 2018). Higher resolution structures obtained with cryo-electron microscopy (CryoEM) reveal that the oligomers generated in this process are cylindrical or donut-shaped and have ~35% β-sheet characteristics (Chen *et al.*, 2015). This differs from mature fibrils where stacked α-synuclein protomers adopt a Greek Key conformation containing eight short β-strands resulting in ~65% β-sheet structure (Chen *et al.*, 2015; Guerrero-Ferreira *et al.*, 2019).

α-synuclein exhibits prion-like behaviour whereby fibrils can template the misfolding of other monomers in solution. Molecular dynamics simulations suggest that interaction between the NAC regions of intrinsically disordered monomeric α-synuclein and the fibrillar template progresses in a C-terminal to N-terminal direction driven initially by electrostatic interactions and van der Waals forces and laterally stabilised by predominantly van der Waals interactions (Zhao *et al.*, 2023). Under physiological conditions fibril elongation is considerably faster than primary nucleation, supporting a key role for seeding in the development of aggregated α-synuclein pathology (Buell *et al.*, 2014). These authors also show the rate of fibril elongation is autoinhibited by the assembly of fibrils into larger, more complex structures. Increasing evidence suggests that secondary nucleation (whereby seeding proceeds via catalysis of *de novo* fibril growth on the surface of existing fibrils rather than through monomers addition onto the fibril end) may be the dominant mechanism of seeded aggregation (Horne *et al.*, 2023; Xu *et al.*, 2024). Interestingly, rate constants for secondary nucleation are elevated by low pH which may be physiologically relevant regarding observations of α-synuclein aggregation in the lysosome (Buell *et al.*, 2014; Kakuda *et al.*, 2024).

α-synuclein fibrils are composed of two twisted protofilaments, with an interface formed by residues in the N-terminus of constituent protomers in opposing filaments (Guerrero-Ferreira *et al.*, 2018, 2019; Li *et al.*, 2018). Interestingly, the *SNCA* point mutations which cause autosomal dominant PD lie in this interface region. *In vitro* generated fibrils exist as four main polymorphs (Type 1a&b and Type 2a&b) which differ not only in their fibrillar architecture, including helical pitch and diameter, but also the fold of constituent protomers (Guerrero-Ferreira *et al.*, 2019). Insoluble fibrils are resistant to harsh detergents and can be extracted and purified from post-mortem tissues. This has enabled

structural characterisation of patient-derived fibrils using similar techniques, which revealed that although the fundamental architecture of two helically-interacting protofilaments is conserved, the fold of α-synuclein protomers differs significantly from *in vitro* observations (Schweighauser *et al.*, 2020). α-synuclein aggregation is a common feature of several neurodegenerative conditions besides PD, including Multiple Systems Atrophy (MSA) and Lewy Body Dementia (LBD) although the histological appearance of aggregates differ (Wiseman, Reddy and Dieriks, 2025). There have now been numerous reports that fibril structures also differ between these synucleinopathies which may in future be a valuable tool for assisting diagnosis/patient stratification (Strohäker *et al.*, 2019; Shahnawaz *et al.*, 2020; Van der Perren *et al.*, 2020). However, results should be interpreted with care since several studies used *in vitro* amplification of the brain derived fibrils to generate sufficient material for structural analysis, which does not fully conserve the fold of α-synuclein from the parent brain-derived fibril (Lövestam *et al.*, 2021; Lee, Civitelli and Parkkinen, 2024).

Much less is known about the structures of patient-derived oligomers formed before mature fibrils. Several key factors play into this relative information scarcity. Firstly, oligomers are both transient and heterogeneous, so the concentration of any single species is proportionally minute. Unlike with fibrils, it is not possible to amplify oligomers *in vitro* limiting material available for downstream assays. Oligomers are also much less stable and are susceptible to denaturation/disassembly in a concentration, temperature and pH-dependent manner and hence are much more challenging to extract from post-mortem tissue (Gould *et al.*, 2014). Finally, there is a more limited array of techniques available with which to efficiently study small oligomers either in or purified from biological systems. In primary rodent neurons single molecule FRET has identified

the two differentially active oligomers measured *in vitro,* suggesting that a similar three-step aggregation process takes place, although we do not currently have corresponding CryoEM structures from cells or tissues (Choi *et al.*, 2022). Advances in super-resolution microscopy allow for interrogation of the non-fibrillar aggregates and larger oligomers in PD post-mortem brain. This has identified abundant small non-fibrillar aggregates in amygdala tissue from PD patients and healthy controls, with more species <50 nm in length PD samples (Emin *et al.*, 2022). However, a recent preprint from the same lab, using a different single molecule imaging approach, found that non-fibrillar aggregates from the orbitofrontal cortex were larger in PD than age matched controls (Fertan *et al.*, 2025). These preliminary findings may indicate regional differences in aggregation pathways, possibly modulated by intracellular environment or cell survival, which are worthy of further investigation.

Building a clear understanding of the structural diversity and conserved features of oligomers in patient-derived tissue and physiologically relevant model systems, is essential for the effective design of disease-modifying drugs to interact with these toxic proteoforms (discussed in Subsection 1.6). While structural insight from *in vitro* studies can provide a useful guide, the differences observed between *in vitro* generated and patient-derived fibril architectures serve as a warning of the dangers of over-reliance on data generated from recombinant protein in simple systems. A key priority for the next decade of α-synuclein research will be to leverage advanced biophysical techniques, paired with appropriate passivation and background-reduction strategies, to elucidate oligomers structures against the complex background of biologically relevant samples.

1.3.2 The elusive native tetramer – a hypothesis under reconsideration?

In addition to the pathological pathway of β-sheet aggregation described above, it has also been suggested that α-synuclein can multimerise in its helical conformation under physiological conditions (Bartels, Choi and Selkoe, 2011; Wang *et al.*, 2011). These authors independently evidenced stable homotetramers of α-synuclein in preparations from a variety of cell lines and human brain tissue (though the α-synuclein used by Wang and colleagues had an additional 10 N-terminal residues). However, independent attempts to replicate these findings have, in large part, failed to evidence the tetrameric species (Binolfi, Theillet and Selenko, 2012; Fauvet *et al.*, 2012; Maltsev, Ying and Bax, 2012; Burré *et al.*, 2013). Subsequent publications form the Bartels and Selkoe groups using in-cell crosslinking to avoid challenging native purifications have identified tetrameric α-synuclein in rodent tissues, human blood and postmortem brain as well as stem cell-derived neurons (Dettmer *et al.*, 2013, 2015; Nuber *et al.*, 2018; De Boni *et al.*, 2022, 2024). These studies suggest that by conferring conformation stability tetrameric organisation inhibits the β-strand conversion and aggregation. Consistent with this, tetramer abundance is reduced in synucleinopathy patients and tetramers are destabilised by familial PD mutations (Dettmer *et al.*, 2015; De Boni *et al.*, 2022).

While these data portray an attractive hypothesis, the fact remains that other studies do not observe tetrameric α-synuclein in disease models or patient tissues. Under certain conditions endogenous α-synuclein may exist as tetramers, but it seems likely that the majority is present as intrinsically disordered monomer. Tetramers may arise transiently during physiological processes and/or be stabilised by certain aspects of the intracellular environment, but their involvement in PD remains under question (Trexler and Rhoades, 2012; Dong *et al.*, 2018; Bhattacharya *et al.*, 2024).

1.3.3 Drivers of α-synuclein aggregation: familial point mutations

All known point mutations in *SNCA* which cause autosomal dominant PD (Fig. 1.2) are associated with altered α-synuclein aggregation kinetics. As discussed above (1.3.1) α-synuclein aggregation is a multistep process throughout which the misfolding of monomers can occur through primary or secondary nucleation as well as recruitment to the end of a polarised fibril. E46K, H50Q and A53T mutations increase the rate of fibril formation, however A30P, G51D and A53E appear to slow fibrilisation (Greenbaum *et al.*, 2005; Ghosh *et al.*, 2014; Rutherford *et al.*, 2014; Ruf *et al.*, 2019). These kinetic changes are paired with altered affinity of α-synuclein for lipid membranes and the rate of lipid-induced aggregation, though the exact consequences of individual mutations vary between reports (Fares *et al.*, 2014; Flagmeier *et al.*, 2016; Ruf *et al.*, 2019).

Most studies to date have tracked the effects of mutations on α-synuclein aggregation using ThT assays. This has provided information regarding primary nucleation (often accelerated by the presence of lipid vesicles), fibril elongation and secondary nucleation processes – for example suggesting that secondary nucleation is markedly attenuated for H50Q and G51D variants (Flagmeier *et al.*, 2016). However, the use of β-sheet binding dyes precludes data collection on prefibrillar oligomers. Since all familial PD mutations are associated with early onset disease it is likely that to achieve a toxic effect even those which slow fibrilisation must destabilise monomer toward oligomeric intermediates. In support of this, the use of time-dependent dynamic light scattering shows that initial oligomerisation is not impaired by the A30P mutation despite the slower time course for mature fibril formation (Ghosh *et al.*, 2014). Similarly, in-cell reporter assays suggest both A30P and G51D do not impair initial oligomerisation (Lázaro *et al.*, 2014).

1.3.4 Drivers of α-synuclein aggregation: Alternative splicing

There is strong evidence for regional differences in the expression of alternatively spliced α-synuclein mRNA with certain transcripts being upregulated in a disease and brain-region-specific manner. 126-amino acid α-synuclein is more abundant in the substantia nigra (but not frontal cortex or cerebellum) of PD patients, while the 98- amino acid isoform is upregulated in PD and pure LBD but not LBD with Alzheimer's co-pathology (Beyer *et al.*, 2008; McLean *et al.*, 2011). The 115-amino acid isoform has not been studied in the context of PD but shows elevated expression in the brains of individuals with alcohol use disorder (Janeczek *et al.*, 2015). Advances in proteomics and long-read mRNA sequencing will be valuable to better understand splice isoform abundance and diversity across synucleinopathies.

α-synuclein transcripts lacking exon 6 (112- and 98-amino acid isoforms) loose a considerable portion of the acidic C-terminus and thus are overall more hydrophobic in nature. *In vitro* this corresponds to faster aggregation kinetics than either full length or 126-amino acid α-synuclein, and even at low concentrations can accelerate the aggregation of the full length isoform (Röntgen *et al.*, 2024). The same authors also found that fibrils formed by these two shorter isoforms were morphologically distinct from wild-type fibrils and had a less filamentous structure. All three shorter isoforms promote the liquid-liquid phase separation of α-synuclein, and within condensates the 126-amino acid isoform also increases aggregation relative to the wild-type sequence (Röntgen *et al.*, 2025). Further *in vitro* work is essential to integrate the oligomerisation/aggregation consequences of primary sequence changes with the loss of residues that can be post-translationally modified.

1.3.5 Drivers of α-synuclein aggregation: Post-translational modifications

Post-translational modification (PTM) refers to the formation or breakage of covalent bonds in a protein after it has been synthesised to add/remove certain groups thus changing its chemical properties. PTMs increase the functional diversity of the proteome and can alter the structure, localisation, interactions and half-life of their target protein. Post-mortem studies demonstrate that α-synuclein can be heavily post-translationally modified (Parra-Rivas *et al.*, 2023). Some modifications appear to have physiological roles, while others are linked to disease processes in PD (Manzanza, Sedlackova and Kalaria, 2021; Parra-Rivas *et al.*, 2023). Most α-synuclein in human brain is N-terminally acetylated, though this modification hinders aggregation and may help to stabilise helical multimers (Öhrfelt *et al.*, 2011; Trexler and Rhoades, 2012; Bell *et al.*, 2022).

1.3.5.1 Truncation

Approximately 15% of the α-synuclein present in Lewy bodies has been enzymatically truncated (Zhang, Li and Li, 2019). Most reported truncations are of the C-terminus and mass spectrometry from post-mortem tissue has identified a range of truncation products: 1-103, 1-115, 1-119, 1-122, 1-133, 1-135 (Anderson *et al.*, 2006; Zhang *et al.*, 2017; Killinger *et al.*, 2018). 1-119 and 1-122 appear to be the most abundant although prevalence varies between brain regions and synucleinopathies (Anderson *et al.*, 2006; Kellie *et al.*, 2014; Hass *et al.*, 2021). Similar to the loss of acidic C-terminal residues through alternative splicing, C-terminal truncations have a pro-aggregation effect (Sorrentino *et al.*, 2018). The more C-terminal residues which are deleted, the more the pH dependence of secondary nucleation shifts towards neutral pH values promoting seeding under physiological conditions (Van Der Wateren *et al.*, 2018). Fibril structures generated by the *in vitro* aggregation of truncated α-synuclein also differ from those

formed by full length monomer, being both more twisted and narrower (Iyer *et al.*, 2017). Crucially, C-terminally truncated α-synuclein co-polymerises with the more abundant full-length protein, increasing aggregation rate (Sorrentino *et al.*, 2018)

Several studies have observed N-terminal truncations including at Met-5, Ser-9, Ala-18, Ala-19 and Tyr-39 in post-mortem tissue (Kellie *et al.*, 2014; Killinger *et al.*, 2018). These render α-synuclein more hydrophilic overall, but also cause loss of the N-terminal helices which stabilise the non-β-strand conformation (Meade *et al.*, 2023). *In vitro* N-terminal deletions slightly reduce the rate of fibrilisation (Terada *et al.*, 2018; McGlinchey *et al.*, 2021). However, in SH-SY5Y cells and in mice exogenous addition of N-terminally truncated fibrils either increase or do not affect the development of α-synuclein pathology (Vamvaca, Lansbury Jr. and Stefanis, 2011; Terada *et al.*, 2018). These properties could be explained by accelerated secondary nucleation of wild-type α-synuclein, but reduced primary nucleation, by N-terminally truncated proteoforms.

Truncation arises as a side-effect of incomplete degradation and as such is largely a lysosomal process. A variety of enzymes including calpain, cathepsins, neurosin and Asparaginyl endopeptidase (AEP) have been implicated in α-synuclein truncation, and several of these have been identified within Lewy bodies (Iwata *et al.*, 2003; Mishizen-Eberz *et al.*, 2005). Emerging evidence suggests that the expression and activation of these proteins may be disease-associated. For example AEP is upregulated during aging and shows higher activity in the SNpc of PD patients compared to less affected brain regions or healthy controls, while cathepsin D activity is increased by oxidative stress (Takahashi *et al.*, 2007; Zhang *et al.*, 2014, 2017; H. Wang *et al.*, 2023).

The consequences of truncation for interactions of α-synuclein with other cellular proteins are currently not well understood. As such, mechanistic studies in cell models that faithfully recapitulate truncation phenotypes observed *in vivo* is required.

1.3.5.2 Phosphorylations

Tyrosine (Tyr-39, Tyr-125, Tyr-133 & Tyr-136), threonine (Thr-64) and serine (Ser-87 & Ser-129) residues in α-synuclein are all substrates for phosphorylation. In healthy people phospho-synuclein levels are extremely low making phosphorylation a key hallmark of PD, which animal and cell models often aim to recapitulate (Manzanza, Sedlackova and Kalaria, 2021).

As the only known phosphorylation site located within the N-terminus phospho-Tyr-39 is particularly interesting, as it directly modifies an amino acid involved in fibril formation. Phosphorylation by c-Abl reduces the association of the 2nd N-terminal α-helix with lipid membranes in a similar way to the familial G51D mutation and increases aggregation in primary neurons and mice (Brahmachari *et al.*, 2016; Dikiy *et al.*, 2016; Zhao *et al.*, 2020). This corresponds with a change to fibril architecture including the appearance of a twisted trimeric polymorph as well as the 'normal' dimer of protofilaments (Zhao *et al.*, 2020). Conversely, Tyr-125, -133 and -136 are all phosphorylated by Syk (and possibly other kinases) which appears to reduce the oligomer and aggregate formation (Negro *et al.*, 2002). Interestingly, recent reports have suggested a degree of crosstalk with phosphorylation on Ser-129, likely due to their proximity in the C-terminus (Kleinknecht *et al.*, 2016; Sano *et al.*, 2021).

Phosphorylation of Thr-64 is elevated not only in PD brain but also downstream of aggregation seeded by pre-formed fibril (PFF) injection in mice (Matsui *et al.*, 2023).

Casein kinase 1 and protein kinase R both phosphorylate this site and phosphorylation (or phosphomimetic mutation) *in vitro* increases the abundance of small oligomers on native PAGE but reduces fibrilisation (Reimer *et al.*, 2022; Matsui *et al.*, 2023).

Serine-129 is the most abundant PTM in PD, with >90% of α-synuclein in Lewy bodies being phosphorylated at this site (Anderson *et al.*, 2006). Unlike the other PD-linked phosphorylation sites low levels of phospho-ser-129 α-synuclein are found in healthy people. Recent studies have suggested that dynamic phosphorylation of ser-129 is both activity-dependent and necessary for the physiological role of α-synuclein at the synapse (Parra-Rivas *et al.*, 2023; Ramalingam, Jin, *et al.*, 2023). Familial mutations A30P and E46K, as well as proteasomal inhibition reduce the reversibility of this process providing clues to how phospho-ser-129 α-synuclein may initially accumulate in PD (Ramalingam, Brontesi, *et al.*, 2023). Consistent with this there are reports of elevated phospho-ser-129 in cell models of PD with familial mutations, although results are inconsistent between studies (Ryan *et al.*, 2013; Lin *et al.*, 2016; Stykel *et al.*, 2021; Virdi *et al.*, 2022; Mubariz *et al.*, 2023). In non-human primates ser-129 phosphorylation increases during normal aging, this may be linked to the increasingly oxidative environment in aged neurons since *in vitro* oxidative stress promotes phospho-ser-129 accumulation (McCormack, Mak and Di Monte, 2012; Perfeito *et al.*, 2014). However, it is likely the largest increases in serine-129 phosphorylation in PD occur after α-synuclein aggregation, since aggregates appear to be better phosphorylation substrates (Ghanem *et al.*, 2022).

Several kinases including polo like kinase-2 and casein kinases have been implicated in serine phosphorylation (Waxman and Giasson, 2008; Inglis *et al.*, 2009). *In vitro* phosphorylation of both serine residues inhibits fibrilisation, supporting phosphorylation

occurring after initial aggregation (Paleologou *et al.*, 2008, 2010; Ghanem *et al.*, 2022). While the exact relationship between physiological and pathological ser-129 phosphorylation requires further study, the utility of this PTM as a proxy for aggregation in PD models cannot be undervalued.

1.3.5.3 Oxidation and nitration

The four methionine residues in α-synuclein (Met-1, Met-5, Met-116 & Met-127) are readily oxidised *in vitro* by exposure to oxidants including products of dopamine metabolism such as DOPAL (Glaser *et al.*, 2005; Coelho-Cerqueira, de Araújo Correia Campos and Follmer, 2019) – Fig. 1.1. Although oxidative stress is widely recognised as a key feature of PD it is challenging to confidently assess oxidation in post-mortem tissue or animal models with mass spectrometry because methionine residues are also oxidised during sample preparation (Bettinger *et al.*, 2019). DOPAL can also interact directly with α-synuclein lysine residues to form covalent adducts which promote the formation of toxic oligomers capable of membrane permeabilisation (Plotegher *et al.*, 2017). Interestingly, there appears to be crosstalk between these two oxidative pathways. Methionine oxidation, particularly oxidation of C-terminal methionines which are less efficiently repaired following oxidative damage, inhibits DOPAL-induced oligomer formation and reduces aggregation (Binolfi *et al.*, 2016; Carmo-Gonçalves *et al.*, 2018; Coelho-Cerqueira, de Araújo Correia Campos and Follmer, 2019).

Oxidative stress also drives nitration of tyrosine residues, causing accumulation of nitrated α-synuclein in PD and other synucleinopathies (Giasson *et al.*, 2000). The oxidative products of dopamine metabolism, specifically MAO-B activity (Fig.1.1), elevate Tyr-39 and possibly Tyr-136 but not Tyr-125 or Tyr-133 nitration (Danielson *et*

al., 2009). At physiological pH Tyr-39 nitration acts similarly to Tyr-39 phosphorylation to add an (albeit smaller) negative charge to this N-terminal residue. Consistent with the results of phosphorylation, Tyr-39 nitration also reduces N-terminal helicity and association with membrane lipids however, fibrilisation is impaired rather than increased (Burai *et al.*, 2015; Chavarría *et al.*, 2024).

1.3.5.4 Glycosylation

o-GlcNAcylation is a dynamic form of glycosylation whereby single sugar moieties, rather than complex glycan chains, are reversibly added to amino acid residues. α-synuclein o-GlcNAcylated on threonine residues as well as Ser-87 has been identified in post-mortem tissue from Alzheimer's and tauopathy patients (Levine *et al.*, 2019). This modification reduces oligomer and aggregate formation *in vitro* and *in vivo* (Marotta *et al.*, 2015; Hu *et al.*, 2024). Accordingly, pharmacological upregulation of o-GlcNAcylation in cells proves neuroprotective and reduces aggregation, possibly representing a novel druggable pathway (Miao *et al.*, 2025).

It is noteworthy that non-enzymatically glycated α-synuclein is also more abundant in the post-mortem brains of synucleinopathy patients than healthy controls (Vicente Miranda *et al.*, 2017). This aging-associated, and diabetes-linked modification increases α-synuclein aggregation and the production of phospho-ser-129 positive inclusions in cell models (Vicente Miranda *et al.*, 2017; Vasili *et al.*, 2025).

1.3.5.6 Peptide conjugation to lysine: Ubiquitination and SUMOylation

α-synuclein in Lewy Bodies is heavily ubiquitinated, consistent with it having been targeted for degradation by a dysfunctional proteasomal system (Manzanza et al. 2021). SUMOylated α-synuclein is also upregulated in PD brains and both modifications inhibit

α-synuclein aggregation in reconstructed *in vitro* systems (Meier *et al.*, 2012; Abeywardana and Pratt, 2015; Rott *et al.*, 2017). Interestingly, in a cellular environment SUMOylation promotes aggregate formation by competing with ubiquitin which reduces α-synuclein degradation (Rott *et al.*, 2017). However, in other cell types SUMOylation has been shown to promote extracellular release (Kunadt *et al.*, 2015).

1.4 What's the problem? α-synuclein-induced neuronal toxicity

During its misfolding and aggregation trajectory α-synuclein exists as an enormous variety of proteoforms, the diversity of which is further expanded by a combinatorial code of post-translational modifications. In the context of disease, it is essential to understand which of these is/are the main drivers of toxicity, neuronal dysfunction and cell loss, and whether this varies with disease progression. The weight of evidence suggests that oligomers, particularly those which have undergone compaction and rearrangement are the most toxic species (Cremades *et al.*, 2012; Ingelsson, 2016). However, the accumulation of monomeric and fibrillar α-synuclein also cause cellular problems for cells which cannot be ignored.

1.4.1 Toxicity of elevated α-synuclein monomer levels

Multiplication of the *SNCA* locus as well as non-*SNCA* familial mutations cause the intracellular accumulation of monomeric α-synuclein prior to the formation of oligomeric and aggregated conformers (Nguyen *et al.*, 2011; Sánchez-Danés *et al.*, 2012; Woodard *et al.*, 2014; Shaltouki *et al.*, 2015; Mazzulli, Zunke, Tsunemi, *et al.*, 2016; Tsunemi *et al.*, 2019; Bono *et al.*, 2020; Laperle *et al.*, 2020; Oji *et al.*, 2020). Furthermore, in mice overexpressing human α-synuclein deficits in dopamine release are observed prior overt aggregation and neuron loss (Janezic *et al.*, 2013). These deficits are caused by aberrant α-synuclein activity in vesicle trafficking pathways similar to, but subtly distinct from, its physiological function. At the synapse, acute increase in local α-synuclein concentration results in impaired synaptic vesicle endocytosis during high but not low frequency stimulation (Busch *et al.*, 2014). This is mediated by the N-terminus and is prevented in mutants which are unable to adopt the helical conformation

necessary for interaction with membrane lipids. Monomeric α-synuclein also directly binds to and inactivates the VAMP2 homologue ykt6, which is involved in intracellular membrane fusion during autophagy (Cuddy *et al.*, 2019; Pitcairn *et al.*, 2023). This interaction inhibits both the fusion of autophagic vesicles and the trafficking of hydrolase enzymes to degradative lysosomes, leading to an overall decrease in autophagic flux, protein clearance and exacerbating the buildup of α-synuclein.

It is likely that *in vivo* these early, oligomer-independent forms of dysfunction arise in parallel with the formation and accumulation of more toxic oligomeric conformers, especially lysosomal inhibition drives oligomer accumulation (Mazzulli, Zunke, Tsunemi, *et al.*, 2016).

1.4.2 Toxicity of small oligomers

An ever-increasing variety of mechanisms through which oligomeric α-synuclein can damage neuronal cells have been identified. The most straightforward of these is direct permeabilisation of membranes by insertion of pore-like annular oligomers resulting in the leakage of cytoplasmic and vesicular contents (Volles *et al.*, 2001; Brochner *et al.*, 2025). At dopaminergic synapses this sets up a toxic cycle whereby oligomers cause dopamine leak from vesicles into the cytosol, which is subsequently metabolised to DOPAL that induces further oligomer formation (Plotegher *et al.*, 2017). Synaptic physiology is further perturbed by oligomers subverting the normal physiological role of α-synuclein and binding VAMP2 in manner that prevents SNARE complex assembly and vesicle release (Choi *et al.*, 2013).

Membrane binding of oligomeric α-synuclein also causes it to accumulate in mitochondrial membrane where its presence induces the externalisation of cardiolipin

from the inner to outer mitochondrial membrane (Ryan *et al.*, 2018). Cytosolic exposure of this anionic lipid both targets mitochondria for degradation through mitophagy and promotes further α-synuclein oligomerisation (Ryan *et al.*, 2018; Choi *et al.*, 2022). Within the mitochondria, proximity ligation and super-resolution microscopy demonstrate that α-synuclein oligomers interact with the ATP synthase and complex I, increasing the production of reactive oxygen species and probability of permeability transition pore opening (Ludtmann *et al.*, 2018). α-synuclein oligomers have also been shown to inhibit mitochondrial protein import, cause mtDNA damage and perturb mitochondrial Ca2+ homeostasis (Mingo, Escobar Galvis and Henderson, 2025).

Like monomers, oligomeric α-synuclein also reduces lysosomal hydrolase activity, likely through disrupted trafficking (Cuddy *et al.*, 2019; Hoffmann *et al.*, 2019). α-synuclein oligomers (but not monomers) further impair their own degradation by inhibiting the 26S ubiquitin proteasome (Zhang, Tang and Liu, 2008; Emmanouilidou *et al.*, 2010). Inhibition is due to the allosteric binding of oligomers to the catalytic 20S subunit which prevents the conformational change required for substrates to traverse the core (Thibaudeau, Anderson and Smith, 2018). Interestingly, while the binding mode of α-synuclein oligomers cannot be mimicked by monomers or fibrils, oligomeric β-amyloid and mutant huntingtin induce the same conformational change, implying shared pathomechanisms between diseases.

Finally, like many neurodegeneration-associated proteins, the accumulation of misfolded α-synuclein oligomers activates the ER unfolded protein response (UPR) (Colla *et al.*, 2012; Heman-Ackah *et al.*, 2017). While this is initially a protective pathway, chronic UPR activation and unresolved protein stress contribute to neurodegeneration (Scheper and Hoozemans, 2013). The UPR effector ATF6 is normally protective during

chronic ER stress, however in PD its trafficking between the ER and Golgi is inhibited by α-synuclein (Wu *et al.*, 2007; Credle *et al.*, 2015). This may contribute to a state of unresolved proteins tress which primes neurons for degeneration.

It is worth noting that while all the studies cited in this section focus on oligomer-specific mechanisms the exact identity of these oligomers is both unknown and likely heterogenous in most reports. This adds an additional layer of complexity as it remains unclear whether distinct oligomeric proteoforms exert divergent pathological effects.

1.4.3 Toxicity of Fibrillar α-synuclein

In addition to the capacity of fibrils to seed α-synuclein aggregation, promoting oligomer formation through secondary nucleation, it has become clear that fibrils themselves disrupt the autophagy-lysosome pathway. Ultrastructural analysis of post-mortem brain reveals autophagosomes and lysosomes incorporated into Lewy bodies (Fellner *et al.*, 2021). Macroautophagy is a major route for clearance of α-synuclein, however while fibrillar α-synuclein is targeted by autophagy machinery it is inefficiently degraded (Tanik *et al.*, 2013). The C-terminus of fibrillar, but not monomeric, α-synuclein directly interacts with key autophagy regulator LC3B, inhibiting its endogenous interaction with p62 in a dose-dependent manner and thus impairing autophagy initiation (Xu *et al.*, 2024). If autophagy proceeds as far as lysosome fusion, fibrils have been shown to alter lysosome structure, localisation and integrity (Senol *et al.*, 2021).

In human PD patients it is likely that α-synuclein exerts toxicity through a 'multi-hit' mechanism which simultaneously dysregulates synaptic communication, proteostasis and energy metabolism. A series of positive feedback loops (e.g. synaptic vesicle permeabilisation, hydrolase trafficking and cardiolipin externalisation) precipitate a toxic spiral that eventually overwhelms compensation strategies and initiate cell death.

1.5 Prion-like spread of α-synuclein pathology

In PD Lewy pathology appears in the brain in a relatively characteristic pattern consistent with the progression of motor and non-motor symptoms. α-synuclein inclusions arise first in the hindbrain (medulla oblongata and pons), then the midbrain including the acutely vulnerable SNpc (Braak *et al.*, 2003). In later stages pathology is found in temporal- and then neo-cortical areas with inclusions only found in association cortices at end-stage disease. More recently it has been suggested that, at least in a subset of patients, pathology first arises in the enteric nervous system and only later in the brain (Borghammer *et al.*, 2021). Although synaptic connectivity does not fully explain the stereotypic manner in which pathology arises it is notable that the order in which brain regions are affected aligns with their neuroanatomical connectivity.

The first evidence that α-synuclein pathology can propagate between cells came from the observation of phosphorylated α-synuclein inclusions in grafted tissue from PD patients who had received fetal cell transplants as part of an experimental therapy (Kordower *et al.*, 2008; Li *et al.*, 2008). It has now been shown that injection of brain homogenate from PD patients into the brains of rodents and monkeys not only seeds aggregation at the injection site but also induces pathology in multiple brain regions in a time-dependent manner (Recasens *et al.*, 2014). Similar time-dependent spread of seeded aggregation is observed if PFFs of recombinant α-synuclein are used rather than patient-derived fibrils (Masuda-Suzukake *et al.*, 2013). Consistent with the polymorph conservation of fibrillar seeds observed *in vitro* (the α-synuclein 'strain' phenomenon), α-synuclein fibrils in mice share biochemical characteristics with the fibrils used for inoculation (Uemura *et al.*, 2023).

PFF experiments have also shown that in animal models α-synuclein spreads between synaptically and neuroanatomically connected regions (Luk *et al.*, 2012). However, when neuroanatomical connections are disrupted, for example through callosotomy, the transmission of α-synuclein aggregates is not completely prevented (Okuzumi *et al.*, 2018). Consistent with the existence of extracellular α-synuclein outside the synaptic cleft, neuronally derived α-synuclein has been identified in the cerebrospinal fluid (CSF) of patients with PD and other synucleinopathies (Mollenhauer *et al.*, 2012). Interestingly, the total α-synuclein content of CSF is actually reduced in PD compared to healthy controls (Mollenhauer, 2014; Førland *et al.*, 2020). In contrast levels of oligomeric and phosphorylated α-synuclein are increased in CSF from PD patients (Park *et al.*, 2011; Majbour *et al.*, 2016). CSF from patients with PD and other synucleinopathies is able to seed the aggregation of recombinant α-synuclein *in vitro* providing crucial evidence for how extracellular misfolded α-synuclein may propagate pathology between brain regions (Fairfoul *et al.*, 2016).

The validity of the prion-like propagation hypothesis relies on the ability of recipient neurons to uptake extracellular α-synuclein oligomers. Although monomers and oligomers can diffuse across membranes they appear to be mostly taken up by endocytosis (Shearer, Petersen and Woodside, 2021). A variety of cell surface receptors have been implicated in this process including FAM171A2, LRP1 and LAG3 (Mao *et al.*, 2016; K. Chen *et al.*, 2022; Wu *et al.*, 2025). Live cell imaging shows that after uptake, aggregated seeds escape from the endolysosomal system into the cytosol where the can seed aggregation of endogenous protein in the recipient neurons (Ivey *et al.*, 2025).

1.6 Therapies targeting extracellular α-synuclein

The discovery of an extracellular oligomeric stage in the α-synuclein propagation cycle raises the important question as to whether this might be a potentially druggable target. Current licenced therapies mainly target the dopamine system, increasing synthesis or impairing breakdown, but as such only treat PD symptoms rather than altering the disease course (Kim and Lee, 2025). Continued SNpc degeneration eventually renders dopamine replacement therapies less effective as the number of neurons left for drugs to act on declines (Riederer *et al.*, 2025). An α-synuclein-directed therapy has the potential to be disease modifying, stalling the spread of pathology and neuronal dysfunction.

Active and passive immunotherapies against α-synuclein have been tested both in animal models of PD and human clinical trials. Immunization with α-synuclein C-terminal peptides UB-312 (Vaxxinity) and ACI-7104.56 (AC Immune) results in the generation of oligomer/aggregate selective antibodies that reduce the α-synuclein oligomer burden, degeneration and motor defects in PD mouse models (Mandler *et al.*, 2014; Nimmo *et al.*, 2020, 2022). Thus far both antigens have shown immunogenicity and tolerability in human PD patients and UB-312 was found to reduce oligomeric and phosphorylated α-synuclein in CSF (Volc *et al.*, 2020; Eijsvogel *et al.*, 2024). Phase II trials for both vaccines are now underway.

An alternative approach to target extracellular α-synuclein for degradation is passive immunotherapy with purified antibodies. So far Phase II trials have been carried for Cinpanemab (Biogen) which binds to an N-terminal epitope, and Prasinezumab (Roche) which targets the α-synuclein C-terminus. Both antibodies are selective for aggregated/oligomeric α-synuclein. Cinpanemab failed to reduce seeding-competent α-

synuclein in CSF and in line with failed target engagement did not improve motor performance in PD patients (Hutchison *et al.*, 2024). By contrast, a reanalysis of Prasinezumab trial results demonstrated slower progression of PD motor symptoms in the treated group compared to controls (Pagano *et al.*, 2022, 2024). Motivated by these findings and positive results from ongoing open-label continuation studies Prasinezumab is being advanced to Phase III trials, making it the first drug targeting oligomeric α-synuclein to reach this stage. How Prasinezumab fares in future trials is not only important in the context of drug development but also to validate the hypothesis that α-synuclein is central to PD pathomechanisms and aetiology.

A variety of small molecular inhibitors of α-synuclein aggregation/dis-aggregation agents have also been developed and demonstrate efficiency in preclinical models. These differ from the biologics described above in their ability to cross cell membranes and thus act both on extracellular and intracellular α-synuclein. Small molecule inhibitors can be broadly categorised by their mechanisms of action. For example, Anle183b and SynuCleanD bind to aggregated fibrils within the hydrophobic core, while CLR01 and NPT100 prevent association of monomers by blocking the amino acid side chains (Sinha *et al.*, 2011; Wrasidlo *et al.*, 2016; Pujols *et al.*, 2018; Antonschmidt *et al.*, 2022). An alternative strategy is to prevent misfolding altogether by stabilising the helical monomer in the absence of direct membrane interaction, for example with constrained N-terminal helical peptides (Meade *et al.*, 2025).

Other α-synuclein-directed approaches aim to reduce α-synuclein levels through modulating *SNCA* gene expression, mRNA stability or translation. However, these pose the risk of loss of function toxicity by also reducing monomer levels (Rodger, Nasser and Carter, 2023).

1.7- Mechanisms of inter-cellular α-synuclein transfer

For α-synuclein to propagate between cells in CSF it must first be released by neurons. Release could occur passively as cells, overwhelmed with α-synuclein pathology, undergo apoptosis. However, in a landmark study Lee and colleagues demonstrated that secretion of monomeric and aggregated α-synuclein is a constitutive and active process (Lee, Patel and Lee, 2005). Consistent with the lack of export signal sequence, these authors also showed that α-synuclein is not secreted by the conventional ER-Golgi route.

In the 20 years following this initial finding numerous possible unconventional secretion mechanisms have been suggested for α-synuclein based mostly on work using exogenous overexpression of pathway components in cancer cell lines (Fig. 1.3). However, it remains unclear which, if any, of these are active in human neurons. A clear understanding of the pathways active and the interplay between these pathways, would allow design of targeted therapeutics to impair α-synuclein secretion and spread acting upstream of the therapeutic approaches described in 1.6.

1.7.1 - Synaptic release

In mouse primary neurons α-synuclein secretion is dependent on electrical activity and can also be inhibited by tetanus toxin which cleaves VAMPs involved in vesicle fusion with the plasma membrane (Yamada and Iwatsubo, 2018; Xie *et al.*, 2022; Nakamura *et al.*, 2024). Activity-coupling could suggest a role for synaptic vesicles in α-synuclein release and consistent with this α-synuclein was found to be secreted from the axons of primary cells grown in microfluidic devices (Danzer *et al.*, 2011). Similarly, exogenously added tagged α-synuclein can also be re-secreted into the axonal chamber by dopaminergic neurons (Tsunemi *et al.*, 2019).

A recent publication using induced pluripotent stem cell-derived dopaminergic neurons (iPSC-DaNs) demonstrated a role for neuronal activity in α-synuclein release in this more disease-relevant model (Nuermaimaiti *et al.*, 2025). However, complete inhibition of firing activity only reduced α-synuclein secretion by ~20%, indicating electrical activity is clearly not the only regulator of α-synuclein secretion in neurons. Moreover, demonstration of activity dependence does not *per se* prove involvement of synaptic vesicles as many intracellular membrane fusion events are regulated by the Ca^{2+} fluxes arising from neuronal activity (Fukuda, 2013; Tsunemi *et al.*, 2019).

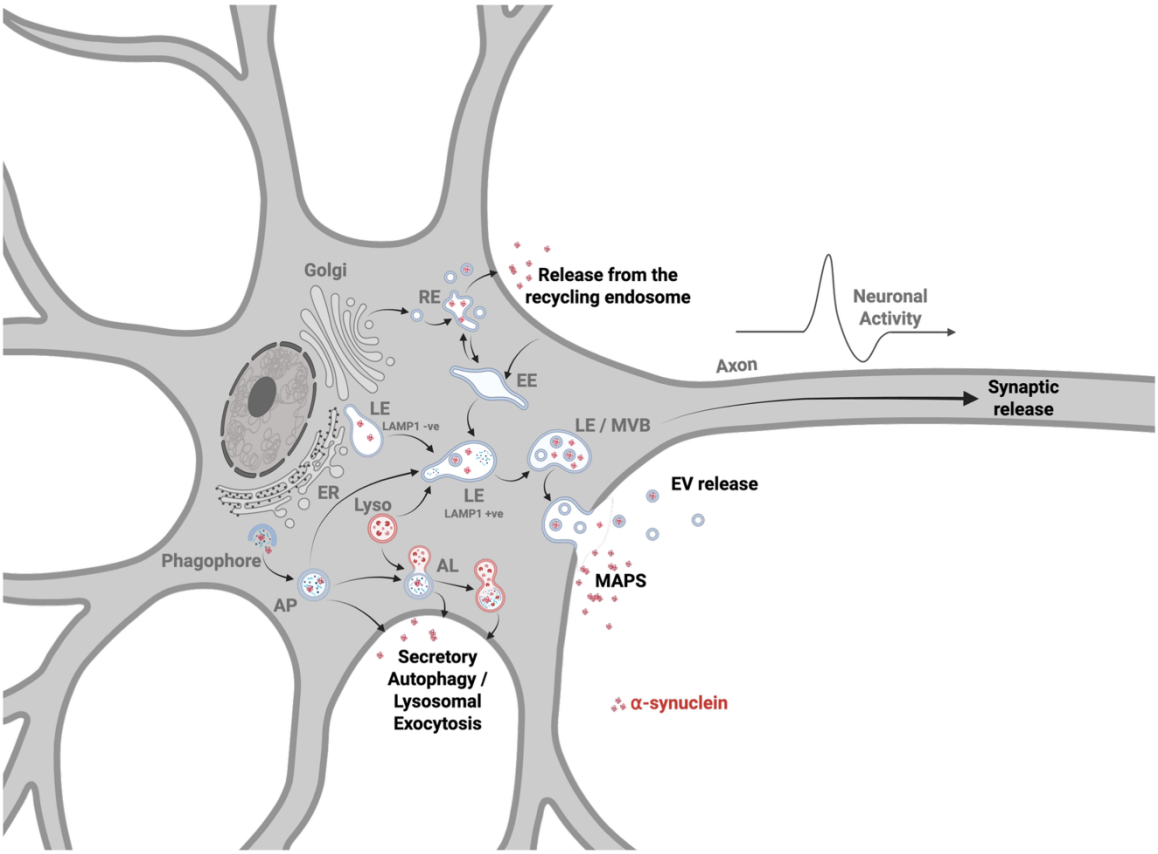

Fig. 1.3 Numerous intracellular pathways implicated in α-synuclein secretion
Schematic representation of the intracellular pathways contributing to α-synuclein release. AP = autophagosome, AL = autolysosome, EE = early endosome, ER = endoplasmic reticulum, LE = late endosome, Lyso = lysosome, MAPS = misfolding associated protein secretion, MVB = multivesicular body and RE = recycling endosome

1.7.2 - Secretion from the recycling endosome

The endosomal recycling system proceeds via two main routes: fast recycling pathways directly from the early endosome to the plasma membrane and slow recycling pathways via proteomically distinct recycling endosomes denoted by markers such as Rab11a (O'Sullivan and Lindsay, 2020). Knockdown of key recycling endosome GTPase Rab11a inhibits free α-synuclein secretion (Liu *et al.*, 2009; Hasegawa *et al.*, 2011). Moreover, overexpression of either Rab11a or Rab13, involved in recycling endosome-Golgi trafficking, increases α-synuclein secretion and intercellular transfer (Gonçalves *et al.*, 2016). Overexpression of these GTPases promotes flux through the recycling endosome pathways as shown by reduced intracellular transferrin. This suggests that α-synuclein can be released through the recycling endosome system, though it is unclear how α-synuclein is initially trafficked into this compartment.

Despite the lack of involvement of canonical ER-Golgi secretion in baseline α-synuclein release, inhibition of the ER-Golgi pathway with Brefeldin A increases the secretion of α-synuclein in a manner which can be attenuated by Rab11 inhibition (Chutna *et al.*, 2014; Fernandes *et al.*, 2016; Y. Yang *et al.*, 2017). Conversely, treatment with ambroxol, which both inhibits autophagic flux and increases α-synuclein release, boosts Rab11a expression (Magalhaes *et al.*, 2018a). While these data do not clarify how α-synuclein comes to be within recycling endosomes they suggest that it may be in response to perturbation of other α-synuclein release pathways.

1.7.3 – Misfolding associated protein secretion via the late endosome

Misfolding associated protein secretion (MAPS) is mediated by ER-tethered ubiquitin-specific protease USP19 which recruits aberrantly folded cytosolic proteins, including α-synuclein, to the ER membrane (Lee *et al.*, 2016). USP19 recognises ubiquitin-like signal peptides (ubiquitin-fold modifier 1, UFM1) which are added to α-synuclein and other misfolded proteins by UFM1-specific ligase 1 (Wang *et al.*, 2024). Protein cargoes are then shuttled into a Rab9-positive, ER-associated late endosome compartment, by the activity of USP19 chaperone HSC70 and its co-chaperone DNAJC5 (Xu *et al.*, 2018). DNAJC5, also known as cysteine string protein-α, is essential for this process, and palmitoylation of its cystine string domain facilitates membrane binding - disruption of which greatly impairs MAPS efficiency (Xu *et al.*, 2018). Interestingly, mice lacking DNAJC5 develop progressive and ultimately fatal neurodegeneration (Fernández-Chacón *et al.*, 2004). Super-resolution and electron microscopy reveal that although MAPS cargo are found inside late endosomes, they are not present in the intraluminal vesicles, consistent with this being a mechanism for the release of free protein (Lee *et al.*, 2016). LAMP2 also contributes to α-synuclein translocation into the late endosome, although it does not interact with DNAJC5 (Lee *et al.*, 2018). SNAP-23 is essential for the subsequent late endosome-plasma membrane fusion, and knockdown abrogates the DNAJC5-mediated boost to secretion (Fontaine *et al.*, 2016; Zhao *et al.*, 2022).

In addition to α-synuclein other neurodegeneration-related proteins can also be secreted through MAPS *in vitro*. Overexpression of USP19 or DNAJC5 in HEK293T cells stimulates the release of Tau, SOD1, Atx3-Q84 and TDP43, but not typical ER-Golgi cargo clusterin, when these proteins are also exogenously expressed (Fontaine *et al.*, 2016; Xu *et al.*, 2018).

1.7.4 - Secretory autophagy / Lysosomal exocytosis

As well as proceeding towards degradation autophagosomes, autolysosomes and degradative lysosomes can release their cargo into the extracellular milieu by direct fusion with the plasma membrane (Buratta *et al.*, 2020). Depending on the stage at which vesicles are exocytosed the nomenclature of this process changes, but the underlying principle of cargo-uptake via macro-autophagy followed by SNARE-mediated vesicular release is conserved.

Although there is less data supporting this route of α-synuclein secretion, it has been demonstrated that conditions which boost lysosomal exocytosis, such as agonism of the lysosomal Ca^{2+} channel TRPML1 or lysosome deacidification with Bafilomycin A1, also boost α-synuclein release (Tsunemi *et al.*, 2019; Scholz *et al.*, 2025). The small GTPase Rab27b is implicated in this pathway as its knockdown abrogates both Bafilomycin A1-induced lysosomal exocytosis and α-synuclein secretion (Underwood *et al.*, 2020; Scholz *et al.*, 2025). However, Rab27b overexpression in the absence of Bafilomycin A1 treatment reduces α-synuclein release, possibly through enhanced activity of lysosomal proteases, suggesting that this route of exocytosis is negligible in the absence of a lysosomal stressor (Scholz *et al.*, 2025).

Syntaxin-4, VAMP7 and SNAP-23 have been shown to regulate both lysosome and late endosome fusion with the plasma membrane (Rao *et al.*, 2004; Dingjan *et al.*, 2018). SNAP-23 and syntaxin-4 knockdown decrease both α-synuclein release and lysosomal exocytosis as measured by the coincident secretion of lysosomal proteases (Xie *et al.*, 2022; Zhao *et al.*, 2022; Sawai, Nakamura and Arawaka, 2025). Accordingly, these authors have argued a role for SNARE-mediated lysosomal exocytosis in basal α-

synuclein secretion, without a lysosomal stressor. Note, only pro-proteases were detected in the extracellular environment leading Sawai and colleagues to suggest that vesicles are secreted prior to lysosomal maturation i.e. a secretory autophagy variant of release. However, although VAMP7 knockdown or dominant negative expression reduces α-synuclein release, only dominant negative expression impairs lysosomal exocytosis (Xie *et al.*, 2022; Zhao *et al.*, 2022). The ability of VAMP7 depletion to impair α-synuclein release without perturbing secretion of lysosomal proteases suggests that the Syntaxin-4/VAMP7/SNAP-23 complex acts on α-synuclein release through late endosome pathway rather than autolysosome/lysosomes where another R-SNARE may be able compensate. While these data do not rule out involvement of lysosomal exocytosis in basal α-synuclein secretion, more evidence is required to demonstrate specificity given the numerous shared genetic regulators with MAPS.

1.7.5 Extracellular vesicles

Secretory extracellular vesicles (EVs) can be categorised into exosomes which are released upon fusion of the multivesicular body with the plasma membrane and microvesicles which are directly derived from the plasma membrane (Doyle and Wang, 2019). Exosomes range in diameter from ~30-150 nm and are released from a variety of cell types in the brain including neurons (Mavroeidi *et al.*, 2022). α-synuclein has been identified within exosomes in CSF from Parkinson's patients and healthy people although this only represents approximately 2% of the total CSF α-synuclein (Stuendl *et al.*, 2016). α-synuclein secretion in exosomes has also been confirmed in SH-SY5Y cells and iPSC dopaminergic neurons where exosomal α-synuclein accounts for 0.1-2 % of secretion in healthy cells (Gustafsson *et al.*, 2018; Wang *et al.*, 2018; Oh *et al.*, 2022).

Disruption of the autophagy-lysosome pathway triggers a concomitant increase in exosomal α-synuclein release. Mechanistic work in SH-SY5Y cells has demonstrated that pharmacological inhibition of autophagosome biogenesis and lysosomal function increases the number of exosomes secreted and their total α-synuclein content (Alvarez-Erviti *et al.*, 2011; Danzer *et al.*, 2012; Ejlerskov *et al.*, 2013; Poehler *et al.*, 2014; Fussi *et al.*, 2018; Minakaki *et al.*, 2018; Tang *et al.*, 2021). This is distinct from the boost to free α-synuclein secretion, possibly through lysosomal exocytosis or secretory autophagy which is also observed when autophagy is inhibited (Lee *et al.*, 2013; Fernandes *et al.*, 2016; Sawai, Nakamura and Arawaka, 2025). When autophagy is inhibited the EVs released express distinct proteomic signatures including LC3B, p62 and LAMP2 (Minakaki *et al.*, 2018; Oh *et al.*, 2022). Intriguingly, DNAJC5 has also be identified in α-synuclein-containing EVs though this is likely to be independent of its role in MAPS which, unlike exosome release, is not inhibited by knock-down of ESCRT complex components (Lee *et al.*, 2016; Deng *et al.*, 2017; Wu, Sirkis and Schekman, 2022; Lee *et al.*, 2023). Indeed, a secondary palmitoylation-independent role of DNAJC5 at peripheral acidified multi-vesicular bodies has recently been reported, which appears to be distinct from its function on perinuclear late endosomes (Lee *et al.*, 2023).

Under conditions of autophagy-lysosome dysfunction, how is α-synuclein re-routed from lysosomal degradation to EV-mediated release? Double membraned autophagosomes fuse with the late-endosome/multi-vesicular body (MVB) releasing their contents, still bounded by the inner autophagosomes membrane, into the lumen of the late-endosome (Zubkova *et al.*, 2024). These so-called amphisomes are then released along with canonical exosomes. The process of autophagosome-late endosome membrane fusion is dependent on the SNAP-29/Syntaxin-17 complex (Zubkova *et al.*, 2024). As well as in

response to harsh experimental autophagy perturbations, this process also occurs physiologically in response to protein stress, during which SCAMP5 inhibits autophagy to promote exosomal α-synuclein release (Yang *et al.*, 2017).

This pathway crosstalk is important in a disease context as many of the mutations which cause inherited PD are associated with dysfunction in the autophagy-lysosome pathway or elevated protein stress in patient-derived cells (Schöndorf *et al.*, 2014; Fernandes *et al.*, 2016; Mazzulli, Zunke, Tsunemi, *et al.*, 2016; Burbulla *et al.*, 2017; Lang *et al.*, 2019; Okarmus *et al.*, 2020). Dysregulated autophagy is even observed in cells from patients with sporadic PD (Sánchez-Danés *et al.*, 2012; S.-Y. Yang *et al.*, 2017; Corenblum *et al.*, 2023). Consistent with this, fibroblasts and neurons derived from patients with PD mutations have been found to secrete more exosomal α-synuclein than cells from healthy controls (Cerri *et al.*, 2021; Stykel *et al.*, 2021; Oh *et al.*, 2022).

1.7.6 Non-secretory transfer: propagation through tunnelling nanotubes

α-synuclein can also be transferred between cells in a contact-dependent manner through intercellular conduits called tunnelling nanotubes (TNTs) (Abounit *et al.*, 2016; Dilsizoglu Senol *et al.*, 2019; Grudina *et al.*, 2019; Senol *et al.*, 2021). These membrane-bound structures are supported by an F-actin-only cytoskeleton and allow transport of various organelles including mitochondria, ER and lysosomes (Wu and Schekman, 2024). α-synuclein transfer through TNTs appears to be within trafficked lysosomes (Abounit *et al.*, 2016; Senol *et al.*, 2021). Accumulating evidence suggests a crucial role of TNT-mediated α-synuclein transfer in neuron-glia and glia-glia communication (Rostami *et al.*, 2017; Chakraborty *et al.*, 2023; Raghavan *et al.*, 2024; Scheiblich *et al.*, 2024).

1.7.7 Release pathway crosstalk and integration

In addition to the regulation of free and exosome-bound α-synuclein release by the autophagy-lysosome pathway, there appears to be a degree of reciprocal regulation between exosomal release and pathways which secrete free α-synuclein. Genetic inhibition of intraluminal vesicle biogenesis and exosome secretion through disruption of the ESCRT machinery (VPS4 or CHMP2B) causes a parallel increase in free α-synuclein secretion mediated by Rab11a (Hasegawa *et al.*, 2011; Spencer *et al.*, 2016). Moreover, when EV-mediated release is already boosted by autophagy disruption, pharmacological inhibition of exosome biogenesis causes a coincident increase in free α-synuclein secretion (Fussi *et al.*, 2018).

Integrating findings from the studies described above suggests a model in which cells have numerous α-synuclein release pathways available and can re-direct between pathways in response to changes in their internal environment. Assuming equal expression of pathway components in any given cell model it appears that constitutive secretion of α-synuclein under normal conditions is predominantly from the endosomal system. Selectivity for the recycling or late-endosome route may be dictated by folding state though further work is required to conclusively prove this hypothesis. Additional pathways including secretory autophagy/lysosomal exocytosis and EV release can be engaged in response to dysfunction in the autophagy-lysosome pathway downstream of pharmacological agents or PD-linked mutations. However, it remains to be determined whether individual cell types, specifically those with links to PD aetiology, exhibit intrinsic preferences to any pathways based on the endogenous expression level of the necessary functional and regulatory proteins. Moreover, while Ca^{2+} has been shown to regulate most routes of α-synuclein secretion, the Ca^{2+} sensors involved as well as extent

and timescale of coupling to neuronal activity remain unclear. Furthermore, in the context of PD it is essential to understand how different disease-causing mutations influence which pathways are active and whether any of the secretion pathways exhibit a preference for oligomeric, aggregated or post-translationally modified and α-synuclein.

1.7.8 – Limitations of mechanistic studies in non-neuronal systems

Other than a limited selection of publications working with primary rodent neurons, mostly in the context of activity-dependent secretion, most mechanistic work has been carried out in immortal cell lines. While these studies have provided useful insights there are important limitations of reconstituting biological processes by overexpression of pathway components including α-synuclein itself. The supraphysiological levels of α-synuclein achieved, in cells where it serves no physiological function, may increase its probability of being targeted for degradation/extrusion, possibly engaging mechanisms which would not occur *in vivo*. Similarly, singular or pairwise overexpression of regulatory proteins can create a background of protein stress as well as competition for endogenous binding partners, confounding data interpretation as seen for Rab11a (Chutna *et al.*, 2014). Moreover, pathways are usually studied in isolation making it challenging to compare relative contributions to total α-synuclein secretion under basal or disease conditions. There are also under-appreciated differences between immortal cell models; for example HeLa cells release far fewer exosomes, which limit the extent to which conclusions can be drawn across multiple studies (Valenzuela *et al.*, 2015). Most crucially, PD-vulnerable dopaminergic neurons are highly specialised cells with distinct transcriptional programs and a vast axonal arbour which itself is the site of axonal mRNA translation further fine-tuning the local proteome (Matsuda *et al.*, 2009; Kilfeather

et al., 2024). It therefore seems unlikely that these cells behave in the same manner as actively dividing non-neuronal cells without any degree of polarisation.

As highlighted above, many of the same genes such as *SNAP23*, *ATG5* and *DNAJC5* have been studied in the context of numerous pathway without sufficient controls to prove that their inhibition in a given experiment is through the mode of action cited by the study authors (Hasegawa *et al.*, 2011; Fontaine *et al.*, 2016; Deng *et al.*, 2017; Fussi *et al.*, 2018; Xu *et al.*, 2018; Xie *et al.*, 2022; Zhao *et al.*, 2022; Sawai, Nakamura and Arawaka, 2025). Even where pleiotropic effects have not been explicitly explored, many of the proteins identified as release-regulators, are also known to be active in other cellular pathways that modulate α-synuclein secretion. For example, Rab11a studied in the context of recycling endosome-mediated α-synuclein secretion also regulates autophagosome-MVB fusion, and ESCRT components facilitate autophagosome biogenesis as well as intraluminal vesicle budding (Zubkova *et al.*, 2024). Hence, a clear understanding of α-synuclein release biology can only be achieved by studying all potential regulators together in the same, physiologically relevant, model. As a high throughput and high relevance model, human iPSC-DaNs are well placed to tackle this challenging question.

1.8 iPSC neuron models

1.8.1 Stem cell reprogramming and differentiation

The discovery of the Yamanaka factors (OCT3/4, SOX2, KLF4 and c-MYC), which can collectively reprogram adult fibroblasts to an embryonic-like pluripotent state, has revolutionised the *in vitro* modelling of human diseases (Takahashi and Yamanaka, 2006). Viral transduction of somatic cells with this cocktail of transcription factors generates stem cells capable of forming all three germ layers. It was rapidly realised that these stem cells can be re-differentiated to cell types of interest in a similar manner to the human embryonic stem cells (hESCs) used up to this point (Dimos *et al.*, 2008). The combination of somatic cell reprogramming and target cell type differentiation enables the study of patient-derived cells where functional deficits caused by disease-associated mutations can be interrogated.

Motivated by the potential to generate dopaminergic neurons for therapeutic transplantation, the Studer lab published the first protocol for midbrain dopamine neuron generation from hESCs using temporally controlled growth factor exposure in 2004 (Perrier *et al.*, 2004). Neural induction was achieved by co-culture with a stromal feeder line but exogenous addition of developmental signalling molecules sonic hedgehog (SHH, ventralisation) and fibroblast growth factor 8 (FGF8, caudalisation) was used for the crucial midbrain dopaminergic pattering. Finally, cells were differentiated by exposure to ascorbic acid and brain-derived neurotrophic factor. In the following years protocol improvements have been made to optimise both differentiation efficiency (the percentage of cells expressing tyrosine hydroxylase) and cell type identity (midbrain marker expression including LMXA1), and although the core principles of neural

induction, midbrain patterning and extended maturation remain unchanged (Marton and Ioannidis, 2019). Today, the most commonly used method induces neuronal identity with dual SMAD inhibition where SB431542 inhibits the activin receptor and SMAD2/3, while LDN193189 antagonises bone morphogenic protein (BMP) signalling and SMAD1/5/8 (Chambers *et al.*, 2009; Kriks *et al.*, 2011; Puspita, Deline and Shim, 2025). Midbrain dopaminergic neurons are then patterned with SHH, (synthetic SHH agonist) puromorphamine and FGF8 with the inclusion of CHIR99021 to specify floorplate identity by activating WNT signalling (Kriks *et al.*, 2011). Electrophysiologically active, dopamine-releasing neurons are matured by inhibiting Notch-Delta signalling with DAPT in the presence of neurotrophic factors (Kriks *et al.*, 2011; Hartfield *et al.*, 2014).

Dopaminergic differentiation (as above) of patient-derived iPSC has enabled an explosion of research into the cellular dysfunction in cells from patients with familial and sporadic PD (Soldner *et al.*, 2011; Sánchez-Danés *et al.*, 2012; Woodard *et al.*, 2014; Chung *et al.*, 2016; Fernandes *et al.*, 2016; Burbulla *et al.*, 2017; A. Ikeda *et al.*, 2019; Barbuti *et al.*, 2020; Bono *et al.*, 2020; Brazdis *et al.*, 2020; Oji *et al.*, 2020). However, the rate of advancement is still limited by the lengthy differentiation protocols where production of mature neurons routinely takes >100 days from thawing iPSCs (Lang *et al.*, 2019). The duration of this process can be massively shortened by replacing SHH/FGF8-mediated neural induction with the overexpression of pioneer transcription factor neurogenin-2 (NGN2) (Hulme *et al.*, 2021).

NGN2 is a master regulator of neurogenesis, capable of binding in regions of previously closed chromatin to rapidly activate gene regulatory networks controlling neuronal identity (Smith *et al.*, 2016). Even in somatic cell types, forced NGN2 expression promotes rapid transdifferentiation to neurons, with an efficiency dictated by the

transgene expression level (Berninger *et al.*, 2007; Heinrich *et al.*, 2010). In combination with different patterning and maturation protocols, forced NGN2 expression, can yield a wide variety of neuron types including cortical, motor, sensory and most recently dopaminergic neurons (Fernandopulle *et al.*, 2018; Hulme *et al.*, 2020; Sheta *et al.*, 2022). Importantly, NGN2 expression during normal neurogenesis is transient necessitating inducible expression systems where NGN2 can be silenced after neuronal induction to permit maturation (Galichet, Guillemot and Parras, 2008).

A key limitation of both growth factor-induced and transcription factor-induced iPSC-derived neuronal models is the loss of cellular aging markers such as CpG methylation, mitochondrial damage and telomer shortening which are effectively 'reset' when cells pass through the iPSC stage (Miller *et al.*, 2013). Aging is the largest risk factor for PD suggesting that phenotypes observed in patient-derived cells *in vitro* may be more pronounced if the iPSC stage was avoided. Ongoing work is seeking to optimise protocols for transdifferentiation of patient fibroblasts to dopaminergic neurons which would retain the biochemical age of donor cells and may be better disease models in future (Huh *et al.*, 2016).

1.8.2 Complex culture systems

With the vast array of iPSC-derived cell types which can now be generated, co-culturing in 2D and 3D systems provides the opportunity to interrogate physiologically relevant interactions between cell types, for example astrocytes and dopaminergic neurons, that may contribute to PD pathology. Improvements in assembloid and organoid production is starting to facilitate cells to be grown in microenvironments more representative of their midbrain niche *in vivo* (Fiorenzano *et al.*, 2021; Reumann *et al.*, 2023; Solana-

Manrique *et al.*, 2025). Encouragingly, these more complex culture systems recapitulate cellular features of PD observed in 2D models such as increased oligomeric α-synuclein downstream of *SNCA* triplication (Mohamed *et al.*, 2021).

Co-cultures can also be established in a more 'supervised' fashion whereby circuit architecture is directly controlled (Do *et al.*, 2024). These authors optimised a tripartite microfluidic model of cortico-striato-nigral circuitry that demonstrated that the dysfunction caused by familial mutations in iPSC-DaNs altered the electrophysiological properties of the striatal medium spiny neurons onto which they project. Furthermore, even in monoculture, combining iPSC-derived neurons with microfluidic technology allows separation of axonal arbours from their soma and dendrites enabling compartment-specific interrogation of these highly polarised cells (Prots *et al.*, 2018; Tsunemi *et al.*, 2019; Bengoa-Vergniory *et al.*, 2020; Vroman *et al.*, 2025).

1.8.3 CRISPR interference in iPSC-derived neurons

The repurposing of bacterial clustered, regularly interspaced, short palindromic repeats (CRISPR) and Cas9 enzymes for gene editing has revolutionised genetic engineering. In the bacterial response to viral pathogens target-directed CRISPR-RNA (crRNA) interacts with trans-activating tracrRNA to recruit and activate the Cas9 enzyme that introduces sequence-specific double stranded DNA breaks (Knott and Doudna, 2018). For the purposes of gene editing, the crRNA and tracrRNA are combined into a single guide RNA (sgRNA) which can be designed against targets of interest. Classic CRISPR has been used extensively in iPSC-derived models to generate permanent knockout of PD-linked genes including *SNCA* (Chen *et al.*, 2019; Inoue *et al.*, 2023). However, CRIPSR can also have permanent off-target effects and the reliance on endogenous double-stranded DNA

repair mechanism generates different mutations at the target site across the cell population (Mandegar *et al.*, 2016; Franks, Heon-Roberts and Ryan, 2024). Moreover, for some essential genes, knockout strategies are not suited to investigate their functionality, as these would greatly impair cell viability.

CRISPR interference (CRISPRi) capitalises on the site-specific targeting of classic CRISPR but uses a catalytically inactive Cas9 mutant fused to the transcriptional repressor domain of the transcription factor KOX1 (dCas9-KRAB) to inhibit the activation of transcription without permanently changing the gene sequence (Gilbert *et al.*, 2013) – Fig. 1.4. In iPSC-derived neurons, CRISPRi has been used to make targeted knockdowns for phenotypic characterisation as well as screens to understand the genes that contribute to a certain phenotype (Tian *et al.*, 2019; Santhosh Kumar *et al.*, 2024; Kumar and Feldman, 2025). The specificity and comparative high throughput of CRISPRi knockdown technology positions it as the ideal approach to probe genes and proteins involved in α-synuclein release and propagation processes.

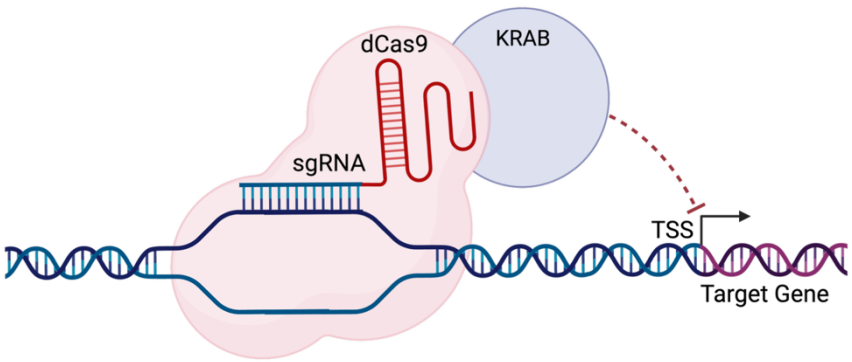

Fig. 1.4 CRISPRi-mediated transcriptional repression
Schematic representation the dCas9-KRAB mediated transcriptional repression. The sgRNA binds via a target specific sequence (blue) to genomic DNA and via a conserved sequence (red) to the catalytically dead Cas9 enzyme localising it close to the transcriptional start site (TSS). dCas9 is fused to the Krüppel associate box (KRAB) domain of the transcription factor KOX1 which inhibits transcription of the target gene.

1.9 Thesis Aims

By integrating techniques from stem cell biology, classical biochemistry and biophysics this thesis aims to:

- Characterise the landscape of post-translational modifications to α-synuclein in iPSC-DaNs (Chapter 3).
- Investigate the cellular mechanisms contributing to α-synuclein secretion from iPSC-DaNs using pharmacological and genetic approaches (Chapters 4 and 5).
- Identify potentially pathogenic conformers of α-synuclein secreted by iPSC-DaNs (Chapter 6).

Chapter 2 – Materials and Methods

2.1 Mammalian Cell Culture

2.1.1 General

Table 2.1.1 Materials and Reagents for Cell Culture

Reagent	Supplier	Catalogue Number
2-bromopalmitic acid	Merck	21604
2-mercaptoethanol	Gibco	21985023
Antibiotic-antimycotic	Gibco	15240096
Ascorbic acid	Merck	A4544
B-27 Supplement with Vit A	Gibco	17504044
B-27 Supplement without Vit A	Gibco	12587010
BAPTA-AM	Abcam	ab120503
BDNF	PeproTech	450-02
Biolaminin LN	BioLamina	LN521-05
Boric acid	Merck	B6768
CCCP	Merck	C2759
Chemgene	STARLAB ltd	SKU075A
CHIR-99021	Tocris	4423/10
Chloroquine	Merck	C6628
Cool Cell Freezing Container	Corning	15552771
Cytosine β-D-arabinofuranoside	Merck	C6645
DAPT	Abcam	ab120633
Db-cAMP	Biosynth	ND07996
DMEM high glucose, GlutaMAX	Gibco	61965026
DMEM/F-12	Gibco	21331020
DMSO	Merck	D2438
Doxycycline	Merck	D9891
Embryonic stem-cell FBS	Gibco	16141079
FGF8a	SinoBiological	16124-HNAE-SIB
GDNF	PeproTech	450-10
Geltrex	Gibco	A1413302
GW4869	Tocris	6741
hESC-qualified Matrigel	Corning	354277
Hygromycin B	Gibco	10687010
Isradipine	Abcam	ab120142
Knockout DMEM	Gibco	10829018
Knockout serum replacement	Gibco	10828010
L-Glutamine	Thermo Scientific	25030024
Laminin	Merck	L2020
Lenti-X 293T cell line	Takara Bio	632180
LDN-193189	Merck	SML0559
MEM non-essential amino acids	Gibco	11140050
Mitomycin C	Abcam	ab120797

MRT68921	Merck	SML1644
mTeSR plus Kit	StemCell Technologies	100-0276
MycoAltert Mycoplasma Detection Kit	Lonza	LT07-318
N2 Supplement	Gibco	17502048
Neurobasal medium	Gibco	21103049
Neurobasal Medium minus phenol red	Gibco	12348017
Penicillin-streptomycin	Gibco	15140122
Poly-L-ornithine	Merck	P3655
Purmorphamine	Tocris	4551/10
Quercetin	Merck	Q4951
Recombinant SHH C24II	R&D Systems	1845-SH-500
ROCK inhibitor (Y27632)	Apex Bio	A3008-APE
Rotenone	Merck	R8875
SB-431542	Apex Bio	A8249-APE
SH-SY5Y	ECACC	94030304
Sodium tetraborate	Merck	221732
STEMdiff Midbrain Differentiation Kit	STEMCELL Technologies	100-0038
STEMdiff Midbrain Maturation Kit	STEMCELL Technologies	100-0041
StemPro Accutase	Gibco	A1110501
TGFβ3	Gibco	100-36E
Trypsin-EDTA	Gibco	25200056
UltraPure 0.5M EDTA	Invitrogen	15575-038

2.1.1.1 Aseptic Technique

Before addition to cells all media were filtered (0.22 µm) to remove potentially contaminating bacteria. Tissue culture work was performed in laminar flow hoods and cells were maintained in 37°C incubators with 5% CO_2. Between August 2024 and October 2025 conditioned media samples were routinely tested for mycoplasma contamination using MycoAlert Detection Kit.

2.1.1.2 Cell counting

Cell suspensions were diluted 1:10 or 1:20 in PBS to a total volume of 100 µL. A 20 µL aliquot was mixed with 1 µL of AO.DAPI (80 µg/mL acridine orange, 40 µg/mL 4′,6 diamidino-2-phenylindole). 10 µL was added to chambers of a NC-slide A8 in duplicate and counted using a Chemometec NucleoCounter NC-250.

2.1.2 Stem Cell Culture

Table 2.1.2 Stem Cell Lines

Genotype	Donor	Sex	Age	Reprogramming	Clone	Transgene(s)	Line Name	Ref
Control	WTC11	M	30	Episomal plasmid	G3dCas9	NGN2, dCas9	dCas9 i3	Tian et al., 2019
Control	JR053	M	68	Retrovirus	01	-	JR053	Lang et al., 2019
Control	SFC065	M	65	Sendai Virus	03-03	-	065	Lang et al., 2019
						mTagBFP2	B065	-
Control	SFC067	M	72	Sendai Virus	03-01	-	067	Lang et al., 2019
						mTagBFP2	B067	-
Control	SFC156	M	75	Sendai Virus	03-01	-	156	Lang et al., 2019
						mTagBFP2	B156	-
Control	SFC856	F	78	Sendai Virus	03-04	-	856	Zambon et al., 2019
						dCas9	dCas 856	-
SNCA-KO	SFC856	F	78	Sendai Virus	03-04	-	12E	Zambon et al., 2019
SNCA-A53T	SFC828	F	51	Cytotune 1	03-06	-	828	Zambon et al., 2019
SNCA-A53T	SFC829	M	46	Cytotune 1	03-06	-	829	Zambon et al., 2019
SNCA-A53T	SFC830	M	51	Cytotune 1	04-09	-	830	Zambon et al., 2019
SNCA-trip	SFC831	F	55	Cytotune 1	03-01	-	831-1	Zambon et al., 2019
						dCas9	dCas9 831-1	-
					03-03	-	831-3	Zambon et al., 2019
						dCas9	dCas9 831-3	-
					03-05	-	831-5	Zambon et al., 2019
GBA-N370S	SCF871	F	70	Sendai Virus	03-09	-	871	Bogetofte et al., 2021
GBA-N370S	MK071	F	81	Retrovirus	03	-	71-3	Fernandes et al., 2016
GBA-N370S	MK082	M	51	Retrovirus	26	-	82-26	Lang et al., 2019
GBA-N370S	MK088	M	46	Retrovirus	01	-	88-1	Fernandes et al., 2016

2.1.2.1 iPSC culture

2.1.2.1.1 Thawing iPSCs

One well of a 6-well plate per cell line was coated with Matrigel diluted in ice cold Knockout DMEM and incubated overnight at 37°C. The next day cryovials of frozen iPSCs were thawed in a 37°C water bath and then centrifuged for 5 minutes at 350 xg in 10 mL of Knockout DMEM. The supernatant was aspirated and pelleted cells were resuspended in 1 mL of filtered mTeSR+ with 10 µM Rho kinase inhibitor (ROCKi). The Matrigel coating was aspirated from the wells and replaced with 1 mL of mTeSR+/ROCKi media, and the cell suspension was added in a drop-wise manner swirling the plate to achieve a homogenous distribution. The next day a full media change was performed with 3 mL mTeSR+ without ROCKi.

2.1.2.1.2 Expanding iPSCs and hygromycin selection

iPSCs were cultured in mTeSR+ medium at 37°C, 5% CO_2 for a maximum of 2 weeks, with media changes every 2-3 days until they reached 80% confluency and were colony passaged. For dCas9 856, dCas9 831-1 and dCas9 831-3 mTeSR+ was supplemented with 300 mg/mL hygromycin after the first passage. Cells were maintained under hygromycin selection (excluding days of passaging) until >90% of the population expressed the nuclear mNeonGreen marker, as determined by eye with the Etaluma Lumascope 620. At this point cells were single cell passaged for differentiation.

2.1.2.1.3 Colony passaging iPSCs

Non-enzymatic passaging with EDTA was preferentially used for iPSCs to reduce the risk of spontaneous differentiation unless a cell count or single cell suspension was required. Plates were coated overnight at 37°C with Matrigel in Knockout DMEM. iPSCs at 80-90% confluency were washed with pre-warmed 0.5 mM EDTA in PBS. The EDTA was immediately aspirated and replaced with a further 1 mL of EDTA per well. Cells were incubated with EDTA at 37°C for 3-5 minutes with regular checks using the EVOS XL Core Imaging System to ascertain dissociation from adjacent cells, indicated by an apparent brightening of small colonies creating a halo effect. The EDTA was aspirated, and wells were resuspended in pre-warmed mTeSR+ using a P1000 pipette. iPSCs were split in 1:3 to 1:5 ratio based on the relative growth rate of that cell line and plated in 3 mL mTeSR+ per well. Cells were checked with the EVOS approximately 1 hour after replating to ensure attachment to the Matrigel coating.

2.1.2.1.4 Single Cell passaging iPSCs

Enzymatic dissociation with Accutase was only used in the 1-2 days directly preceding the start of differentiation or before cryopreservation. iPSCs were washed once with room temperature PBS, which was aspirated and replaced with 0.6 mL per well of room temperature Accutase. Cells were then incubated with Accutase at 37°C for 3-10 minutes, checking every minute from 3 minutes onwards. Dissociation was ascertained by gently knocking on the side of the plate to determine if cells would lift. P1000 pipette was used to add 1 mL of Knockout DMEM per well and homogenise the cell suspension. The cell suspension was transferred into a spin falcon containing Knockout DMEM. Wells of the same line were pooled, ensuring a minimum 1:10 dilution of Accutase in DMEM. Cells were centrifuged for 5 minutes at 350 xg and the knockout DMEM aspirated. Cell pellets were resuspended in mTeSR+ supplemented with 10 μM ROCKi and counted as described in 2.1.1.2.

2.1.2.1.5 Cryopreserving iPSCs

iPSCs were single cell passaged using Accutase, but cell pellets were resuspended in warmed freezing media (90% Stem cell grade FBS, 10% DMSO) before counting. Cells suspensions were further diluted to $4x10^6$ cells/mL in freezing media and aliquoted into cryovials, 1 mL per vial. Vials were moved to -80°C freezers in CoolCell Freezing containers to slow the rate of freezing to 1°C per minute. The CoolCell containers were removed after 24 hours, and the frozen vials were transferred to liquid nitrogen containers for long-term storage.

2.1.2.2 Dopaminergic differentiation - modified from Kriks et al (2011)

Differentiation days are referred as DayX where Day0 represents the first day iPSCs are no longer cultured in mTeSR+. Full feeds refer to complete media changes whereas half feeds indicate removal of 45% of the well volume and replacement with 50% of the intended volume to account for evaporation.

Table 2.1.2.2A Kriks Protocol Base Media Composition

Base Media Name	Composition	Concentration % (v/v)
KSR	Knockout DMEM	85
	Knockout Serum Replacement	15
	2-mercaptoethanol	1
	L-Glutamine	1
	MEM non-essential amino acids	1
NNB	Neurobasal medium	97.5
	N2 Supplement	0.5
	B-27 Supplement without Vit A	1
	L-Glutamine	1
NB	Neurobasal Medium	97
	B-27 Supplement without Vit A	2
	L-Glutamine	1
NG	Phenol-free Neurobasal Medium	99
	L-Glutamine	1

2.1.2.2.1 Neural induction and patterning

On Day-3 6-well plates were coated with Geltrex diluted in cold Knockout DMEM and incubated overnight at 37°C. iPSCs were single cell passaged on Day-2 replating at a density of 1.2 million cells per well in 3 mL mTeSR+ with ROCKi and fully fed again on Day-1 with mTeSR+ only. On Day0 mTeSR was replaced with KSR supplemented with 100 nM LDN-193189 and 10 µM SB-431542. Between Day0 and Day10 base media composition is gradually changed from KSR to NNB while exposing the cells to dual SMAD inhibition followed by activation of SHH and WNT signalling (Fig. 2.1A). Cells were maintained in 4 mL of culture media with half feeds on days 2, 4, 6, 8 and 10.

Table 2.1.2.2B Kriks Protocol Media Composition Day0-10

	Day1-2	Day3-4	Day5-6	Day7-8	Day9-10
Base media	100% KSR	100% KSR	75% KSR 25% NNB	50% KSR 50% NNB	25% KSR 75% NNB
Growth factors	LDN 100 nM SB 10 µM SHH 100 ng/mL Puromoph 2 µM FGF8 100 ng/mL	LDN 100 nM SB 10 µM SHH 100 ng/mL Puromoph 2 µM FGF8 100 ng/mL CHIR 3 µM	LDN 100 nM SHH 100 ng/mL Puromoph 2 µM FGF8 100 ng/mL CHIR 3 µM	LDN 100 nM CHIR 3 µM	LDN 100 nM CHIR 3 µM

2.1.2.2.2 NPC expansion and single cell passaging

After Day10 NPCs were expanded for 7 to 23 days to improve final differentiation efficiency. During this time cells were maintained in Day9-10 media (above) alternating daily between half and full feeds. On Day10+1 NPCs were single cells passaged in a ratio of 1:2. 6-well plates were coated overnight with Geltrex, and NPCs were dissociated with room temperature Accutase, as described in 2.1.2.1.4 and centrifuged for 5 minutes at 350 xg in spin falcons containing neurobasal. Cell pellets were resuspended in Day9-10 media supplemented with 10 µM ROCKi. The following day a full feed was performed to remove remaining ROCKi. The same passaging procedure was carried out approximately every 7 days during the expansion.

2.1.2.2.3 Cryopreservation of NPCs

It was possible to bank NPCs for future experiments directly after any of the expansion splits. For cryopreservation cell pellets were resuspended in freezing media (90% Day9-10 media, 10% DMSO) using 1 mL of freezing media per confluent well of a 6-well plate that had been dissociated. The cell suspension was aliquoted into pre-labelled cryovials, 1 mL per vial. Vials were moved to -80°C freezers as described in 2.1.2.1.5.

2.1.2.2.4 Neuronal maturation to Day20

2 days after the final expansion split (approximately Day10+8, Day10+15 or Day10+22) NPCs were guided towards dopaminergic fate by switching to maturation media (NB base media supplemented with BDNF, 20 ng/mL; GDNF, 20 ng/mL; TGFβ3, 1 ng/mL; DAPT, 10 µM; Ascorbic Acid, 200 µM and db-cAMP 500 µM) – Fig. 2.1A. The first day in maturation media is referred to as Day11. On Day11 and Day12 maturation media was further supplemented with 3 µM CHIR. Between Day11 and Day20 cells were fed daily alternating between half and full feeds. Neuronal processes became visible with light microscopy from Day13.

2.1.2.2.5 Final neuronal replating

Neurons were replated from 6-well plates into their final assay format on Day20. In advance of this, plates were coated on Day18 with poly-L-ornithine in borate buffer (PLO-borate: 0.01% PLO, 100 mM boric acid, 25 mM sodium tetraborate, 72 mM NaCl pH8.4) and incubated overnight at 37°C. PLO-borate was aspirated on Day19 plates were washed 3 times with PBS and then coated with 10 µg/mL biolaminin (96-well plates and microfluidic devices) or Geltrex (24-well, 12-well and 6-well plates), see Table 2.1.2.2C. On Day20 cells were dissociated with Accutase as described in 2.1.2.1.4, processing a maximum of 3 cell lines at one time. Dissociated cells were resuspended in spin falcons containing neurobasal medium and centrifuged for 5 minutes at 350 xg. Neurobasal was aspirated and cell pellets were resuspended in maturation media supplemented with 10 µM ROCKi and 1% antibiotic-antimycotic. Cells were counted as described in 2.1.1.2 and plated at the densities described in Table 2.1.2.2C after aspirating the coating medium. Plates were left for five minutes at room temperature in the tissue culture hood for cells to settle before returning to the incubator.

For cells plated in microfluidic devices, the devices were washed in Trypsin-EDTA followed by ethanol and then dried overnight on Day-3 before mounting on 13 mm glass coverslips and coating with PLO-borate and biolaminin. Cells were plated in an initial volume of 70 µL in the somatic chambers and 50 µL in the axonal chamber and incubated at an angle for 2 hours to encourage cells to attach near the microgroove array. Devices were then returned to a horizontal plane and chamber filled to their final full-feed volume. The axonal chamber was supplemented with BDNF (200 ng/mL) and Laminin (200 ng/mL) which was maintained for approximately 10 days until axons had traversed the microgroove array.

Table 2.1.2.2C Neuron Plating Densities, Plate-coating and Feeding Volumes

Plate type	Cells per Well	Coating volume (µL)	Full-feed volume (µL)
Half-area 96-well	30,000	30	50
Full-area 96-well	120,000	60	100
24-well	625,000	300	500
12-well	1,125,000	500	1000
6-well	2,850,000	1000	3000
Microfluidic device (soma chamber)	70,000	80	200
Microfluidic device (axon chamber)	-	60	150

2.1.2.2.6 Lentiviral transduction of Kriks dopaminergic neurons

Cells to be transduced with lentivirus were replated on Day16 rather than Day20 but following the same procedure as described in 2.1.2.2.5. All lentiviral transduction was done in full-area 96-well plates. Lentivirus aliquots were thawed on ice and diluted to 2x final concentration in maturation media supplemented with 10 µM ROCKi and 1% antibiotic-antimycotic in a separate source plate and kept on ice in the tissue culture hood. Two hours after replating 50 µL of media was removed from every well of the cell

plate and replaced with 50 µL of diluted virus from the source plate using a multichannel pipette. From Day16 onwards all consumables used in the feeding and harvesting of transduced cells were considered as lentiviral waste and were decontaminated in 10% Chemgene for 24-hours before disposal.

2.1.2.2.7 Post-replating neuronal maturation

Neurons were visually inspected but not fed on Day21. On Day22 they were treated with mitomycin C to remove dividing cells. Maturation media was aspirated and replaced with warmed NB base media containing 1 µg/mL mitomycin C and protected from light. Plates were returned to the 37°C incubator for 1 hour and then mitomycin C was removed and cells were washed gently with neurobasal. Neurobasal was aspirated and cells received a full feed with maturation media supplemented with 1% antibiotic-antimycotic. After Day22 cells were half-fed every second day until Day30 and then half-fed every third day from Day30 until harvesting (between Day35 and Day100). Cells for α-synuclein release experiments received a full media change on their final feed and then were maintained in the same media for 2-4 days prior to media harvest. For CN-PAGE, RT-QuIC, Mass photometry and SiMPull experiments the final media was made with NG rather than NB as a base and BDNF, GDNF, TGFβ and DAPT were excluded.

2.1.2.3 Dopaminergic differentiation - modified from Sheta et al (2023)

The protocol presented here represents the result of several modifications to the published protocol to improve compatibility with the dCas9 i3 neurons, CRISPRi and α-synuclein release assays. Dr Razan Sheta (Université Laval) provided remote advice and guidance which streamlined this optimisation process.

2.1.2.3.1 Neuronal Induction

On Day-2 6-well plates were coated with Geltrex diluted in cold knockout DMEM and incubated overnight at 37°C. dCas9 i3 iPSCs were single cell passaged on Day-1 replating at a density of 1 million cells per well in 3 mL mTeSR+ with ROCKi. On Day0 mTeSR+ was replaced with 4 mL DMEM induction media (iDM) supplemented with BDNF (10 ng/mL), GDNF (10 ng/mL), Laminin (1 µg/mL) and Doxycycline (2 µg/mL) – Fig. 2.1B. Cells were washed 4 times with DPBS on Day 1 and then received another full feed with the same media.

2.1.2.3.2 Final replating of NGN2 dopaminergic neurons

Neuronal progenitors were replated from 6-well plates into their final assay format on Day2. In advance of this, plates were coated overnight at 37°C on Day0 with PLO-borate then with 10µg /mL Laminin overnight at 4°C on Day 1. On Day2 cells were dissociated with Accutase as described in 2.1.2.1.4 and resuspended in spin falcons containing DMEM/F12 with 1% antibiotic-antimycotic. Following centrifugation for 5 minutes at 350 xg DMEM/F12 was aspirated and cell pellets were resuspended in Neurobasal induction media (iNM) supplemented with BDNF (10 ng/mL), GDNF (10 ng/mL), Laminin (1µg/mL), Doxycycline (2 µg/mL), Cytosine β-D-arabinofuranoside, AraC (1 µM) and ROCKi (10 µM). Cells were plated at a density of 100,000 cells per well of full-area 96-well plates for α-synuclein release assays, 25,000 cells per well of half-area 96-well plates for immunocytochemistry and 1 million cells per well of 12-well plates for western blot. Following replating neurons were more prone to pealing than those grown using the Kirks et al. protocol and were fed with an automated multichannel pipette on the lowest speed to reduce shear forces contributing to detachment.

Table 2.1.2.3 NGN2 Protocol base media composition

Base Media Name	Composition	Concentration % (v/v)
iDM	DMEM/F12	96
	B-27 Supplement with Vit A	2
	N2 Supplement	1
	MEM non-essential amino acids	1
iNM	Neurobasal Medium	95
	B-27 Supplement with Vit A	2
	N2 Supplement	1
	MEM non-essential amino acids	1
	L-Glutamine	1

2.1.2.3.3 Neuronal Differentiation

On Day3 cells were washed once with DPBS and then fed with differentiation media (STEMdiff Midbrain Neuron Differentiation Media with doxycycline and 200 ng/mL SHH) supplemented with AraC Between Day4 to Day8 the same differentiation media was used without AraC supplementation (Fig. 2.1B).

2.1.2.3.4 Lentiviral transduction of *NGN2* dopaminergic neurons

dCas9 i3 neurons were transduced with lentivirus on Day7. Differentiation media was aspirated and replaced with 50 µL per well, lentiviruses were diluted to 2x final concentration as described in 2.1.2.2.6 and added to cells with an automated multichannel pipette from the source plate.

2.1.2.3.5 Neuronal Maturation

From Day9 neurons were fed with STEMdiff Midbrain Neuron Maturation Media. After the first full feed cells received a half feed every 3 days until Day20 after which they received full feeds every 4 days for media collection as shown in Fig. 5.8A.

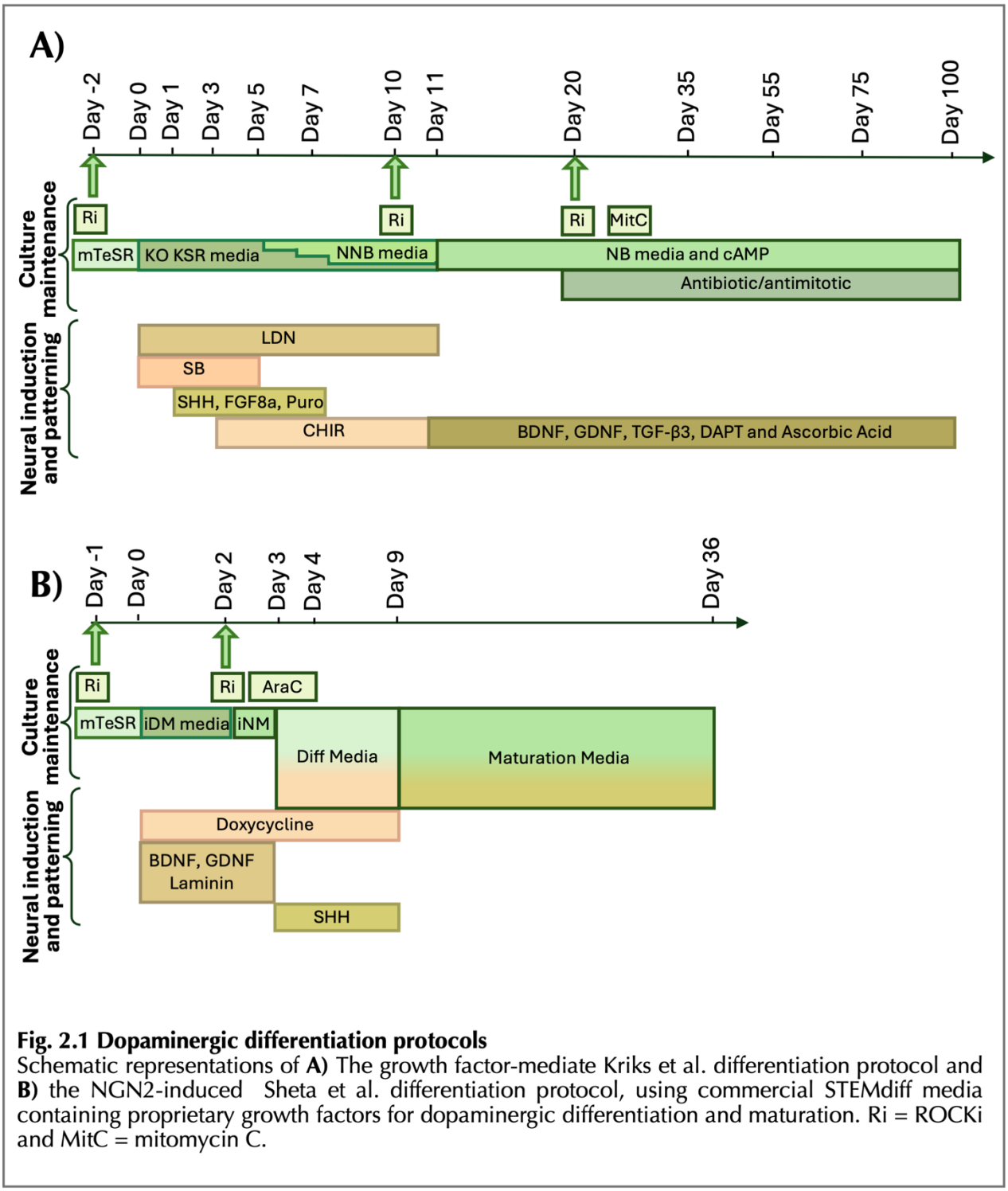

Fig. 2.1 Dopaminergic differentiation protocols
Schematic representations of **A)** The growth factor-mediate Kriks et al. differentiation protocol and **B)** the NGN2-induced Sheta et al. differentiation protocol, using commercial STEMdiff media containing proprietary growth factors for dopaminergic differentiation and maturation. Ri = ROCKi and MitC = mitomycin C.

2.1.3 SH-SY5Y Cell Culture

2.1.3.1 SH-SY5Y culture maintenance

dCas9-BFP-KRAB undifferentiated SH-SY5Y cells (Carling *et al.*, 2022) were maintained in T75 flasks in DMEM/F12 supplemented with 10% FBS, 100 Units/mL Penicillin-streptomycin and 1% L-glutamine. Cells were passaged using Typsin-EDTA when they reached 90% confluency, to a maximum of 20 passages.

2.1.3.2 SH-SY5Y lentiviral transduction

Following dissociation with Trypsin-EDTA cells were plated at a density of 10,000 cells per well of a full-area 96-well plate. The next day 50% of the media was removed and replaced with media containing 2x final concentration of sgRNA lentivirus. Media containing lentivirus was removed after 24 hours and decontaminated in 10% Chemgene. Cells were maintained in fresh media for a further 24 hours before imaging.

2.1.4 HEK Cell Culture

Lenti-X HEK293T cells were maintained in T175 flasks in high glucose DMEM supplemented with 10% FBS and 100 Units/mL Penicillin-streptomycin. Cells were passaged using Trypsin-EDTA when they reached 70% confluency, to a maximum of 15 passages.

2.2 sgRNA cloning and lentivirus production

2.2.1 General

Table 2.2.1 Materials and Reagents for lentivirus library preparation

Reagent	Supplier	Catalogue Number
Ampicillin	Merck	A0166
Carbenicillin	Gibco	10177012
LB Agar, powder	Invitrogen	22700025
LB broth, powder	Invitrogen	12780052
Lenti-X Concentrator	Takara Bio	631232
Lipofectamine 3000	Invitrogen	L3000015
Mighty Mix DNA Ligation Kit	Takara Bio	6023
Mix & Go E. coli Transformation Kit	ZymoResearch	T3002
OptiMEM	Gibco	31985062
QIAprep Spin MiniPrep kits	Qiagen	27106
Stbl3 Chemically Competent *E. coli*	Invitrogen	C737303
ViralBoost	Alstem	VB100
Zymobroth	ZymoResearch	M3015

All sgRNA lentiviruses were packaged specifically for this study. Plasmid DNA for guides *SNCA_1, SNCA_2, NT_1* and *NT_2* were kind gifts from Dr Rachel Heon Roberts and Dr Gizem Onal in the Ryan and Wade-Martins Groups respectively.

2.2.2 Plasmid Preparation

2.2.2.1 Generation of sgRNA inserts for cloning

Horlbeck et al. (2016) published a list of sgRNAs against the whole transcriptome, with high predicted knock down efficiencies. Using this tool, 2 sgRNA sequences were selected per target gene, as well as two non-targeting controls, and the corresponding oligonucleotide sequences ordered (Table 2.2.2). Complementary oligonucleotide strands were diluted to 100 µM in annealing buffer (100 mM potassium acetate, 30 mM HEPES, 2 mM magnesium acetate) and heated to 95°C for 5 minutes. Oligonucleotides annealed generating sticky ends for ligation into the plasmid backbone while cooling to room temperature for 20 minutes.

Table 2.2.2 sgRNA Insert sequences 5′ to 3′

sgRNA	Strand 1	Strand 2
ATG5_1	TTAGCTCTTAAACCTCCTTCCTACCACACCTACCAACAAG	TTGGTAGGTGTGGTAGGAAGGAGGTTTAAGAGC
ATG5_2	TTAGCTCTTAAACGACACACTGTCCTGCGGGGCCAACAAG	TTGGCCCCGCAGGACAGTGTGTCGTTTAAGAGC
DNAJC5_1	TTAGCTCTTAAACGTGCCGCACCCGCGCCCTCCCAACAAG	TTGGGAGGGCGCGGGTGCGGCACGTTTAAGAGC
DNAJC5_2	TTAGCTCTTAAACACGTCAGGCCCGGGCAGGCCCAACAAG	TTGGGCCTGCCCGGGCCTGACGTGTTTAAGAGC
GBA1_2	TTAGCTCTTAAACTCAGAGTCTTACTGCGCGGCCAACAAG	TTGGCCGCGCAGTAAGACTCTGAGTTTAAGAGC
GBA1_2	TTAGCTCTTAAACGCCTTAGCTATAGGCACTACCAACAAG	TTGGTAGTGCCTATAGCTAAGGCGTTTAAGAGC
HSPA8_1	TTAGCTCTTAAACGTCTCATTGAACTCGCCTGCCAACAAG	TTGGCAGGCGAGTTCAATGAGACGTTTAAGAGC
HSPA8_2	TTAGCTCTTAAACTCGTTATTGGAGCCAGGCCCCAACAAG	TTGGGGCCTGGCTCCAATAACGAGTTTAAGAGC
HSPA8_3	TTAGCTCTTAAACTGGTTCTTCAGAGCTGTTCCCAACAAG	TTGGGAACAGCTCTGAAGAACCAGTTTAAGAGC
MICAL1_1	TTAGCTCTTAAACTCGTCCGGGCCACCCGCAGCCAACAAG	TTGGCTGCGGGTGGCCCGGACGAGTTTAAGAGC
MICAL1_2	TTAGCTCTTAAACTCATGAGATTCCGTCTGCCCCAACAAG	TTGGGGCAGACGGAATCTCATGAGTTTAAGAGC
RAB11A_1	TTAGCTCTTAAACTTTCGCTCCTCGGCCGCGCCCAACAAG	TTGGGCGCGGCCGAGGAGCGAAAGTTTAAGAGC
RAB11A_2	TTAGCTCTTAAACCAGATACCACTGCTGCTCCCCAACAAG	TTGGGGAGCAGCAGTGGTATCTGGTTTAAGAGC
RAB13_1	TTAGCTCTTAAACACCAGTGCCGGGCGCTCCCCCAACAAG	TTGGGGGAGCGCCCGGCACTGGTGTTTAAGAGC
RAB13_2	TTAGCTCTTAAACTCCAGTCCCGCCTACCAGTCCAACAAG	TTGGACTGGTAGGCGGGACTGGAGTTTAAGAGC
RAB27A_1	TTAGCTCTTAAACGTCCCCGCCTGGCTCGGGTCCAACAAG	TTGGACCCGAGCCAGGCGGGGACGTTTAAGAGC
RAB27A_2	TTAGCTCTTAAACCCCGGTTCATTCCTCCCTCCCAACAAG	TTGGGAGGGAGGAATGAACCGGGGTTTAAGAGC
RAB27B_1	TTAGCTCTTAAACACCTGTGGCTCCGGATGGGCCAACAAG	TTGGCCCATCCGGAGCCACAGGTGTTTAAGAGC
RAB27B_2	TTAGCTCTTAAACCTCGCAGTCCTGACGGGCACCAACAAG	TTGGTGCCCGTCAGGACTGCGAGGTTTAAGAGC
RAB35_1	TTAGCTCTTAAACCCATGGCCCGGGACTACGACCAACAAG	TTGGTCGTAGTCCCGGGCCATGGGTTTAAGAGC
RAB35_2	TTAGCTCTTAAACAGGGGAGGTTGGGGCGCGGCCAACAAG	TTGGCCGCGCCCCAACCTCCCCTGTTTAAGAGC
RAB5A_1	TTAGCTCTTAAACCTGTCGGGCTCCGTCTCCGCCAACAAG	TTGGCGGAGACGGAGCCCGACAGGTTTAAGAGC
RAB5A_2	TTAGCTCTTAAACCCGGAGCCACTTCCGCTGCCCAACAAG	TTGGGCAGCGGAAGTGGCTCCGGGTTTAAGAGC
RAB7A_1	TTAGCTCTTAAACCGGTAAGCAGCGGGCCCAGCCAACAAG	TTGGCTGGGCCCGCTGCTTACCGGTTTAAGAGC
RAB7A_2	TTAGCTCTTAAACCCGCCTCAGGCTTTATGGCCCAACAAG	TTGGGCCATAAAGCCTGAGGCGGGTTTAAGAGC
RAB8A_1	TTAGCTCTTAAACACCCTCAGCCCGCTCGTTACCAACAAG	TTGGTAACGAGCGGGCTGAGGGTGTTTAAGAGC
RAB8A_2	TTAGCTCTTAAACACGATTACCTGTTCAAGCTCCAACAAG	TTGGAGCTTGAACAGGTAATCGTGTTTAAGAGC
RAB9A_1	TTAGCTCTTAAACCGGTAGCGCAGCCAGGCTCCCAACAAG	TTGGGAGCCTGGCTGCGCTACCGGTTTAAGAGC
RAB9A_2	TTAGCTCTTAAACTGTTGTTCCCTCCGCGCTGCCAACAAG	TTGGCAGCGCGGAGGGAACAACAGTTTAAGAGC
SCAMP5_1	TTAGCTCTTAAACCGGAGCGGCTCGCGGCCGGCCAACAAG	TTGGCCGGCCGCGAGCCGCTCCGGTTTAAGAGC
SCAMP5_2	TTAGCTCTTAAACCATCGCTCGGGTGCAGCGCCCAACAAG	TTGGGCGCTGCACCCGAGCGATGGTTTAAGAGC
SNAP23_1	TTAGCTCTTAAACCCGGAGAGGAGTGGCCTCGCCAACAAG	TTGGCGAGGCCACTCCTCTCCGGGTTTAAGAGC
SNAP23_2	TTAGCTCTTAAACGACCTGGCGCTGCACCCTACCAACAAG	TTGGTAGGGTGCAGCGCCAGGTCGTTTAAGAGC
SNAP29_1	TTAGCTCTTAAACTAGTGACTCGATGGTGGTACCAACAAG	TTGGTACCACCATCGAGTCACTAGTTTAAGAGC
SNAP29_2	TTAGCTCTTAAACAGACCGAGAGCCGCGCCGGCCAACAAG	TTGGCCGGCGCGGCTCTCGGTCTGTTTAAGAGC
STX17_1	TTAGCTCTTAAACAAGTGCGAGCGCCATGGTGCCAACAAG	TTGGCACCATGGCGCTCGCACTTGTTTAAGAGC
STX17_2	TTAGCTCTTAAACTTACCTCCCGCCGGGGCGCCCAACAAG	TTGGGCGCCCCGGCGGGAGGTAAGTTTAAGAGC
STX1A_1	TTAGCTCTTAAACAGGAGCTCCGCACGGTGAGCCAACAAG	TTGGCTCACCGTGCGGAGCTCCTGTTTAAGAGC
STX1A_2	TTAGCTCTTAAACCTGCCACTCCCGGGAGCATCCAACAAG	TTGGATGCTCCCGGGAGTGGCAGGTTTAAGAGC
STX3_1	TTAGCTCTTAAACCGGACGCTCCTCCTAGCTACCAACAAG	TTGGTAGCTAGGAGGAGCGTCCGGTTTAAGAGC
STX3_2	TTAGCTCTTAAACCTCCTTCCTACCACACCTACCAACAAG	TTGGGGAGGAGCGTCCGAGGCCAGTTTAAGAGC
STX4_1	TTAGCTCTTAAACCCCACTGCCTCGAAAGGCCCCAACAAG	TTGGGGCCTTTCGAGGCAGTGGGGTTTAAGAGC
STX4_2	TTAGCTCTTAAACCTCCCTATCCCGAAGACCACCAACAAG	TTGGTGGTCTTCGGGATAGGGAGGTTTAAGAGC
STX5_1	TTAGCTCTTAAACCCGAAACCCGACCAAAGACCCAACAAG	TTGGGTCTTTGGTCGGGTTTCGGGTTTAAGAGC
STX5_2	TTAGCTCTTAAACTCACTGGCCCTCCCGGAGGCCAACAAG	TTGGCCTCCGGGAGGGCCAGTGAGTTTAAGAGC
SYT1_1	TTAGCTCTTAAACCTGCTAACTGCTGCTGCCGCCAACAAG	TTGGCGGCAGCAGCAGTTAGCAGGTTTAAGAGC
SYT1_2	TTAGCTCTTAAACTAGGTCTCAGACTCCCACCCCAACAAG	TTGGGGTGGGAGTCTGAGACCTAGTTTAAGAGC
SYT7_1	TTAGCTCTTAAACCTCGATCCCGCGCCCCCGGCCAACAAG	TTGGCCGGGGGCGCGGGATCGAGGTTTAAGAGC
SYT7_2	TTAGCTCTTAAACCCGAACAGCGCCGAGCCGCCCAACAAG	TTGGGCGGCTCGGCGCTGTTCGGGTTTAAGAGC
SYTL5_1	TTAGCTCTTAAACTTGTGAACTACTTGGAGCACCAACAAG	TTGGTGCTCCAAGTAGTTCACAAGTTTAAGAGC
SYTL5_2	TTAGCTCTTAAACCTCATATTCCCACAATCTACCAACAAG	TTGGTAGATTGTGGGAATATGAGGTTTAAGAGC
UBE2I_1	TTAGCTCTTAAACTTTGTCTCGGGACTTCCCTCCAACAAG	TTGGAGGGAAGTCCCGAGACAAAGTTTAAGAGC
UBE2I_2	TTAGCTCTTAAACCTCGGTCCTCCACCTGTCCCCAACAAG	TTGGGGACAGGTGGAGGACCGAGGTTTAAGAGC
USP19_1	TTAGCTCTTAAACTGAACAGGCCGCCGCGGCCCCAACAAG	TTGGGGCCGCGGCGGCCTGTTCAGTTTAAGAGC
USP19_2	TTAGCTCTTAAACGAACGGAGAGCGGGTTGCCCCAACAAG	TTGGGGCAACCCGCTCTCCGTTCGTTTAAGAGC
USP19_3	TTAGCTCTTAAACTTCCGGTTCCGGCGCAGGTCCAACAAG	TTGGACCTGCGCCGGAACCGGAAGTTTAAGAGC
VAMP3_1	TTAGCTCTTAAACTCTCTCGTCGCCGCTGCCGCCAACAAG	TTGGCGGCAGCGGCGACGAGAGAGTTTAAGAGC
VAMP3_2	TTAGCTCTTAAACCCGGTCCCAACTTCGCTTCCCAACAAG	TTGGGAAGCGAAGTTGGGACCGGGTTTAAGAGC
VAMP7_1	TTAGCTCTTAAACCTGGGAGCGGGCAGTTGGCCCAACAAG	TTGGGCCAACTGCCCGCTCCCAGGTTTAAGAGC
VAMP7_2	TTAGCTCTTAAACTGCACTGACCCGCGTCCCTCCAACAAG	TTGGAGGGACGCGGGTCAGTGCAGTTTAAGAGC
VSP35_1	TTAGCTCTTAAACTGGCGACTCCCCAGAGCCTCCAACAAG	TTGGAGGCTCTGGGGAGTCGCCAGTTTAAGAGC
VSP35_2	TTAGCTCTTAAACCAGAGCCTGCAGCAAGCAGCCAACAAG	TTGGCTGCTTGCTGCAGGCTCTGGTTTAAGAGC
VTI1B_1	TTAGCTCTTAAACTAGGGGGCGTGTCTGAGGACCAACAAG	TTGGTCCTCAGACACGCCCCCTAGTTTAAGAGC
VTI1B_2	TTAGCTCTTAAACCGGGATTCAGTTCCCTGGGCCAACAAG	TTGGCCCAGGGAACTGAATCCCGGTTTAAGAGC
WDR44_1	TTAGCTCTTAAACTTACTGCGAGGAGCCACCGCCAACAAG	TTGGCGGTGGCTCCTCGCAGTAAGTTTAAGAGC
WDR44_2	TTAGCTCTTAAACCTGAAGATGTGCACCTAGGCCAACAAG	TTGGCCTAGGTGCACATCTTCAGGTTTAAGAGC

2.2.2.2 Ligation of sgRNA inserts into H25-U9-sgRNA-NucBlue backbone

The H25-U9-sgRNA-NucBlue backbone (Fig. 5.2A) was linearised via restriction enzyme digest with BlpI and BstXI by Dr Sandor Szunyogh, and annealed oligos (2.2.1.1) were ligated into the backbone using the Might Mix DNA Ligation Kit. Ligation was carried out at 16°C for 30 minutes using 20 ng of H25-U9-sgRNA-NucBlue and 0.5 µL of annealed insert per reaction in a final reaction volume of 5 µL.

2.2.2.3 Bacterial Culture

Stbl3 *E. coli* was used for DNA preparation. *E. coli* were cultured either in solution in lysogeny broth (LB), prepared by dissolving 25 g of LB in 1 L of distilled water, or on LB agar plates, prepared by dissolving 37 g LB agar in distilled water. Both LB broth and LB agar were autoclaved before use.

2.2.2.4 Preparation of chemically competent Stbl3 *E. coli*

The Mix & Go Kit was used to generate competent bacteria for DNA uptake. Stbl3 *E. coli* were streaked on LB agar plates and incubated for 8 hours at 37°C. A single colony was picked and inoculated into 5 mL of LB broth which was grown overnight in a shaking incubator. The following day, 500 µL of the turbid culture was used to inoculate 50 mL of ZymoBroth and cultured in the shaking incubator until the optical density at 600 nm reached 0.5. The culture was then incubated on ice for 10 minutes followed by centrifugation at 2,500 xg for 10 minutes at 4°C. The supernatant was discarded and the bacterial pellet resuspended in Mix & Go Wash Buffer, and once again pelleted by centrifugation. This second pellet was suspended in 5 mL of Mix & Go Competent Buffer and rapidly divided into 25 µL aliquots that were stored at -80°C until use.

2.2.2.5 Transformation of chemically competent bacteria

1 µL of ligated plasmid (2.2.2.2) was mixed with a 25 µL aliquot of competent Stbl3 *E. Coli* and incubated on ice for 5 minutes. Bacteria were streaked onto LB agar containing 100 µg/mL carbenicillin and incubated for 16 hours at 37°C.

2.2.2.6 DNA preparation

Three small to medium sized colonies (2.2.2.5) were picked per sgRNA guide and inoculated into 6 mL of LB broth supplemented with 100 µg/mL ampicillin. Bacteria were cultured overnight in the shaking incubator. The next day turbid cultures were centrifuged for 10 minutes at 3,000 xg and supernatants discarded. Bacterial pellets were lysed and DNA extracted and purified using QIAprep Spin MiniPrep kits according to the manufacturer's instructions. Ligation efficiency and sgRNA sequence integrity were verified by sequencing, performed by Eurofins Genomics.

2.2.3 Lentiviral Packaging

2.2.3.1 HEK Transfection

H25-U9-sgRNA-NucBlue plasmids containing target-specific inserts were packaged into lentiviruses for delivery to cells using three packaging vectors: psPAX2 (packaging plasmid) pMD2G (envelope plasmids) and pAdvantage (translation enhancer plasmid). 10 cm dishes were coated with PLO-Borate overnight and then air dried for 2-3 hours. Lenti-X HEK293T (2.1.4) were dissociated with Trypsin-EDTA and plated at a density of 15 million cells per dish in 18 mL of media. After 24 hours HEK cells were transfected with the four plasmids using Lipofectamine 3000 according to the manufacturer's instructions. The following day the media was replaced and supplemented with 1:500 dilution of ViralBoost. Viral waste was decontaminated in 10% Chemgene.

2.2.3.3 Virus concentration

Three days after ViralBoost addition all media was harvested and centrifuged for 10 minutes at 500 xg to pellet cell debris. The supernatant was mixed with 6 mL of Lenti-X Concentrator and incubated at 4°C for a further 3 days. Once a white precipitate had formed samples were centrifuged for 45 minutes at 1,500 xg at 4°C and the supernatants discarded. The virus pellet was resuspended in PBS and divided between 20 µL aliquots which were stored at -80°C until use.

2.3 RNA Analysis

2.3.1 General

Table 2.3.1 Materials and Reagents for RNA extraction and analysis

Reagent	Supplier	Catalogue Number
10x Tris-Borate-EDTA buffer	Merck	T4415
Agani Needle 25G x 5/8 Inches	VWR Internation Ltd	613-5379
Direct-Zol 96	ZymoResearch	R2055
Quick-Load 100bp DNA Ladder	BioLabs	N0467S
Fast SYBR Green Master Mix	Gibco	4385618
GoTaq Hot Start Polymerase	Promega	M5001
Oligo dT primers	Invitrogen	18418020
RNaseZAP	Invitrogen	AM9780
RNeasy Mini kit	QIAGEN	74106
SuperScript III	Invitrogen	18080044
SYBR™ Safe DNA Gel Stain	Gibco	S33102
Terumo Disposable Syringe 1 mL	Appleton Woods Ltd	GS572

RNA work was carried out at 4°C on ice, cleaning equipment with RNaseZAP before use. RNA concentrations were determined by absorbance at 260 nm measured using DeNovix DS-11 UV-Vis Spectrophotometer.

2.3.2 RNA extraction

2.3.2.1 RNeasy Mini kit

Cells were resuspended in RLT buffer and homogenised with passage through 25G needle connected to a 1 mL syringe for 3 minutes. RNA extraction was carried out using spin columns according to the manufacturer's instructions. RNA was eluted using RNase-free water preheated to 65°C.

2.3.2.2 Direct-Zol 96

Cells were resuspended in TRIzol by vigorous pipetting. Four wells of a 96-well plate were pooled and applied to a single well of the spin plate. RNA extraction was carried out according to the manufacturer's instructions. RNA was eluted using room temperature RNase-free water.

2.3.3 Reverse transcription

cDNA was synthesised using SuperScript III reverse transcriptase according to the manufacturere's instructions with oligo dT primers. 100-500 ng of RNA was used per reaction in a total reaction volume of 30 µL.

2.3.4 PCR and agarose gel electrophoresis

cDNA for the whole *SNCA* transcript was amplified using the GoTaq Hot Start PCR kit according to the manufacturer's instructions. Using the NCBI primer BLAST tool, forward and reverse primers were designed against the most common 5'UTR (exon 2a) and the most common 3'UTR (exon 7) found in human brain:

Forward primer: GGCCATTCGACGACAGTGTG

Reverse primer: GCTCCCAGTTTCTTGAGATCTGC

Agarose gels (1.4% w/v) were prepared by dissolving powdered agarose in 1x Tris-Borate-EDTA (TBE) buffer using intermittent microwave heating. 10 µL of SYBR safe DNA stain was added to the gel for visualisation and the gel was cast and allowed to cool. The gel was submerged in TBE buffer and the comb removed. The entire PCR reaction mixture was loaded and run at 120 V for 30-40 minutes alongside a 100 bp DNA ladder. Gels were imaged using a Chemidoc with the SYBR safe filter.

2.3.5 qPCR

qPCR was carried out in 384-well plate format using the Fast SYBR green qPCR mix with 40 amplification cycles (denaturation at 95°C for 15 seconds, annealing at 60°C for 25 seconds, and extension at 72°C for 20 seconds). Primers (Table 2.3.5) were designed with the NCBI primer BLAST tool and assessed for specific amplification by melt-curve analysis. Gene expression was calculated using the $\Delta\Delta C_T$ method relative to three housekeeping genes and expressed relative to gene expression in cells treated with non-targeting sgRNA lentivirus. Housekeeping genes*, CYC1, UBE2D2* and *RPL13,* were selected based on reported stable expression between disease states in human brain (Rydbirk *et al.,* 2016) and gave C_T of 20-24, 23.5-27.5 and 19.5-24 respectively.

Table 2.3.5 Primers used for qPCR

Target	Forward Primer	Reverse Primer
SNCA	ATGTTGGAGGAGCAGTGGTG	AATTCCTTCCTGTGGGGCTC
UBE2D2	AGCCTACAAGAAAGTTTGCCTAT	TCGCATACTTCTGAGTCCATTCC
CYC1	AGCCTACAAGAAAGTTTGCCTAT	AGCCTACAAGAAAGTTTGCCTAT
RPL13	CCTGGAGGAGAAGAGGAAAGAGA	TTGAGGACCTCTGTGTATTTGTCAA
DNAJC5	GGGAAGTGTAAGCCCAAGG	TGTCTGTGGCCTCCCTCTC
SYT1	GCTGAGAAGGAAGAGCAAGAG	CGGATAAGCCACCCACATCC
SYT7	CGAGATGCTCATGCTCTCC	TGTAGCCGACACTGAACTGG
USP19	CGGGAATGACCCAGTCTCTC	ACTCGGGCTCATCCACCAAG
HSPA8	ACCACCATTCCTACCAAGCAG	CGCTCGCCTTCATAAACCTG
ATG5	TCACAAGCAACTCTGGATGGG	AAGGTCTTTCAGTCGTTGTCTG
GBA1	ACTTTGTGAAGTTCCTGGATGC	CACTCAACAGCCCAGCAGAAG
RAB5A	AATTGGGTTAAAGAACTTCAGAGG	TGCATAGGACTGTGCTTCCTG
RAB7A	TTAAGCAGGAAACGGAGGTGGAG	CTTGGCCCGGTCATTCTTGTC
RAB8A	CGGTTTCGGACGATCACAACG	GCAGAGGCGTGCTCCTCAATG
RAB9A	TAAGCGAACGGCAGGTGTCTAC	AACCGCTTCAAAGGCTGCT
RAB11A	AGCACCATTGGAGTAGAGTTTGC	AAGGCACCTACAGCTCCACGA
SNAP23	ACGAGGAGAATCCTGGGTTTAGC	TCTTCTATGCGGTTTAGTTGTTCC
SNAP29	GCCAGCCACCCAAACCTTAG	TGGACAGCTCATCTAGGTTGC
SYTL5	AACCCAAGGTGGAGTTTGCTC	GTTGTTCTGGTGGAAGCATCAGG
VAMP7	GGCCTAGACAAAGTGATGGAGAC	AGCTACCAGATCTATGTTTCTGACC
STX5	AGGATTTCGTGAGAGCCAAGGG	GAAGCCAGTTTCGACTGCAAGG
VTI1B	GGACCTTGCTAAACTCCATCGG	TGCCCTTTGAGACTGTAGCCGA

2.3.6 RNA sequencing

Bulk RNA-sequencing (RNAseq) experiments and raw data processing were carried out by Dr Benjamin Vallin.

2.3.6.1 Bulk RNA Sequencing (*SNCA*-triplication and Control iPSC-DaNs)

RNA was purified using the RNeasy Mini Kit and RNA integrity numbers (RINs) were measured on a Bioanalyzer (Agilent Technologies), ranging between 8.6 and 9.0 for all samples. cDNA library preparation and bulk RNA-seq were conducted by Novogene Company Limited: cDNA libraries were constructed using a dUTP protocol with polyA enrichment and sequenced on an Illumina NovaSeq 6000 instrument (PE 150, ≥ 20 million read pair/sample).

2.3.6.2 Preprocessing of raw sequencing data

SNCA-triplication and control iPSC-DaNs: raw sequencing reads were quality checked with FastQC/MultiQC and adaptor trimming was performed with Trim Galore (non-default arguments: --stringency 3, --trim-n). Reads were aligned onto a decoy-aware human reference transcriptome (GRCh38.p14 - GENCODE Release 44) with Salmon using an index built with k-mers of length 31 (optional arguments: --gcBias, --seqBias).

Healthy, prodromal and sporadic/familial PD iPSC-DaNs: data were produced by the Foundational Data Initiative for Parkinson's Disease (FOUNDIN-PD) study and obtained on 2024-09-16 from the Parkinson's Progression Markers Initiative (PPMI) database (www.ppmi-info.org/access-data-specimens/download-data), RRID:SCR_006431.

Sequencing reads were aligned onto a custom human reference transcriptome (GRCh38.p12 - GENCODE Release 29 combined with LNCipedia version 5.2) with

Salmon and shared by the PPMI *via* an Aspera transfer platform. Analyses were performed on a subset of the original dataset which included, for each combination of iPSC donor and timepoint, the RNA-seq sample with the smallest batch and version indices. This resulted in a total of 94, 93 and 91 RNA-seq samples from distinct iPSC donors at Day0, 25 and 65, respectively. For up-to-date information on the PPMI study, visit www.ppmi-info.org. PPMI – a public-private partnership – is funded by the Michael J. Fox Foundation for Parkinson's Research, and funding partners (full list available at www.ppmi-info.org/about-ppmi/who-we-are/study-sponsors).

2.3.6.3 RNA-seq analyses

Transcript-level quantification data was loaded and optionally summarized to gene-level with the R package tximport. Abundance estimates, transcripts per million (TPM), were used to compute $\log_2$(TPM+1) expression values. The relative proportion of transcripts encoding each α-synuclein isoform were computed using the R package rnaseqtools. Differential gene expression analyses were conducted on gene-level raw counts with the R package DESeq2. The effect of explanatory variables on gene expression was estimated using either a likelihood ratio test or a Wald test, and p-values were adjusted for multiple comparison using the Benjamini & Hochberg method.

2.4 Protein extraction, purification and fractionation

2.4.1 General

Table 2.4.1A Materials and Reagents for protein preparation

Reagent	Supplier	Catalogue Number
4x Sample Laemmli Buffer	BioRad	1610747
CaptureSelect™ C-tagXL affinity Resin	Thermo Scientific	2943072010
cOmplete EDTA-free Protease Inhibitor	Merck	11836170001
DTT	Thermo Scientific	R0861
Dynabeads Protein G	Invitrogen	10004D
EDTA	Merck	EDS-100G
EGTA	Merck	324626
Pierce BCA Protein Assay Reagent A	Thermo Scientific	23228
Pierce BCA Protein Assay Reagent B	Thermo Scientific	23224
PMSF Protease Inhibitor	Thermo Scientific	36978
SDS 20% Solution	Santa Cruz	sc-24950
SEPEA peptide	GenScript	Custom Order
Sodium deoxycholate	Merck	D6750
Superdex 200 16/60 PG column	GE Healthcare	GE28-9893-35
Triton-X 100	Merck	T8787
Tween-20	Merck	P1379

Protein work was carried out at 4°C on ice and samples were stored at -80°C between protocol stages where necessary. Protease inhibitor cocktail was added at 1x to all lysate samples and at 0.1x to all conditioned media samples.

Table 2.4.1B Compositions of buffers for protein preparation

Buffer	Composition	pH
Triton buffer	1% Triton X-100, 150mM NaCl, 50mM Tris-HCl	7.4
RIPA buffer	10mM Tris-HCl, 1mM EDTA, 1mM EGTA, 140mM NaCl, 1% Triton X-100, 0.1% SDS, 0.5% Sodium deoxycholate	7.4
HEPEPS buffer	20mM HEPES, 150mM NaCl, 0.0001% Tween-20	7.4
Glycerol extraction buffer	10% glycerol, 1% Triton X-100, 150mM NaCl, 50 mM NaF, 20mM HEPES, 2 mM Na_3VO_4, 1 mM EDTA, 0.5 mM PMSF	7.4
SDS buffer	2 % SDS, 50 mM Tris-HCl	7.4

2.4.2 Protein extraction and clarification

2.4.2.1 Native cell lysis

Cell pellets were resuspended in 100 µL PBS / ~2.5million cells and homogenised by passage through 25G needle connected to a 1 mL syringe for 3 minutes.

2.4.2.2 Mild cell lysis – Triton-X100

Cell pellets were resuspended in 300 µL Triton buffer / ~2.5 million cells and homogenised by passage through 25G needle connected to a 1 mL syringe for 3 minutes.

2.4.2.3 Harsh cell lysis – RIPA

Cell pellets were resuspended 50 µL RIPA buffer / ~2.5 million cells by vigorous pipetting and incubated for 30 minutes on ice.

2.4.2.4 Brain tissue homogenisation

300-600 mg of each brain region was resuspended by vigorous pipetting in RIPA buffer and homogenised for 3 minutes using a Dounce homogeniser and washing thoroughly with ultrapure water between samples.

2.4.2.5 Lysate/homogenate/conditioned media clarification

Samples were centrifuged at 10,000 xg for 10 minutes at 4°C and supernatants collected and transferred to clean Eppendorf tubes.

2.4.2.6 Determining concentration

For western blot, the concentration of clarified protein samples was determined by BCA assay according to the manufacturer's instructions. For mass spectrometry and mass photometry approximate concentration was determined by absorbance at 280 nm measured using a DeNovix DS-11 UV-Vis Spectrophotometer.

2.4.3 α-synuclein immunoprecipitation

2.4.3.1 Immunoprecipitation from cell lysates for gel electrophoresis

Cells were lysed (2.4.2.2) and clarified lysates were incubated overnight with 1 µg MJFR1 α-synuclein antibody. The following day 600 µg protein G DynaBeads were washed three times in triton buffer and incubated with lysate for 1 hour at 4°C followed by 15 minutes at room temperature. Beads were separated from the α-synuclein depleted fraction/flow through on a magnetic rack and washed three times with 200 µL of triton buffer. Beads were resuspended in 100 µL of triton buffer and transferred to a clean Eppendorf. Triton buffer was aspirated and protein was eluted at 75°C for 10 minutes with 30 µL of 2x Laemmli in triton buffer supplemented with 50 mM DTT.

2.4.3.2 Immunoprecipitation from cell lysates for mass spectrometry

Cells were lysed (2.4.2.1) and clarified lysates were incubated overnight with 2 µg MJFR1 α-synuclein antibody. The following day 1000 µg protein G DynaBeads were washed twice in triton buffer and then a further three times in PBS and incubated with lysate for 1 hour at 4°C followed by 30 minutes at room temperature. Beads were separated from the α-synuclein depleted fraction/flow through on a magnetic rack and washed three times with 200 µL of PBS. Beads were resuspended in 100 µL of PBS transferred to a clean Eppendorf.

2.4.3.3 Native Immunoprecipitation from cell lysates

1 µg MJFR1 α-synuclein antibody was conjugated to 600 µg protein G DynaBeads using 5 mM BS_3 cross-linking reagent in 20 mM sodium phosphate, 150 mM sodium chloride according to the manufacturer's instructions. Beads were washed three times in HEPES buffer and then incubated overnight with clarified cell lysates (2.4.2.1). The following

day beads were washed three times with 200 µL of HEPES buffer. Beads were resuspended in 100 µL of triton buffer, transferred to a clean Eppendorf and the buffer aspirated. Protein was eluted with low pH glycine at room temperature (as shown in Fig. 6.10A) and pH adjusted with 1:10 1 M Tris pH 8.5. Beads were then resuspended in 2x Laemmli in triton buffer supplemented with 50 mM DTT and heated to 75°C for 10 minutes to elute remaining proteins.

2.4.3.4 Immunoprecipitation from culture media

3 mL of four-day conditioned culture media was clarified and incubated overnight with 1 µg MJFR1 monoclonal α-synuclein antibody. The following day 600 µg protein G DynaBeads were washed, incubated with sample and immunoprecipitation performed as described in 2.4.3.1.

2.4.4 α-synuclein nanobody affinity purification

NbSyn2 C-Tag resin for affinity purification was a kind gift from the Draper Group. Dr Barnabas Williams provided technical guidance for use of the ÄKTA PureTM 25 system (GE Healthcare) fluid handling apparatus.

2.4.4.1 Loose resin affinity Purification – cell lysates

Resin was washed three times with PBS, using 5 minutes of centrifugation at 3000 xg for sedimentation. Clarified lysates (2.4.2.1) were incubated overnight with resin at 4°C. The next day, samples were centrifuged discarding the supernatants and the resin was washed three times with 20 mL of PBS. Samples were eluted with 100 µL of 2 mM SEPEA competing peptide in 20 mM Tris by vortexing for 2 minutes.

2.4.4.1 On-column affinity Purification – conditioned media

Conditioned media was filtered through 0.22 µm filters to remove cell debris and α-synuclein isolated using a CaptureSelect™ C-tag affinity column equilibrated with TBS as described previously (Jin *et al.*, 2017). 2 M magnesium chloride in 20mM Tris-HCl (pH 7.4) was used for elution and eluate was collected in 500 µL fractions.

2.4.5 Size exclusion chromatography

Conditioned media (after 0.22 µm filtration) or C-tag eluted fractions were fractionated using a HiLoad 26/60 Superdex 200 column as described previously (Fauvet *et al.*, 2012). Proteins were eluted at a flow rate of 2 mL/minute in 20 mM Tris–HCl, 150 mM NaCl, pH 7.4 and collected in 500 µL fractions.

2.4.6 Ultracentrifugation-based protein fractionation

2.4.6.1 Detergent Fractionation

Solubility of neuron-derived α-synuclein in Triton vs SDS was analysed as described previously, with slight modifications (Stojkovska and Mazzulli, 2021). Briefly, cells were lysed in glycerol extraction buffer by passage through a 25G needle connected to a 1 mL syringe for 3 minutes followed by incubation on ice for 30 minutes. Samples were snap frozen on dry ice for three freeze-thaw cycles and then centrifuged in a T70.1 fixed rotor (Beckman Coulter) at 100,000 xg for 30 minutes at 4°C. The supernatant (Triton-soluble material) was harvested, and the pellet resuspended in glycerol extraction buffer and ultracentrifuged again. This supernatant was discarded and the pellet resuspended in SDS buffer, boiled for 10 minutes at 95°C and bath sonicated for 10 minutes to ensure solubilisation. The SDS sample was ultracentrifuged at 100,000 xg for 30 minutes at 21°C and the supernatant (SDS-soluble material) was harvested.

2.4.6.2 Sucrose Density Gradient Fractionation

Density gradient ultracentrifugation was performed as described previously (Emin *et al.*, 2022). Briefly, discontinuous sucrose step gradients (10-50% w/v in PBS, 400 µL per layer) were made up by snap freezing between addition of each layer. Gradients were stored at -20°C until use. Cells were lysed (2.4.2.1) and clarified (2.4.2.5) and layered on top of the gradient pooling lysates from at least 4 wells of a 6 well plate to a total volume of 400 µL. Gradients were thawed and then ultracentrifuged for 4 hours at 113,000 xg at 4°C in a swinging bucket SW 60 Ti rotor (Beckman Coulter). Following centrifugation, layers were carefully removed using a P200 pipette and collected in separate Eppendorf tubes which were stored at -80°C until analysis.

2.4.6.3 Extracellular Vesicle isolation

8 mL of clarified conditioned media was ultracentrifuged in a T70.1 fixed rotor (Beckman Coulter) at 100,000 xg for 1 hour at 4°C. The supernatant was aspirated and the pellet resuspended in 2x Laemmli in RIPA buffer supplemented with 50 mM DTT.

2.5 Protein Gel Electrophoresis and visualisation

2.5.1 General

Table 2.5.1 Materials and Reagents for gel electrophoresis

Reagent	Supplier	Catalogue Number
α-synuclein (4B12) Antibody	BioLegend	39730-200
α-synuclein (4D6) Antibody	Abcam	Ab1903
α-synuclein (MJFR1) Antibody	Abcam	ab138501
α-synuclein (MJFR14) Antibody	Abcam	ab209538
α-synuclein (Syn1) Antibody	BD Biosciences	610787
10 kDa Amicon 0.5 Centrifugal filter unit	Merck	UFC501024
16% Formaldehyde solution (w/v)	Thermo Scientific	28908
4-15% TGX Gel 18W 30 µl	BioRad	5671084
4–15% TGX Stain-Free Gel 18W 30 µl	BioRad	5678084
Anti-Guinea Pig IgG HRP Antibody	BioRad	AHP863P
Anti-Mouse IgG for IP	Abcam	ab131368
Anti-Mouse IgG HRP Antibody	BioRad	170-6516
Anti-Rabbit IgG HRP Antibody	BioRad	1706515
Bromophenol blue	Thermo Scientific	A16899.09
Calnexin (C5C9) Antibody	Cell Signalling	2679
Calreticulin Antibody	Abcam	Ab22683
Cas9 Antibody	Invitrogen	7A9-3A3
DNAJC5 Antibody	RayBiotech	144-10489-200
Dopa decarboxylase Antibody	Sigma	AB1569
ECL Primer Western Blotting Detection	VWR International	RPN2236
Flottilin-1 (Clone18) Antibody	BD Bioscience	610821
GAPDH Antibody	Abcam	ab9484
LAMP1 Antibody	Santa Cruz	Sc20011
LASH 1-10	Gift from Prof Lashuel	5B10-A12
LASH 1-20	Gift from Prof Lashuel	LASH-EGTNter
LC3B Antibody	Cell Signalling	2775S
Mitofusin-2 Antibody	Abcam	Ab56889
Monoamine oxidase-B Antibody	Abcam	Ab137778
Pan-synuclein Antibody	Newmarket Scientific	R-060-100
Proteasome 19S S4/PSMC1 Antibody	Abcam	ab3317
Silver Stain for Mass Spectrometry Kit	Thermo Scientific	24600
SimplyBlue SafeStain	Invitrogen	LC6060
Skimmed milk powder	Merck	70166
Spectra Multicolour Broad Range Ladder	Thermo Scientific	26634
Trans-Blot Turbo Midi 0.2um PVDF Transfer	BioRad	1704157
Tyrosine Hydroxylase Antibody	Merck	AB152
VMAT2 Antibody	Abcam	Ab70808
β-actin-HRP (AC-15) Antibody	Abcam	ab49900
β3-tubulin Antibody	Abcam	ab52623

2.5.2 SDS-PAGE

Clarified cell lysates were diluted to load 10-25 µg of total protein for western blot or up to 600 µg of total protein for silver staining. 22 µL (in a total volume of 30 µL) was used for all other sample types. Samples were mixed with 1x Laemmli buffer and 50 mM DTT and boiled for 10 minutes at 75°C unless otherwise stated. Boiled samples were resolved alongside a broad-range protein ladder using pre-cast 4-15% gradient polyacrylamide gels in SDS running buffer (25 mM Tris base, 192 mM glycine, 0.1% SDS, pH 8.3). A voltage of 180 V was applied for the first 10 minutes until samples had left the stacking gel and then the voltage was increased to 200 V.

2.5.3 CN-PAGE

Clarified cell lysates (15 µg total protein) or 25 µL of conditioned media concentrated 70x using Amicon 10 kDa ultrafiltration columns, were mixed with native loading buffer (62.5 mM Tris-HCl, 40% glycerol, 0.01% bromophenol blue, pH 6.8) without boiling. Samples were resolved on 4-15% gradient polyacrylamide gels in native running buffer (25 mM Tris base, 192 mM glycine, pH 8.3), applying a constant voltage of 150 V until ~10 minutes after the dye front reached the end of the gel.

2.5.4 Total Protein visualisation

2.5.4.1 Stain-Free Detection

BioRad stain-free gels contain a Tri-halo compound permitting direct in-gel fluorescence visualisation of proteins. Stain-free imaging was used as a loading control for post-mortem samples.

2.5.4.2 Coomassie Staining

SimplyBlue safe Coomassie G-250 was used according to the manufacturer's instructions for evaluation of sample purity following immunoprecipitation and affinity purification.

2.5.4.3 Silver Staining

The Pierce Silver Stain for Mass Spectrometry Kit was used to identify gel bands for mass proteomic digest. Staining and destaining were carried out according to the manufacturer's instructions.

2.5.5 Immunoblotting

Resolved proteins were transferred to PVDF membranes using the BioRad Trans-Blot Semi-Dry transfer system. Membranes were washed once in TBS with Tween-20 (TBS-T; 20 mM Tris, 150 mM NaCl, 0.1% Tween-20) and fixed for 30 minutes in 4% PFA to reduce loss of small proteins (Lee and Kamitani, 2011; Sasaki *et al.*, 2015). Membranes were blocked for 1 hour, in 5% skimmed milk or 5% bovine serum albumin (BSA) in TBS-T and incubated overnight at 4°C with primary antibodies made up in blocking buffer (Table 2.5.5). The next day membranes were washed three times in TBS-T, incubated for 1 hour with a 1:1000 dilution of secondary antibodies and washed a further three times. A Bio-Rad ChemiDoc was used for visualisation: auto-optimal settings were used for SDS-PAGE and signal-accumulation mode for CN-PAGE.

2.5.6 Protein band quantification

BioRad ImageLab Software was used for densitometric quantification of stained gels and immunoblot membranes.

Table 2.5.5 Primary Antibodies Used for Western blot

Antibody	Species	Dilution	Blocking
α-synuclein (4B12)	Mouse	1:1,000	Skimmed milk powder
α-synuclein (4D6)	Mouse	1:1,000	Skimmed milk powder
α-synuclein (MJFR1)	Rabbit	1:10,000	Skimmed milk powder
α-synuclein (MJFR14)	Rabbit	1:1,000	Skimmed milk powder
α-synuclein (Syn1)	Mouse	1:1,000	Skimmed milk powder
19S RP	Rabbit	1:1,000	Skimmed milk powder
Calnexin	Rabbit	1:1,000	Skimmed milk powder
Calreticulin	Mouse	1:1,000	Skimmed milk powder
Cas9	Mouse	1:500	BSA
DNAJC5	Rabbit	1:1,000	Skimmed milk powder
Dopa decarboxylase	Rabbit	1:1,000	Skimmed milk powder
Flottilin-1	Mouse	1:1,000	Skimmed milk powder
GAPDH	Mouse	1:1,000	Skimmed milk powder
LAMP1	Mouse	1:1,000	Skimmed milk powder
LASH 1-10	Mouse	1:250	Skimmed milk powder
LASH 1-20	Mouse	1:250	Skimmed milk powder
LC3B	Rabbit	1:1,000	Skimmed milk powder
Mitofusin	Mouse	1:1,000	Skimmed milk powder
Monoamine oxidase-B	Rabbit	1:1,000	Skimmed milk powder
Pan-synuclein	Rabbit	1:500	Skimmed milk powder
Tyrosine Hydroxylase	Rabbit	1:1,000	Skimmed milk powder
VMAT2	Rabbit	1:500	BSA
β-actin-HRP	Mouse	1:5,000	Skimmed milk powder
β3-tubulin	Rabbit	1:1,000	Skimmed milk powder

2.6 Mass Spectrometry

2.6.1 General

Table 2.6.1 Materials and Reagents for mass spectrometry

Reagent	Supplier	Catalogue Number
Acetonitrile	Merck	34851
C18 resin	Empore	2215-C18
Chymotrypsin	Promega	V1061
Chloroacetamide	Merck	C0267
Iodoacetamide	Merck	I1149
Elastase	Promega	V189A
Formic Acid	Thermo Scientific	28905
GluC	Promega	V165A
TCEP	Merck	C4706
Trypsin	Promega	V5111
Urea	Merck	U5378

2.6.1 Sample preparation

Sample preparation was carried out at room temperature using reagents and protocols provided by the Biochemistry Department Advanced Proteomics Facility or Dr Neha Kalmankar.

2.6.2.1 In-solution digest of recombinant α-synuclein

5 µg of α-synuclein were denatured for 10 minutes with 4 M urea in 100 mM ammonium bicarbonate buffer, while shaking at 650 rpm. Cysteine residues were reduced for 30 minutes with 10 mM Tris(2-carboxyethyl)phosphine (TCEP) and alkylated with 50 mM 2-chloroacetamide (ClAM) for 30 minutes protected from light. Samples were diluted in ammonium bicarbonate buffer to reduce the urea concentration. For tryptic digests 2 mM calcium chloride was added. Samples were incubated with enzyme (Trypsin 0.25 µg, GluC 0.25 µg or Elastase 0.2 µg) overnight at 37°C while shaking at 800 rpm. Reactions were stopped with 5 % formic acid and samples were centrifuged for 30 minutes at 14,000 xg and supernatants were collected.

2.6.2.2 On-bead digest of immunoprecipitated samples

Beads were resuspended in 1.5x their original volume of 8 M urea in ammonium bicarbonate buffer and then reduced, alkylated and digested as described in 2.6.2.1. Following formic acid addition samples were placed on a magnetic rack and the supernatants collected for centrifugation as in 2.6.2.1.

2.6.2.3 C18 clean up and desalting

Desalting tips were prepared by inserting 2 mm diameter discs of C18 resin into P10 pipette tips. The resin was activated with two 100% acetonitrile washes centrifuging for 5 minutes at 4000 xg until all the liquid had passed through. Resin was then washed with 0.1% trifluoroacetic acid (TFA) and the sample loaded. Resin was washed a further two times with 0.1% TFA and peptides eluted with 50% acetonitrile in 0.1% TFA. Eluates were dried in a SpeedVac and peptides stored at -20°C until injection.

2.6.2.4 In-gel digest of silver-stained gel band

Following destaining (2.5.4.3) gel pieces were further dissected with a P200 pipette tip into ~1 mm^3 cubes and washed with ammonium bicarbonate buffer for 15 minutes. The buffer was aspirated and gel pieces were equilibrated in 50% acetonitrile (v/v) in ammonium bicarbonate buffer for 15 minutes and then dehydrated in 100% acetonitrile until they turned white. Acetonitrile was aspirated and proteins were then reduced with 10 mM DTT for 45 minutes at 56°C while shaking at 400 rpm and then alkylated with 55 mM iodoacetamide for 30 minutes in the dark at room temperature. Gel pieces were washed in ammonium bicarbonate buffer, dehydrated with 100% acetonitrile and then allowed to air dry for 10 minutes. Overnight digests were carried out at 37°C with 1.5 µg trypsin and 1.5 µg chymotrypsin in ammonium bicarbonate buffer.

The following day reactions were stopped with 5% formic acid and the supernatants were collected. Peptides were sequentially extracted in 1% formic acid, 50% acetonitrile and 100% acetonitrile for 15 minutes each pooling the supernatants. Pooled supernatants were dried using a SpeedVac. Peptides were stored at -20°C until injection.

2.6.3 LC-MS/MS

2.6.3.1 In solution and on-bead digest samples

Sample injection and data analysis were performed by Dr Marjorie Fournier in the Department of Biochemistry Advanced Proteomics Facility. Briefly, using the nano liquid chromatography system (Thermo Scientific Ultimate 3000 RSLC) peptides were first trapped onto a short C18 precolumn (Thermo Scientific PepMap100) in 0.1% formic acid and then separated on an analytical C18 column (Thermo Scientific Easy-Spray 50 cm, 75 µm inner diameter) using a 15-minute linear gradient of 0.1% formic acid in acetonitrile (15-38%). Data were acquired with a Q Exactive mass spectrometer using the orbitrap analyser in data-dependent acquisition mode. The 5 most abundant ions from the full MS1 scan (Resolution 70,000, scan range 350-1500 m/z) were fragmented using higher-energy collisional dissociation (HCD) (30% normalized collision energy) and MS2 spectra acquired (Resolution 17,500). Ions with 0 or +1 charge were excluded.

PEAKS Studio software v10.0. MS/MS spectra were searched for semi-GluC/trypsin specific peptides against a protein sequence database of 20,288 *Homo sapiens* proteins (Uniprot release 2025-04) and common contaminants. A pan-PTM search was performed including 304 post-translational modifications configured in PEAKS software. Two missed cleavages were permitted. Peptide mass tolerance was set at 20ppm on the

precursor and 0.6 Da on the fragment ions. Data were filtered at FDR below 1% at PSM level. Post-translational modifications of interest were manually validated.

2.6.3.2 In-gel digest samples

Peptides were resuspended in 0.1% formic acid and separated on a C18 column (Thermo Scientific Acclaim PepMap100, 75 μm × 2 cm) using an Ultimate 3000 UHPLC system (Thermo Scientific) with a 60 minute linear gradient of 0.1% formic acid in 80% acetonitrile (5-40%), at a flow rate of 300 nL/minute. Separated peptides were electrosprayed in positive mode into an Orbitrap Eclipse Tribrid mass spectrometer through an EASY-Spray nano-electrospray ion source (Thermo Scientific). Precursor peptides were analysed in the Orbitrap analyser (Resolution 120,000, scan range 300–2,000 m/z). Precursor peaks above an intensity threshold of 5.0 × 104, corresponding to multiply charged peptide ions (charge states 2–5), were selected with the quadrupole using a 0.7 m/z selection window and fragmented using HCD (30% normalized energy). MS2 spectra were also acquired in the Orbitrap (Resolution 30,000).

Peptide identification and data analysis were carried out by Dr Neha Kalmankar using Thermo Proteome Discoverer software v2.1. MS/MS spectra were searched with the SEQUEST HT engine against a database of *Homo sapiens* proteins (Uniprot release 2025-04) and common contaminants. Data were filtered at FDR below 1% or 5% at peptide level. Peptides were manually validated.

2.7 α-synuclein ELISAs

2.7.1 General

Table 2.7.1 Materials and Reagents for ELISA

Reagent	Supplier	Catalogue Number
DuoSet ELISA Ancillary Reagent Kit	Bio-Techne	DY008B
ELAST ELISA Amplification System	Revvity	NEP116E001EA
Human α-synuclein DuoSet ELISA Kit	Bio-Techne	DY1338-05
LEGEND MAX Human α-synuclein Aggregate ELISA kit	BioLegend	448807
U-PLEX Human α-synuclein kit	Mesoscale Discovery	K151WKK

All conditioned media for ELISAs was centrifuged for 5 minutes at 1,000 xg to remove cell debris and only the supernatant added to the ELISA plate.

2.7.2 MSD α-synuclein ELISA

The U-PLEX Human α-synuclein kit was used according to the manufacturer's instructions. 20 µL of conditioned media was used per well and samples were run in technical duplicate.

2.7.3 Bio-Techne DuoSet α-synuclein ELISA

Details of the optimisation and modification of this protocol to improve sensitivity along with the corresponding assay validation can be found in Subchapter 4.4.

2.7.3.1 Manufacturer's protocol

The kit was used according to the manufacturer's instructions with slight modifications. Blocking was carried out for 90 minutes, four washes were used after each step from sample addition onwards and serial dilutions of α-synuclein standards were made up in NB media (Table 2.1.2.2A) rather than blocking buffer. 100 µL of conditioned media was used per well and samples were run in technical triplicate.

2.7.3.2 ELAST amplification

Bio-Techne DuoSet ELISA plates were coated with capture antibody as per manufacturer's instructions and blocked overnight with 1% or 2% BSA in PBS. Plates were incubated with sample/standards, biotinylated detection antibody, and streptavidin-HRP as in 2.7.3.1. Following incubation with streptavidin-HRP, plates were washed four times and incubated with biotinyl tyramide from the Revvity ELAST kit according to the manufacturer's instructions. Plates were washed a further four times and then incubated for 25 minutes in 1:500 or 1:1000 dilutions of Revvity Streptavidin-HRP in BSA with 0.5% Tween-20. After the second HRP incubation plates washed and developed as in 2.7.3.1.

2.7.3.3 Optimised BioT3

The Bio-Techne DuoSet ELISA was carried out as in 2.7.3.1, however after the first hour of incubation with conditioned media, those samples were removed and discarded. A second 100 µL aliquot of media harvested from the same cells at a different time point was added for one hour without washing. This process was repeated a total of three times before plates were washed and detection antibodies added. The rest of the protocol was the same as in 2.7.3.1 but four to six technical replicates were run for each condition (see plate map in Fig. 5.8B).

2.7.4 BioLegend aggregated α-synuclein ELISA

The LEGEND MAX α-synuclein aggregate ELISA was carried out according to the manufacturer's instructions using 50 µL of media per well in technical triplicate.

2.8 RT-QuIC

2.8.1 General

Table 2.8.1 Materials and Reagents for RT-QuIC

Reagent	Supplier	Catalogue Number
100 kDa Amicon 0.5 Centrifugal filter unit	Merck	UFC510024
50 kDa Amicon 0.5 Centrifugal filter unit	Merck	UFC505024
Clear bottom 96-well plate	Nalgene Nunc	165305
PIPES	Merck	P6757
Recombinant α-synuclein	rPeptide	S-1001
ThT	Merck	T3516

Details of the development of this protocol along with the corresponding assay validation can be found in subchapter 6.2. Only the final optimised protocol is presented below.

2.8.2 Sample preparation

Four-day conditioned media was centrifuged for 10 minutes at 10,000 xg at 4°C and then ultracentrifuged for an hour at 100,000 xg using a T70.1 fixed rotor (Beckman Coulter). Supernatants were concentrated 10x or 20x using 10 kDa or 50 kDa Amicon ultrafiltration columns and stored at -80°C until use.

2.8.3 Reaction Set Up

Recombinant α-synuclein was re-monomerised by Dr Civitelli. Briefly, recombinant protein was resuspended in 6 M Guanidium hydrochloride and centrifuged at 20,000 xg for one hour at 4°C. The supernatant was dialysed into distilled water overnight and then concentrated using 10 kDa Amicon ultrafiltration columns.

The monomer was passed through a 100 kDa Amicon ultrafiltration column to remove aggregates and the concentration of the flow through determined by nanodrop. Recombinant α-synuclein was diluted to 0.12 mg/mL in filtered assay buffer (1 mM

Thioflavin-T, 500 mM PIPES, 500 mM sodium chloride, 500 mM EDTA at pH 7) and 85 µL was mixed with 15 µL of media sample (2.8.2) per well of the 96-well assay plate. Plates were sealed with film.

2.8.4 Reaction Conditions

The RT-QuIC reaction was carried out as described previously (Lee, Civitelli and Parkkinen, 2024) for 80 to 220 hours with cycles of 1 minute double orbital shaking at 400 rpm and 1 minute rest. ThT fluorescence was measured every 30 minutes.

2.8.5 Data Analysis

RT-QuIC data was analysed using the QuICSeedR package (M. Li *et al.*, 2024). Lag time was defined as the time to exceed 5x standard deviation of baseline fluorescence as calculated between 2.5 and 5 hours of the assay. The bin width for maximal slope determination was set as 4. For each experiment, lag time was calculated separately for each of the four technical replicate wells per cell line and then averaged to give a mean lag time per cell line. Lag times for the same cell line across experimental replicates (independent differentiations) were then averaged and compared by genotype with one-way ANOVA and Dunnett's multiple comparisons post-hoc test.

2.9 – Mass Photometry

2.9.1 General

Table 2.9.1 Materials and Reagents for Mass Photometry

Reagent	Supplier	Catalogue Number
24 x 50 mm Glass Coverslips	Menzel Gläser	VWR 630-2603
DOPC	Avanti Polar Lipids	850375 P
DOPS	Avanti Polar Lipids	840035 P

2.9.2 Sample preparation

Cells were lysed (2.4.2.1) and clarified (2.4.2.5) and diluted to the working concentration with 20 mM HEPES, 150 mM potassium chloride, 1 mM magnesium chloride at pH 7.4. Four-day conditioned media was clarified and concentrated 20x through Amicon 10 kDa ultrafiltration columns. Samples were incubated overnight with 10-200 nM MJFR1 α-synuclein antibody.

2.9.3 Mass Measurements

Supported lipid bilayers (SLBs) were prepared by Raman Van Wee as described previously (Foley *et al.*, 2021). Briefly, from DOPC and DOPS were mixed in a 60:40 molar ratio to form liposomes which were sonicated and incubated on plasma-cleaned glass coverslips for a minimum of 30 minutes before use.

Mass estimation was performed using a Refeyn OneMP mass photometer and 40 µL of sample was loaded to a total volume of 60 µL in the gasket. Data was acquired in 1 minute recording periods and dynamic mass photometry movies were analysed as described previously (Foley *et al.*, 2021)

2.10 Single Molecule Pull down

2.10.1 General

Table 2.10.1 Materials and Reagents for SiMPuLL

Reagent	Supplier	Catalogue Number
NeutrAvidin	Thermo Scientific	31050
Normal Goat Serum	Abcam	Ab7481
Syn211-AF647 Antibody	Santa Cruz	Sc-12767 AF647
Syn211-Biotin Antibody	Santa Cruz	Sc-12767 B

2.10.2 Sample preparation

Four-day conditioned media samples were clarified (2.4.2.5) and concentrated 20x using Amicon 10 kDa ultrafiltration columns. Samples were snap frozen and shipped to Cambridge on dry ice.

2.10.3 Staining and microscopy

Single molecule pull down and image acquisition were performed by Florence Layburn as described previously (Emin *et al.*, 2022). Briefly, Rain-X coated glass coverslips, were blocked with 10% BSA/10 % normal goat serum and incubated with Neutravidin (0.1 mg/mL). Coverslips were washed three times in PBS, 0.05% Tween-20 and coated with biotinylated α-synuclein antibody Syn211 (10 nM). Coverslips were washed and blocked again, then incubated with media samples (2.10.2) for 3 hours. After a further three washes, coverslips were incubated with Alexa Fluor647-labelled Syn211 (5 nM), washed and exchanged to PBS for imaging. Image acquisition was carried out with a custom-built total internal reflection fluorescence (TIRF) microscope and analysis was performed in ImageJ using the ThunderSTORM plugin described previously (Ovesný *et al.*, 2014).

2.11 Cellular Assays

2.11.1 General

Table 2.8.1 Materials and Reagents for cellular assays

Reagent	Supplier	Catalogue Number
Anti-Chicken 488 Antibody	Invitrogen	A78948
Anti-Chicken 647 Antibody	Invitrogen	A78952
Anti-Mouse 555 Antibody	Invitrogen	A31570
Anti-Rabbit 488 Antibody	Invitrogen	A21206
Anti-Rabbit 555 Antibody	Invitrogen	A31572
DAPI	Merck	D9542
HCS CellMask Far Red	Thermo Scientific	H10294
MAP2 Antibody	Abcam	Ab92434
Mouse IgG	Abcam	Ab3735S
Normal Donkey Serum	Stratech	017-000-121-JIR
pSer129 α-synuclein (EP1536Y) Antibody	Abcam	Ab51253
Rabbit IgG	Cell Signalling	2729S
Toxilight kit	Lonza Biologics	LT07-217

2.11.2 Toxilight

Toxilight cell viability assay was carried out according to the manufacturer's instructions using 20 µL of conditioned media and running samples in technical triplicate.

2.11.3 Confocal fluorescence microscopy

2.11.3.1 Live Imaging

Cells were incubated with 1:250 dilution of HCS CellMask for 30 minutes at 37°C in NB, washed once with neurobasal and returned to culture media for imaging. 96-well plates were maintained at 37°C, 5% CO_2 throughout imaging using the OperaPhenix (Perkin Elmer).

2.11.3.2 Immunocytochemistry

Neurons were fixed with 4% PFA in PBS for 20 minutes at room temperature, then permeabilised and blocked with 0.1% triton-X100 in PBS for 15 minutes followed by

0.1% triton-X100 in 5% Normal donkey serum (NDS) for 1 hour. Permeabilised cells were incubated with primary antibodies overnight at 4°C in 0.1% Triton-X100 and 1% NDS, washed three times and then incubated with secondary antibodies and DAPI for 1 hour at room temperature. All antibodies were used at a dilution of 1:500. Cells were washed a further three times and transferred to PBS for imaging. Images were acquired at 43x resolution using the OperaPhenix (Perkin Elmer).

2.11.3.3 Image analysis

Images were analysed using Harmony Software (Perkin Elmer). Intensity thresholds were set relative to un-transduced or untreated controls for live imaging and to isotype controls for immunocytochemistry.

2.12 Statistical analysis

Data analysis and statistical testing were carried out using GraphPad Prism and RStudio. Details of the sample sizes and statistical tests are provided in the relevant figure legends.

Chapter 3 - Characterising α-synuclein PTMs in iPSC-DaNs

3.1 Introduction

α-synuclein has been reported to accumulate in iPSC-DaNs from patients with a variety of familial PD mutations, including *SNCA* multiplications and point mutations, as well as sporadic disease (Devine *et al.*, 2011; Mazzulli *et al.*, 2011; Nguyen *et al.*, 2011; Chung *et al.*, 2016; Kouroupi *et al.*, 2017; Burbulla *et al.*, 2019). However, these observations vary dramatically between differentiation protocols and the stage of maturation at which the accumulation phenotype is measured (Sánchez-Danés *et al.*, 2012; Dettmer *et al.*, 2015; Fernandes *et al.*, 2016; Cuddy *et al.*, 2019; Zambon *et al.*, 2019). α-synuclein modified by phosphorylation at serine-129 has been detected in mature iPSC-DaNs by some groups though the abundance is low and often undetectable without exogenous insult from α-synuclein PFFs (Ryan *et al.*, 2013; Lin *et al.*, 2016; Kouroupi *et al.*, 2017; Luo *et al.*, 2020; Stykel *et al.*, 2021; Tanudjojo *et al.*, 2021; Iannielli *et al.*, 2022; Virdi *et al.*, 2022). The publications above use immunoblotting or immunocytochemistry with phospho-selective antibodies to quantify phospho-ser-129 and total α-synuclein abundance. A reliance on antibodies for PTM quantification is hindered by issues of specificity and affinity, parameters which are both altered by other modifications proximal to the epitope of interest (Lashuel *et al.*, 2022). Moreover, sole reliance on antibody detection greatly limits the range of interrogable PTMs to those for which antibodies have already been generated, thus preventing the discovery of novel modified sites.

While targeted mass spectrometry is the obvious solution to achieve an unbiased characterisation of the PTM landscape for any individual protein, α-synuclein has a scarcity of tryptic cut sites in the C-terminus, hindering the use of canonical trypsin digests (Pons *et al.*, 2022). A limited number of studies in post-mortem brain tissue have used different enzymes or employed alternative strategies to ionise large tryptic peptides to achieve full sequence coverage, although whether these are suitable for the much lower abundance α-synuclein in iPSC-DaNs remains to be determined (Li *et al.*, 2005; Zhang *et al.*, 2017; Killinger *et al.*, 2018). A better understanding of α-synuclein PTMs in iPSC-DaNs, compared to human brain, is essential for the design of experiments dissecting the functional consequences and pathological significance of such modifications in disease. To that end this chapter investigates the modifications of α-synuclein, and specifically a lower molecular weight form of α-synuclein identified in patient-derived iPSC-DaNs. Neurons carrying the *SNCA*-triplication mutation which increase α-synuclein expression, and *GBA1-N370S* heterozygous point mutations, the most common genetic risk factor for PD, were used for this work.

Chapter Aims

1. To determine the α-synuclein expression profile in iPSC-DaNs harbouring the *SNCA*-triplication or *GBA1-N370S* mutations.
2. To optimise a mass-spectrometry approach suitable for unbiased assessment of additive PTMs on α-synuclein derived from iPSC-DaNs.
3. To characterise any modified proteoforms of α-synuclein expressed by iPSC-DaNs.

3.2 Generating iPSC-derived dopaminergic neurons expressing α-synuclein

Overt α-synuclein pathology is only detectable comparatively late in life for PD patients. Accordingly, iPSCs from healthy controls and PD patients with *SNCA*-triplication or *GBA1-N370S* mutations were differentiated according to Kriks et al. (2011) with slight modifications (Fig. 3.1A, Subchapter 2.1.2.2) and extensively matured to Day100. At Day35 cells already showed expression of neuronal marker MAP2 as well as tyrosine hydroxylase (TH), a crucial enzyme for monoamine synthesis, suggesting dopaminergic fate (Fig. 3.1B&C). Expression of α-synuclein (but not TH) increased with neuronal maturation, consistent with its role as a synaptic protein (Fig. 3.1C-F). Moreover, a lower molecular weight α-synuclein band was detected in both PD and control genotypes (Fig. 3.1C). The relative abundance of this lower band increased throughout differentiation in control and *GBA1-N370S* lines and showed a trending increase with neuronal maturity in *SNCA*-triplication neurons (Fig. 3.1E). To further examine genotypic differences in α-synuclein expression, 3-4 additional differentiations of iPSC-DaNs were matured to Day75 and probed for α-synuclein as well as TH and dopa-decarboxylase (DDC), the next enzyme in the dopamine synthesis pathway (Figs. 1.1 & 3.1G). Cells also expressed vesicular monoamine transporter-2 (VMAT2) required for synaptic vesicle dopamine loading, and monoamine-oxidase B, further confirming their dopaminergic identity (Fig. 3.1G). Densitometric quantification revealed that TH expression was reduced in *SNCA*-triplication neurons while, DDC was unchanged and α-synuclein expression was increased, consistent with triplication of the *SNCA* gene locus (Fig. 3.1H). It is worth noting that, as in Fig. 3.1G, a lower band for α-synuclein was not always observed, with approximately 1 differentiation in 5 only showing the dominant upper band.

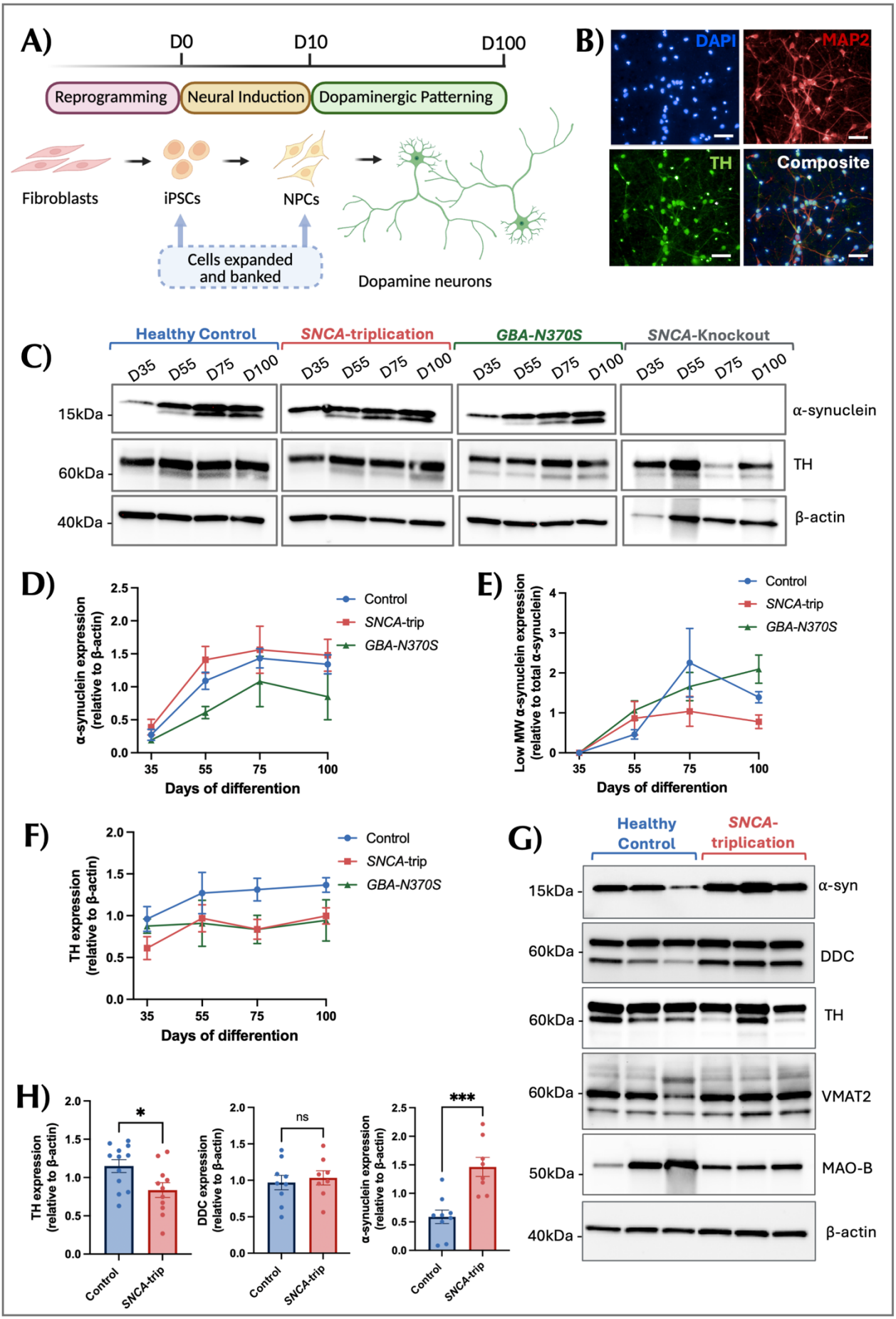
A)
D0
D10
D100
Reprogramming
Neural Induction
Dopaminergic Patterning
Fibroblasts
iPSCs
NPCs
Cells expanded and banked
Dopamine neurons
B)
DAPI
MAP2
TH
Composite
C)
Healthy Control
SNCA-triplication
GBA-N370S
SNCA-Knockout
D35
D55
D75
D100
15kDa
60kDa
40kDa
α-synuclein
TH
β-actin
D)
α-synuclein expression (relative to β-actin)
Days of differention
Control
SNCA-trip
GBA-N370S
E)
Low MW α-synuclein expression (relative to total α-synuclein)
F)
TH expression (relative to β-actin)
G)
Healthy Control
SNCA-triplication
α-syn
DDC
TH
VMAT2
MAO-B
50kDa
H)
DDC expression (relative to β-actin)
ns
***

Fig. 3.1 α-synuclein expression increases throughout maturation and is elevated by triplication of the *SNCA* gene locus. A) Schematic describing the differentiation of dopaminergic neurons from patient-derived fibroblasts according to the Kriks et al. (2011) protocol. **B)** Representative images of Day35 iPSC-DaNs stained for neuronal marker MAP2 and monoamine synthetic enzyme TH. Scale bar = 50 μm. **C)** Representative western blots for α-synuclein and TH expression throughout differentiation. **D)** Densitometric quantification of α-synuclein relative to β-actin. Linear regression shows a significant increase in α-synuclein expression over time for all the three genotypes: $p_{Control}$=0.0003, $p_{SNCA\text{-}trip}$=0.0235, $p_{GBA1\text{-}N370S}$=0.0489. N=3 cell lines, 2 differentiations per genotype, per timepoint. **E)** Densitometric quantification of low molecular weight α-synuclein relative to total α-synuclein throughout differentiation. Linear regression shows significant increases in the proportion of low molecular weight α-synuclein over time for controls and *GBA1-N370S* neurons: $p_{Control}$=0.0137, $p_{SNCA\text{-}trip}$=0.1562, $p_{GBA1\text{-}N370S}$<0.0001. N=3 cell lines, 2 differentiations per genotype, per timepoint. **F)** Densitometric quantification of TH expression relative to β-actin throughout differentiation. Linear regression shows no significant difference in TH expression over genotypes. N=3 cell lines, 2 differentiations per genotype, per timepoint. **G)** Representative western blots from Day75 neurons showing expression of α-synuclein, TH, DDC, VMAT2 and MAO-B **H)** Densitometric quantification of α-synuclein, DDC and TH relative to β-actin. Student's two-tailed t-test *p<0.005, **p<0.01, ***p<0.0001. N = 3 cell lines per genotype from 3 or 4 independent differentiations.

3.3 Assessment of additive PTMs on neuron-derived α-synuclein

To determine the presence of additive PTMs on α-synuclein in our iPSC model it was necessary to identify proteases that give optimal coverage of the α-synuclein sequence. Trypsin, elastase and GluC are all predicted to generate peptides covering the N-terminus while C-terminal coverage is only expected from elastase and GluC (Fig. 3.2A). Mass spectrometry, carried out Biochemistry Department Advanced Proteomics Facility, demonstrated that contrary to expectation, in-solution digestion of recombinant α-synuclein with trypsin yielded large C-terminal peptides, but the N-terminus was not covered. The efficiency of the elastase digest was extremely low, but the GluC digest provided 88% sequence coverage including the N- but not C-terminus (Fig. 3.2A).

To investigate cell-derived α-synuclein it was first necessary to extract and enrich for soluble α-synuclein which was achieved using magnetic bead immunoprecipitation (IP) (Fig. 3.2B). Immunoblotting the eluted protein demonstrated successful pull down of α-synuclein from iPSC-DaN lysates (Fig. 3.2C). In line with meaningful enrichment, digestion of *SNCA*-triplication samples with trypsin or GluC showed that α-synuclein was the most abundant human protein present (Fig. 3.2D). In contrast to the recombinant protein, both enzymes provided full sequence coverage of α-synuclein. A pan-PTMs search in PEAKS filtering with FDR 1% identified numerous modified peptides from each digestion (Fig. 3.2E). However, the biological validity and disease relevance of these modifications is likely to be low.

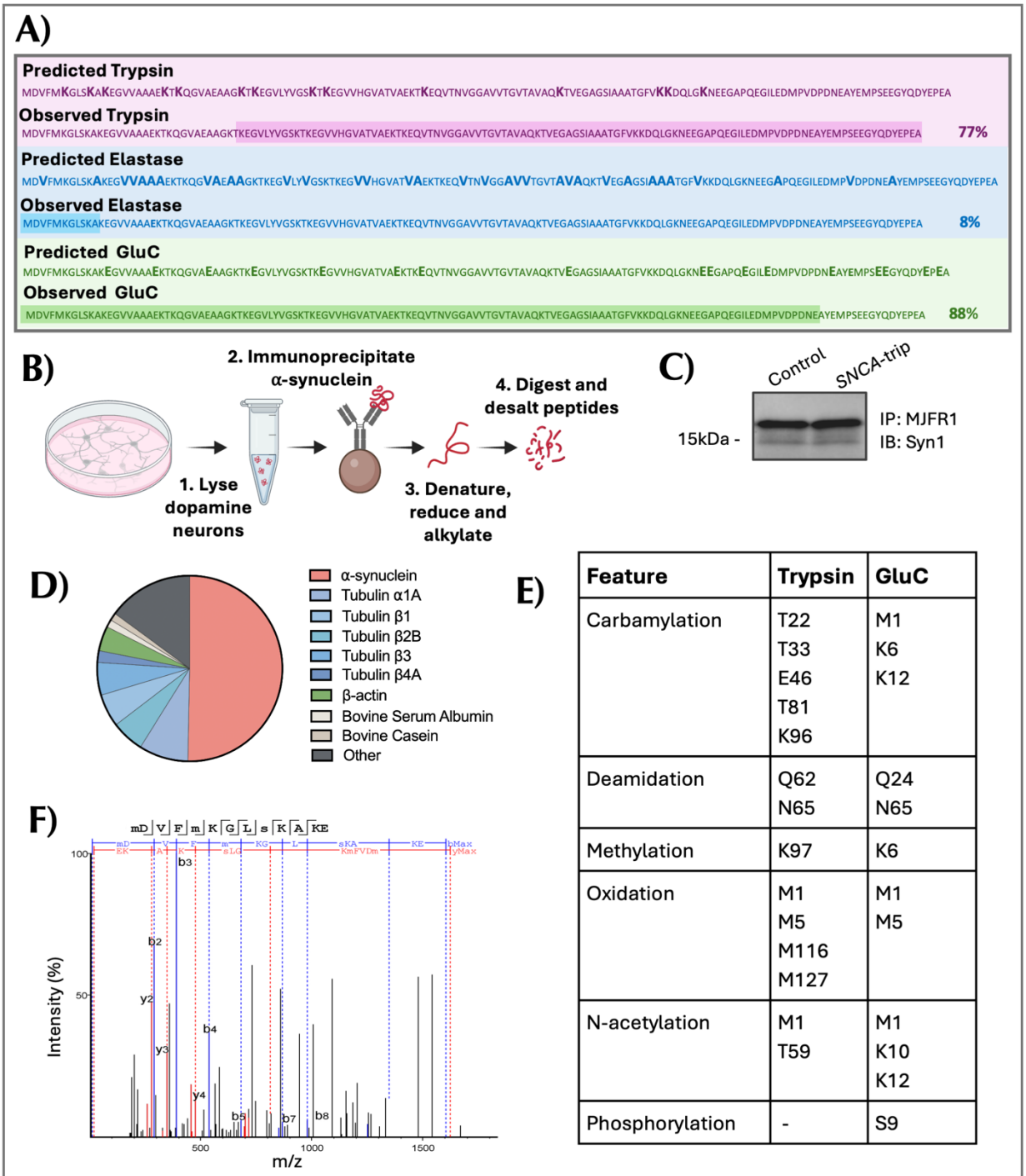

Feature	Trypsin	GluC
Carbamylation	T22 T33 E46 T81 K96	M1 K6 K12
Deamidation	Q62 N65	Q24 N65
Methylation	K97	K6
Oxidation	M1 M5 M116 M127	M1 M5
N-acetylation	M1 T59	M1 K10 K12
Phosphorylation	-	S9

Fig. 3.2 α-synuclein from iPSC-derived dopamine neurons lacks PD-associated additive PTMs **A)** α-synuclein sequence with enzyme cut sites predicted by Expasy Peptide Cutter in bold and the actual sequence coverage for recombinant α-synuclein highlighted. **B)** Schematic showing the procedure for α-synuclein extraction, enrichment and preparation ahead of mass spectrometry. **C)** western blot of immunoprecipitated α-synuclein from control and *SNCA*-triplication neuron lysates after stage 2 in B). **D)** Relative abundance of human proteins in the IP eluate following tryptic digest, as approximated by spectral area of each protein in mass spectrometry. Peptides were searched against the human proteome so antibody fragments (rabbit) from the IP are not detected. **E)** Modifications identified on α-synuclein peptides generated from GluC/Trypsin digests. (pan-PTMs search, FDR <1%). Data are from Day65 *SNCA*-triplication neurons pooled across two experimental replicates. **F)** MS2 spectrum for N-terminal GluC peptide covering ser-9.

Carbamylation occurs non-enzymatically when isocyanate, present in the aqueous 8 M urea solution used for protein denaturation, reacts with primary free amines on the N-termini of peptides or in lysine side chains (Stark, Stein and Moore, 1960). Deamidation also occurs spontaneously; and although the timescale for hydrolysis is slow, overnight enzymatic digestions (as used here) increase the abundance of this modification (Krokhin *et al.*, 2006). Lysine mono-methylations were only detected (at low abundance) in one peptide per digest from only one of the two experimental replicates, calling into question the validity of this finding. Moreover, this modification has no known link to PD.

While methionine oxidation can play a physiological role it also occurs *in vitro* during sample preparation and requires specialised methods to discriminate endogenous and artifactual oxidation (Glaser *et al.*, 2005; Bettinger *et al.*, 2019). Accordingly, the recombinant α-synuclein used as a negative control in these experiments was also oxidised on methionine. N-acetylation is a relatively abundant modification which can occur co- or post-translationally to modulate peptide targeting, interactions or stability (McTiernan, Kjosås and Arnesen, 2025). It stabilises α-helices in a variety of proteins including α-synuclein through hydrogen bonding of the acetyl carbonyl group with un-paired hydrogen bond donors at the N-terminal end of the helix (Kang *et al.*, 2012; Trexler and Rhoades, 2012). Met-1 N-acetylation has been widely reported *in vivo* and is accepted to be the default state of α-synuclein, which is not known to be altered by disease status (Öhrfelt *et al.*, 2011; Burré *et al.*, 2013). The identification of N-acetylated Lys-10, Lys-12 and Thr-59 (which must have occurred after digestion), suggests a degree of non-enzymatic N-acetylation in these samples.

Finally, in one experimental replicate three peptides were identified corresponding to phosphorylation of ser-9 in the N-terminus of α-synuclein following the GluC digest. α-

synuclein phosphorylation on Thr-64, Ser-87, Tyr-39, Tyr-125, Ser-129, Tyr-133 and Tyr-136 is strongly linked to PD but ser-9 phosphorylation has never previously been identified (N. de O. Manzanza, Sedlackova and Kalaria, 2021). Moreover, neither UniProt nor PhosphoSitePlus (Cell Signalling Technologies) list ser-9 as a known α-synuclein phosphorylation site in any tissue or disorder. While the peptide intensity was strong in MS1, the putative modification was not observed in the corresponding MS2 spectrum (Fig. 3.2F). Since the exact site could not be localised, the putative phosphorylation was only seen with one of two enzymes in one experiment and there is no known record of this PTM, I concluded that the phospho-ser-9 peptides may be an artifact of our data collection and did not warrant follow-up.

These data suggest that the disease-associated additive PTMs reported in post-mortem tissue are not abundant in mature iPSC-DaNs from PD patients. Other than N-terminal acetylation, phosphorylation on ser-129 is the most abundant PTM *in vivo* (Anderson *et al.*, 2006). Thus, *a priori*, one would expect phospho-ser-129 to be the most abundant modification in iPSC-DaNs from PD patients. Despite coverage of Ser-129 with both enzymes, no peptides with masses corresponding to a phosphorylation in this region were identified. Seeking orthogonal verification, mature *SNCA*-triplication iPSC-DaNs were immunostained for phospho-ser-129 α-synuclein (Fig. 3.3). As a positive control neurons were challenged with α-synuclein PFFs to seed endogenous aggregation which elevates ser-129 phosphorylation (Volpicelli-Daley, Luk and Lee, 2014) – Fig. 3.3A. Consistent with the mass spectrometry results, phospho-ser-129 signal was negligible in the untreated iPSC-DaNs whereas somatic and neuritic staining was detected after 2 weeks of PFF-induced aggregation (Fig. 3.3B).

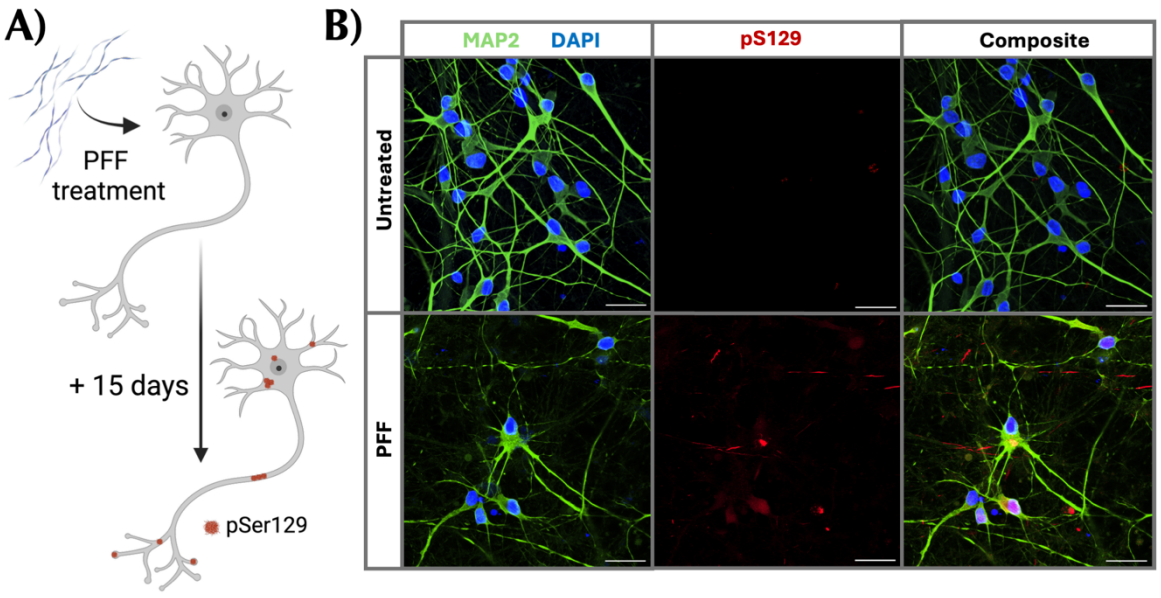

Fig. 3.3 α-synuclein from iPSC-derived dopamine neurons is not phosphorylated on Ser-129 under quiescent conditions. A) Schematic showing the PFF treatment paradigm for positive controls. *SNCA*-triplication neurons at Day35 were treated with 10 µg/ml of PFFs for 48 hours. PFFs were washed out and neurons were incubated for 15 days to allow seeded aggregate pathology to develop. **B)** Representative confocal fluorescence images of Day50 *SNCA*-triplication iPSC-DaNs. Phospho-ser-129 signal is absent in untreated neurons. Scale bar = 25 µm.

Together these data show that in the absence of seeded aggregation, the additive PTMs observed in post-mortem brain tissue are not well modelled in iPSC-DaNs. This finding aligns with the consensus that iPSC-derived neurons model early-stage disease, possibly prior to the accumulation of modifications linked to a pro-aggregation phenotype.

3.4 Biological relevance of low molecular weight α-synuclein

Despite the lack of additive PTMs on α-synuclein in mature iPSC-DaNs, the presence of the maturation-dependent lower molecular weight band (Fig. 3.1C&E, 3.2C) suggests there is heterogeneity in the proteoforms expressed and is worthy of further investigation.

iPSC-DaNs from PD patients exhibit widespread cellular dysfunction including oxidative stress, mitochondrial depolarisation, lysosomal swelling and decreased autophagic flux which arise as a function of time in culture (Cuddy *et al.*, 2019; Virdi *et al.*, 2022; Pitcairn *et al.*, 2023). To examine whether these age-dependent phenotypes were causally involved in the maturation-dependent appearance of low molecular weight α-synuclein, neurons were pharmacologically/nutritionally challenged to modulate dysfunction at Day35 when the low molecular weight proteoform is normally less abundant (Fig. 3.4A). Conditions which respectively cause mitochondrial depolarisation, lysosomal dysfunction, oxidative stress and autophagy activation caused trending increases in low molecular weight α-synuclein abundance but only maturation to Day65 had a significant effect (Young, Martinez and La Spada, 2009; Neely *et al.*, 2017; Zambon *et al.*, 2019; Hasan *et al.*, 2023) - Fig. 3.4B. This suggests that disruption of individual cellular processes contributes only weakly to aberrant α-synuclein processing while the compounded dysfunction caused by aging is required for a more robust effect.

SNpc dopaminergic neurons are preferentially vulnerable to degeneration in PD and α-synuclein-induced toxicity in PD-like animal models, this suggests that the intracellular environment of these cells may be particularly favourable for aberrant α-synuclein processing (Sulzer and Surmeier, 2012; Janezic *et al.*, 2013; Abdelmotilib *et al.*, 2017). Therefore, the cell-type specificity of the α-synuclein lower band was investigated using

a variety of iPSC-derived neuronal models obtained from collaborators in the Kavli Institute[1] (Fig. 3.4C). This demonstrated that the lower molecular weight band was almost exclusively present in dopaminergic neurons. However, total α-synuclein expression was also highest in dopaminergic neurons which may influence detection threshold due to the inherent non-linearity of ECL-based visualisation. To control for this an attempt was made to normalise for α-synuclein expression between the neuron types which still demonstrated a dopaminergic-selective appearance of the lower band (Fig. 3.4D). Interestingly, iPSC-derived sensory neurons also expressed very low levels of the low molecular weight α-synuclein. Capitalising on this low-level expression, sensory and cortical neuronal lysates (which express full length α-synuclein at similar levels) were titrated to further confirm that cell-type specificity was not an artifact of α-synuclein expression level (Fig. 3.4E).

Sensory neurons were also the only other cell type to express TH, raising the possibility that dopamine metabolism is involved in low molecular weight α-synuclein formation. The relationship between TH expression and the abundance of low molecular weight α-synuclein was examined by linear regression using the western blot data presented in Fig. 3.1C. This demonstrated significant linear correlations both at Day75 and Day100 (Fig. 3.4F). However, since western blotting represents bulk analysis of a somewhat heterogenous neuronal culture it remains unclear whether the correlation is simply driven by a higher proportion of the culture being the target dopaminergic cell type or a more causal relationship with monoamine metabolism.

[1]Motor neurons from Dr Lucy Farrimond and Lara Nickel (Talbot Group), Sensory neurons from Dr Jakub Scaber (Talbot Group), Cerebellar neurons from Dr Elizabeth Apsley (formerly Becker Group), Cortical neurons from Féodora Bertherat (Wade-Martins Group), Microglia from Anne Sophie Gry Larsen (Wade-Martins Group) and Astrocytes from Dr Naroa Ibarra Aizpurua (formerly Wade-Martins Group).

A)

Treatment	Desired effect
CCCP dose	A protonophore/uncoupler which depolarizes mitochondria
Chloroquine (CQ) dose	Inhibits autophagosome-lysosome fusion reducing autophagic flux
Rotenone (ROT) dose	Inhibition of Complex I increases production of ROS
Nutrient starvation	B27 deprivation induces neuronal autophagy through mTOR

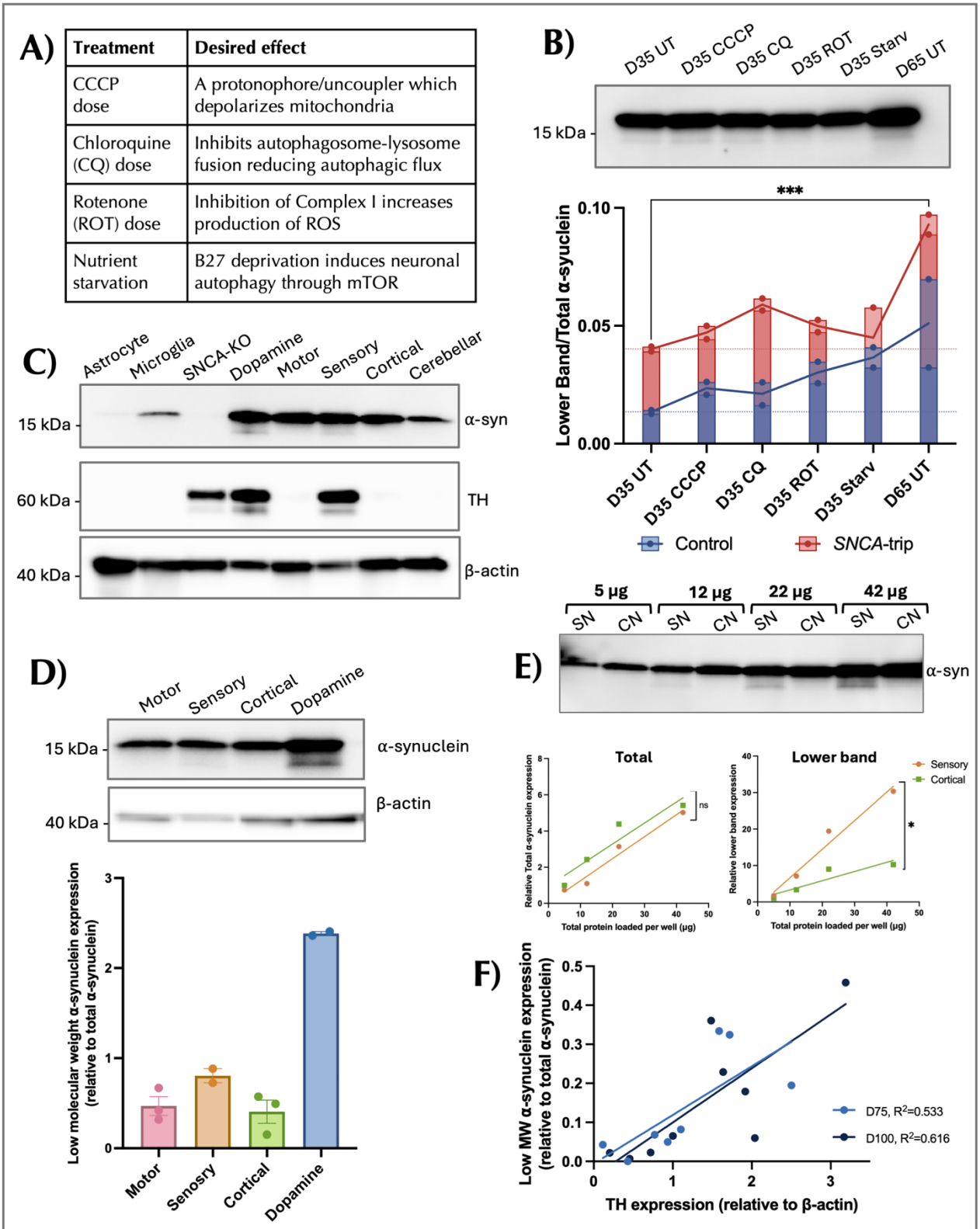

Fig. 3.4 Assessing cellular causes of low molecular weight α-synuclein.
A) Table of treatment conditions used to mimic age-dependant dysfunction in iPSC dopamine neurons. Treatments lasted 72 hours at the following dosages: CCCP 1 µM, CQ 2 µM and ROT 25 nM **B)** Representative western blot from *SNCA*-triplication dopamine neurons and relative quantification of low molecular weight band intensity. N = 2 cell lines per genotype. Two-way ANOVA shows a significant effect of genotype ($p_{Genotype}$<0.0001) and treatment ($p_{Treatment}$=0.005) and Dunnett's Multiple Comparisons test only showed a significant increase for… (cont. over leaf)

…maturation to Day65 but not any of the treatments. **C)** western blot showing full length and low molecular weight α-synuclein, as well as TH and β-actin expression from iPSC-derived neurons and glia from healthy controls. The *SNCA-KO* iPSC line was differentiated to dopaminergic neurons as a negative control. All cells were considered mature according to their respective protocols and were harvested between Day40 and Day65. 10 µg of total protein was loaded per lane. **D)** Representative western blot and densitometric quantification showing low molecular weight α-synuclein in iPSC neuron lines normalizing input for total α-synuclein expression based on the results of C). **E)** Western blot and densitometric quantification from healthy control sensory (SN) and cortical (CN) neurons loading 5-42 µg of total protein per lane, showing the abundance of total and lower molecular weight α-synuclein as a function of protein input. ANCOVA showed a significant effect of cell type on low molecular weight α-synuclein, but not total α-synuclein with increasing protein concentration $F(1,4) = 17.36$ $p=0.0141$. **F)** Simple linear regression correlating β-actin normalised TH expression and fractional low molecular weight α-synuclein abundance across control, *SNCA*-triplication and *GBA1-N370S* cell lines at Day75 and Day100 of differentiation. N=2 differentiations, each data point represents one cell line from one differentiation. $p_{Day75}=0.0396$ and $p_{Day100}=0.0122$.

Soluble α-synuclein can also be detected in post-mortem human brain tissue using a similar procedure for protein extraction and sample preparation (Fig. 3.5A). In line with previous findings, this demonstrates that soluble α-synuclein in the cortex is reduced in PD patients compared to age-matched healthy controls (Zhou *et al.*, 2011) - Fig. 3.5B, likely due to sequestration in detergent-insoluble aggregates. Comparing the western blot migration of α-synuclein across brain regions from one Braak Stage 5 PD patient demonstrated region-specific appearance of low molecular weight α-synuclein with the same gel shift as found in iPSC-DaNs (Fig. 3.5C&D). As for the iPSC-derived neuronal lysates, post-mortem brain homogenates were reblotted adjusting for total α-synuclein expression, which demonstrated that the selective appearance of the lower band in amygdala and substantia nigra was not an artifact of higher total α-synuclein expression. In the post-mortem samples there was no correlation between regions expressing high levels of TH and low molecular weight α-synuclein, although it is worth noting that these tissue samples contained a mixture of cell types including neurons, glia and to a lesser extent, neurovasculature.

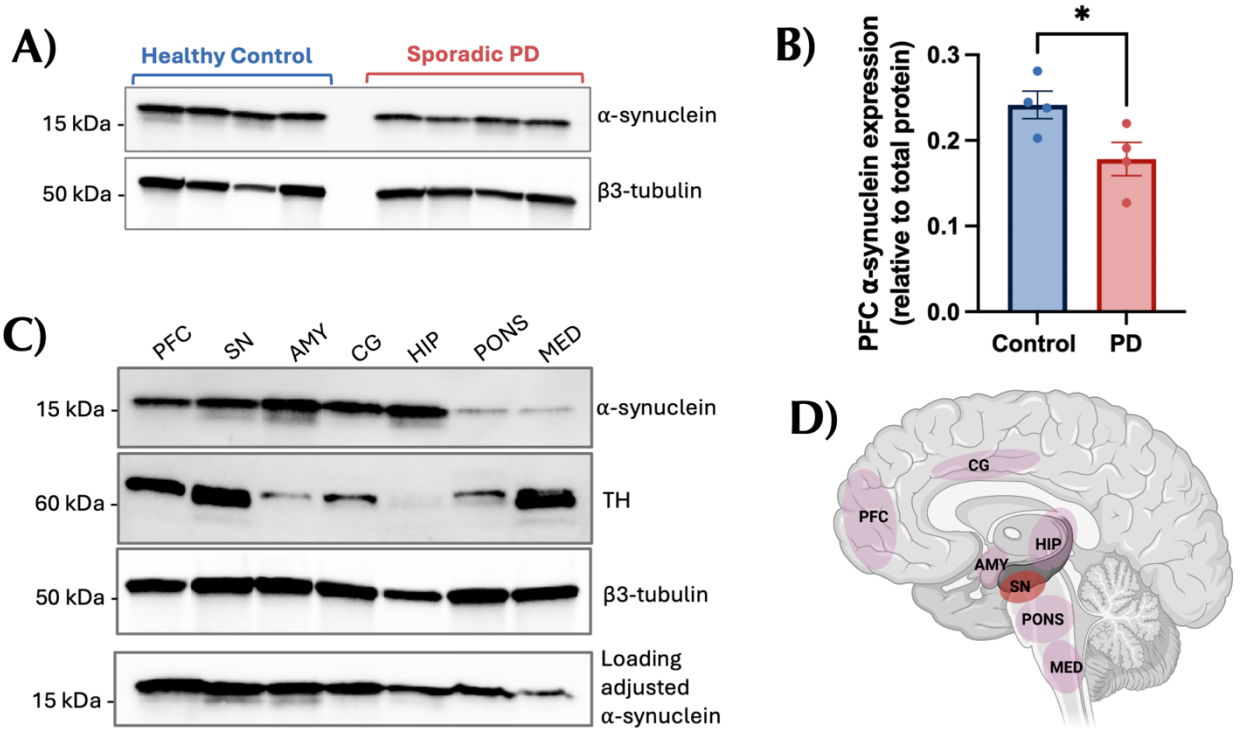

Fig. 3.5 Expression of low molecular weight α-synuclein varies between brain regions. **A)** Western blot and **B)** densitometric quantification of soluble α-synuclein in human post-mortem prefrontal cortex from four Braak Stage 4-6 PD patients and four age-matched controls. Results are normalised to total protein loaded per lane determined by stain-free tri-halo imaging. Two-tailed students t-test p=0.046. **C)** Western blot of soluble α-synuclein, β3-tubulin and TH extracted from the brain regions shown in D) from one 75-year-old male PD patient (Braak stage 5). Blots from 20 µg total protein, or input adjusted for total α-synuclein expression are shown. **D)** α-synuclein was quantified in the prefrontal cortex (PFC), substantia nigra (SN), amygdala (AMY), cingulate gyrus (CG), hippocampus (HIP), Pons (PONS) and medulla (MED).

Due to limited tissue availability, it was not possible to compare the expression of low molecular weight α-synuclein in the amygdala or substantia nigra between PD patients and controls. In iPSC-DaNs there was no difference between genotypes, however the maturation-dependence and cell-type specificity suggest a possible association with disease processes. Moreover, the abundance in post-mortem brain correlates with regions that develop a higher burden of aggregate pathology and are more vulnerable to degeneration (Braak *et al.*, 2003). Overall, these findings motivated further work to identify the origin and identity of the low molecular weight proteoform.

3.5 Alternative splicing of α-synuclein in iPSC-DaNs

A reduction to the observed molecular weight of α-synuclein on SDS-PAGE could be caused either by alternative mRNA splicing or post-translational truncation. In this section I use two transcriptomic datasets to investigate the former possibility.

The skipping of exons 4, 6 or both result in 126-, 112- or 98-amino acid isoforms of α-synuclein, while inclusion of a small portion of intron 4 gives rise to a 115-amino acid form (Beyer and Ariza, 2013; Janeczek *et al.*, 2015) – Fig. 3.6A. Alternative splicing also occurs within the 5′ untranslated region (UTR) giving rise to 4 possible 5′ UTRs. Of these, inclusion of exon 2a (giving rise to SNCA-205/NM_000345 when no coding exons are skipped) is the most common (Beyer and Ariza, 2013; Gámez-Valero and Beyer, 2018)[2]. Primers were designed spanning exon 2a/exon 3 ~20bp upstream of the start codon and ~20bp downstream of the stop codon in exon 7. These should amplify the entire coding sequence for 140-, 126-, 112- and 98-amino acid α-synuclein (though not the 115-amino acid isoform, due to the distinct 3′ UTR) which use exon 2a in the 5′ UTR. Primers may also provide lower efficiency amplification of transcripts with exon 1 or 2b in the 5′ UTR based on sequence homology. mRNA was reverse transcribed and then PCR amplified. Agarose gel electrophoresis of the PCR products yielded a single band at ~500bp corresponding to the 498bp sequence expected in the absence of exon skipping, i.e. mRNA encoding 140-amino acid α-synuclein (Fig.3.6B). This finding suggests that the majority of *SNCA* mRNA transcripts in healthy control and *SNCA*-triplication iPSC-DaNs are not alternatively spliced.

[2] The nomenclature for different transcript variants is inconsistent in the literature. In this thesis all transcripts are referenced by their NCBI RefSeq and Ensembl Transcript names.

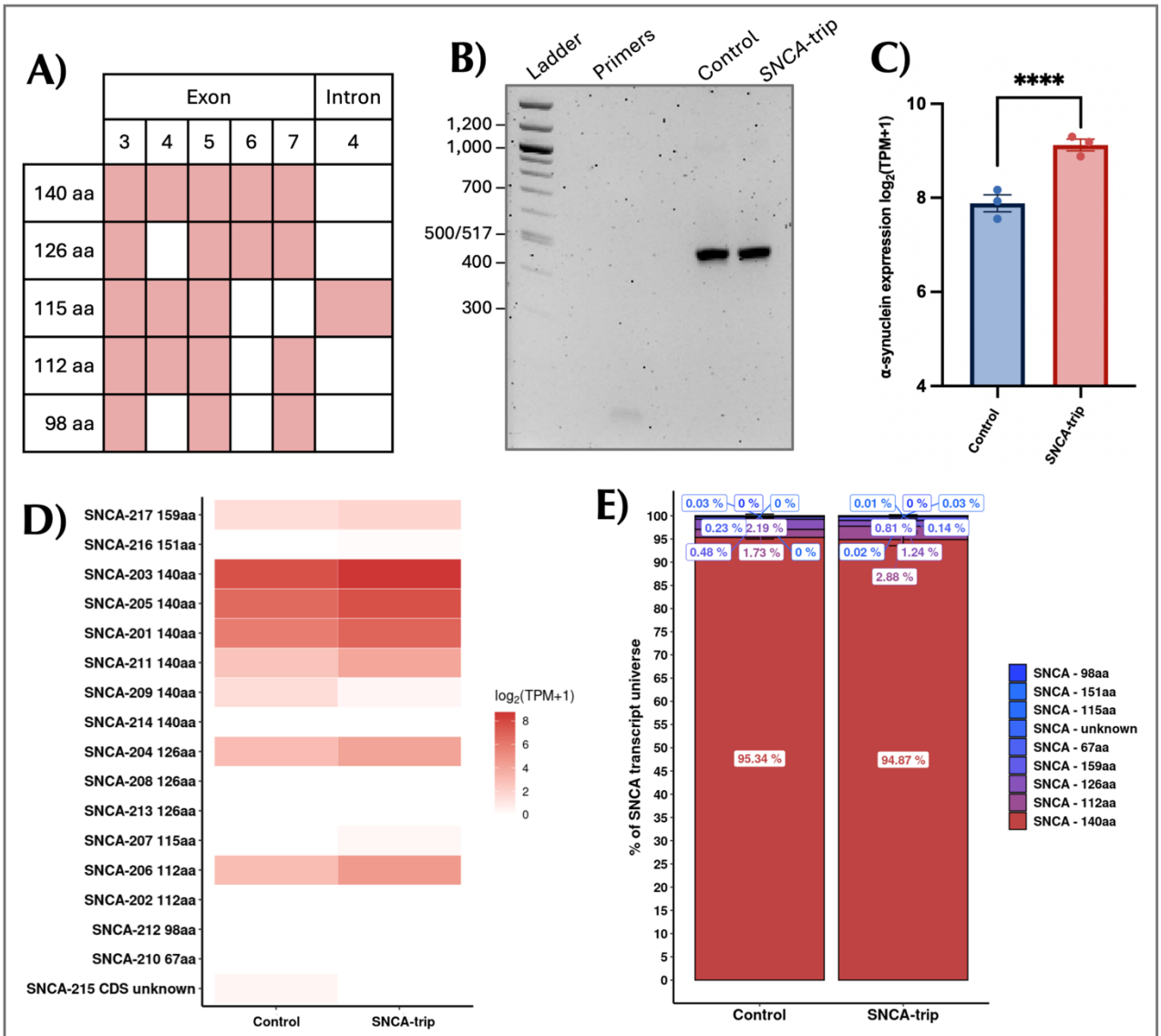

Fig. 3.6 Low molecular weight α-synuclein is not caused by alternative mRNA splicing.
A) Table showing the exons which are spliced together to generate the known isoforms of alternatively spliced α-synuclein that could correlate to the molecular weight of the lower α-synuclein band on SDS-PAGE. For 115aa α-synuclein a small section of intron 4 is included rather than exons 6 and 7. **B)** Agarose gel following PCR of the entire *SNCA* coding sequence using cDNA reverse transcribed from mRNA extracted from Day100 neurons. Only one dominant *SNCA* band at approximately 500bp was observed (expected length of PCR product 498bp). **C)** Total *SNCA* expression in control and *SNCA*-triplication dopamine neurons at Day70 presented as $\log_2$(TPM+1) values. Differential gene expression analysis was carried out using raw counts using DESeq2, and a Wald test shows significant difference in expression between genotypes. **** p_{adj} <0.0001. **D)** Tile plot showing the abundance of distinct *SNCA* splice variants. **E)** Proportional abundance of transcripts corresponding to full length or shortened coding sequences as well as one non-coding transcript. Data presented as mean ± standard deviation.

To validate this finding with a more sensitive approach, short-read bulk mRNA sequencing data from healthy control and *SNCA*-triplication iPSC-DaNs (a dataset

gathered by Dr Benjamin Vallin) was interrogated for evidence of alternative *SNCA* splicing. As expected, the expression of all mRNA transcripts encoding α-synuclein was elevated in the *SNCA*-triplication neurons compared to control (Fig. 3.6C). Separate analysis of the abundance of all 32 known transcript variants, showed that SNCA-203/NM_001146054.2, encoding 140-amino acid α-synuclein with use of exon 2b in the 5′ UTR was most abundant in the iPSC-DaNs from patients and controls.

This analysis showed that whilst a variety of transcripts were expressed the majority encode full length 140-amino acid α-synuclein, differing only in their untranslated regions (Fig. 3.6D). By summing the abundance (TPM) of transcripts encoding the same α-synuclein isoforms and rescaling the summed abundances it was clear that ~95% of the mRNAs encode full length α-synuclein in both *SNCA*-triplication and control iPSC-DaNs while 112- and 126-amino acid isoforms contribute only fractionally to the total *SNCA* transcript pool (Fig.3.6E).

Together these data suggest that low molecular weight α-synuclein detected by western blot in *SNCA*-triplication and control iPSC-DaNs cannot be the product of alternative splicing, since the abundance of transcripts encoding isoforms of this molecular weight is too low. However, the identification of low molecular weight α-synuclein in brain tissue from a sporadic PD patient (Fig. 3.5C) motivated further study in iPSC-DaNs from patients with sporadic PD. The FOUNDIN-PD dataset includes short-read mRNA sequencing from 95 iPSC lines including healthy controls, prodromal/SWEDD, unaffected mutation carriers and sporadic or monogenic PD patients (Bressan *et al.*, 2023). Both the *SNCA*-triplication and *GBA1-N370S* mutations studied in this chapter are represented among the monogenic PD group. Pooling data for sporadic and

monogenic PD lines, as well as for prodromal and asymptomatic mutation-carriers, total *SNCA* expression was compared across groups and found not to differ with disease status (Fig. 3.7A). As for the iPSC-DaNs grown in-house (Fig. 3.6), a variety of transcripts were expressed, though in the FOUNDIN-PD neurons SNCA-201/NM_001146055 which includes exon 1 in the 5′ UTR was the most abundant (Fig. 3.7B). The abundance of transcript variants encoding the same α-synuclein isoform were summed and rescaled, demonstrating that while most transcripts encode full length α-synuclein the 115- and 112-amino acid isoforms were markedly more abundant than in our neurons though this did not differ with disease status (Fig. 3.7C).

A key advantage of the FOUNDIN-PD dataset is the availability of sequencing data for Day0 and Day25 timepoints as well as mature Day65 neurons. The abundance of low molecular weight α-synuclein measured by western blot increased with neuronal maturity (Fig. 3.1C&E), motivating investigation of splice isoforms over time. Total α-synuclein expression increased with differentiation from iPSCs to neurons in all three groups in line with its function as a synaptic protein and results at the protein level (Fig. 3.1C&D, 3.7D). Interestingly, the proportion of transcripts encoding full length (140-amino acid) α-synuclein showed a trending increase throughout differentiation in healthy controls, which became significant in the prodromal and PD groups (Fig. 3.7E-G). This trend appears to be driven by increased abundance of shorter splice isoforms at the iPSC stage. Although these results do not provide further insight toward the origin of the low molecular weight α-synuclein in mature neurons, they suggest large differences in *SNCA* mRNA processing through neuronal development. Overall, analysis of both transcriptomic datasets indicates that the lower molecular weight α-synuclein observed by western blot must arise through post-translational processing.

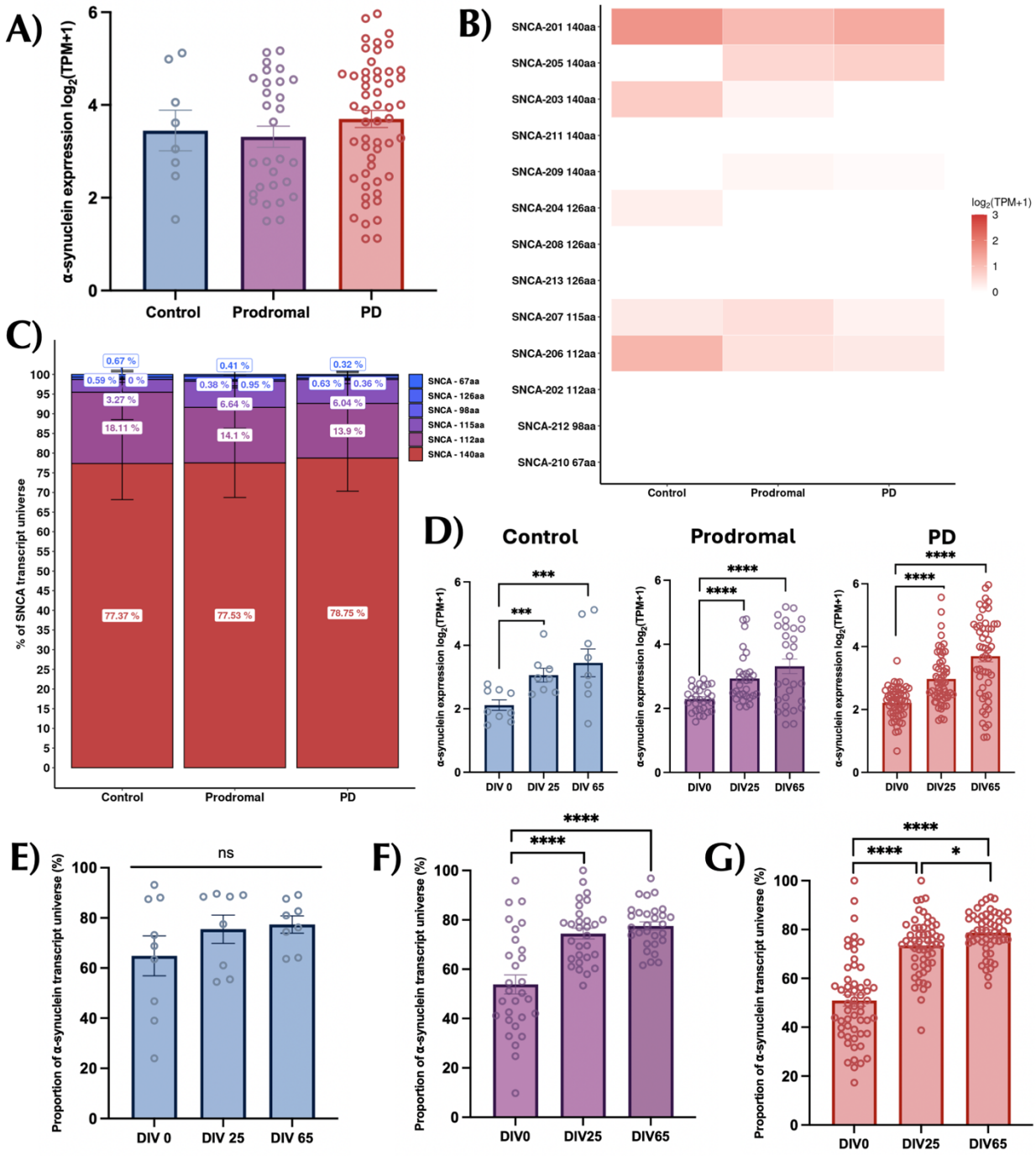

Fig. 3.7 Alternatively spliced α-synuclein is more abundant early in differentiation in FOUNDIN-PD iPSC-DaNs. A) Total *SNCA* expression in healthy control, prodromal and PD patient neurons from the FOUNDIN-PD dataset at Day65 of differentiation. Each data point represents a distinct donor. Likelihood ratio testing shows a significant effect of disease status ($p<0.0001$), but no pair-wise Wald tests reach significance. **B)** Tile plot showing abundance of distinct *SNCA* splice variants. **C)** Proportional abundance of transcripts corresponding to full length or shortened coding sequences. Data presented as mean ± standard deviation. **D)** Total *SNCA* expression throughout differentiation by disease status. Wald tests show a highly significant increase in α-synuclein over time. The percentage of transcripts corresponding to 140-amino acid α-synuclein in **E)** Healthy control, **F)** Prodromal and **G)** PD patient-derived cells. Repeated measures ANOVA and Bonferroni post-hoc testing shows significant effects of maturation to Day 25 and Day65 in prodromal and PD neurons. *p_{adj} <0.05, **p_{adj} <0.01, ***p_{adj} <0.001, **** p_{adj} <0.0001.

3.6 Investigating proteolytic truncation of α-synuclein

The only known α-synuclein PTM which can reduce its apparent molecular weight on SDS-PAGE is proteolytic truncation. Studies in post-mortem brain have identified a range of truncation sites in the N- and C-termini of α-synuclein giving rise to numerous truncated products with increased aggregation propensity (Li *et al.*, 2005; Suthar and Lee, 2023). To investigate this, four commercially available antibodies with epitopes against the C-terminus of α-synuclein were used for western blot detection. In the case of a C-terminal truncation antibodies with epitopes distal to the cut-site should not detect the low molecular weight band.

All four antibodies detected the lower band (Fig. 3.8A), although it was only observed with 4D6 in two out of three replicate experiments. The final 6 amino acids (loss of which would generate a truncation product of 13.6 kDa) were not covered in this paradigm. As a complementary approach α-synuclein was immunoprecipitated from cell lysates using either the antibody MJFR1 (Subchapter 2.4.3.1) or the nanobody NbSyn2 (Subchapter 2.4.4.1) and detected with Syn1 (Fig. 3.8B&C). Since the epitope of Syn1 is in the NAC region this should detect all isoforms such that only the antibody/nanobody used for IP conveys sequence selectivity. Low molecular weight α-synuclein was detected even with pull-down using NbSyn2 which targets only the final 4 amino acids of the α-synuclein sequence (Fig. 3.8C), suggesting that the putative truncation cannot be C-terminal. Interestingly, following nanobody pull-down blots revealed two low molecular weight bands which had not previously been resolved.

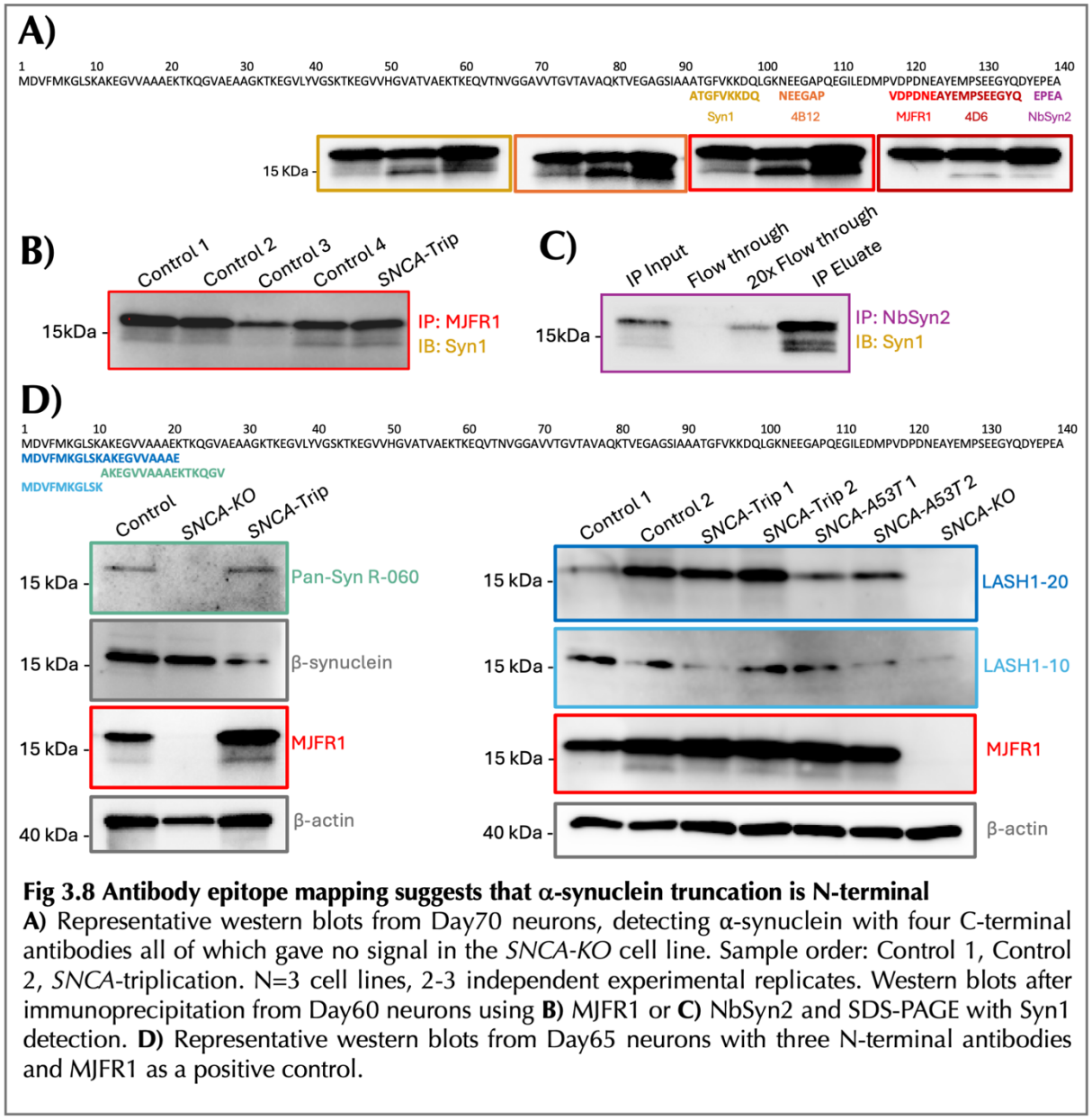

Fig 3.8 Antibody epitope mapping suggests that α-synuclein truncation is N-terminal
A) Representative western blots from Day70 neurons, detecting α-synuclein with four C-terminal antibodies all of which gave no signal in the *SNCA-KO* cell line. Sample order: Control 1, Control 2, *SNCA*-triplication. N=3 cell lines, 2-3 independent experimental replicates. Western blots after immunoprecipitation from Day60 neurons using **B)** MJFR1 or **C)** NbSyn2 and SDS-PAGE with Syn1 detection. **D)** Representative western blots from Day65 neurons with three N-terminal antibodies and MJFR1 as a positive control.

If low molecular weight, putatively truncated α-synuclein has an intact C-terminus then the truncation must be N-terminal. Unfortunately, the intrinsically dynamic nature of the N-terminus (existing in disordered, helical, and β-stranded conformations) poses significant challenges for antibody design. Cinepanemab, trialled as a passive immunotherapy for PD, binds residues 1-10 but exhibits >800-fold increased affinity for aggregated rather than monomeric α-synuclein highlighting the profound impact of conformational flexibility in this region (Weihofen *et al.*, 2019). Additionally, the N-

terminus of α-synuclein shares considerable sequence homology with β- and ɣ-synucleins resulting in a lack of commercially available high-affinity, high-specificity antibodies. The pan-synuclein antibody pan-syn-R-060 showed a single band for α-synuclein which was absent in *SNCA-KO* iPSC-DaNs, while the double band was observed with C-terminal MJFR1 in the same samples (Fig. 3.8D). Two custom-made antibodies gifted by the Lashuel lab were trialled with iPSC-DaN lysates from a range of familial PD genotypes, both of which failed to detect the low molecular weight α-synuclein band (Fig. 3.8D).[3] However, the LASH1-10 antibody also detected a small amount of protein in the *SNCA-KO* cell line suggesting possible non-specific detection of β- and ɣ-synucleins (Fig. 3.8D).

Together the epitope mapping data tentatively suggest that low molecular weight α-synuclein is the result of an N-terminal truncation which wholly or partially deletes the epitopes of Pan-Syn R-060, LASH1-10 and LASH1-20. However, orthogonal validation was necessary to overcome the caveats of epitope mapping with low specificity antibodies and to more exactly localise the cleavage site.

The mass spectrometry experiments described in Subchapter 3.3 were not expected to detect truncation products since full length and truncated α-synuclein were digested together. Intact mass spectrometry, without proteolysis, should avoid this caveat since full length and truncated α-synuclein would be detected as different molecular weights. In collaboration with Dr Neha Kalmankar in the Robinson Group[4] immunoprecipitated

[3] Detection of α-synuclein with LASH1-10 in *SNCA-KO* iPSC-DaNs is expected as the knockout strategy used to generate this line allows a short N-terminal sequence to be translated before the frame-shift deletion and premature stop codon which were introduced with CRISPR/Cas9 gene editing.

[4] Intact mass spectrometry and gel band digests were undertaken in collaboration with Dr Kalmankar. I grew the cells, carried out the immunoprecipitation, gel staining and mass spec sample preparation. Neha assisted with gel band excision and set the parameters LC-MS/MS run which I carried out according to her instructions. We contributed equally to experimental design and planning.

α-synuclein was subjected to intact mass spectrometry under native conditions. Although it was possible to detect clear peaks for recombinant α-synuclein controls (with charge states varying between +5 and +8) the low concentration of cell-derived α-synuclein, even after immuno-enrichment, rendered it undetectable with this approach (data not shown).

As an alternative approach full length and putatively truncated α-synuclein were immunoprecipitated, separated by SDS-PAGE and silver stained, after which bands excised and digested separately. Silver staining demonstrated that in addition to the full length and low molecular weight bands observed previously by western blot there were also faint bands at an even lower molecular weight, which were not detected with antibodies (Fig. 3.9A). To be within the working range of silver stain detection (~0.5-5 ng α-synuclein per band), cell lysates from ~30 million iPSC-DaNs were pooled, representing a 10-15-fold increase in the amount of cell material usually used for a single assay. It was therefore not feasible to carry out parallel experiments digesting with trypsin and GluC to achieve full sequence coverage. Based on analysis of predicted cut sites of all available enzymes we decided to combine trypsin and chymotrypsin in a single digestion to increase the probability of both N- and C-terminal coverage (Fig. 3.9B). Peptides from all three identified bands were search against the UniProtKB/Swiss-Prot database using trypsin, chymotrypsin or semi-trypsin parameters (to find peptides with two tryptic ends, two chymotryptic ends or which had been generated by cleavage with both enzymes). This approach gave full coverage of the full-length band, but the N-

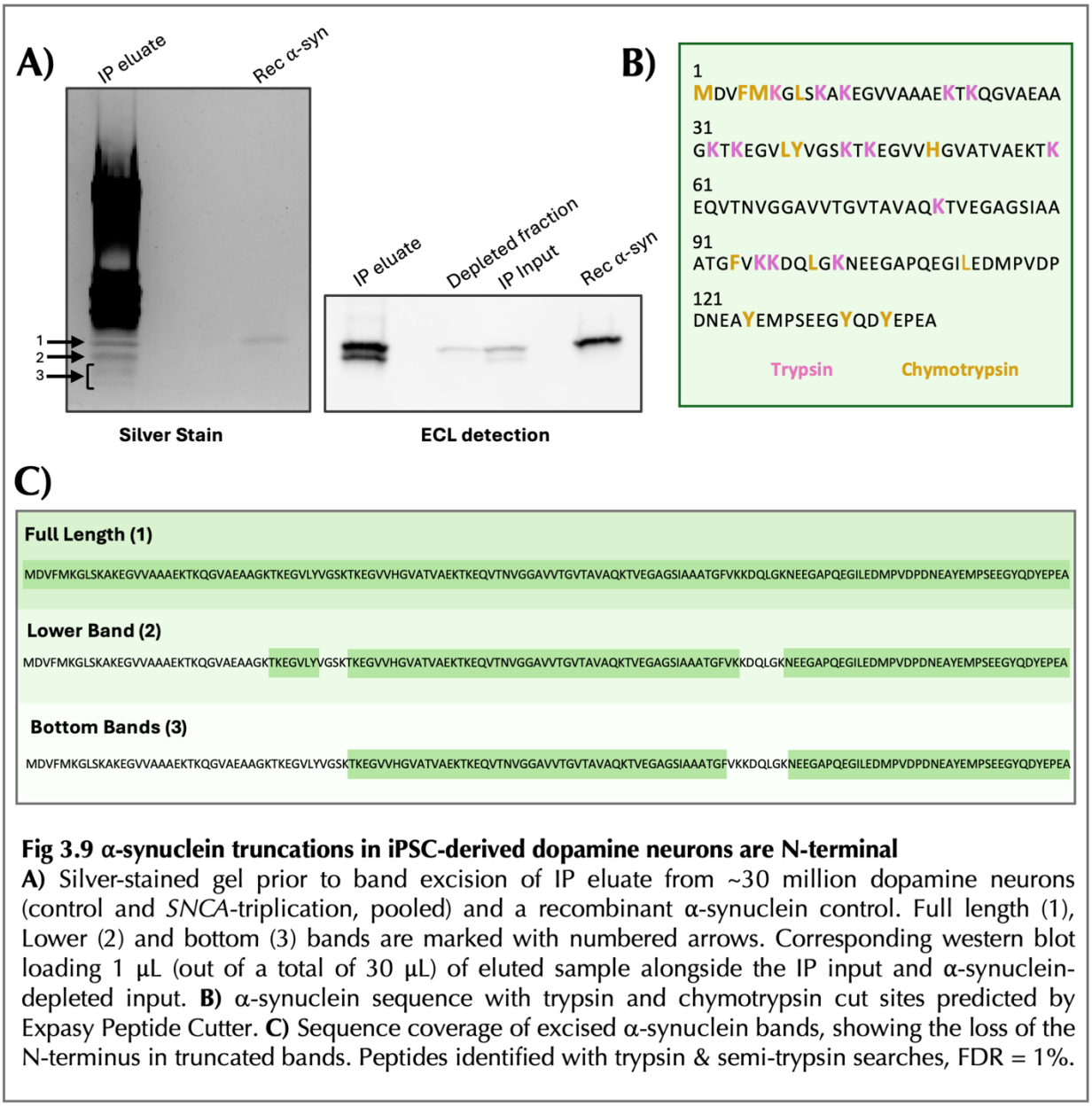

Fig 3.9 α-synuclein truncations in iPSC-derived dopamine neurons are N-terminal
A) Silver-stained gel prior to band excision of IP eluate from ~30 million dopamine neurons (control and *SNCA*-triplication, pooled) and a recombinant α-synuclein control. Full length (1), Lower (2) and bottom (3) bands are marked with numbered arrows. Corresponding western blot loading 1 µL (out of a total of 30 µL) of eluted sample alongside the IP input and α-synuclein-depleted input. **B)** α-synuclein sequence with trypsin and chymotrypsin cut sites predicted by Expasy Peptide Cutter. **C)** Sequence coverage of excised α-synuclein bands, showing the loss of the N-terminus in truncated bands. Peptides identified with trypsin & semi-trypsin searches, FDR = 1%.

terminus (amino acids 1-32) was missing for the low molecular weight band (labelled 2) – Fig. 3.9C. To confirm this was not a false negative result, i.e. failing to identify N-terminal peptides if they were less abundant, we relaxed the search parameters to a false discovery rate of 5% and repeated the analysis. Even with these less stringent settings we no N-terminal peptides were identified for the lower band. Hence, we can conclude that lower molecular weight proteoform results from N-terminal truncation.

The N-terminus was also missing in the lowest bands which were only identified with silver staining but not antibodies. Corresponding to their lower apparent molecular weight on SDS-PAGE a larger region of the N-terminus was absent (Fig. 3.9C). Given that the C-terminus (containing antibody epitopes) appeared to be intact it is surprising that these truncated products were not visualised with antibody detection.

Overall, the epitope mapping and mass spectrometry presented in this section confirm that α-synuclein in iPSC-DaNs is N-terminally truncated in a maturation-dependent manner. While this does not differ between genotypes, dopaminergic neurons appear to be selectively vulnerable to this aberrant α-synuclein processing.

3.7 Discussion

iPSC-DaNs expressing multiple markers of dopaminergic fate, and which previous work has shown to be electrophysiologically active (Beccano-Kelly *et al.*, 2023), abundantly express α-synuclein. α-synuclein protein expression increased over time in healthy controls and two familial PD genotypes (Fig. 3.1D), corresponding to an increase in mRNA expression in control, prodromal and sporadic PD neurons (Fig. 3.7D). In line with the increased gene dosage and previous literature α-synuclein expression was approximately 2-fold higher in *SNCA*-triplication iPSC-DaNs than controls (Devine *et al.*, 2011; Oliveira *et al.*, 2015) - Fig. 3.1H. Consistent with our group's published findings there was no evidence of α-synuclein accumulation in the heterozygous *GBA1-N370S* iPSC-DaNs, although this contrasts with other reports that have shown increases in protein but not mRNA (Woodard *et al.*, 2014; Fernandes *et al.*, 2016; Kim *et al.*, 2018; Yang *et al.*, 2020). Where reported, accumulation is explained by impaired degradation due to lysosomal dysfunction, although this is a subtle phenotype with some authors only observing significant α-synuclein accumulation in homozygotes but not heterozygous *GBA1-N370S* lines (Schöndorf *et al.*, 2014). While time course SDS-PAGE demonstrated a trending increase in α-synuclein expression in *SNCA*-triplication iPSC-DaNs (Fig. 3.1D), repetition with four differentiations was required to reach statistical significance (Fig. 3.1H). Similarly powered experiments were not performed with *GBA1-N370S* neurons; hence a potentially milder phenotype could have been missed.

Here, I show that mature iPSC-DaNs from the Kriks protocol do not abundantly express the shorter mRNA transcripts for *SNCA* which have been reported to arise through alternative splicing. Short read RNA-sequencing and PCR demonstrate that ~95% of

transcripts encode 140-amino acid full length α-synuclein although there is some variability in the 5'UTR included. This correlates well with previous work in control, PD and DLB brain samples where 95-97% transcripts also contain all 6 exons (Tseng *et al.*, 2019). Interestingly, SNCA-203 which has a much longer 5'UTR through use of exon 2b rather than the canonical exon 2a was the most abundant in these neurons. Except for a short sequence of ~30bp at the 3' end, all of exon 2a is conserved in exon 2b with the addition of 279 bases. This indicates that secondary structural regulatory elements including G-quadruplexes, internal ribosome entry sites and iron response elements which have been well-studied in exon 2a of SNCA-205/NM_000345 are likely to be conserved in SNCA-203. Furthermore, it opens the possibility for additional regulatory sites which may be important in the iPSC-DaNs (Koukouraki and Doxakis, 2016). By contrast exon 1 seems more commonly in the FOUNDIN-PD dataset (Fig. 3.7B). Exon 1 is markedly shorter and shares little to no homology with the exon 2 variants, and as such must use a distinct mode of translational regulation. These findings are important for the use of iPSC-DaNs in developing α-synuclein-targeting therapeutics. For example, Synucleozoid is a small molecule which binds to iron response elements in the 5' UTRs encoded by exon 2 variants to reduce α-synuclein translation (Zhang *et al.*, 2020). Since exon 1 lacks these iron response elements any potential efficacy of this drug could be missed if only trialled in a SNCA-201 dominant cell populations.

Whilst still representing the majority of transcripts, mRNA encoding full length α-synuclein was of lower relative abundance in the FOUNDIN-PD neurons independent of disease status. The relative abundance of full length α-synuclein increased over time from iPSCs to mature neurons (Fig. 3.7E-G). While α-synuclein is expressed in the developing nervous system, it does not have a known role in stem cells before

commitment to neural fate. Assuming, therefore, that exon skipping is a developmental phenotype the lower proportion of full length α-synuclein in Day65 FOUNDIN-PD neurons compared to those grown in our lab may indicate comparative immaturity. While a modified version of the Kriks protocol was used in both cases it is worth noting that scRNAseq suggests that only 23% of the Day65 population of FOUNDIN-PD cells are mature dopaminergic neurons with a further 10% being immature dopaminergic neurons (Bressan *et al.*, 2023). However, it is worth noting that the total expression of α-synuclein at Day0 is low, so a seemingly large reduction in proportion of 140-amino acid α-synuclein corresponds to only a small change in absolute terms (Fig. 3.7D).

Low expression of 112- and 126-amino acid α-synuclein was observed in Dr Vallin's dataset, while 112- and 115- amino acid α-synuclein were found in control, prodromal and PD iPSC-DaNs from the FOUNDIN-PD dataset. The exclusion of exon 6 and consequent deletion of a large proportion of the acidic C-terminus in the 112-amino acid isoform increases aggregation, whereas there is no effect of 126-amino acid α-synuclein on aggregation kinetics in solution, though it accelerates aggregation within phase separated condensates (Röntgen *et al.*, 2024, 2025). The 115-amino acid isoform has not been linked to PD but shows elevated expression in the brains of individuals with alcohol use disorder (Janeczek *et al.*, 2015). This splicing event also causes loss of negative amino acids from the C-terminus, increasing the predicted isoelectric point from 4.67 to 9.12. Hence, 115-amino acid α-synuclein is also likely to be more aggregation prone.

It is worth noting that a recent pre-print identified numerous previously-unknown splice isoforms of α-synuclein in iPSC-DaNs using long read RNA sequencing (Evans *et al.*, 2024). Even if highly abundant these, and other, novel transcripts would not be detected

in the above analysis which used Salmon to map sequencing reads to known transcripts (Patro *et al.*, 2017). It is therefore possible that a greater transcript diversity exists than I have reported, although PCR and agarose gel electrophoresis suggest that any such transcripts are unlikely to be abundant (Fig. 3.6B). Future work could perform *de novo* transcriptome assembly with tools such as StringTie to investigate the possibility of novel *SNCA* isoforms in the bulk mRNA sequencing datasets used here (Pertea *et al.*, 2015).

To the best of our knowledge this is the first study to take a proteomic mass spectrometry approach to analysing α-synuclein PTMs in iPSC-DaNs. Creating an assay suitable for studying a stem cell disease model marks a notable achievement in experimental downscaling since input material is heavily limited compared to classical expression systems used in biochemistry/biophysics. α-synuclein expressed by mature *SNCA*-triplication iPSC-DaNs was found to be carbamylated, deamidated, mono-methylated, N-acetylated, oxidised and possibly phosphorylated, however there was no robust evidence of disease-linked modifications. Carbamylation, deamidation and oxidation are all non-enzymatic processes which can occur during sample preparation or with time post-translation as a hallmark of cellular aging (Gorisse *et al.*, 2016; Adav and Sze, 2020). As such they have been linked to various neurodegenerative disease including PD as one of many mechanisms through which aging-associated cellular dysfunction precipitates amyloidogenesis. For example, carbamylation reduces the charge of a protein by neutralising amine groups and *in vitro* work suggests that carbamylation of the KTKEGV repeats increases aggregation of α-synuclein (Gadhavi *et al.*, 2025). Oxidised α-synuclein has been detected with the putatively oxidation-selective antibody syn303 in iPSC-DaNs but LC-MS/MS identification requires specialised experimental design to discriminate cell-derived and sample preparation-induced modifications

(Glaser *et al.*, 2005; Burbulla *et al.*, 2017, 2019; Bettinger *et al.*, 2019; Kim *et al.*, 2023). To specifically study these disease-linked but non-enzymatic PTMs alternative approaches, e.g. alkylation of unoxidized methionine residues, are required prior to sample preparation. Such measures were not adopted here as enzymatic processes, specifically phosphorylation, were the target.

Although peptides with masses corresponding to a possible phosphorylation on serine-9 were identified, these could not be verified in MS2 spectra. Moreover, this site is not known to be a phosphorylated in PD or any other conditions. No other phospho-peptides were identified including phospho-ser-129 phosphorylation which is detected in post-mortem brain by mass spectrometry even when other modifications are below the detection limit (Anderson *et al.*, 2006). Despite being undetected in our neurons with mass spectrometry and immunocytochemistry other groups have occasionally reported phospho-ser-129 α-synuclein in *SNCA*-triplication iPSC-DaNs (Lin *et al.*, 2016; Virdi *et al.*, 2022). These reports differ from the current study regarding the differentiation protocols used as well as their reliance on phosphorylation-selective antibodies in the absence of de-phosphorylated/recombinant α-synuclein controls. Virdi and colleagues argue that phosphorylation occurs as a late phenotype, arising after oligomerisation in their differentiation protocol which could suggest that this PTM may eventually be detectable in our cells with longer maturation. In the absence of PFF insult, serine-129 phosphorylation has been more widely reported in iPSC-DaNs carrying the pro-aggregation *SNCA-A53T* mutation (Kouroupi *et al.*, 2017; Ryan *et al.*, 2018; Stykel *et al.*, 2021). This alludes to a double-hit hypothesis where both α-synuclein accumulation and accelerated aggregation are required to induce phosphorylation within a tractable differentiation timescale (Kouroupi *et al.*, 2017; Ryan *et al.*, 2018; Stykel *et al.*, 2021). In

future work, combining longer differentiation with a phospho-protein enrichment strategy such as immobilised metal affinity chromatography or titanium oxide affinity chromatography, may increase sensitivity for any super-low abundance phosphorylated α-synuclein proteoforms (Yu and Veenstra, 2021). Enrichment protocols also exist for other reported α-synuclein PTMs which were not detected in my experiments such as o-GlcNAcylation (Wang *et al.*, 2010). However, the risk of sample loss from additional preparative steps for such low volume/concentration samples should be carefully considered. Moreover, it is likely that genotypic differences would be difficult to infer when working close to the detection limit of these approaches. Instead, the data presented here suggest that iPSC-DaNs model an earlier stage of disease prior to the formation of large, phosphorylated aggregates, and should be used accordingly to investigate the first stages of cellular dysfunction.

Despite the lack of additive PTMs, α-synuclein was found to be N-terminally truncated in control, *SNCA*-triplication and *GBA1-N370S* iPSC-DaNs (Figs. 3.1C, 3.8 & 3.9). In mice and cell lines this modification has been associated with increased seeded aggregation (Terada *et al.*, 2018; Taguchi, Watanabe and Tanaka, 2025). My mass spectrometry data localises the truncation to the first ~30 amino acids of α-synuclein though it was not possible to confirm the exact site of this truncation. Theoretically a semi-tryptic peptide with a tryptic end at Lys-32 and an N-terminus defined by the *in cellulo* truncation site could have been identifiable under the paradigm used. However, if this peptide was shorter than 6 amino acids its detection would be impaired by low ionisation efficiency and was thus filtered out in our analysis.

Since the N-terminus of α-synuclein is responsible for its membrane binding, N-terminal truncation may result in mis-localisation of α-synuclein from cellular membranes (Bartels

et al., 2010). This could perturb its function at the synapse where simultaneous C-terminal interactions with vesicular VAMP2 and N-terminal interaction with plasma membrane phosphatidyl serine contribute to the regulation of synaptic vesicle docking (Lou *et al.,* 2017). To investigate this, future work should leverage subcellular fractionation approaches to determine whether N-terminally truncated α-synuclein is selectively depleted in cellular membranes including synaptic vesicles.

It has recently been reported that N-terminally truncated α-synuclein is generated by mouse primary neurons in culture after of PFF treatment (Taguchi, Watanabe and Tanaka, 2025). These authors showed that the lysine endopeptidase sentrin-specific protease 2 (SENP2) cleaves 4 of the 5 N-terminal KxKxGV repeats generating 12-140, 23-140, 34-140 and 45-140 α-synuclein. The predicted molecular weights of these truncation products are 13.25 kDa, 12.27 kDa, 11.13 kDa and 9.96 kDa respectively. Based on my mass spectrometry results it is plausible that SENP2 cutting at Lys-12 or Lys-23 might give rise to the truncated α-synuclein in iPSC-DaNs. SENP2 activity can be pharmacologically inhibited with NSC632839. In PFF-injected mice, NSC632839 treatment reduced the formation of phospho-ser-129 positive aggregates suggesting that normally N-terminal truncations worsen pathology (Terada *et al.*, 2018; Taguchi, Watanabe and Tanaka, 2025). Future experiments should treat iPSC-DaNs with this inhibitor to determine whether levels of N-terminally truncated α-synuclein decrease.

Other truncation sites including Met-5, Ser-9, Ala-18 and Ala-19 have been identified in post-mortem brain and the vermiform appendix (Kellie *et al.*, 2014; Killinger *et al.*, 2018). Ser-9, Ala-18 and Ala-19 would be compatible with my mass spectrometry results and the SDS-PAGE gel shift for the lower molecular weight α-synuclein band. Other than SENP2, the proteases implicated in N-terminal truncation are mostly lysosomal,

including Calpain (Ser-9) and Cathepsins D, B and L (Suthar and Lee, 2023). It has been suggested that truncated α-synuclein is formed when aggregates are incompletely degraded in the lysosome (McGlinchey *et al.*, 2019). Lysosomal dysfunction is widely reported in iPSC-DaNs from PD patients and arises in an aging/maturation-dependant manner (Cuddy *et al.*, 2019; Pitcairn *et al.*, 2023). It is therefore possible that the maturation-dependence of the N-terminal truncation may arise downstream of lysosome impairment. Interestingly, chloroquine treatment at Day35 had the largest single effect of any of the 'age mimetic' pharmacological manipulations in *SNCA*-triplication iPSC-DaNs (Fig. 3.4B). Increasing the dosage, duration or using another lysosome inhibitors such as bafilomycin A1 might exhibit a more profound effect.

SENP2, is not lysosomal and in fact shuttles between the nucleus and cytoplasm so its efficiency is unlikely to be modulated by age-dependant lysosomal dysfunction (Itahana, Yeh and Zhang, 2006). Capitalising on the multi-timepoint FOUNDIN-PD transcriptomic dataset I compared SENP2 expression between Day25 and Day65 timepoints, a period during which N-terminal truncation of α-synuclein greatly increases in my neurons. SENP2 expression was upregulated ~11% in PD neurons during this time frame though there was no significant change to expression in controls (Wald tests: Control $P_{adj\ (D25vsD65)} = 0.955$ & PD $P_{adj\ (D25vsD65)} = 0.00079$). This could suggest that increased SENP2 expression contributes to the maturation-dependence of N-terminal truncation though whether such as small expression change is biologically meaningful remains to be determined. SENPs are also subject to regulation of their proteolytic activity and stability through PTM addition to their own N-termini (Nayak and Müller, 2014). Future work should investigate the protein level expression of SENP2 in iPSC-DaNs during maturation to compliment pharmacological modulation.

N-terminally truncated α-synuclein was more abundant in iPSC-derived dopaminergic neurons than any other iPSC-derived cell type investigated. This may explain differences in the abundance of N-terminal truncations between dopaminergic differentiations, if those cultures with minimal low molecular weight α-synuclein, e.g. Fig. 3.1G, contained higher proportions of contaminating cell types. Numerous factors could contribute to cell-type specific truncation, including differences in protease expression and lysosome function, different conformers of α-synuclein in dopaminergic neurons which are better substrates for N-terminal proteolysis or features of the microenvironment such as oxidative stress from dopamine metabolism which results in more α-synuclein being targeted for degradation. Although further experiments are needed to dissect the above possibilities, these findings highlight the value of iPSC-derived neuron monoculture for analysis of factors contributing to dopaminergic preferential vulnerability.

The dopaminergic specificity of α-synuclein truncation *in vitro* motivated investigation across postmortem brain regions (Fig. 3.5C). Although the gel shift of low molecular weight α-synuclein in postmortem samples exactly matched that seen in iPSC-DaNs it is not possible to definitively conclude that this band is also an N-terminal truncation without repeating the silver staining and mass spectrometry in postmortem samples (for which there was insufficient biological material). Regional differences in α-synuclein truncation are not without precedent. Using a panel of modification selective antibodies, region- and cell type-specificity has been identified for C-terminal truncations in PD and LBD (Hass *et al.*, 2021). Although there are no antibodies selective for N-terminal truncation products, a recent publication found that the percentage of α-synuclein aggregates immunostaining for the N-terminus was lower in the substantia nigra and hippocampus compared to the middle frontal gyrus (pre-frontal cortex), entorhinal cortex

and olfactory bulb (Wiseman *et al.*, 2024). These brain regions correlate where I found higher abundance of truncated α-synuclein. The reduced labelling observed by Hass and colleagues could result from either N-terminal truncation or the presence of distinct conformers with less accessible N-termini (or both). Overall, my findings fit with a growing literature in support of regional heterogeneity in α-synuclein pathology and proteoforms which *in vitro* models must aim to recapitulate.

Chapter 4 - α-synuclein secretion by patient neurons

4.1 Introduction

Having demonstrated in Chapter 3 that α-synuclein is robustly expressed in a maturation-dependent manner in iPSC-DaNs, I sought to examine α-synuclein secretion in these cells. In line with increased gene dosage, our lab and others have previously reported elevated α-synuclein secretion in *SNCA*-triplication dopaminergic neurons (Devine *et al.*, 2011; Zambon *et al.*, 2019; Iannielli *et al.*, 2022). Moreover, we have also shown that secretion is elevated in *GBA1-N370S* iPSC-DaNs although intracellular expression of α-synuclein in the *GBA1* mutants is not consistently upregulated (Fernandes *et al.*, 2016).

Study of α-synuclein in the conditioned media of cell culture systems aims to mimic the secretion of α-synuclein into CSF *in vivo*. In patient CSF α-synuclein has been identified as free soluble protein as well as inside extracellular vesicles (EVs) (Anagnostou *et al.*, 2023). α-synuclein from iPSC-DaNs has been identified associated with the membranes of L1CAM-positive EVs and its abundance in the EV fraction appears to be increased by *SNCA* mutations (Oh *et al.*, 2022; Yan *et al.*, 2025). A recent pre-print also suggested that secretion of pathological α-synuclein in EVs is increased by build-up of GCase substrates in *GBA1* mutants (Jacquemyn *et al.*, 2025). However, it appears that only a tiny fraction of secreted α-synuclein is EV-associated (Fernandes *et al.*, 2016; Oh *et al.*, 2022). The role of this low-level EV-mediated secretion as well as crosstalk with/reciprocal regulation of pathways that release free α-synuclein remains to be determined.

Pharmacological perturbation of lysosomal function with chloroquine and bafilomycin A1 increases free α-synuclein secretion, suggesting a role for the endosomal system in release (Fernandes *et al.*, 2016). However, the same study showed that inhibition of ER-Golgi secretion with brefeldin A also increased secretion, not only demonstrating that multiple mechanisms are involved but also that there may be interplay between pathways. This is consistent with extensive work in non-neuronal models which have identified a plethora of possible pathways which secrete α-synuclein when the necessary components are overexpressed (Liu *et al.*, 2009; Emmanouilidou *et al.*, 2010; Alvarez-Erviti *et al.*, 2011; Hasegawa *et al.*, 2011; Tsunemi, Hamada and Krainc, 2014; Fontaine *et al.*, 2016; Gonçalves *et al.*, 2016; Lee *et al.*, 2016; Xu *et al.*, 2018; Underwood *et al.*, 2020; Xie *et al.*, 2022). It is not known which (if any) of these pathways are responsible for secretion of endogenous α-synuclein in dopaminergic neurons, and whether certain mechanisms exhibit specificity for pathologically relevant proteoforms.

The low levels of secretion, and limited culture volumes for iPSC-DaNs, necessitate sensitive methods for extracellular α-synuclein detection. Commercial ELISAs have previously been used to measure α-synuclein release, however these kits are prohibitively expensive for high throughput analysis. To more exhaustively investigate secretion mechanisms with a panel of pharmacological or genetic manipulations a lower cost but equal/higher sensitivity approach is required. In this chapter I set out to modify a low-sensitivity 'DIY-ELISA' kit from BioTechne to detect soluble α-synuclein iPSC-DaN conditioned media. Using this assay and complementary techniques I then probe α-synuclein secretion mechanisms in patient-derived neurons using pharmacological tools.

Chapter Aims:

1. To validate published effects of PD-linked mutations on α-synuclein secretion in patient-derived iPSC-DaNs.
2. To optimise a low-cost high throughput assay with which to measure α-synuclein secretion after experimental perturbation.
3. To assess the involvement of proposed secretion mechanisms from non-neuronal models in the release of α-synuclein from patient neurons using pharmacology.

4.2 *SNCA*-triplication and *GBA1-N370S* neurons release α-synuclein from the soma

Previous work from our group suggests that *SNCA*-triplication and *GBA1-N370S* mutations increase α-synuclein release, and that this phenotype becomes more evident as neurons mature from Day22 to Day32 (Fernandes *et al.*, 2016; Zambon *et al.*, 2019). Building on these results, the α-synuclein content of conditioned media was assayed between Day35 and Day100, revealing a progressive increase up to Day75 at which point the genotype differences were most pronounced (Fig. 4.1A&B). α-synuclein immunoprecipitation from culture media at this time-point exhibited the same trend as the MSD ELISA and demonstrated that trace amounts of truncated α-synuclein, as characterised in Chapter 3, are also secreted (Fig. 4.1C&D).

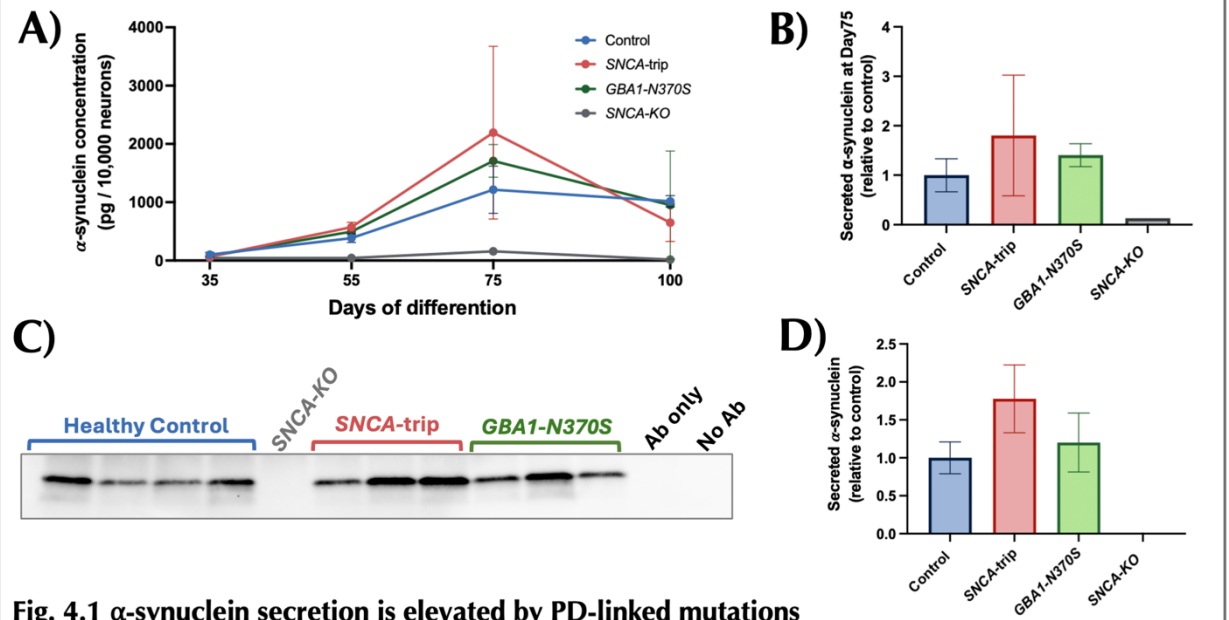

Fig. 4.1 α-synuclein secretion is elevated by PD-linked mutations
A) α-synuclein concentration of conditioned media measured by electrochemical MSD ELISA. N=2-4 lines per genotype from one differentiation. **B)** α-synuclein concentration of conditioned media at Day75 from A) represented relative to secretion in healthy controls. **C)** Western blot after SDS-PAGE for α-synuclein immunoprecipitated from culture media from Day75. N=3-4 cell lines per genotype, except for *SNCA-KO*. **D)** Densitometric quantification of C).

Studies *in vivo* suggest that α-synuclein spreads through synaptically connected routes and recently it was demonstrated that α-synuclein secretion from iPSC-DaNs can be regulated by neuronal activity (Nuermaimaiti *et al.*, 2025). Despite having a synaptic function α-synuclein is also expressed ubiquitously in the cell body of iPSC-DaNs (Fig. 4.2A). Therefore, I sought to determine whether α-synuclein secretion is predominantly somatic or axonal.

The axonal compartment of iPSC-DaNs can be isolated from soma/dendrites using microfluidic devices (Do *et al.*, 2024). Cells were plated into one chamber of a two-chamber device and axons encouraged to grow through the 5 µm wide microgrooves with a gradient of BDNF and laminin (Fig. 4.2B). After 50 days in culture the microgrooves appeared to be completely filled with axonal bundles which fanned out in the axonal chamber (Fig. 4.2C). Prior to assessing α-synuclein concentration in the respective chambers it was necessary to ensure there was no diffusion of media through any microgrooves which were only partially filled with axons. Although visual inspection with light microscopy enabled an approximate assessment of microgroove filling, this does not provide certainty of fluid separation. An alternative quality control method was required. Culture media usually contains pH indicator phenol red which has a characteristic absorption spectrum between 500 and 580 nm. Somatodendritic chambers were fed with phenol red media while the axonal chamber received media lacking phenol red. The absorbance of media from the axonal chamber therefore provided a read-out of fluid separation where a peak at ~560 nm indicated that inter-chamber diffusion had taken place (Fig. 4.2D). Such devices were not used for analysis of secreted α-synuclein. Measuring media α-synuclein content from somatodendritic and axonal chambers of devices which passed quality control (See Supplementary Fig. 4.2),

demonstrated that axonal α-synuclein secretion across all three genotypes was barely above background of the assay as determined by the *SNCA*-knockout control (Fig. 4.2E). Even when normalising for total protein concentration of cell material in each chamber, secretion was almost an order of magnitude higher in the somatodendritic compartment. Although these data do not rule out a low-level α-synuclein secretion from axon terminals they suggest that in iPSC-DaNs most free α-synuclein release is from the soma and dendrites.

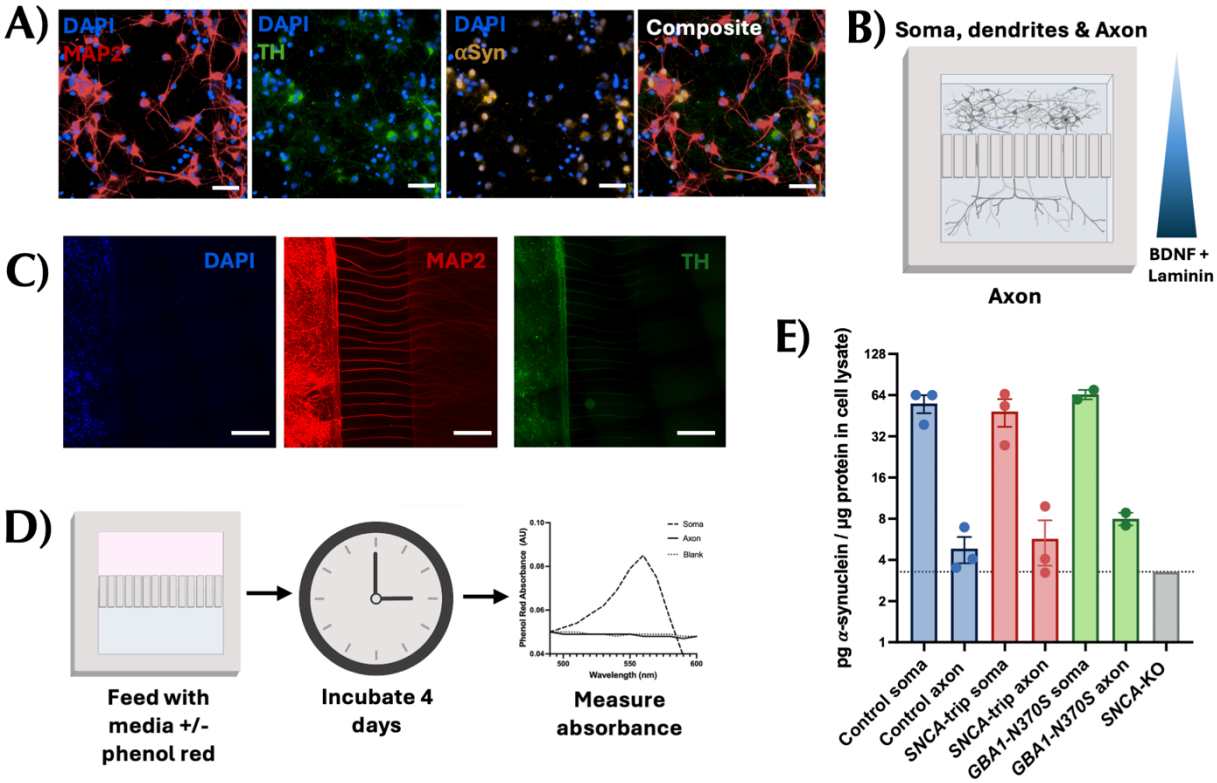

Fig. 4.2 α-synuclein secretion is mostly from the soma of iPSC-derived dopamine neurons
A) Representative images of control neurons at Day40 expressing α-synuclein as well as neuronal marker MAP2 and dopaminergic marker TH. Scale bar = 50 µm **B)** Schematic showing the microfluidic set up. **C)** Representative images of *GBA1-N370S* neurons at Day50 after growing in a microfluidic device showing compartmentalisation of axons. Scale = 200 µm. **D)** Schematic describing the method used to assess fluid separation between axonal and somatodendritic compartments. **E)** α-synuclein concentration of conditioned media at Day60 from the two microfluidic compartments normalised to the total protein content of lysed material from that compartment measured by BCA.

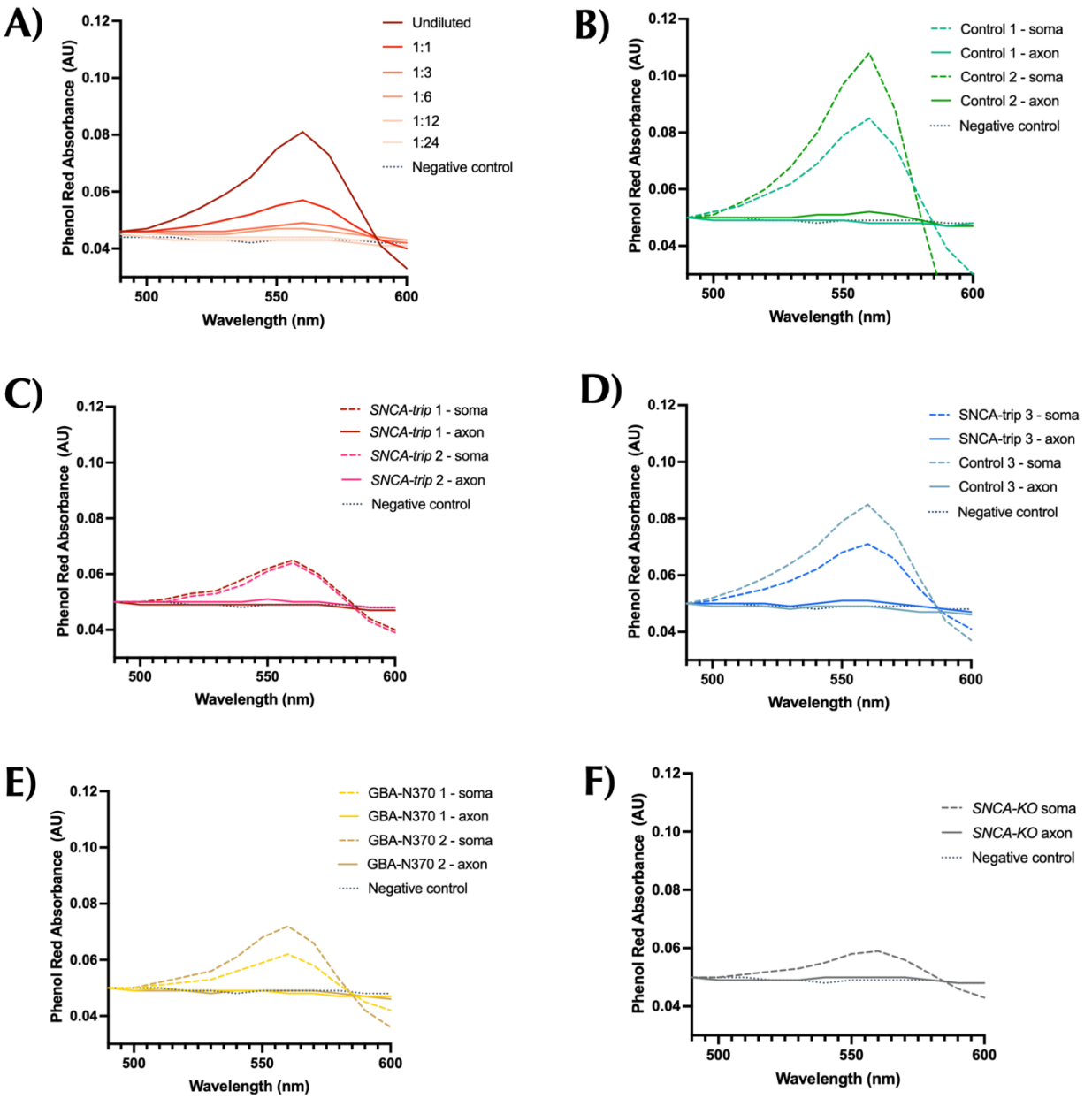

Supplementary Fig. 4.2 Quality control for media compartmentalisation in microfluidic devices **A)** Phenol red absorbance spectra for serially diluted culture media. **B)-F)** Phenol red absorbance spectra for somatodendritic (containing phenol red) and axonal (not containing phenol red) chambers after 4 days of incubation showing that there was no diffusion of phenol red between compartments and hence complete fluid separation.

4.3 Release of α-synuclein through misfolding-associated protein secretion

Recently there has been considerable interest in the misfolding-associated protein secretion (MAPS) pathway as an unconventional secretion route for proteins involved in neurodegenerative diseases including α-synuclein (Fontaine *et al.*, 2016; Xu *et al.*, 2018). In collaboration with the Schekman group at UC Berkeley I investigated whether MAPS contributes to α-synuclein secretion in patient-derived iPSC-DaNs.[5] DNAJC5 palmitoylation and subsequent membrane localisation is essential for MAPS (Wu, Sirkis and Schekman, 2022). Palmitoylation can be inhibited using palmitate analogue 2-bromopalmitic acid while DNAJC5 function and interaction with Hsc70 can be inhibited with plant-derived flavonoid quercetin (Resh, 2006; Xu *et al.*, 2010).

In iPSC-DaNs from *GBA1-N370S* PD patients and healthy controls most DNAJC5 was palmitoylated although 2-bromopalmitic acid induced some de-palmitoylation (Fig. 4.3A). The total expression level of DNAJC5 was not altered by either drug. Quercetin, but not 2-BA, reduced α-synuclein release in healthy controls and *GBA1-N370S* dopamine neurons showing a dose-dependent suppression of secretion (Fig. 4.3B-D). Previous work from our group shows that chloroquine increases α-synuclein secretion (Fernandes *et al.*, 2016). Using this drug as a positive control, *SNCA*-triplication iPSC-DaNs were also challenged with quercetin and 2-BA (Fig. 4.3E-G). The reduction of secretion by quercetin and trending increase with 2-BA was replicated in these neurons both by MSD ELISA and immunoprecipitation from culture media.

[5] This work was published in eLife (Wu et al., 2023). The broader study design focussing on palmitoylation and DNAJC5 oligomerisation was devised by the Schekman group. I optimised drug concentrations and dosing regimens for iPSC-DaNs and carried out all iPSC-DaN experiments. Special thanks to Dr Kalina Naidoo and Dr William McGuinness who grew some of the cells used for this work.

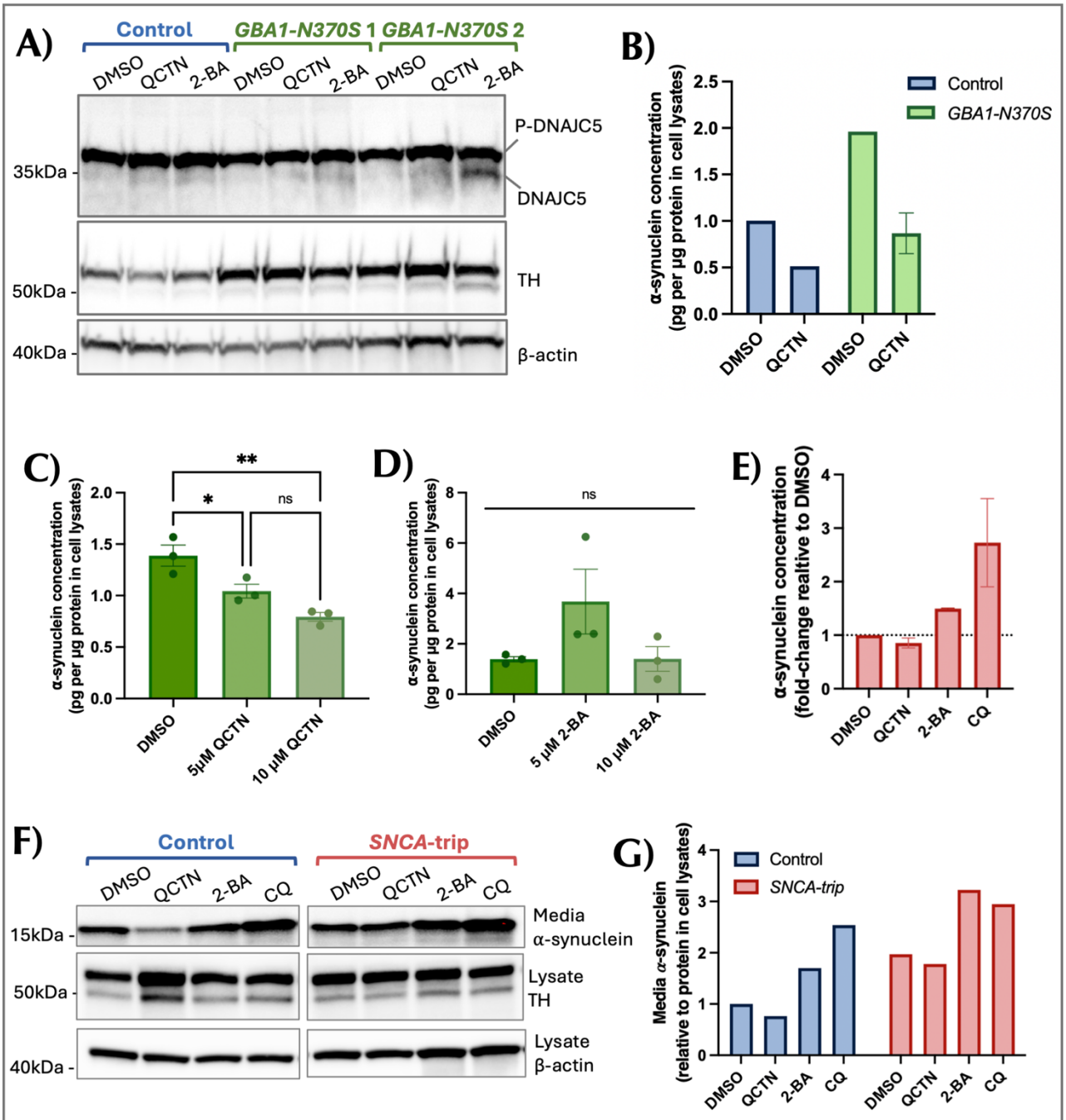

Fig. 4.3 DNAJC5-mediated secretion of α-synuclein in patient-derived neurons.
A) Western blot after SDS-PAGE showing palmitoylated and de-palmitoylated DNAJC5 in Day68 neurons following 72 hours of treatment with quercetin (QCTN, 7.5 µM) or 2-bromopalmitic acid (2-BA, 10 µM). **B)** α-synuclein concentration of conditioned media from Day60 neurons treated for 72 hours with 7.5 µM quercetin measured by electrochemical MSD ELISA. N=1-3 lines per genotype from one differentiation. α-synuclein concentration in conditioned media from Day38 *GBA1-N370S* neurons treated for 72 hours with 5 µM or 10 µM **C)** quercetin and **D)** 2-bromopalmitic acid measured by electrochemical MSD ELISA. N=3 lines from one differentiation. One-way ANOVA and Dunnett's multiple comparisons tests show a significant effect of quercetin but not 2-BA. **E)** α-synuclein concentration of conditioned media from *SNCA*-triplication iPSC-DaNs at Day44 following 48 hours of treatment with 7.5 µM quercetin, 10 µM 2-BA or 50 µM chloroquine (CQ) measured by electrochemical MSD ELISA. N=2 cell lines. **F)** Western blot after SDS-PAGE for α-synuclein immunoprecipitated from culture media at Day44, following 48 hours of treatment with 7.5 µM quercetin, 10 µM 2-BA or 50 µM chloroquine. **G)** Densitometric quantification of F).

Overall, these data show that DNAJC5 is palmitoylated in iPSC-DaNs and its activity contributes to α-synuclein release both in healthy neurons and those from PD patients where baseline secretion is elevated.

4.4 Development of a low-cost ELISA for α-synuclein

The results of the electrochemical MSD ELISA, presented in Figs. 4.1-4.3 show that α-synuclein is robustly secreted and this secretion can be modulated by PD causing mutations and pharmacological intervention. However, at the cost of £600-700 per plate, reliance on this technique limits technical replication as well as the range of pathways which can be investigated. Therefore, it was necessary to find an alternative lower-cost approach to measuring α-synuclein concentration of conditioned media.

MSD experiments demonstrated that prior to normalisation, conditioned media α-synuclein concentration varies between ~120-3000 pg/mL for untreated neurons, suggesting that an assay should be robust below 100 pg/mL to reliably detect any reduction to secretion caused by experimental manipulation. Of the numerous commercial ELISAs available, several would fulfil this sensitivity requirement (Fig. 4.4A). However, for the number of assays needed to complete this study (>30 including optimisation experiments) the Bio-Techne DY1338-05 DuoSet kit (henceforth Bio-Techne ELISA) was the only financially viable option. This is a DIY ELISA kit, with all reagents sold separately and no published sensitivity, precision or linearity data. The sensitivity/limit of detection (LOD) was calculated on 3-times blank standard deviation as 321 pg/mL (Hasibeder *et al.*, 2015). Compared to the MSD ELISA, where standards remained tight down to 10 pg/mL, dilution of the Bio-Techne standards below their intended range yielded considerable variability (Fig. 4.4B-D). The Bio-Techne ELISA remained linear with sample dilution at the upper and lower ends of the assay window demonstrating the absence of significant matrix effects form other components of the media (Fig. 4.4E&F). Spike recovery using 400 pg/mL recombinant α-synuclein was also

performed against a range of conditioned media dilutions which also showed acceptable recovery rates down to 1:4 dilution (Dutta *et al.*, 2023) – Fig. 4.4G. Finally, the Bio-Techne ELISA was able to discriminate the biologically relevant difference in α-synuclein secretion between healthy control and *SNCA*-triplication neurons, with all values falling above the calculated LOD.

While the results of the Bio-Techne ELISA without modification were encouraging I remained concerned that manipulations which reduce α-synuclein secretion would yield concentrations below the LOD. I therefore set out to improve the sensitivity of this assay. Tyramide signal amplification (TSA) uses a dual incubation with horseradish peroxidase to first catalyse biotinyl tyramide addition to electron-rich groups on surrounding protein and a second incubation to catalyse the TMB colour change reaction (Yamamori *et al.*, 2007). Compared to the unamplified reaction, TSA increased the signal intensity, shifting the response sigmoid to lower α-synuclein concentrations (Fig. 4.5A). Lower variance was achieved with 1:1000 dilution of biotinyl-tyramide however backgrounds was increased compared to the unamplified reaction. Blocking with 2% BSA reduced the inter-replicate variability, but only the unamplified reaction yielded a standard curve with a significantly non-zero slope between 12.5 and 100 pg/mL (Fig. 4.5B). Moreover, there was no significant improvement to the percentage recovery of standards compared to the unamplified reaction (Figs. 4.4D & 4.5C). In summary, for low analyte concentrations TSA increases the background more than true signal so was unsuitable for improving assay sensitivity.

A)

Product Code	Sensitivity (pg/mL)	Standards (pg/mL)	Cost
Abbexa	Abx358545	9.38	15.6 -1000	£420
Abcam	ab260052	504	615 - 7000	£570
AnaSpec	AS-55550-H	5	5 - 800	£520
Bio-Techne	NBP2-62771	7.5	12.5 - 800	£691
Bio-Techne	DY1338-05	N/A	313 - 20000	£101
Biolegend	448607	1.8	10.2 - 650	£407
Euroimmun	6545-L	24.42	41.3 - 6000	£3100
Invitrogen	KHB0061	200	23 - 15000	£564

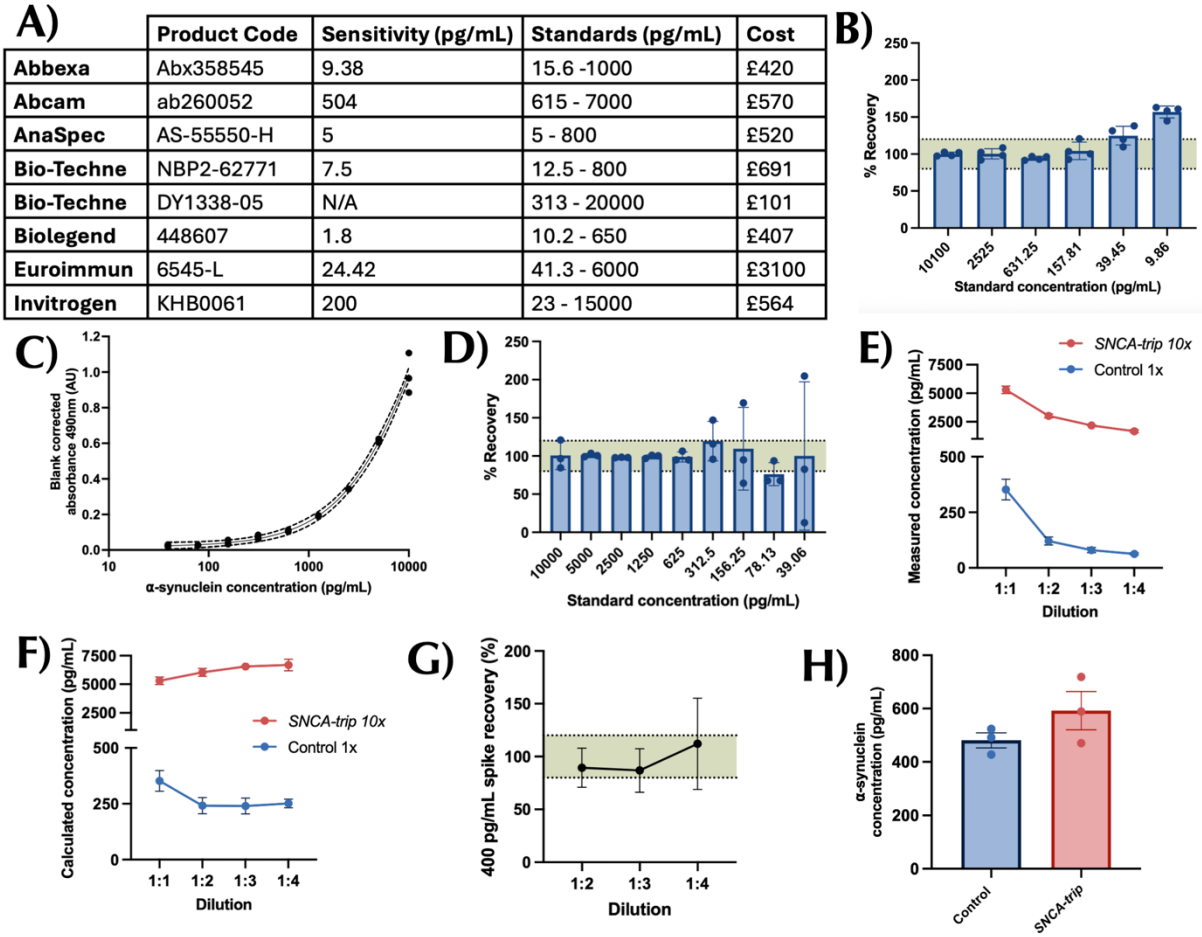

Fig. 4.4 Validation of Bio-Techne 'self-build' α-synuclein ELISA.
A) Table showing the commercially available α-synuclein ELISAs and respective prices per 96-well plate. **B)** Percentage recovery of recombinant α-synuclein standards from the electrochemical MSD ELISA. Data pooled from two technical replicates. **C)** Standard curve for the Bio-Techne ELISA fitted with four-parameter logistic regression (R^2=0.99) **D)** Percentage recovery of recombinant α-synuclein standards from the Bio-Techne ELISA. **E)** Interpolated α-synuclein concentration for samples at either end of the assay range diluted in culture media. The *SNCA*-trip sample was concentrated 10x with a 10 kDa Amicon ultrafiltration column to mimic an abnormally high concentration sample. **F)** Calculated concentrations accounting for dilution from E) demonstrating assay linearity. **G)** Percentage recovery of 400 pg/mL recombinant α-synuclein spiked into serially diluted conditioned medium from healthy control neurons. **H)** α-synuclein concentration from Day60 dopaminergic neurons. N=3 lines per genotype from one differentiation. Acceptable sample recovery was taken as 100 ± 20% and is shown in green.

Alternatively, I sought to increase the analyte concentration. While concentration columns can be used (Fig. 4.4E&F) this would greatly increase cost and processing time. Culture media can be sequentially collected from the same cells to accumulate a larger volume than required for single ELISA. Since α-synuclein is rapidly pulled down by immobilised antibody, we reasoned that sequential additions of culture media to the

same wells of the ELISA plate would increase the effective concentration of each sample. Three additions of media collected from cells between Day52 and Day65 markedly increased signal intensity (Fig. 4.5D) and greatly improved the percentage recovery and variability of standards (Fig. 4.5E). The LOD of the triple addition ELISA (henceforth BioT3 ELISA) was calculated to be 47.2 pg/mL, a notable improvement compared to the unmodified Bio-Techne ELISA. The BioT3 ELISA effectively detected biologically relevant differences in α-synuclein secretion between healthy control and *SNCA*-triplication iPSC-DaNs as well as the CRISPRi knock-down of the *SNCA* gene in controls (Fig. 4.5F&G). Despite the high biological variation between cell lines, technical replicates were concordant on and between ELISA plates (Fig. 4.5H). Together these validation experiments demonstrate that the BioT3 ELISA is a robust and reliable assay, sensitive over the range required for conditioned media analysis.

Finally, I was keen to investigate whether a live nuclei count could be used to normalise ELISA results between conditions rather than the laborious total protein quantification by BCA used up to this point. Total protein and nuclei counts were found to be significantly correlated (Fig. 4.5I), and this method reduced the processing time per plate from 120 to 30 minutes so was used for all future experiments.

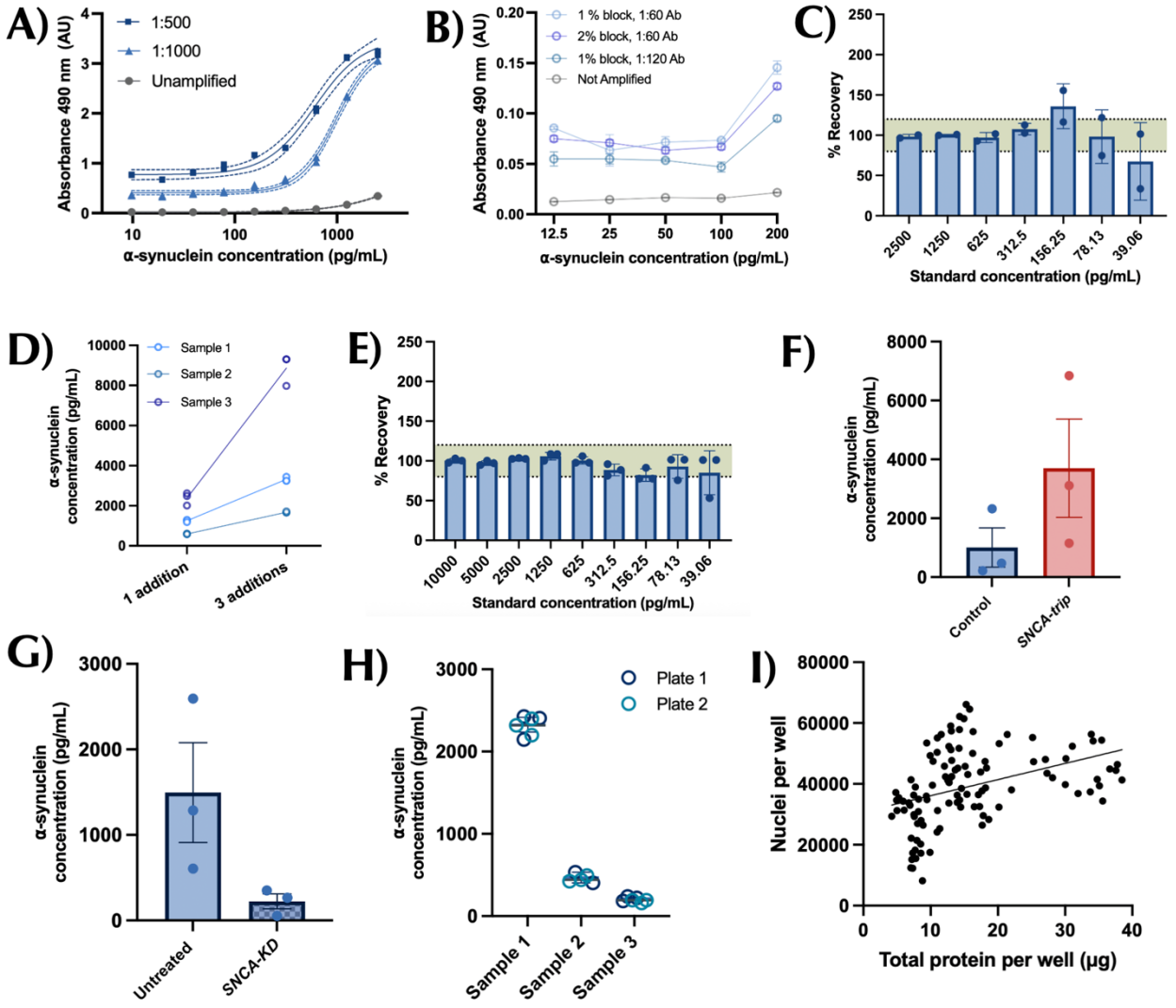

Fig. 4.5 Development and validation of a more sensitive α-synuclein ELISA.
A) Standard curves for the unamplified or TSA amplified ELISAs with 1:500 or 1:1000 dilutions of biotinyl tyramide solution, 1% BSA blocking and 1:60 dilution of detection antibody. Standard curves were fitted with four-parameter logistic regression ($R^2_{unamplified}$=1, $R^2_{1:500}$=0.98, $R^2_{1:1000}$=1). **B)** Plotted standards for unamplified or TSA amplified ELISAs varying blocking and detection antibody concentration. Simple linear regression shows that only the unamplified reaction gives a positive gradient for standards between 12.5 and 100 pg/mL ($p_{unamplified}$=0.036, $p_{1\%\ block,\ 1:60Ab}$=0.6826, $p_{2\%\ block,\ 1:60\ Ab}$=0.3027 and $p_{1\%\ block,\ 1:120\ Ab}$=0.1065). **C)** Percentage recovery of recombinant α-synuclein standards from the TSA ELISA blocked with 2% BSA, incubated with 1:1000 biotinyl tyramide and detected with 1:60 antibody dilution of anti-α-synuclein antibody. **D)** Interpolated α-synuclein concentrations for 3 conditioned media samples added sequentially to the ELISA plate for 1 hour at a time. **E)** Percentage recovery of recombinant α-synuclein standards from the triple addition ELISA. **F)** α-synuclein concentration from Day60 dopaminergic neurons. N=3 lines per genotype from one differentiation. **G)** α-synuclein concentration from Day50 healthy control dopaminergic neurons expressing dCas9 and the same cells treated with lentivirus containing sgRNA to knock down *SNCA* using CRISPRi. **H)** α-synuclein concentration of healthy control technical replicates measured across two separate ELISA plates processed separately. **I)** Correlation of total protein content of cell lysates from neurons grown in full-area 96-well plates used for ELISA with live nuclei counts from each well demonstrating a significant correlation with simple linear regression (p<0001). Acceptable sample recovery was taken as 100 ± 20% and is shown in green.

4.5 Pharmacological modulation of free α-synuclein secretion

Capitalising on the cost-effective Bio-Techne ELISA I sought to further probe α-synuclein secretion mechanisms active in neurons from healthy controls and *SNCA*-triplication PD patients using a variety of drugs.[6]

In SH-SY5Y cells α-synuclein secretion is dependent on intracellular Ca^{2+} but is unaffected by extracellular Ca^{2+} chelation (Emmanouilidou *et al.*, 2010; Zhao *et al.*, 2022). Similarly in mature iPSC-DaNs membrane permeable BAPTA-AM, but not impermeant EGTA, reduced α-synuclein release (Fig. 4.6A). This suggests that intracellular Ca^{2+} dynamics, but not entry across the plasma membrane, is required for release.

A recent publication demonstrated that α-synuclein secretion in iPSC-DaNs neurons partially depends on their electrical activity (Nuermaimaiti *et al.*, 2025). These authors found that complete suppression of neuronal firing caused ~20% reduction in α-synuclein release. The canonical mode of coupling electrical activity to intracellular processes involves voltage-gated channels (CaVs and NMDARs) which permit Ca^{2+} entry across the plasma membrane to activate intracellular Ca^{2+}-dependant processes. Despite the apparent lack of dependence on extracellular Ca^{2+} (Fig. 4.6A), treatment with L-type Ca^{2+} channel blocker isradipine significantly reduced α-synuclein secretion in healthy control and *SNCA*-triplication neurons (Fig. 4.6B).

[6] Due to the parallel nature of experimentation during this project the BioT3 ELISA had not been fully optimised at the time of the work presented in Subchapter 4.5. Accordingly, the unmodified Bio-Techne ELISA was used to monitor α-synuclein secretion in these experiments with the rationale that pharmacological perturbation is unlikely to decrease α-synuclein secretion as much as genetic manipulations, so the lower sensitivity did not pose a problem.

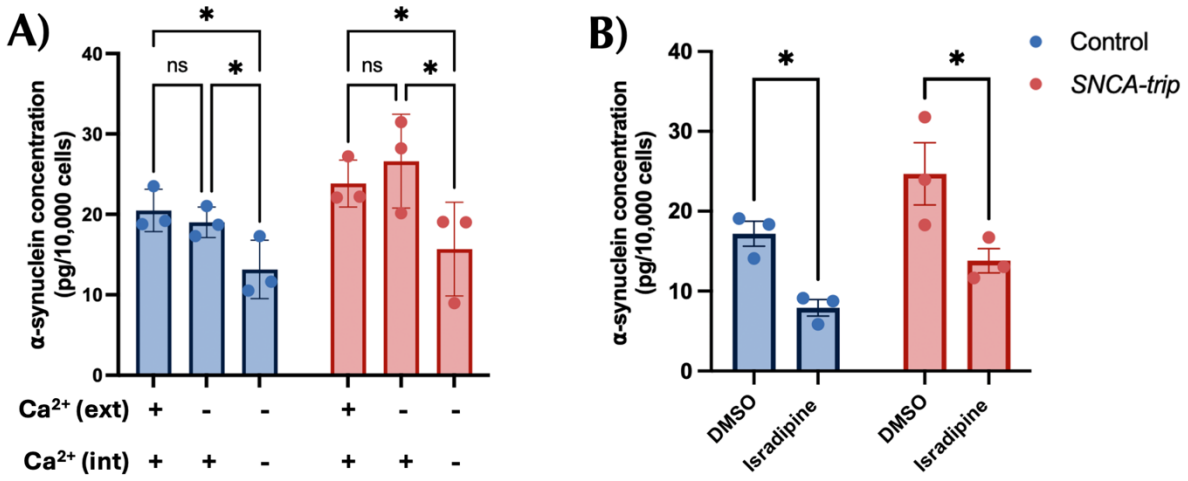

Fig. 4.6 α-synuclein secretion in iPSC-derived neurons is Ca^{2+}-dependent.
A) α-synuclein concentration of conditioned media from Day60 dopaminergic neurons cultured for 24 hours in 1.3 mM extracellular Ca^{2+} with membrane impermeable Ca^{2+} chelator EGTA (0.5 mM) or EGTA & cell permeable Ca^{2+} chelator BAPTA-AM (2 µM). Two-way ANOVA with Dunnett's multiple comparisons test shows a significant effect of EGTA & BAPTA-AM treatment for both genotypes. N=3 lines per genotype from one differentiation. **B)** α-synuclein concentration of conditioned media from Day60 dopaminergic neurons cultured for 24 hours with L-type CaV channel blocker isradipine (300 nM). Two-way ANOVA with Šídák's multiple comparisons test shows a significant decrease in α-synuclein release in both genotypes. N=3 lines per genotype from one differentiation.

Previous reports suggest that a small proportion of secreted α-synuclein is associated with EVs (Oh *et al.*, 2022). In the absence of membrane permeabilisation intravesicular α-synuclein is not exposed to ELISA antibodies and will not be detected by this approach (Alvarez-Erviti *et al.*, 2011). EVs, isolated by ultracentrifugation from 10 mL of conditioned media, contained trace amounts of α-synuclein but not the cytoplasmic marker calnexin (Fig. 4.7A). Compared to the results of immunoprecipitation of free α-synuclein from just 2 mL of media (Fig. 4.1C) this represents a tiny fraction of the total secreted α-synuclein.

In neuroblastoma cells genetic perturbation of EV release increases free α-synuclein secretion (Hasegawa *et al.*, 2011; Spencer *et al.*, 2016). Exosome biogenesis can be inhibited pharmacologically with sphingomyelinase inhibitor GW4869 which depletes ceramide needed for the formation of intraluminal vesicles in the multivesicular body (Fussi *et al.*, 2018). GW4869 treatment resulted in a dose-dependent increase in free α-synuclein secretion in both healthy control and *SNCA*-triplication iPSC-DaNs (Fig. 4.7B). This drug is also reported to suppress autophagosome formation which could contribute to perturbed α-synuclein release (Back *et al.*, 2018). However, in the iPSC-DaNs 10 μM GW4869 did not alter LC3-II/LC3-I levels as a marker of autophagy initiation (Fig. 4.7C&D). Moreover, treatment with Ulk1 inhibitor MRT68921 to mimic an autophagy initiation defect did not increase α-synuclein secretion (Fig. 4.7C-E). These data suggest that sphingomyelinase inhibition increases α-synuclein secretion through a pathway independent of perturbed autophagy. Future work should use quantitative measures of EV release such as nanoparticle tracking analysis to confirm that the drug is acting on target. If GW4869 is shown to be reducing EV release this would suggest that there is also crosstalk between secretion pathways in iPSC-DaNs (like in non-neuronal cells).

Together these data and the modulation of DNAJC5 presented in Fig. 4.3, demonstrate that many mechanisms identified in non-neuronal models are conserved in disease-relevant iPSC-DaNs. This motivates further investigation using more precise, genetic, manipulation of candidate pathways.

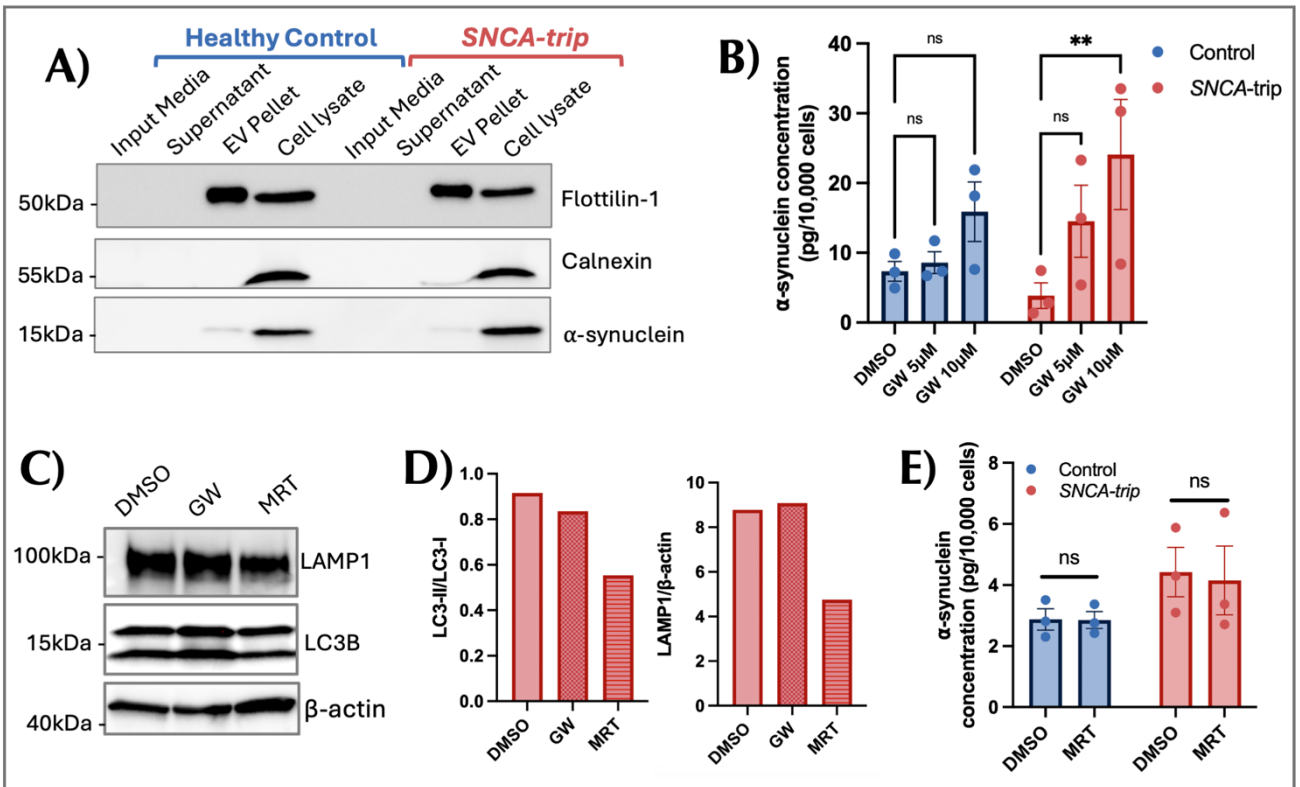

Fig. 4.7 Crosstalk between EV-associated and free α-synuclein secretion pathways.
A) Western blot after SDS-PAGE for EVs pelleted from 10 mL culture media at 100,000 xg showing trace amounts of α-synuclein in the EV pellet. **B)** α-synuclein concentration of conditioned media from Day60 dopaminergic neurons cultured for 48 hours in GW4869 (GW). Two-way ANOVA with Dunnett's multiple comparisons test shows a significant effect of 10 μM GW4869 for *SNCA*-triplication neurons. N=3 lines per genotype from one differentiation. **C)** Western blot after SDS-PAGE for LC3B and LAMP1 as markers of autophagy initiation and lysosomal accumulation respectively for iPSC-DaNs treated for 48 hours with 10 μM GW4869 or 500 nM MRT68921 (MRT). **D)** Densitometric quantification of C). **E)** α-synuclein concentration of conditioned media from Day60 dopaminergic neurons cultured for 48 hours in 500 nM MRT68921. Two-way ANOVA with Šídák's multiple comparisons test shows no significant effect of drug treatment. N=3 lines per genotype from one differentiation.

4.6 Discussion

Mature iPSC-DaNs release α-synuclein into their culture media. In line with previous reports, α-synuclein secretion was raised by PD-linked mutations (Devine *et al.*, 2011; Fernandes *et al.*, 2016; Zambon *et al.*, 2019; Iannielli *et al.*, 2022) – Fig. 4.1. The elevated secretion down-stream of *SNCA*-triplication is consistent with increased gene dosage and higher intracellular expression (Fig. 3.1G&H, 3.4C). However, the cause of the elevated release in *GBA1-N370S* neurons is less clear since the intracellular expression of α-synuclein in these cells does not differ from controls (Fig. 3.1C). Homozygous deletion of *GBA1* in SH-SY5Y cells also increases α-synuclein secretion suggesting that the N370S mutation acts through lysosomal loss of function rather than toxic gain of function from GCase misfolding in the ER (Bae *et al.*, 2014; Smith and Schapira, 2022). Consistent with this, both *GBA1-/-* and patient-derived *GBA1-N370S* iPSC-DaNs exhibit lysosomal dysfunction (Schöndorf *et al.*, 2014; Fernandes *et al.*, 2016; Sanyal *et al.*, 2020). In cell lines, artificially impairing lysosomal function also increases α-synuclein secretion through elevated release of extracellular vesicles with an autophagosome-like proteome. (Alvarez-Erviti *et al.*, 2011; Ejlerskov *et al.*, 2013; Minakaki *et al.*, 2018). However, the α-synuclein secreted by iPSC-DaNs with either the *GBA1-N370S* mutation or chloroquine-induced lysosomal dysfunction is free in the culture media and accessible to ELISA antibodies (Fernandes *et al.*, 2016) – Figs. 4.1 & 4.3E-G. Therefore, although lysosomal dysfunction in *GBA1* lines appears to be the trigger for elevated α-synuclein secretion, the actual mechanism through which this occurs in iPSC-DaNs remains unclear.

The increase in secretion over time in all genotypes parallels the increase in α-synuclein intracellular expression (Fig. 3.1D & 4.1A). However, between Day55 and Day75 α-

synuclein release increase considerably more than intracellular expression. Spontaneous activity increases markedly between Day50 and Day70 in these cells (Beccano-Kelly *et al.*, 2023). Since the electrical activity of iPSC-DaNs partially regulates α-synuclein secretion it is possible that maturation of pace-making behaviour may underlie the differences in time course of α-synuclein expression vs secretion (Nuermaimaiti *et al.*, 2025). Unlike total expression, secretion decreased by Day100 whereas intracellular expression remained high. The health of iPSC-derived neuron cultures decreases with extended culture duration and since α-synuclein release is an energy-dependent process this late-stage decline is likely linked more to suboptimal culture conditions than a biologically relevant phenotype (Lee, Patel and Lee, 2005).

For all three genotypes α-synuclein release was mostly from the cell body and dendrites rather than axon terminals (Fig. 4.2E). The ultra-low concentrations measured in the axonal chamber of the microfluidic devices were similar to the *SNCA-KO* negative control making it impossible to conclude whether any axonal secretion had occurred. When overexpressed in primary cortical neurons α-synuclein has been detected at low levels in the axonal compartment media (Danzer *et al.*, 2011). Similarly, exogenously added α-synuclein PFFs can be re-secreted from axons in primary cortical and iPSC-DaNs (Brahic *et al.*, 2016; Tsunemi *et al.*, 2019). However, none of these publications made efforts to control for α-synuclein diffusion through unfilled micro-grooves. Moreover, although α-synuclein was present at vastly supraphysiological concentrations, the conditioned media α-synuclein concentration of the axonal compartment was substantially below the sensitivity of most commercial ELISAs.

While *in vitro* evidence for secretion from axon terminals is sparse, work in rodents suggests that α-synuclein can spread trans-synaptically through neuroanatomically

connected routes. Intramuscular injection of PFFs progressively seeds pathology in the spinal cord, pons, midbrain and then motor cortex (Sacino *et al.*, 2014; Schaser *et al.*, 2020). *In vivo* studies measure α-synuclein transfer between synaptically connected neurons rather than release from an 'unpaired' axon terminal in cultured cells. Given the extent of axon terminal remodelling upon target dendrite recognition, it is conceivable active synapses may be required for axonal α-synuclein secretion (Fox and Umemori, 2006). Indeed, a recent study using an advanced microfluidic setup recapitulated trans-synaptic anterograde α-synuclein transfer *in vitro* (Courte *et al.*, 2023). However, only a tiny proportion of exogenously added oligomers and fibrils were propagated to the secondary cells and over much slower time scales than non-axonal secretion, leading the authors to conclude that synaptic release plays only a minor role in α-synuclein propagation. The results presented here and published data suggest that synaptic release of α-synuclein contributes minimally to the total intercellular spread of α-synuclein. Although this raises questions regarding peripheral seeding in rodents it is more consistent with the pattern of α-synuclein pathology in human brain where several highly connected regions such as the locus coeruleus develop aggregates considerably later than would be expected from a connectivity model alone (Surmeier, Obeso and Halliday, 2017).

In line with previous reports a tiny amount of α-synuclein was identified in the EV pellet in healthy control and *SNCA*-triplication iPSC-DaNs, although no efforts were made to quantitatively compare abundance between genotypes (Fernandes *et al.*, 2016; Oh *et al.*, 2022; Yan *et al.*, 2025). These results are consistent with findings in patient CSF where only ~2% of α-synuclein is exosome-associated (Stuendl *et al.*, 2016). Despite the low overall abundance, studies in non-neuronal cells suggest that EV-associated α-

synuclein is more easily taken up by recipient cells and is more potent at seeding aggregation than free α-synuclein (Danzer *et al.*, 2012; Grey *et al.*, 2015; Delenclos *et al.*, 2017). However, the mechanism underpinning this phenomenon remains unclear since many proposed uptake pathways require direct interaction of α-synuclein with cell surface receptors which would be impossible for intravesicular α-synuclein (Delenclos *et al.*, 2017; Shippey *et al.*, 2022). Moreover, although injection of α-synuclein-containing exosomes into mouse brain seeds aggregation of endogenous mouse α-synuclein, this is far less efficient than injection of free PFFs (Ngolab *et al.*, 2017; Karampetsou *et al.*, 2020). In a therapeutic context, free but not EV-associated α-synuclein is exposed to passive immunotherapy so the mild improvement in MDS-UPDRS Part III with Prasinezumab must result from free α-synuclein clearance (Pagano *et al.*, 2024). In light of these findings and inherent technical difficulties of quantitatively studying EV-associated α-synuclein, only mechanisms of free α-synuclein secretion were pursued going forward.

The interest in α-synuclein as a biomarker of PD has motivated the development of numerous high-sensitivity commercial immunoassays to measure low concentration α-synuclein in biofluids. These include classical colourimetric ELISAs, conjugated SULFO-TAGs electrochemiluminescence and bead array-based detection in SIMOA. However, the cost of these ultra-high sensitivity approaches is prohibitive for basic research, particularly screening. Here, I characterise the DIY α-synuclein ELISA kit from Bio-Techne (with small modifications) (Fig. 4.4C-H) and a modified triple sample addition assay which yielded significantly improved sensitivity and sample detection for iPSC-DaNs conditioned media (Fig. 4.5D-H). Surprisingly, TSA did not significantly improve the assay sensitivity. Previous work demonstrated that TSA improved α-synuclein ELISA

sensitivity 400-fold and remained linear in the 20-100 pg/mL range which could not be discriminated from background in my experiments (Lee *et al.*, 2011). However, these authors used chemiluminescent rather than chromogenic detection which is more sensitive and provides a larger dynamic range (Lewkowich, Campbell and HayGlass, 2001). If future work requires further improvement to ELISA sensitivity, exchanging the chromogenic HRP substrate TMB for luminol should be considered as first priority.

Ca^{2+} was shown to modulate α-synuclein secretion (Fig. 4.6A). Consistent with work in non-neuronal models, depletion of intracellular but not extracellular Ca^{2+} impaired release (Emmanouilidou *et al.*, 2010; Zhao *et al.*, 2022; Nakamura *et al.*, 2024). However, in apparent challenge to this result, the L-type CaV channel blocker isradipine significantly impaired release implying a role for Ca^{2+} entry from the extracellular space (Fig. 4.6B). As well as coupling neuronal activity to Ca^{2+}-dependent vesicle release at the synapse, L-type CaVs also regulate autophagy through a calpain-dependent pathway triggering secondary Ca^{2+} release from intracellular stores (Williams *et al.*, 2008). As such, other dihydropyridines have been shown to induce autophagy and α-synuclein clearance (Siddiqi *et al.*, 2019). Given the weight of evidence showing that inhibition of the autophagy-lysosome pathway causes elevated α-synuclein secretion it is possible that the effect of isradipine is mediated through this more specific pathway rather than larger scale cytoplasmic Ca^{2+} dynamics (Emmanouilidou *et al.*, 2010; Danzer *et al.*, 2012; Lee *et al.*, 2013; Fernandes *et al.*, 2016; Zhao *et al.*, 2022). Isradipine has previously been investigated for efficacy in PD, showing neuroprotective effects in preclinical studies but not PD patients (Ilijic, Guzman and Surmeier, 2011; The Parkinson Study Group STEADY-PD III Investigators, 2020).

Independent of the mode of action of L-type CaV blockers, it is clear that free α-synuclein secretion must involve a Ca^{2+} sensing molecule. Synaptotagmins and synaptotagmin-like proteins, including Doc2 family members and rabphilin, all of which contain Ca^{2+}-binding C2 domains, are the main regulators of Ca^{2+}-dependent organelle fusions with the plasma membrane though inter-organelle Ca^{2+}-dependent fusion events are regulated by other effectors including calmodulin and Hrs (Yan *et al.*, 2004; Hay, 2007; Fukuda, 2013). Distinct synaptotagmin isoforms associate with different secretory pathways such that an understanding of the Ca^{2+} sensor for α-synuclein secretion would provide insight to the rest of the release mechanism (Fukuda, 2013). Discrimination between synaptotagmins necessitates a genetic rather than pharmacological approach.

Quercetin, GW4869 and Chloroquine but not 2-bromopalmitic acid or MRT68921 were shown to modulate α-synuclein secretion (Fig. 4.3B-G, 4.7B&E). Although these results suggest that some of the mechanisms identified in non-neuronal systems may also be active in iPSC-DaNs, they also highlight the challenges of relying on drugs to draw specific cell biology conclusions. 2-bromopalmitic acid showed only limited target engagement at 10 μM (Fig. 4.3A) and lacked dose dependence in its effect on α-synuclein secretion, suggesting possible off-target toxicity. Although quercetin reduced α-synuclein secretion in all three genotypes (Fig. 4.4B-G) this drug is known to have an extensive polypharmacology making it impossible to conclude that its effects are solely mediated through DNAJC5 (Vijayan *et al.*, 2016; Georgiou *et al.*, 2023). Many other pharmacological agents have been used to study of α-synuclein secretion in cell lines, but these also pose problems. For example, ambroxol increases α-synuclein secretion apparently through inhibition of autophagy, but also reduces ER stress, increases

lysosomal hydrolase activity and was recently found to interact with at least 19 intracellular targets (Magalhaes *et al.*, 2018b; Dhanve *et al.*, 2023; Z. Wang *et al.*, 2023).

Overall, it is clear that active secretion of α-synuclein by iPSC-DaNs occurs through a variety of mechanisms which exhibit a degree of crosstalk and reciprocal regulation. To better map these pathways and obtain a clearer understanding of the protein families and isoforms involved a targeted genetic approach is required.

Chapter 5 – CRISPRi screen for regulators of α-synuclein secretion

5.1 Introduction

Having demonstrated in Chapter 4 that α-synuclein secretion can be manipulated in iPSC-DaNs to probe the underlying mechanisms, I sought to expand on these findings with a targeted genetic approach. Mechanistic studies in immortal cell lines have identified a range of potential regulatory genes which modulate α-synuclein secretion when knocked down using shRNA or siRNA technology (Table 5.1). These genes map to four main pathways: misfolding-associated protein secretion (MAPS), release from the recycling endosome, lysosomal exocytosis or extracellular vesicle release. There is notable overlap between the molecular regulators of these pathways particularly converging around late-endosomal/lysosomal biology.

Work in non-neuronal models has suggested that α-synuclein secretion is boosted by disruption to the autophagy-lysosome system and additional mechanisms are recruited to achieve this effect. I confirmed that in iPSC-DaNs pharmacological perturbation of lysosomes (but not autophagy) also increased free α-synuclein secretion (Figs. 4.3E-G & 4.7C-E). Moreover, in line with previous studies *GBA1-N370S* patient neurons, which exhibit a clear lysosomal deficit, secreted more α-synuclein than controls despite similar levels of intracellular expression (Fernandes *et al.*, 2016) – Fig. 4.1. However, not all PD-linked genes cause strong lysosomal phenotypes, instead inducing degeneration through mitochondrial or proteasomal pathways (Korczyn and Hassin-Baer, 2015). Furthermore, only around 10% of PD cases are familial (Poewe *et al.*, 2017), and increasing evidence

Table 5.1 – Genes whose knockdown is reported to modulate α-synuclein secretion

Gene	Effect of KD/KO/inhibition	Cell model	Pathway	Publication
DNAJC5	Reduced	HEK293T	MAPS	Xu et al (2018)
USP19	Reduced	HEK293T	MAPS	Lee et al (2016) Wang et al (2024)
HSPA8	Reduced	HEK293T	MAPS	Xu et al (2018) Fontaine et al (2016)
ATG5	Increased	LUHMES cells	Exosomes	Fussi et al (2018)
	Reduced	SH-SY5Y	-	Nakamura et al (2024) Sawai et al (2025)
GBA1	Increased	SH-SY5Y	Lyso exocytosis	Sawai et al (2025) Bae et al (2014)
RAB8A	Reduced	SH-SY5Y	Secretory Autophagy	Nakamura et al (2024) Sawai et al (2025)
RAB11A	Reduced	HEK293T	RE secretion	Hasegawa et al (2011)
		SH-SY5Y	RE secretion	Hasegawa et al (2011)
		MES23.5	-	Liu et al (2009)
	Increased	SH-SY5Y	Not RE secretion	Chutna et al (2014)
RAB27A	Reduced	PC12	LE fusion	Ejlerskov et al (2013)
RAB27B	Reduced but HMW increased	M17	Not exosomes	Underwood et al (2020)
SCAMP5	Reduced	SH-SY5Y	Exosomes	Yang et al (2017
SNAP23	Reduced	HEK	MAPS	Fontaine et al (2016)
		M17	MAPS	Fontaine et al (2016)
		SH-SY5Y (diff)	-	Zhao et al (2022)
		SH-SY5Y	Lyso exocytosis	Sawai et al (2025)
		Primary neurons	Lyso exocytosis	Xie et al (2022)
STX1A	No effect	SH-SY5Y (diff)	-	Zhao et al (2022)
STX4	Reduced	SH-SY5Y (diff)	-	Zhao et al (2022)
		SH-SY5Y	Lyso exocytosis	Sawai et al (2025)
UBC9	Reduced	N2a	Exosomes	Kundt et al (2015)
VAMP3	Reduced	SH-SY5Y (diff)	-	Zhao et al (2022)
VAMP7	Reduced	SH-SY5Y (diff)	-	Zhao et al (2022)
		Primary neurons	Lyso exocytosis	Xie et al (2022)
VAMP8	Reduced	SH-SY5Y (diff)	-	Zhao et al (2022)
SNAP25	Increased	SH-SY5Y (diff)		Zhao et al (2022)
HSP90	No effect	HEK293T	MAPS	Xu et al (2018)
	No effect	H4	-	Danzer et al (2011)
	Reduced	MES23.5	-	Liu et al (2009
ATG7	Increased	MEF	Not exosomes	Lee et al (2013)
BECN1	Reduced	SH-SY5Y	Lyso exocytosis	Sawai et al (2025)
FIP200	Reduced	SH-SY5Y	Lyso exocytosis	Sawai et al (2025)
14-3-3θ	Reduced	M17	-	Wang et al (2018)
GRASP55	Reduced	SH-SY5Y	Lyso exocytosis	Sawai et al (2025)
CHMP2B	Increased	B103	-	Spencer et al (2016
UFM1	Reduced	HEK293T	MAPS	Wang et al (2024)
LAMP2	Reduced	HEK293T	MAPS	Lee et al (2018)
UBA5	Reduced	HEK293T	MAPS	Wang et al (2024)
UFBP1	Reduced	HEK293T	MAPS	Wang et al (2024)
VPS4	Increased	HEK293T	RE secretion	Hasegawa et al (2011)
		SH-SY5Y	RE secretion	Hasegawa et al (2011)

HMW = high molecular weight α-synuclein, Lyso = lysosome, RE = recycling endosome
Black: target assessed in this study, Grey: Target not assessed in this study

suggests that some sporadic cases show mitochondrial-dominant pathology with little lysosomal perturbation (Poewe *et al.*, 2017; Carling *et al.*, 2020; Arena *et al.*, 2024). Carling and colleagues demonstrated that fibroblasts from sporadic PD patients can be stratified by lysosomal or mitochondrial dysfunction and that this stratification is predictive of response to neuroprotective agents.

Although additional secretion pathways, namely lysosomal exocytosis and EV release, may be recruited during autophagy-lysosome dysfunction, work in non-neuronal models suggests that basal secretion mechanisms are not down-regulated (Hasegawa *et al.*, 2011; Spencer *et al.*, 2016; Wu, Sirkis and Schekman, 2022). Hence, inhibition of basal pathways active in the absence of lysosomal stress is expected to reduce α-synuclein release indiscriminate of PD genotype. Therefore, to ensure the broadest applicability of mechanistic findings from this study, I decided to interrogate the α-synuclein secretion pathways used by iPSC-DaNs in the absence of overt autophagy-lysosome dysfunction. If a suitable cell model and study design are established here, future work could build on these results by probing the effects of lysosomal perturbation on the genetic regulators involved.

Regulatory genes identified to date cluster into three major families including Rab GTPases which control membrane trafficking, SNARE proteins responsible for membrane fusion (both intracellularly and with the plasma membrane), and a more heterogenous category of regulators of autophagosome biogenesis (Table 5.1). I selected the 17 best-studied which also have the most direct effects on α-synuclein release for inclusion in the knockdown screen. A further 15 genes were selected which have either not yet been studied in the context of α-synuclein release but contribute to implicated pathways (such

as cognate SNARE proteins) or which have only previously been assessed with overexpression, not knockdown (Table 5.2). In Chapter 4 I demonstrated that α-synuclein secretion is Ca^{2+}-dependent in iPSC-DaNs indicating the presence of a Ca^{2+} sensor. Ca^{2+}-responsive synaptotagmin-like protein 5 (*SYTL5*) overexpression has previously been found to boost α-synuclein secretion in SH-SY5Y cells (Gonçalves *et al.*, 2016). Synaptotagmins 1 and 7 also act as Ca^{2+} sensors for SNARE-mediated membrane fusion complexing with SNAP-25/Syntaxin-1A/VAMP2 and SNAP-23/Syntaxin-4/VAMP7 respectively (Rao *et al.*, 2004; Dingjan *et al.*, 2018). Therefore, these three synaptotagmins were also investigated (Table 5.2). Finally, I selected two negative controls, Syntaxin-5 and Rab5, involved in ER-Golgi trafficking and early-endosome fusion respectively and which have no known links to pathways implicated in α-synuclein release (Dingjan *et al.*, 2018; Zhang, Jiang and Shi, 2022). These are expected not to specifically impact α-synuclein secretion but serve as controls for generalised perturbation of protein trafficking.

CRISPRi was used for target gene knockdown. This approach exhibits higher specificity and fewer off target effects than the RNAi used in previous studies (Franks, Heon-Roberts and Ryan, 2024). CRISPRi requires cells to stably express the dCas9 enzyme required for transcriptional repression. Unpublished work from our research group has engineered a selection of healthy control and PD iPSC lines expressing the dCas9 enzyme which, following validation, may be suitable for interrogating the effect of gene knockdown on α-synuclein secretion. Pairing these neurons with the optimised ELISAs presented in Chapter 4, I set out to identify the genes and pathways involved in α-synuclein secretion from iPSC-DaNs with a CRISPRi screen.

Table 5.2 Additional CRISPRi targets and associate rationale for inclusion

Gene	Function	Reason for inclusion
STX5	ER to TGN trafficking	Does not interact with α-synuclein (Cuddy *et al.*, 2019). Negative control.
RAB5A	EE transport	Involved in α-synuclein endocytosis (Jy *et al.*, 2001). Negative control.
SYT1	Ca^{2+} regulation of SNAREs	Regulation of axonal & somatodendritic dopamine release (Banerjee *et al.*, 2020; Lebowitz *et al.*, 2022).
SYT7	Ca^{2+} regulation of SNAREs	Activity-dependent plasticity of dopamine release (Lebowitz *et al.*, 2024).
SYTL5	Ca^{2+} regulation of SNAREs	Overexpression increases α-synuclein release (Gonçalves et al., 2016).
RAB13	TGN to RE trafficking	Overexpression increases α-synuclein release (Gonçalves et al. 2016).
RAB7A	AP, Lyso & LE transport	Overexpression increases α-synuclein release (Ejlerskov *et al.*, 2013).
RAB9A	LE transport	Co-localises with α-synuclein (Xu et al. 2018).
RAB35	RE & SV transport to PM	Overexpression increases α-synuclein release (Chiu *et al.*, 2016).
MICAL1	RE to PM trafficking	Rab8a, 8b and 10 effector for RE secretion of newly synthesised protein (Lucken-Ardjomande Häsler *et al.*, 2020).
WDR44	RE to PM trafficking	Rab11a effector for RE secretion (Lucken-Ardjomande Häsler *et al.*, 2020).
SNAP29	AP-Lyso fusion	Directly interacts with α-synuclein, knockdown boosts release of exosomes, but α-synuclein content was not examined (Tang et al. 2021).
STX17	AP-Lyso fusion	Cognate SNARE of SNAP-29 and VAMP8 (Itakura, Kishi-Itakura and Mizushima, 2012).
VTI1B	AP and LE fusion	Cognate SNARE of VAMP7 and Syntaxins 7+8, important for autophagosome maturation (Antonin, 2000; Moreau *et al.*, 2011).
VSP35	LE transport	Linked to late-onset PD, causes LE dysfunction (Bono *et al.*, 2020).

AP, autophagosome, EE = early endosome, LE = late endosome, Lyso = Lysosome, PM = plasma membrane, RE = recycling endosome, SV = synaptic vesicle, TGN = Trans-Golgi network

Chapter Aims:

1. To generate a library of CRISPRi guides against genes implicated in α-synuclein secretion.
2. To validate an iPSC-DaN model suitable for high-throughput screening of α-synuclein release.
3. To carry out a CRISPRi screen to determine genetic regulators of α-synuclein secretion in iPSC-DaNs.

5.2 Target expression in patient and control iPSC-DaNs

To further refine the list of proposed CRISPRi target genes (Table. 5.1 & 5.2), the mRNA expression level of these genes was assessed in healthy control and *SNCA*-triplication iPSC-DaNs using the short-read bulk mRNA sequencing dataset (gathered by Dr Vallin). This demonstrated that *VAMP8* is barely expressed in iPSC-DaNs, so it was removed from the target list (Fig. 5.1A). All other genes were expressed at reasonable levels with *HSPA8* (encoding Hsc70) being the most abundant. Expression of *SNCA* is high in both genotypes compared to the other genes of interest. The finalised set of target genes for CRISPRi interrogation is shown in Fig. 5.1B.

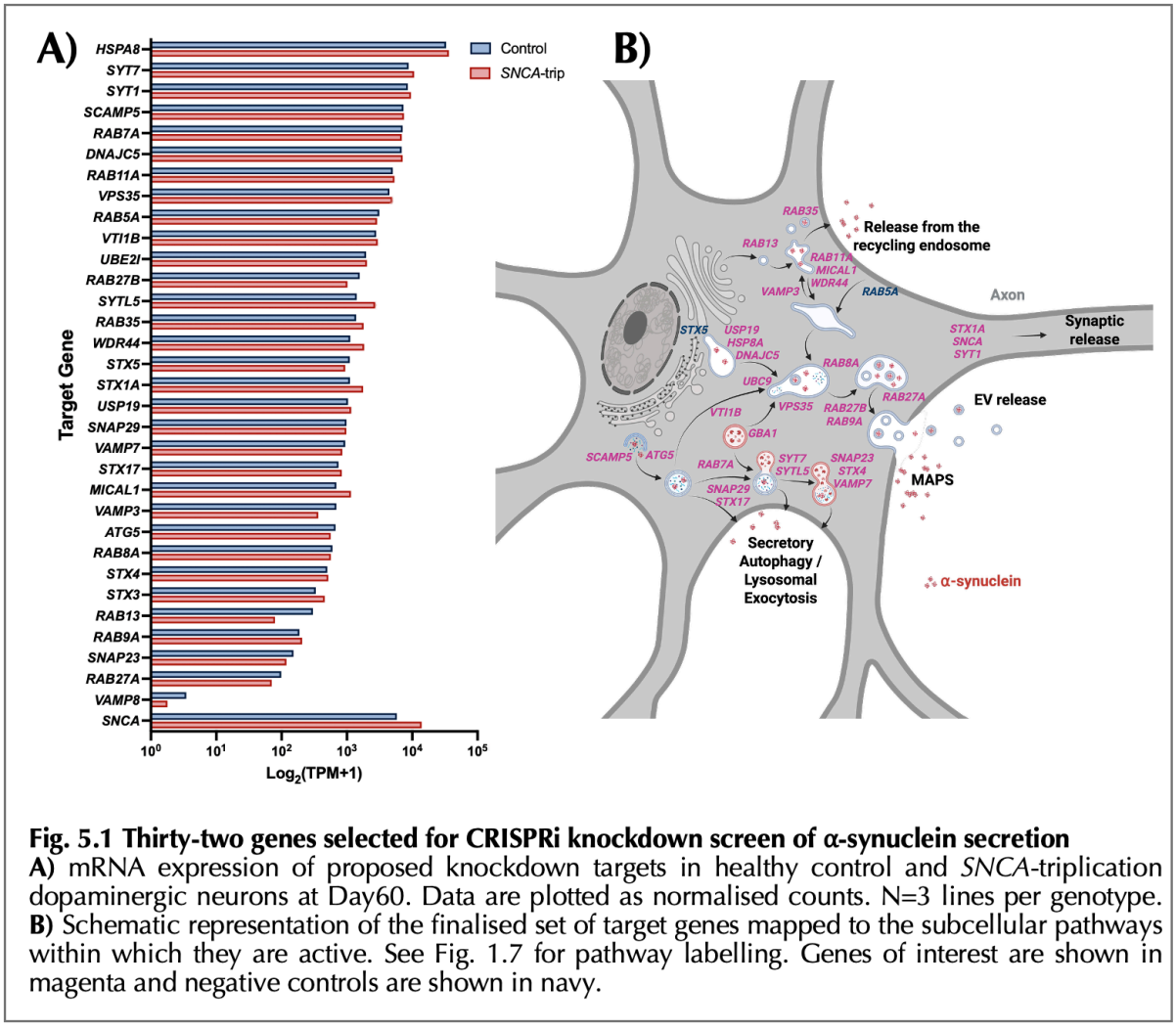

Fig. 5.1 Thirty-two genes selected for CRISPRi knockdown screen of α-synuclein secretion
A) mRNA expression of proposed knockdown targets in healthy control and *SNCA*-triplication dopaminergic neurons at Day60. Data are plotted as normalised counts. N=3 lines per genotype. **B)** Schematic representation of the finalised set of target genes mapped to the subcellular pathways within which they are active. See Fig. 1.7 for pathway labelling. Genes of interest are shown in magenta and negative controls are shown in navy.

5.3 Cloning, lentiviral production and titering

Using the tool developed by Horlbeck and colleagues two sgRNA guide sequences were selected per target gene with high predicted efficiency and specificity (Horlbeck *et al.*, 2016). These sequences were cloned into the published H25-U6-sgRNA-NucBlue backbone plasmid (Tian *et al.*, 2019) – Fig. 5.2A, which contains the mTagBFP2 coding sequence fused to a nuclear localisation signal to enable assessment of transduction efficiency. Three clones were prepared per sgRNA guide and DNA sequencing demonstrated a ligation efficiency of ~80% with minimal point mutations (Fig. 5.2B). Error-free DNA sequences were packaged into lentiviruses for efficient delivery of the sgRNA to iPSC-DaNs.

Success of lentiviral packaging was demonstrated in SH-SY5Y neuroblastoma cells expressing the dCas9 enzyme. These cells took up the virus in a dose-dependent manner and robustly expressed the nuclear mTagBFP2 marker (Fig. 5.2 C&D). For the four guides assessed, 20 µL of undiluted virus per well of a full-area 96-well plate gave 70-90% transduction efficiency (Fig. 5.2D). Three out of the four guides reduced the expression of their target gene (Fig. 5.2E), although it is worth noting that the endogenous expression of *SYT7* is considerably lower in SH-SY5Y than in iPSC-DaNs. Since the guide sequences generated by Horlbeck and colleagues are genome-wide predictions, not validated for knockdown efficiency it is unsurprising that one of the guides had no effect on gene expression. Unpublished work from our research group suggests that ~60% of predicted guide sequences do not reduce gene expression, hence the decision to design two guides per target gene in the screen.

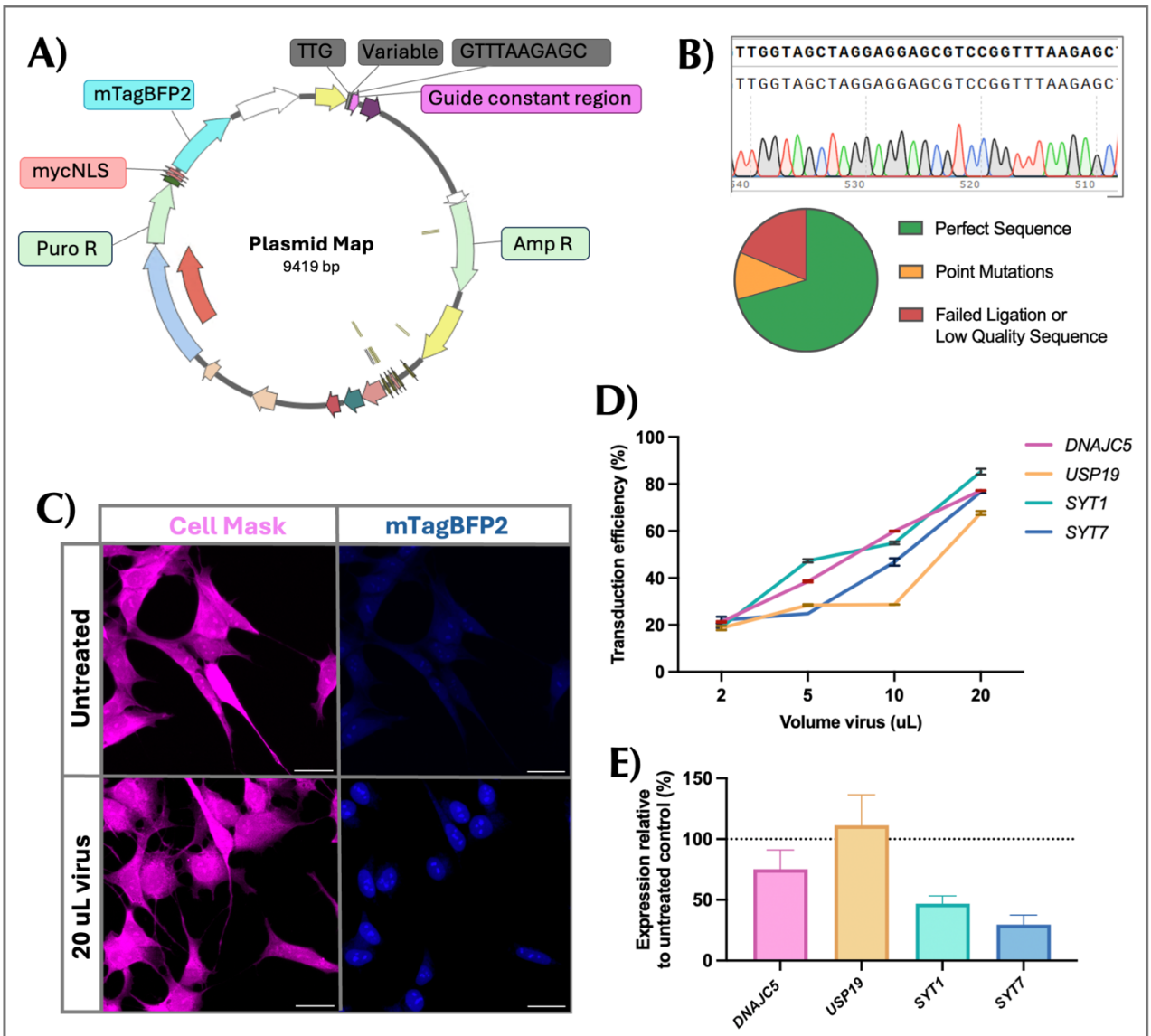

Fig. 5.2 sgRNA packaged in lentiviruses reduce gene expression in neuroblastoma cells
A) Schematic representation of the sgRNA plasmid containing antibiotic resistance selection markers, the nuclear mTagBFP2 and the variable and constant regions of the CRISPRi sgRNA guide. **B)** Example sequencing results for the variable region of a Syntaxin-3 guide and pie chart showing the proportion of successful cloning reactions **C)** Representative images of dCas9 SH-SY5Y cells transduced with 20 µL lentivirus containing *SNCA*-targeting sgRNA. Scale bar = 25 µm. **D)** Percentage of dCas9 SH-SY5Y cells with mTagBFP2+ nuclei 48 hours after transduction with 2, 5, 10 or 20 µL of four sgRNA lentiviruses. The guides used were: *DNAJC5_1, USP19_2, SYT1_1* and *SYT7_2* **E)** Knockdown efficiency of the same four lentiviruses represented as expression of the target gene relative to expression in untreated cells determine by qPCR. Data represented as means ± S.E.M.

Motivated by successful transduction and knockdown of the guides tested in SH-SY5Y cells I moved to iPSC-DaNs. To avoid the proposed impact of lysosomal dysfunction on α-synuclein release, neurons from a healthy control (856) were used for the following experiments. The iPSCs were engineered to express the dCas9-KRAB machinery and nuclear mNeonGreen marker by Dr Maria-Claudia Caiazza using a PiggyBac system (unpublished). Following differentiation, these cells exhibited a neuronal morphology and expressed the neuronal marker MAP2 (Fig. 5.3A). Some of the differentiated dCas9 neurons also express dopaminergic marker tyrosine hydroxylase (TH), although this was only 31% of the total population compared to a 60-70% differentiation efficiency which is usually achieved for cells that have not been subject to genetic engineering.

Treatment of the dCas9 neurons with sgRNA lentiviruses demonstrated co-localisation of sgRNA (mTagBFP2) and dCas9 (mNeonGreen) expression (Fig. 5.3B). The dCas9 marker was expressed in 62% of neurons and expression level was not influenced by lentivirus treatment. In SH-SY5Y cells, lentiviruses demonstrated considerable variability in transduction efficiency, particularly at intermediate titer volumes (Fig. 5.2E). The full set of 68 lentiviruses was generated in 5 batches over a one-year period, potentially introducing batch-to-batch variability. To tackle this the viruses were titered on dCas9 856 neurons, calculating the percentage positive for mTagBFP2 out of the total population detected with a live-cell nuclear mask (Fig. 5.3C). This showed significant variability between viruses, with some e.g. *SYTL5* achieving a transduction efficiency of >95% while others e.g. *HSPA8* transduced only 40% of neurons. Assaying the same virus over two experimental replicates (independent differentiations) showed that there was very little difference in the transduction efficiency, demonstrating that viral titres calculated from these experiments should be valid for future differentiations (Fig. 5.3D).

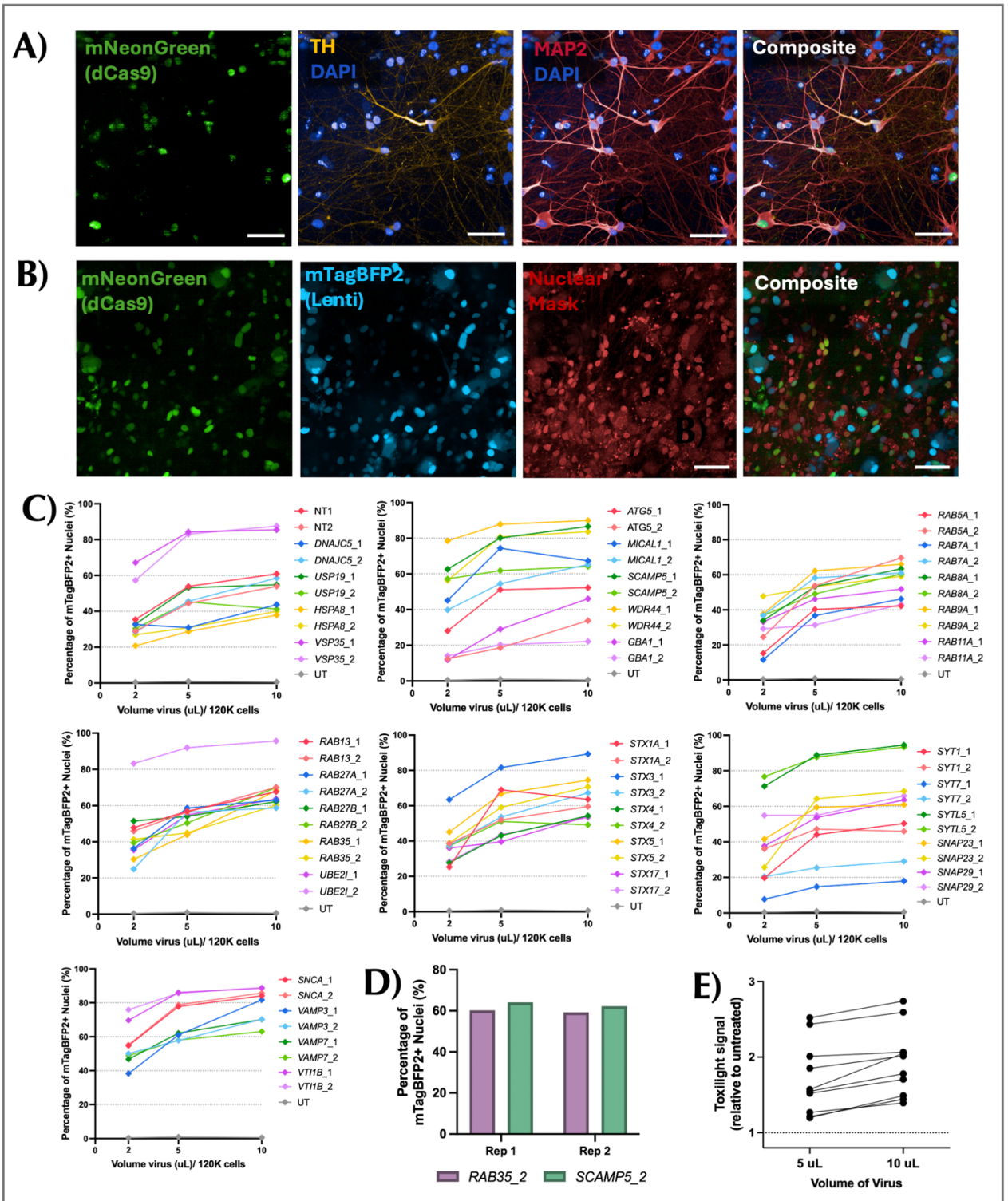

Fig. 5.3 sgRNA lentivirus uptake by iPSC-derived dopaminergic neurons

A) Representative confocal microscopy images of dCas9 856 healthy control neurons immunostained for differentiation markers TH and MAP2 at Day50. Scale bar = 50 µm. **B)** Representative live fluorescence microscopy images of dCas9 856 nuclei at Day25. Scale bar = 50 µm. **C)** Graphs of transduction efficiency for each of the 68 viruses added to cells at Day16 and imaged at Day25. **D)** The calculated transduction efficiency of 10 µL of two viruses is constant between two experimental replicates. **E)** Adenylate kinase release measured with Toxilight as a marker of cytolysis shows that 10 µL of lentivirus is more toxic to cells than 5 µL. Each data point is a different sgRNA lentivirus at either of the two doses.

For a selection of 10 lentiviruses tested increasing the viral titer from 5 to 10 µL was found to subtly increase cytolysis measured by adenylate kinase release (Fig. 5.3E). Although these changes were subtle, and lower in magnitude than the differences in toxicity between viruses, it indicated that 5 µL should be used in cases where the increase in transduction efficiency achieved with 10 µL was minimal. As such it was decided:

- For viruses with maximum transduction efficiency of <60%, 10 µL should be used.
- For viruses with maximum transduction efficiency of 60-85%, 5 µL should be used unless 10 µL increased the percentage transduction by >1.1-fold compared to 5 µL.
- For viruses with a transduction efficiency of >85% for 5 µL, then 5 µL should be used independent of the increased efficiency using 10 µL.

Using this method, I determined that a titer of 5 µL could be used for one third of the sgRNA lentiviruses generated.

5.4 Pilot Screen: Improvement to assay window required

To trial all components of the screen (neuronal maturation, virus treatment, media collection, α-synuclein ELISA and qPCR) in tandem a pilot screen was carried out using the appropriate titer of 28/68 sgRNA lentiviruses. Healthy control iPSC-DaNs expressing dCas9 were transduced with lentivirus at Day16 and matured until Day70 when α-synuclein secretion is maximal (Fig. 4.1A). Conditioned media and cells were harvested for ELISA and RT-qPCR analysis of knockdown efficiency respectively.

ELISA measurements of secreted α-synuclein demonstrated that the two non-targeting guides did not alter α-synuclein release compared to the untreated control, indicating that viral transduction itself does not perturb α-synuclein secretion (Fig. 5.4A). Both *SYT1* and *SYT7* guides reduced the α-synuclein concentration of conditioned media while it was increased by *GBA1_1 and* possibly by *ATG5* (Fig. 5.4A&B). However, the α-synuclein measurements were below the range of the ELISA. standards, so concentrations could not be interpolated. These experiments were undertaken in parallel with the ELISA optimisations presented in Chapter 4. At the time of this pilot the BioT3 ELISA had not yet been optimised so the less sensitive Bio-Techne ELISA was used for media analysis. Therefore, the assay window was greatly compressed with a difference of only 0.005 absorbance units between the lowest value for a non-targeting guide and the blank.

RT-qPCR showed that 13/16 (81%) of the sgRNA guides reduced the expression of their target gene relative to non-targeting controls, and expression was reduced by >50% for 7/16 (44%) (Fig. 5.4C). Neither guide against *USP19* reduced target expression and only one *HSPA8* guide reduced the expression while the other appeared to increase expression >2-fold. The mRNA yield was too low to assess the knockdown efficiency of

several guides using the QIAGEN RNeasy Mini Kit, indicating that an alternative approach to RNA extraction was required going forward. For samples with a sufficient mRNA yield the expression of *SNCA* was also assessed, compared to knockdown using the *SNCA_1* guide which was previously validated by Dr Rachel Heon-Roberts. sgRNAs against other targets did not alter α-synuclein expression (Fig. 5.4D).

Overall, this pilot screen demonstrated that CRISPRi is able to modulate α-synuclein secretion in iPSC-DaNs through specific knockdown of target genes. However, the ELISA assay window and mode of RNA extraction needed improvement before assessing all sgRNA guides.

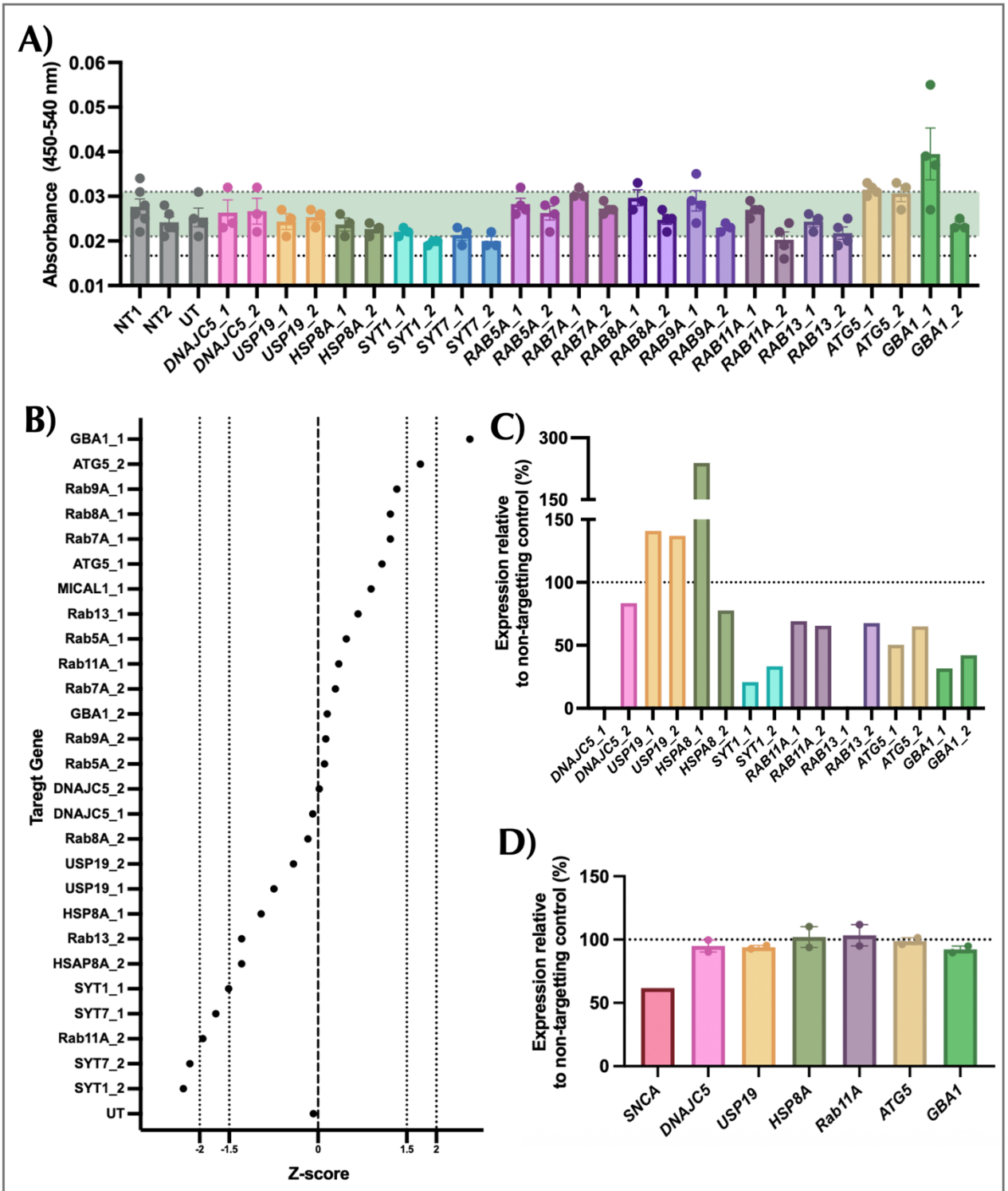

Fig. 5.4 sgRNA lentiviruses knockdown target expression and modulate α-synuclein secretion in iPSC-derived dopaminergic neurons. A) Raw absorbance values from the Bio-Techne ELISA for four-day conditioned media harvested from Day70 dCas9 856 dopaminergic neurons. The range of values recorded for technical replicates of the untreated control is shown in green and the value of the naïve media blank is marked with a black dotted line. **B)** Z-scores calculated from the data shown in A) relative to the the non-targeting controls on each ELISA plate. **C)** mRNA expression of CRISPRi targets relative to expression of each gene in the non-targeting controls (100%). **D)** mRNA expression of *SNCA* relative to expression in the non-targeting controls. Each data point represents one sgRNA guide. The housekeeping genes *UBE2D2, CYC1* and *RPL13* were used for inter-sample normalisation in all RT-qPCR experiments.

5.5 Optimisations 1: Knockdown efficiency & RNA extraction

USP19 and *HSPA8* are both essential genes for MAPS (Lee *et al.*, 2016; Xu *et al.*, 2018; Wu, Sirkis and Schekman, 2022). In chapter 4 I demonstrated a putative role for MAPS in α-synuclein secretion from iPSC-DaNs using *DNAJC5* inhibitor quercetin (Fig. 4.3). The transduction efficiency of both guides against *HSPA8* and one of the *USP19* guides was very low (Fig. 5.3C), and neither *USP19* guide reduced gene expression in iPSC-DaNs or SH-SY5Y cells while *HSPA8_1* increased gene expression (Figs. 5.2F & 5.4C). Therefore, I decided to make a new sgRNA guide for each target using a different predicted sequence from the Horlbeck et al. tool. Viral titering showed an improved transduction efficiency for *HSPA8_3* compared to *HSPA8_1* & *HSPA8_2* but no improvement in transduction efficiency for *USP19_3* (Figs. 5.3C & 5.5A). To increase the probability of successful knockdown I decided to use all three guides for these two genes going forward.

A minimum of 100 pg (concentration >5.5 pg/µL) of RNA was required to measure target expression relative to housekeeping genes. Using the QIAGEN RNeasy mini kit for extraction several samples failed to meet this minimum criterion, preventing verification of knockdown efficiency. Therefore, I tested a plate-based TRIzol extraction kit (DirectZol-96) which both increased the RNA yield and reduced experimental complexity by enabling the parallel processing of up to 96 samples (Fig. 5.5B). ELISA normalisation requires a live nuclei count before RNA extraction. To verify that staining did not hinder RNA extraction or subsequent qPCR iPSC-DaNs were stained and live imaged with a nuclear mask, followed by RNA extraction and RT-qPCR (Fig. 5.5C-E). This demonstrated that sufficient RNA could be harvest after staining, with only a slight

decrease to yield (Fig. 5.5D). Moreover, the C_T values obtained for housekeeping genes were barely affected by staining, indicating that the media harvest -> cell count -> RNA harvest -> RT-qPCR workflow is suitable for use in the main screen (Fig. 5.5E).

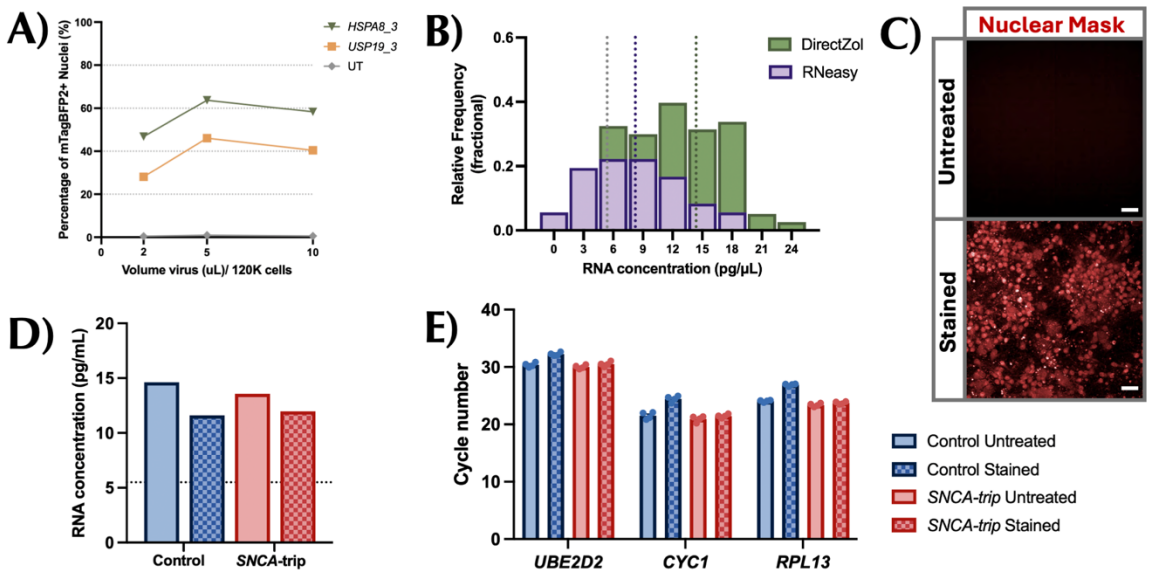

Fig. 5.5 Optimising transduction efficiency and RNA yield
A) Transduction efficiency for new *USP19* and *HSPA8* lentiviruses added to cells at Day16 and imaged at Day25. **B)** Histogram of RNA yield from samples harvested with RNeasy or DirectZol extraction kits. Coloured dotted lines indicate the median RNA concentration from each extraction method (green/purple), and the grey dotted line shows the minimum required RNA concentration for successful RT-qPCR. **C)** Representative live fluorescence microscopy images of nuclei from healthy control neurons at Day60, stained with HCS far red NuclearMask. Scale bar = 50 µm. **D)** Yield of RNA extracted using the DirectZol kit for Day60 neurons pre-incubated with the live nuclear mask shown in C). **E)** Raw CT values for house-keeping genes from Day60 neurons pre-incubated with the live nuclear mask.

5.6 Optimisations 2: Cell line and differentiation protocol

Despite the development of a more sensitive ELISA than that used in pilot screen (Figs. 4.5 & 5.4) I was concerned that the dCas9 856 healthy control line does not secrete enough α-synuclein to be used for screening. The α-synuclein concentration of conditioned media from untreated dCas9 856 neurons measured with the BioT3 ELISA was 350 ± 60 pg/mL (mean ± standard deviation). While this is considerably above the LOD of the assay I remained apprehensive that additional variability introduced by the multi-plate nature of the main screen would render the assay window too small for confident identification of all hits. Moreover, although the dCas9 856 neurons exhibited typical neuronal morphology (Fig. 5.3A) the TH expression was concerningly low. Given that the ELISA is a whole-well assay with no way to specifically select for dopamine neuron-derived α-synuclein I set out to find an alternative cell line for screening.

Both *GBA1-N370S* and *SNCA*-triplication patient-derived dopaminergic neurons secrete considerably more α-synuclein than healthy controls (Fig. 4.1). While *SNCA*-triplication dopaminergic neurons do exhibit a degree of lysosomal dysfunction these phenotypes are less profound than in *GBA1-N370S* neurons and arise as a direct result of α-synuclein accumulation (Zambon *et al.*, 2019; McGuinness *et al.*, 2025). I therefore decided to capitalise on the, as yet uncharacterised, dCas9 *SNCA*-triplication iPSC lines generated by Dr Caiazza dCas9 831-1 and dCas9 831-3.

The dCas9 *SNCA*-triplication cells were markedly more vulnerable than dCas9 healthy control neurons or *SNCA*-triplication neurons which had not been genetically engineered. In total, 11 differentiations of these lines were carried out during this study; dCas9 831-1 survived past the neural progenitor stage (Day8-10) in 4 differentiations,

and dCas9 831-3 only survived to maturity twice. In differentiations where the cells survived until Day60 both patient lines retained dCas9 expression but the expression level was higher for dCas9 831-3 (Fig. 5.6A). Consistent with this the *SYT1_1* guide which showed effective knockdown in dCas9 SH-SY5Y cells and dCas9 856 healthy control neurons, only reduced *SYT1* expression in dCas9 831-3 but not dCas9 831-1 (Fig. 5.6B). Due to their vulnerability, it was not possible to assess α-synuclein secretion in dCas9 831-3, but dCas9 831-1 released 2-3-fold more α-synuclein than the dCas9 856 neurons (Fig. 5.6C). Unsurprisingly there was no effect of *SYT1* sgRNA lentiviruses on α-synuclein release from these dCas9 831-1 cells, likely due to the low dCas9 expression and resultant failure to knockdown to *SYT1*.

The low dCas9 expression in 831-1 was further confirmed by immunocytochemistry, which demonstrated that signal intensity for the mNeonGreen marker also differed between lines (Fig. 5.6D). More concerningly the dCas9 *SNCA*-triplication lines contained abundant non-neuronal cells which were positive for MAP2 but had a fibroblast-like appearance. These cells had larger nuclei than dopaminergic neurons and could be approximately quantified by the proportion of cells with nuclei greater than 130 μm^2. This analysis demonstrated that 15-25% of the dCas9 831-1 and dCas9 831-3 cultures were composed of fibroblast-like cells. Moreover, very few of the remaining 75-85% of cells expressed dopaminergic marker TH, resulting in a differentiation efficiency of only 17±3% (mean ± S.E.M) for dCas9 831-1 across three independent differentiations. Together these results demonstrate that the dCas9 *SNCA*-triplication cells are completely unsuitable for CRISPRi screening as it appears that engineering to express dCas9 has disrupted not only viability but also their differentiation potential.

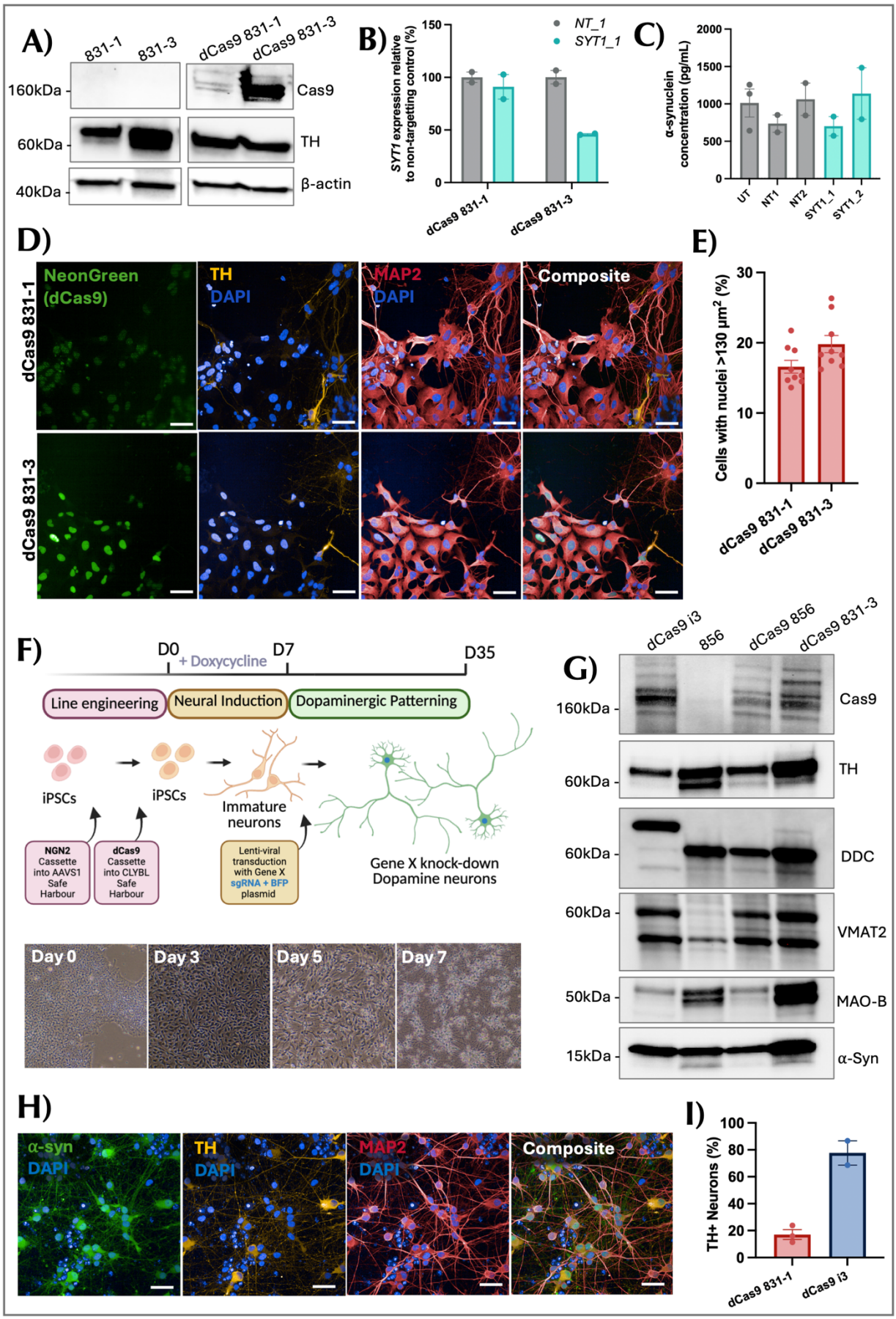
A)
831-1
831-3
dCas9 831-1
dCas9 831-3
160kDa
60kDa
40kDa
Cas9
TH
β-actin
B)
SYT1 expression relative to non-targetting control (%)
NT_1
SYT1_1
dCas9 831-1
dCas9 831-3
C)
α-synuclein concentration (pg/mL)
UT
NT1
NT2
SYT1_1
SYT1_2
D)
NeonGreen (dCas9)
TH DAPI
MAP2 DAPI
Composite
dCas9 831-1
dCas9 831-3
E)
Cells with nuclei >130 µm² (%)
dCas9 831-1
dCas9 831-3
F)
D0
+ Doxycycline
D7
D35
Line engineering
Neural Induction
Dopaminergic Patterning
iPSCs
iPSCs
Immature neurons
NGN2 Cassette into AAVS1 Safe Harbour
dCas9 Cassette into CLYBL Safe Harbour
Lenti-viral transduction with Gene X sgRNA + BFP plasmid
Gene X knock-down Dopamine neurons
Day 0
Day 3
Day 5
Day 7
G)
dCas9 i3
856
dCas9 856
dCas9 831-3
160kDa
60kDa
60kDa
60kDa
50kDa
15kDa
Cas9
TH
DDC
VMAT2
MAO-B
α-Syn
H)
α-syn DAPI
TH DAPI
MAP2 DAPI
Composite
I)
TH+ Neurons (%)
dCas9 831-1
dCas9 i3

Fig. 5.6 Transdifferentiation generates homogeneous dopaminergic neurons expressing dCas9
A) Western blot after SDS-PAGE for dCas9 expression in Day60 neurons from two *SNCA*-triplication lines dCas9 831-1 and dCas9 831-3. **B)** Expression of *SYT1* mRNA in Day60 dCas9 *SNCA*-triplication neurons transduced on Day16 with lentivirus containing the *SYT1_1* guide or a non-targeting sgRNA. **C)** Concentration of secreted α-synuclein in conditioned media measured with the BioT3 ELISA from Day60 831-1 neurons transduced with sgRNA against *SYT1* or non-targeting controls**. D)** Representative confocal fluorescence microscopy images of both dCas9 *SNCA*-triplication cell lines, showing abundant non-neuronal cells. Scale bar = 50 µm. N=2-3 differentiations. **E)** Proportion of cells in *SNCA*-triplication cultures with a nuclear area greater than 130 μm^2 as a proxy measure of non-neuronal identity. N=1 differentiation. **F)** Schematic showing the protocol for transdifferentiation of *NGN2*-induced dopaminergic neurons from i3 (G3dCas9) iPSCs, a modification of the Sheta et al. (2023) protocol. Phase contrast images show the rapid change in morphology from stem cells to neurons in the first 7 days of differentiation. **G)** Western blots after SDS-PAGE for dCas9, α-synuclein and enzymes involved in dopamine metabolism in mature neurons. dCas9 i3s were differentiated for 35 days according to a modified version of the Sheta et al. (2023) protocol and 856, dCas9 856 and dCas9 831-3 were matured to Day50 according to the modified protocol from Kriks et al. (2011) used for the generation of all dopaminergic neurons presented up to this point. **H)** Representative confocal fluorescence microscopy images of dCas9 i3 dopaminergic neurons at Day35 immunostained for α-synuclein, neuronal marker MAP2 and dopaminergic marker tyrosine hydroxylase. Scale bar = 50 µm. **I)** Percentage of MAP2+/TH+ neurons in mature cultures of dCas9 831-1 neurons differentiated to Day60 according to the Kriks protocol or dCas9 i3 neurons differentiated to Day35 according to the Sheta protocol. Data points represent the average of technical replicates from 2-3 independent differentiations from iPSCs.

Successful knockdown of various targets in glutamatergic neurons has been published previously with the same sgRNA backbone as used in this thesis (Tian *et al.*, 2019). The i3 neurons generated by Tian and colleagues express dCas9-BFP-KRAB from the CLYBL safe harbour locus but were induced with forced *NGN2* expression rather than growth factors (Zhang *et al.*, 2013; Wang *et al.*, 2017; Fernandopulle *et al.*, 2018; Tian *et al.*, 2019). Recently the Oueslati group published a protocol for *NGN2*-induction of dopaminergic neurons following transduction of patient iPSCs with a doxycycline-inducible *NGN2* lentivirus (Sheta *et al.*, 2022, 2023). I reasoned that these two protocols could be combined to differentiate the dCas9 i3 iPSCs, generated by Tian and colleagues, to dopaminergic neurons in a much shorter timeframe than the growth-factor mediated Kriks et al. differentiation. Moreover, the stable *NGN2* integration in the dCas9 i3 cells avoids complications of *NGN2* lentivirus transduction efficiency and reduces the protocol duration by a week.

Differentiation according to the schematic shown in Fig. 5.6F rapidly generated cells with a neuronal morphology that developed a branched axonal network visible by phase contrast microscopy in just 7 days. Based on personal communication with Dr Razan Sheta from the Oueslati group at Université Laval I decided that neurons should be matured to Day35 since this was the timepoint at which α-synuclein expression and culture health were maximal (unpublished). At this timepoint cells exhibited a neuronal morphology and expressed α-synuclein as well as numerous markers of dopaminergic fate including TH, DDC, VMAT2 and MAO-B (Fig. 5.6G&H). dCas9 expression was also maintained in mature dCas9 i3 iPSC-DaNs (Fig. 5.5G). It is worth noting that the banding pattern for DDC was different in the dCas9 i3 iPSC-DaNs compared to the three cell lines differentiated with the Kriks et al. protocol. This may indicate differential abundance of post-translational modifications, but since this data is from a single differentiation it is not possible to conclude whether it is a consistent phenomenon of the *NGN2* protocol and if there are functional consequences. Immunocytochemistry demonstrated that 100% of the cells in dCas9 i3 cultures express neuronal marker MAP2 and 70-85% were positive for TH (Fig. 5.6I). These encouraging results suggested that *NGN2*-induced dCas9 i3 neurons have a majoritively dopaminergic identity, robustly express α-synuclein and may be suitable for screening.

Robust α-synuclein secretion is essential for the success of the screen but has never been investigated in *NGN2* dopamine neurons generated using the published *NGN2* lentiviral transduction protocol (Dr Razan Sheta, personal communication). *NGN2* dopamine neurons are typically grown at a lower plating density of 60-80,000 cells per well compared to the 120,000 neurons used for α-synuclein release experiments up to this point. Accordingly, the α-synuclein concentration of 4-day conditioned media from

dCas9 i3 dopaminergic neurons was measured at Day35 using the BioT3 ELISA. This revealed that α-synuclein secretion was ~3-fold higher than Kriks dCas9 *SNCA*-triplication neurons and ~10-fold higher than Kirks dCas9 healthy control neurons when seeded at a comparable density (Fig. 5.7A). More cell death was observed (necrotic nuclei with DAPI stain) when cells were seeded at 120,000 cells per well. Since this density gave no additional increase to media α-synuclein concentration, I decided to use 100,000 cells per well going forwards.

To identify the optimal time at which to transduce dCas9 i3 iPSC-DaNs, cells were treated with 2, 5 or 10 µL of four sgRNA lentiviruses at Day5, Day7 and Day10 of differentiation. Neurons took up lentivirus at all timepoints, but the highest transduction efficiency was achieved at Day7 when the cells already exhibit a neuronal morphology but are still in the differentiation rather than maturation phase (Fig. 5.7 B&C). At Day7 the transduction efficiency for all four viruses increased with viral titer, though for all except *DNAJC5_2* the maximum transduction efficiency achieved with 10 µL of virus was lower than for the same sgRNA lentivirus in the dCas9 856 neurons (Fig. 5.7D). In spite of this, it was decided that titers already calculated in dCas9 856 should still be used for the main screen because further increasing the volume of each virus used may incur greater toxicity and would also prevent future replication by using too much of the lentivirus stock. Finally, I demonstrated the functionality of CRISPRi machinery in the dCas9 i3 iPSC-DaNs. Treating cells on Day7 with 10 µL of sgRNA lentivirus against *SNCA* reduced α-synuclein secretion >3-fold compared to untreated cells (Fig. 5.7E). Importantly, α-synuclein concentration of conditioned media was still within the range of the BioT3 ELISA even for *SNCA* knockdown neurons, defining a large assay window.

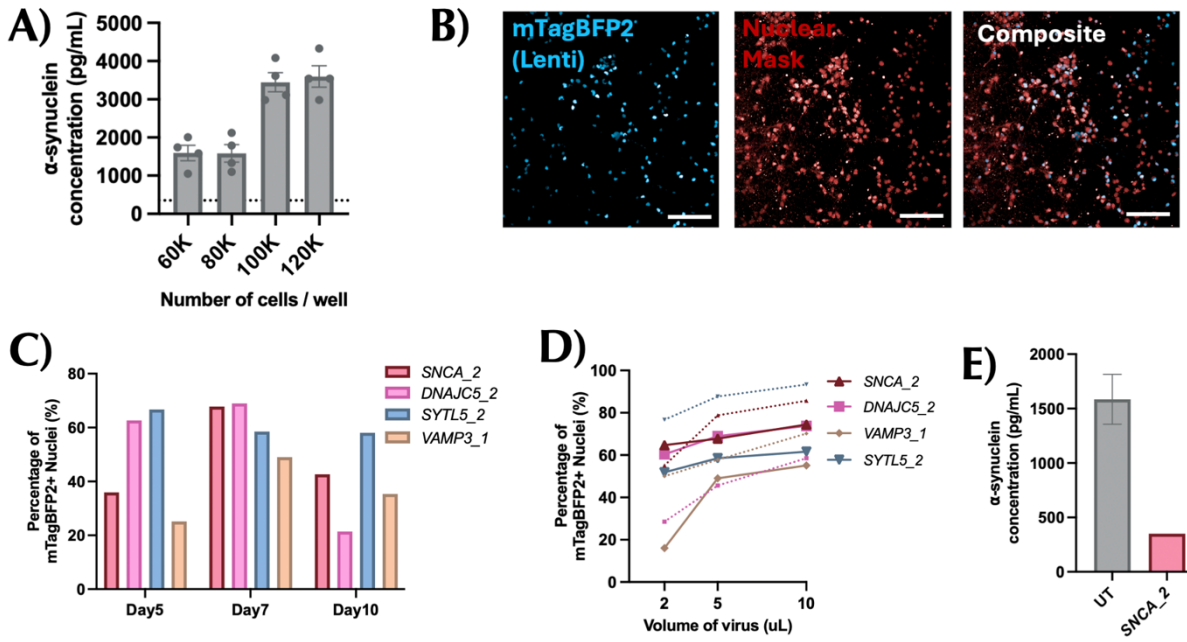

Fig. 5.7 NGN2-induced dopamine neurons secrete α-synuclein and are amenable to CRISPRi. **A)** Concentration of secreted α-synuclein in conditioned media at Day35 measured with the BioT3 ELISA for four plating densities of dCas9 i3 dopaminergic neurons. The α-synuclein concentration of media from dCas9 856 plated at a density of 120K cells per well measured with the same ELISA is shown with a dotted line. **B)** Representative confocal fluorescence live images of dCas9 i3 dopamine neuron nuclei at Day20 following viral transduction with 5 µL *SNCA_1* lentivirus on Day7. Scale bar = 100 µm. **C)** Transduction efficiency measured on Day20 following transduction with 5 µL of four sgRNA lentiviruses on either Day5, Day7 or Day10 of differentiation. **D)** Transduction efficiency of 2, 5 and 10 µL of lentivirus in dCas9 i3 dopamine neurons transduced on Day7 (solid lines with large symbols) or dCas9 856 neurons transduced on Day16 (dotted lines with small symbols). **E)** Concentration of secreted α-synuclein in conditioned media at Day35 measured with the BioT3 ELISA following *SNCA* knockdown with 10 µL of the validated *SNCA_2* guide.

Overall, these data show that the dCas9 i3 iPSC-DaNs are ideal for screening modulators of α-synuclein secretion. Not only are these NGN2-induced cultures more homogenous with a higher proportion of TH+ neurons than neurons grown according to the Kriks protocol but the expression and secretion of α-synuclein is also higher. Finally, the differentiation protocol takes just 35 days compared to a total of ~80 days (including differentiation, expansion and maturation) required for the Kirks et al. (2011) protocol.

5.7 Knockdown screen: identification of four regulatory genes

In light of the optimisations to cell line, differentiation protocol, RNA extraction, transduction efficiency and ELISA methodology the screen of all 70 lentiviruses was carried out in dCas9 i3 iPSC-DaNs as shown in Fig. 5.8A. Target genes were spread over seven plates which all had the same layout corresponding to 10 viruses against 4-5 genes of interest as well as non-targeting and untreated controls and two Triton-X100 positive controls for cytolysis in the toxilight assay (Fig. 5.8B). Target genes were grouped by gene family or pathway as shown in Fig. 5.8C.

Quantification of transduction efficiency by mTagBFP2+ nuclei after the final media harvest demonstrated that the majority of sgRNA lentiviruses transduced more than 60% of cells (Fig. 5.8D). None of the lentiviruses were found to induce significant cytolysis measured with toxilight (data not shown). The α-synuclein concentration of culture media as determined by the BioT3 ELISA was considerably lower than in the pilot study with dCas9 i3 iPSC-DaNs. Across all plates untreated cells secreted 228 ± 24 pg/mL α-synuclein i.e. 12.4 ± 1.4 pg / 10,000 cells (mean ± S.E.M.). After normalisation by cell number ELISA data were further normalised relative to non-targeting controls *NT_1* and *NT_2* for inter-plate comparison. Fig. 5.9A shows results plotted as fold-change of α-synuclein release in pg/10,000 cells relative to the mean of non-targeting controls on each assay plate. Statistical significance is indicated with bar colours but does not account for the effect size. Fig. 5.9B shows Z-scores for α-synuclein release by guide calculated against the mean and standard deviation of non-targeting controls on each assay plate. This approach considers the effect size of the change to α-synuclein secretion but not the variability of technical replicates for each guide.

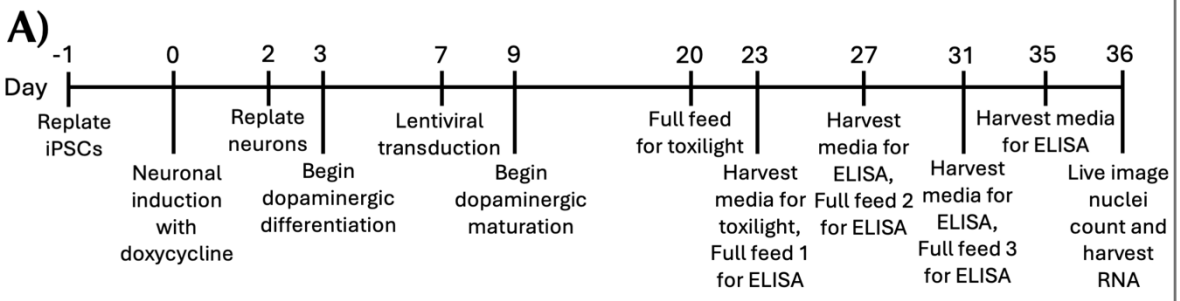

B)

1	1	1	1	NT1	Tx-100	UT	UT	UT	NT2
2	2	2	2	NT1	6	6	6	6	NT2
3	3	3	3	NT1	7	7	7	7	NT2
4	4	4	4	NT2	8	8	8	8	NT1
5	5	5	5	NT2	9	9	9	9	NT1
Tx-100	UT	UT	UT	NT2	10	10	10	10	NT1

C)

	Genes
Rabs 1	*RAB5A, RAB7A, RAB8A, RAB9A, RAB11A*
Rabs 2	*RAB13, RAB27A, RAB27B, RAB35, UBC9*
Syntaxins	*STX1A, STX3, STX4, STX5, STX17*
Synaptic proteins 1	*VAMP3, VAMP7, VTI1B, SNCA*
Synaptic Proteins 2	*SYT1, SYT7, SYTL5, SNAP23, SNAP29*
MAPS	*DNAJC5, USP19, HSPA8, VPS35*
Autophagy and RE	*MICAL1, WDR44, ATG5, GBA1, SCAMP5*

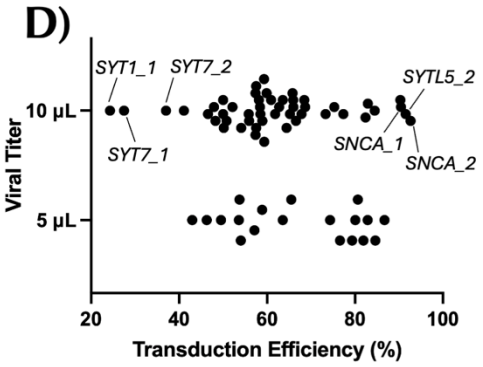

Fig. 5.8 CRISPRi screen design and planning.
A) Schematic showing the timeline of differentiation and screening experiments. The toxilight assay for cytolysis was carried out on the day of media collection. Media for ELISA from the three consecutive harvests was snap frozen and stored at -80°C until ELISAs were performed. Cells were stored in TRIzol at -80°C until RNA was extracted and reverse transcribed. **B)** Plate map for lentivirus treatment. Each of the 7 assay plates had the same layout. **C)** Gene sets on each of the 7 assay plates. Guides for the same target were always on the same plate. **D)** Transduction efficiency of all the sgRNA lentiviruses calculated at Day36, plotted by viral titer used for each guide. Lentiviruses which yielded the three lowest and three highest transduction efficiencies are highlighted. The transduction efficiency of non-targeting guides *NT_1* and *NT_2* was consistent across all plates: 83.68 ± 0.6% and 84.17 ± .3 % (mean ± S.E.M.) respectively.

Most of the guides tested caused a trending reduction in α-synuclein release, with only seven increasing α-synuclein release, though none significantly (Fig. 5.9A). Both *SNCA* guides clearly reduced α-synuclein secretion, providing important positive controls for data interpretation. The largest reduction to α-synuclein secretion was observed with *SYT1_1*, in line with the findings in Kriks neurons (Fig. 5.4A&B).

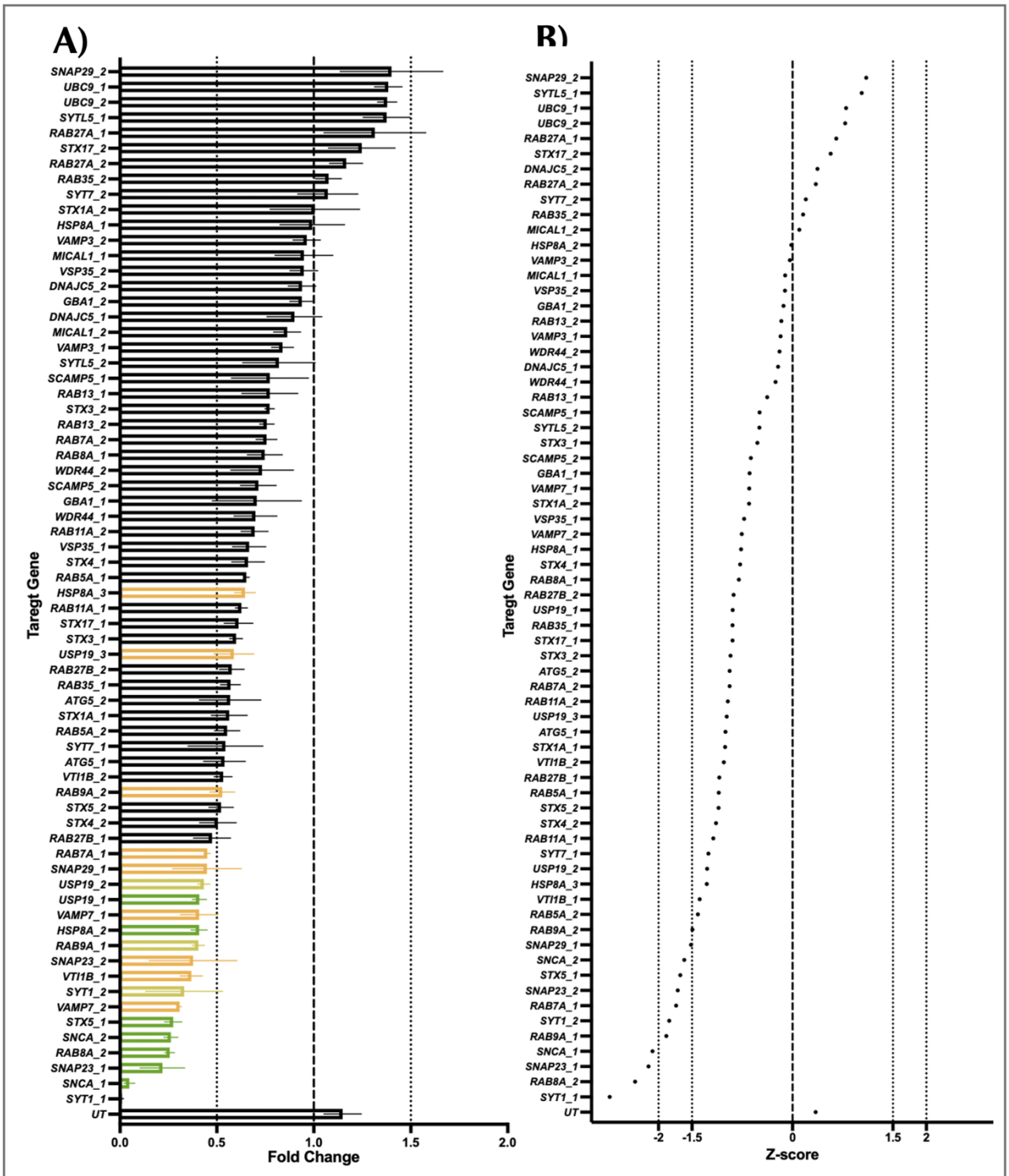

Fig. 5.9 CRISPRi guides modulate α-synuclein secretion in iPSC-derived dopaminergic neurons. **A)** Fold change of media α-synuclein concentration determined by the BioT3 ELISA normalised by live nuclei count, relative to the mean of the non-targeting controls on each ELISA plate. Data presented as mean ± S.E.M. Statistical significance determined by One-Way ANOVA and Dunnett's Multiple comparison's tests: **Orange** $p<0.05$, **Yellow** $p<0.01$, **Green** $p<0.001$ **B)** Z-scores for the mean α-synuclein concentrations for each sgRNA guide relative to the non-targeting controls on each ELISA plate.

Since RT-qPCR verification of gene knockdown is a labour-intensive process, only genes for which at least one of the sgRNA guides significantly reduced α-synuclein secretion by 50% were prioritised (Fig. 5.10A). Additionally, motivated by the pharmacology results presented in Chapter 4, the knockdown efficiencies of guides against *ATG5, GBA1, DNAJC5, SYT7*, *SYTL5* and *RAB11A* were also assessed, none of which had significant effects on α-synuclein secretion (Fig. 5.10B). Relative to non-targeting controls 22/38 (58%) of the guides tested reduced expression of their target gene. Despite significantly reducing α-synuclein secretion none of the guides against *USP19, SNAP29, STX5* or *SYT1* decreased expression of their intended targets (Fig. 5.10A). The latter is particularly surprising given both the extent of suppression of α-synuclein secretion and the previous evidence that these guides are effective (Figs. 5.2E, 5.4C, 5.6B & 5.9A). For *HSPA8, RAB7A, RAB8A* and *VAMP7*, one of the two/three sgRNA guides did not have a significant effect on α-synuclein secretion. The other *HSPA8* and *RAB7A* sgRNA guides yielded the same or greater suppression of gene expression suggesting that the effect on α-synuclein release was not specific to target knockdown. However, for both *RAB8A* and *VAMP7* only the guide which caused a significant reduction in α-synuclein secretion reduced the expression of the target gene suggesting that this was a specific, on-target effect. Finally, both the guides against *SNAP23, RAB9A* and *VTI1B* resulted in efficient gene knockdown. For SNAP23 and RAB9A this corresponded to both guides significantly reducing α-synuclein secretion, while *VTI1B_2* caused a trending but non-significant reduction in α-synuclein release (Fig. 5.9A). Gene expression was reduced by ~50% for both guides against *ATG5* and *GBA1* as well as *RAB11A_2* and by ~70% for *DNAJC5_1* and *SYT7_2* (Fig. 5.9B).

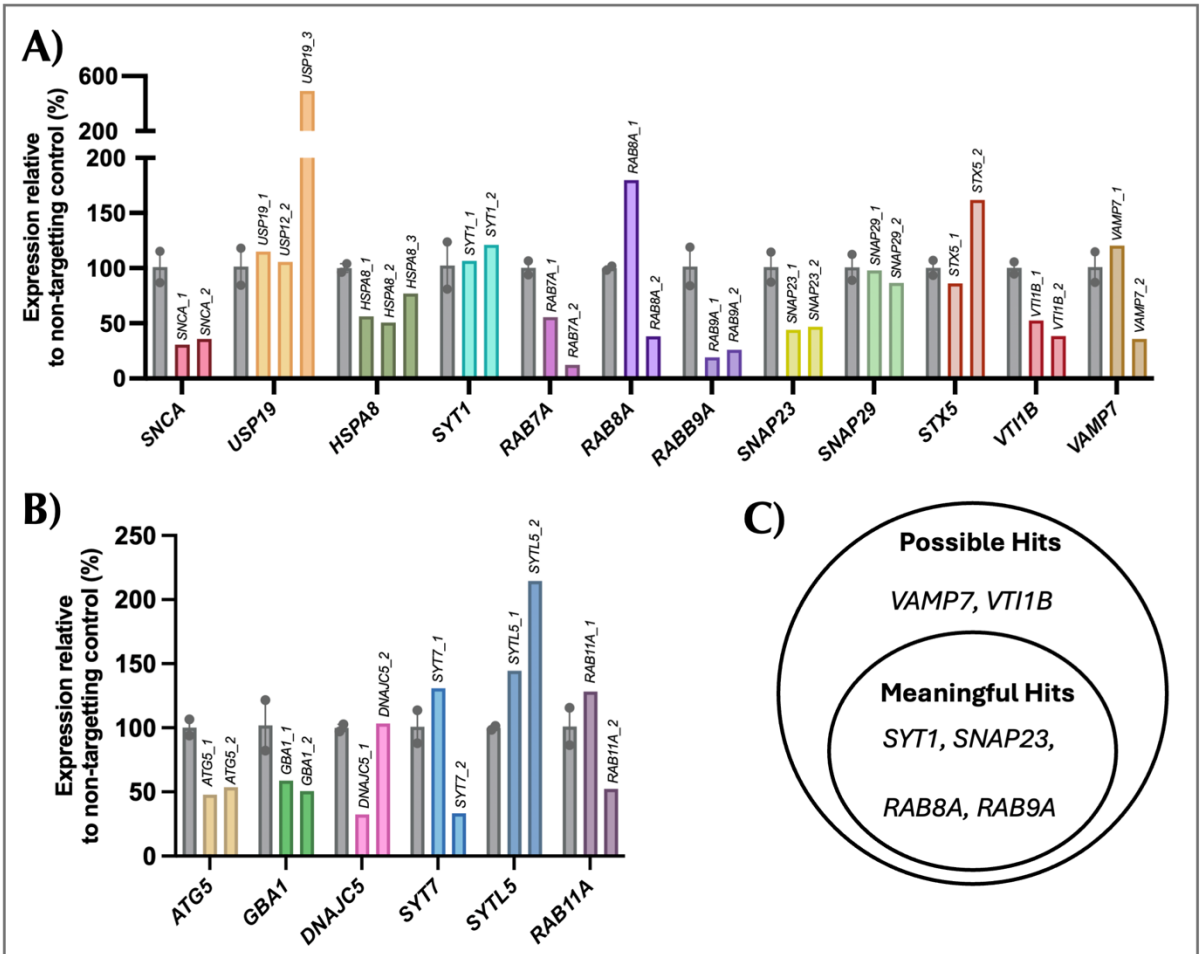

Fig. 5.10 *SYT1, SNAP23, RAB8A and RAB9A* identified as putative regulators of α-synuclein secretion in iPSC-DaNs. mRNA expression of CRISPRi targets relative to expression of each gene in the non-targeting controls for **A)** genes knockdowns which significantly reduced α-synuclein secretion by >50% **B)** other genes knockdowns of interest motivated by pharmacology results in Chapter 4 and previous literature. **C)** List of possible hits (fold change α-synuclein release < -0.5, $p < 0.05$) and meaningful hits (fold change α-synuclein release < -0.5, $p < 0.05$; Z-score < -1.645).

α-synuclein secretion from iPSC-DaNs treated with *SNCA_1* and *SNCA_2* differed from the non-targeting controls by 2.08 and 1.62 standard deviations respectively. Therefore, to select only the hits with a meaningful effect size, a 90% confidence level (Z-score < -1.645) was used for hit identification. From the knockdown validated guides, two nested groups of potential modulatory genes (Fig. 5.10C) were identified using the following criteria:

Possible Hits: Fold change < -0.5, $p < 0.05$

Meaningful Hits: Fold change < -0.5, $p < 0.05$; Z-score < -1.645

Despite the apparent failure of both *SYT1* guides to reduce gene expression in this experiment, I decided to include *SYT1* because the guides had shown efficacy in three previous experiments (Figs. 5.2E, 5.4C, 5.6B). While it is possible that *SYT1_1* and *SYT1_2* were effective in SH-SY5Y cells and Kriks iPSC-DaNs but not *NGN2*-induced iPSC-DaNs, this seems unlikely. It is more probable that in the process of extracting RNA from >200 wells of cells and carrying out >1300 wells of qPCR I made an error with sample or primer labelling. It is therefore essential that future follow-up work should confirm both knockdown efficiency (mRNA and protein expression) and reduction to α-synuclein secretion for all hits including *SYT1*.

The expression of hits was interrogated in the bulk RNA sequencing dataset gathered by Dr Vallin as well as the FOUND-IN PD dataset at Day65, however there were no significant differences in expression between PD and healthy controls in either analysis (Wald Tests $P_{adj} > 0.05$).

Overall, these data demonstrate that pairing the *NGN2* protocol for rapid generation of homogenous dopaminergic cultures with the optimised BioT3 ELISA provides a suitable screening platform for genetic modulators of α-synuclein release. Moreover, *SYT1, SNAP23, RAB8A* and *RAB9A* were identified as potential regulators of α-synuclein release in the absence of lysosomal dysfunction (under quiescent conditions). These findings require further replication in an independent differentiation, before firm conclusions can be drawn.

5.8 Discussion

Numerous genes, across a complex array of pathways, have previously been implicated in α-synuclein secretion from non-neuronal models. CRISPRi knockdown of an assortment of these genes significantly reduced α-synuclein secretion for 18/66 guide sequences, corresponding to 11 genes. Of these, *SYT1, SNAP23, RAB8A* and *RAB9A* were identified as putative hits with a potentially meaningful effect size.

An essential component of the CRISPRi approach is a cell line which robustly expressed the dCas9-KRAB repressor in mature neurons. In iPSC-DaNs differentiated according to the Kriks et al (2011) protocol it appears that dCas9 expression (or the PiggyBac engineering required to achieve this) may impair viability and differentiation potential. Healthy control dCas9 856 neurons did not exhibit overt signs of toxicity however the differentiation efficiency of these cells (~30%) was considerably lower than is routinely observed with this protocol. Moreover, both dCas9 *SNCA*-triplication lines showed markedly reduced viability and survival as well as reduced differentiation efficiency (Fig. 5.6E&I). Interestingly, the dCas9 expression was higher in the 831-3 neurons compared to 831-1 which corresponded with an increased proportion of non-neuronal cells in culture and fewer differentiations which survived to maturity (Fig. 5.6A, D&E). dCas9 831-1 and dCas9 831-3 required hygromycin selection to enrich for cells still expressing the CRISPRi machinery. Anecdotally it seemed that the longer iPSCs were maintained under selection pressure (and hence the higher the proportion of dCas9+ cells at Day0) the more vulnerable the cultures were to spontaneous death as neural progenitors.

Problems with the differentiation of dCas9 Kriks neurons were resolved by optimising the differentiation protocol from Sheta and colleagues (2023) for dCas9 i3 iPSCs. In these neurons dCas9 expression did not appear to hinder differentiation efficiency and beautiful cultures of neurons expressing numerous markers of dopaminergic fate were generated in a more rapid time frame (Fig. 5.6F-I). Interestingly, the western blot banding patterns for several of these markers differed for dCas9 i3 iPSC-DaNs compared to non-engineered control neurons grown using the Kriks protocol. In this respect dCas9 i3 neurons appeared more like dCas9 856 which also showed weaker intensity of TH lower bands and a more prominent upper band for VMAT2 (Fig. 5.6G). While these likely represent different PTM profiles (Tong *et al.*, 2011), the significance of these results in the context of a differentiation effect of dCas9 is low since banding patterns for the same markers also varies between differentiations of un-edited Kriks neurons (Fig. 3.1G).

The second key component of CRISPRi is the sgRNA guides. 58% of guides tested achieved significant knockdown of their intended targets in dCas9 i3 iPSC-DaNs (Fig. 5.10A&B). This reflects what others in the lab have experienced using the same sequence prediction tool and plasmid backbone (Dr Gizem Onal, unpublished). Encouragingly, the same guides showed concordant results across multiple experiments. For example, *DNACJ5_1* yielded efficient knockdown in SH-SY5Y, dCas9 856 and dCas9 i3 iPSC-DaNs while *DNAJC5_2* did not (Fig2. 5.2E, 5.4C & 5.10B). The only exception to this were the *SYT1* guides (discussed above). Transduction efficiencies of the guides which reduced expression of their targets varied from 37-92% and there was no correlation between transduction efficiency and knockdown efficiency (Simple linear regression, p=0.48). This suggests that low transduction efficiency was compensated by high efficacy of the sgRNA sequences for some guides.

α-synuclein secretion was measured using the optimised BioT3 ELISA which was sensitive across the range of media α-synuclein concentrations detected. Toxilight confirmed that α-synuclein secretion was through specific pathways rather than cytolysis as the levels of cytosolic adenylate kinase in conditioned media were extremely low and did not differ between sgRNA lentiviruses for target genes and non-targeting controls. Strangely, the concentration of secreted α-synuclein in culture media was >10-fold higher in the dCas9 i3 iPSC-DaN pilot experiments than the final screen for the same seeding density at the same timepoint. The interval between media harvesting and carrying out the ELISA was longer for the final screen, so it is possible that more α-synuclein was degraded by proteases in the media or adsorbed to the plastic of storage plates (Abdi *et al.*, 2021). Moreover, α-synuclein secretion can be elevated by various cellular stresses independent of cell lysis and release of cytoplasmic contents (Jang *et al.*, 2010). It is plausible that in the final screen neurons were in more optimal culture conditions, as aspects of plate coating and feeding schedules were optimised between the two NGN2 differentiations, and thus cells were perhaps less stressed.

The lower-than-expected level of α-synuclein secretion resulted in sub-optimal separation between the positive controls (*SNCA* sgRNA guides) and negative controls (non-targeting guides). Even though both *SNCA* guides reduced α-synuclein expression by >65% and release by >75%, the variability between *SNCA_1*&*_2* and *NT_1*&*_2* technical replicates resulted in a Z' of -1.08. Despite this, 6 knockdown-validated hits were identified which significantly reduced α-synuclein secretion by >50%, 4 of which had |Z-scores| larger than *SNCA_2,* the positive control with smallest effect size. For an assay to be considered as robust Z'>0.5 is typically required (Zhang, Chung and Oldenburg, 1999). However, for cell-based assays it can be argued that the inherent

variability necessitates a more lenient threshold of Z'>0, although this still represents much less overlap between positive and negative control distributions than achieved here (Bar and Zweifach, 2020). The study design necessitated the use of *SNCA* knockdown as the positive control although it is still expected that these cells release some α-synuclein into culture media. An alternative approach to increase Z', would be to use a naïve media which would not contain any α-synuclein, however due to the method of normalisation chosen (pg/10,000 cells) this was not possible. Overall, we can conclude that while the screen succeeded in identifying putative hits worthy of follow up, the intrinsic variability necessitates cautious interpretation of results at this stage, until hits are orthogonally validated.

Bearing in mind the above caveats *SYT1, SNAP23, RAB8A* and *RAB9A* were identified as putative hits (Fig. 5.10C). These genes are robustly expressed in iPSC-DaNs (Fig. 5.1A), but only *SNAP23* and *RAB8A* have previously been investigated in the context of α-synuclein secretion (Tables 5.1 and 5.2). The interpretation of these findings is discussed in detail in the general discussion, though it is interesting to note at this stage that the four genes are implicated in numerous release pathways, including but not limited to MAPS, lysosomal exocytosis/secretory autophagy and synaptic release (Zhang, Jiang and Shi, 2022; Nakamura *et al.*, 2024; Sawai, Nakamura and Arawaka, 2025).

Chapter 6 – Secreted proteoforms of α-synuclein

6.1 Introduction

Chapter 4 demonstrated that α-synuclein is constitutively secreted from iPSC-DaNs. For secreted α-synuclein to contribute to the spread of pathology it must contain seeds capable of templating further misfolding elsewhere. Oligomeric α-synuclein is elevated in CSF from PD patients compared to controls and larger soluble aggregates have also been identified (Park *et al.*, 2011; Lobanova *et al.*, 2022). Mass spectrometry demonstrates that phospho-ser-129 α-synuclein is also secreted into CSF and immunoassays show it is elevated in PD patients (Wang *et al.*, 2012; Majbour *et al.*, 2016). Recently, studies have begun to investigate the seeding/templating activity of CSF α-synuclein caused by these pro-aggregation proteoforms. *In vitro* seeded amplification assays (SAA) demonstrate that CSF from patients with various synucleinopathies, including PD, can template aggregation of recombinant α-synuclein (Fairfoul *et al.*, 2016; Fernandes Gomes *et al.*, 2023; Bsoul *et al.*, 2025).

Interest in post-translationally modified, oligomeric/aggregated and seeding-competent α-synuclein proteoforms in CSF, as well as robust assays with which to measure them, is largely driven by their promise as potential PD biomarkers (Hatano *et al.*, 2024). This growing field lacks well-characterised cellular models to investigate mechanisms driving secretion of the proteoforms identified as predictors of disease. An *in vitro* model which secretes seeding-competent α-synuclein would represent a valuable tool with which to investigate whether certain release mechanisms selectively contribute to the secretion of pathological vs physiological α-synuclein. Such proteins/pathways would be highly relevant molecular targets for drug design and repurposing. In this chapter I investigate

whether iPSC-DaNs recapitulate the secretion of seeding-competent α-synuclein observed in human brain.

While the *in vitro* seeding of α-synuclein secreted from iPSC-DaNs has not previously been demonstrated, co-culture studies from the Ryan lab evidence transmission of α-synuclein pathology from *SNCA-A53T* to healthy neurons providing solid rationale for the experiments presented herein (Ryan *et al.*, 2018; Stykel *et al.*, 2021). These authors find that phospho-ser-129 α-synuclein increases in control neurons after co-culturing with patient lines but this is reduced by adding antibodies against α-synuclein to the culture media (Ryan *et al.*, 2018). While promising, these results do not confirm templated seeding. It is unclear whether the endogenous α-synuclein in controls is undergoing templated aggregation followed by phosphorylation, or whether phospho-ser-129 α-synuclein from PD lines is being endocytosed and then detected in controls. To conclusively determine if misfolded seeds are present in conditioned media the templating of recombinant α-synuclein must be demonstrated.

Determinants of seeding include folding state, oligomerisation and PTMs. In Chapter 3 intracellular α-synuclein from iPSC-DaNs was found to be N-terminally truncated though no PD-linked additive PTMs were detected. In Chapter 4 I showed that truncated α-synuclein is secreted but it remains to be determined whether this truncation alters α-synuclein aggregation/seeding. Due to the low concentration of α-synuclein in conditioned media, immunoprecipitation followed by mass spectrometry failed to achieve full sequence coverage (data not shown), preventing assessment of additive PTMs in media samples. However, it is unlikely that modified α-synuclein is secreted if not intracellularly expressed. This chapter focuses on experiments to detect

oligomers/aggregates which could follow from truncation and may contribute to putative seeding activity. iPSC-DaNs have been shown to contain oligomeric α-synuclein intracellularly but whether it is actively secreted remains uncertain (Mazzulli, Zunke, Isacson, *et al.*, 2016; Zunke *et al.*, 2018; Cuddy *et al.*, 2019; Stykel *et al.*, 2021; Drobny *et al.*, 2023). These studies use classical biochemical techniques such as detergent fractionation and size exclusion chromatography. I set out to down-scale these, and other, methods for compatibility with low concentration conditioned media samples. Finally, in light of the advances in sensitivity and resolution of single-molecule techniques for studying aggregation-prone proteins, I sought to determine whether novel biophysical approaches could be applied in a cell biology context to provide further insight on the proteoforms of α-synuclein secreted.

Chapter Aims:

1. Optimise an assay to study templated misfolding in conditioned culture media from iPSC-DaNs and compare PD genotypes.
2. Use classical biochemistry approaches to investigate the secretion of oligomeric/aggregated α-synuclein by iPSC-DaNs.
3. Determine the scope of novel biophysical techniques to study the aggregation status of secreted α-synuclein in complex mixtures.

6.2 Seeding-competent α-synuclein secretion by iPSC-DaNs

To increase the probability of identifying oligomeric α-synuclein seeds in conditioned media, iPSC-DaNs from three PD patients heterozygous for the *SNCA-A53T* point mutation were used in this chapter alongside the *SNCA*-triplication lines presented previously. Recombinant A53T α-synuclein aggregates faster than the wildtype sequence and iPSC-DaNs carrying this mutation have more intracellular oligomers per cell measured with DNA-PAINT (Ohgita *et al.*, 2022; Virdi *et al.*, 2022). Like control and *SNCA*-triplication lines, *SNCA-A53T* neurons differentiated into highly branched MAP2/TH positive neurons which expressed α-synuclein (Fig. 6.1A&B). These cells also released α-synuclein into culture media and this secretion increased over time (Fig. 6.1C&D). Unlike the *SNCA*-triplication neurons there was no difference in total α-synuclein secretion at Day75 (Fig. 6.1E).

Numerous commercial ELISAs have been developed which claim to selectively detect aggregated α-synuclein. As a first step toward characterising the secreted α-synuclein from *SNCA*-mutant lines, the LEGEND MAX α-synuclein Aggregate ELISA was used to quantify oligomeric/aggregated species in conditioned media. This demonstrated a trending but non-significant increase in both PD lines compared to controls (Fig. 6.1F). The manufacturers claim this assay only has 0.105% cross-reactivity with monomeric α-synuclein, suggesting that the elevated signal, notably in *SNCA-A53T* where there is no increase in total secreted α-synuclein, may represent increased secretion of oligomeric seeds. However, raw absorbance values from the ELISA were below the range of the assay standards, so results should be interpreted cautiously. To further study this tentative disease phenotype, optimisation of a SAA for cell-derived media samples was required.

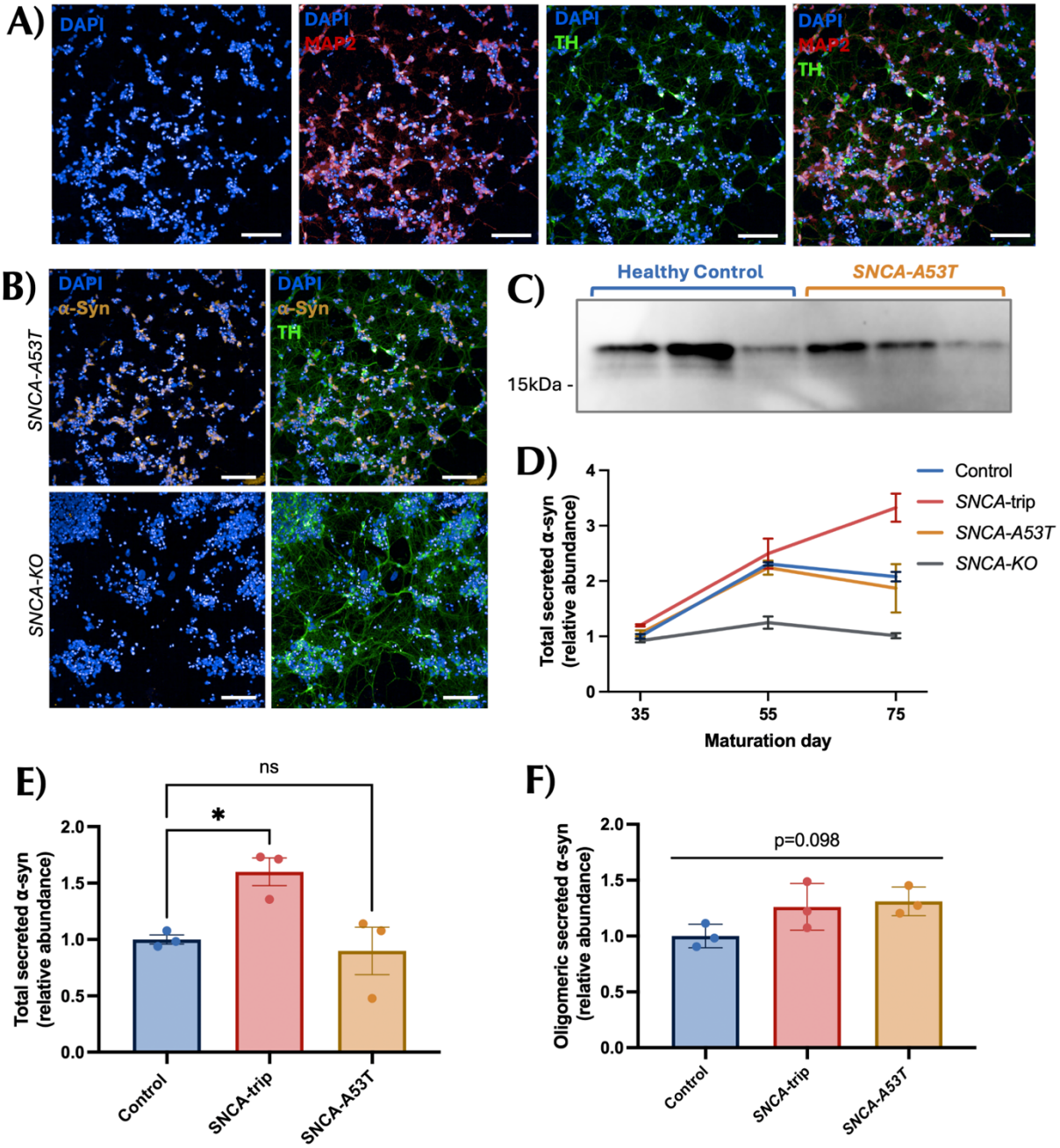

Fig. 6.1 Expression and secretion of α-synuclein by iPSC-DaNs with *SNCA*-mutations.
A) Representative confocal fluorescence images of *SNCA-A53T* neurons at Day35 stained for neuronal marker MAP2 and dopaminergic marker TH. Images taken at 20x resolution, scale bar = 100 µm. **B)** Representative confocal fluorescence images of *SNCA-A53T* and *SNCA-KO* neurons at Day35 stained for total α-synuclein expression, showing α-synuclein signal in *SNCA-A53T* but not the knock-out. Images at 20x resolution, scale bar = 100 µm. **C)** Western blot after SDS-PAGE for α-synuclein immunoprecipitated from culture media from Day70 healthy control and *SNCA-A53T* dopamine neurons. N=3 cell lines per genotype. **D)** Bio-Techne ELISA quantification of total α-synuclein in conditioned media over time and **E)** at Day75 showing a significant increase in secretion for *SNCA*-triplication but not *SNCA-A53T* dopamine neurons compared to control. One-way ANOVA with Dunnett's multiple comparisons test, N=3 lines from one differentiation. *p<0.05 **F)** BioLegend ELISA quantification of putatively oligomeric α-synuclein in conditioned media at Day75. One-way ANOVA shows no significant differences between genotypes. N=3 lines from 3 independent differentiations.

SAA can be broadly categorised into protein misfolding cycle amplification (PMCA) and real-time quaking induced conversion (RT-QuIC) depending on the mode of agitation employed to break apart growing fibrils into smaller seeds (Bougea, 2024; Huang *et al.*, 2024). PMCA relies on ultra-sound while in RT-QuIC the samples are shaken at intervals making it more compatible with high-throughput plate-based experiments in 96-well format (Fig. 6.2). In collaboration with Dr Livia Civitelli in the Parkkinen group and supported by an ARUK Pump Priming grant I sought to modify an existing CSF α-synuclein RT-QuIC protocol for use with conditioned media[7]. Published α-synuclein RT-QuIC protocols differ in the shake time and speed, duration of inter-shake interval, temperature and buffer composition. The assay is extremely sensitive and small changes to these parameters can have a marked effect on kinetics and assay window (Huang *et al.*, 2024). The CSF protocol published by Lee and colleagues (2024) was used as a starting point for optimisation.

Culture media usually contains phenol red as a pH indicator; however, its absorbance spectrum overlaps with the emission spectrum of Thioflavin T (ThT). To reduce potential signal variability phenol red was removed. Media samples were ultracentrifuged to remove cell fragments, and supernatants (which were assumed to contain soluble seeds) were used for the RT-QuIC assay. 5, 10 or 15 µL of undiluted CSF per reaction has been used previously in α-synuclein RT-QuIC (Fairfoul *et al.*, 2016; Poggiolini *et al.*, 2022). The α-synuclein concentration in conditioned media is approximately 10-fold lower than in CSF so 1x and 10x media added in 5 or 15 µL volumes were trialled (Mollenhauer

[7] This work was undertaken as a collaboration between myself and Dr Civitelli using reaction conditions previously published by the Parkkinen group (Poggiollini et al., 2022). I grew the cells, carried out the sample preparation and associated methodological optimisations. Livia trained me in the RT-QuIC assay and assisted with initial replicates. Laterally, I carried out the assay independently with technical guidance from Dr Civitelli. I performed the data analysis using the analysis package QuICSeedR (M. Li *et al.*, 2024).

et al., 2011). While 15 µL 1x conditioned media and 5 µL 10x conditioned media failed to amplify within 120 hours, 15 µL of the 10x concentrate from *SNCA*-triplication neurons seeded aggregation (Fig. 6.3A). This demonstrated that the ultracentrifugation step, needed for removal of cell debris, had not also removed soluble α-synuclein seeds. The lag time for the amplification reaction was comparable to CSF and brain homogenate samples run on the same plate (data not shown). Crucially, the neurobasal controls, where recombinant α-synuclein was mixed with naïve media, failed to amplify demonstrating the specificity of the reaction.

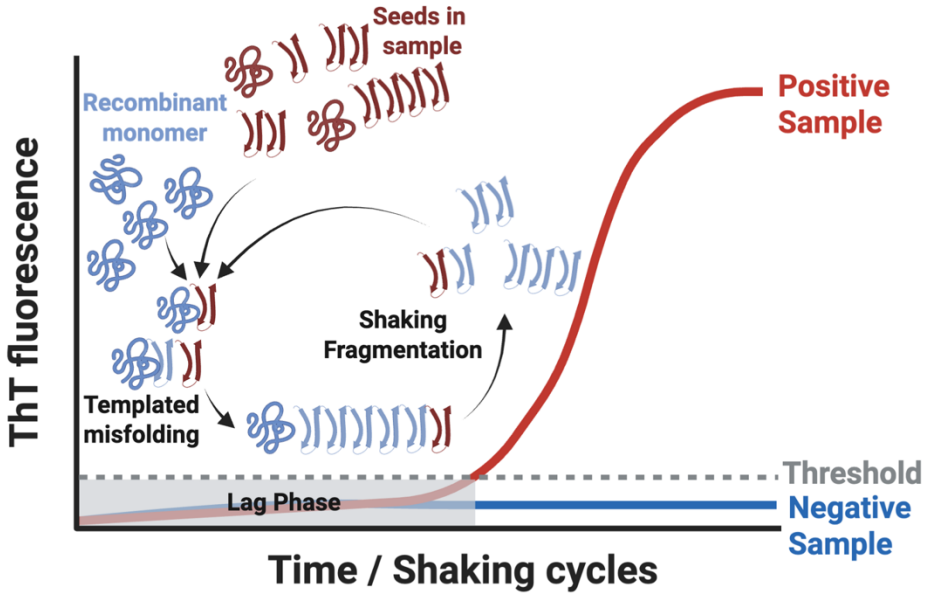

Fig. 6.2 Amplification of neuron-derived misfolded seeds in the RT-QuIC assay.
Schematic representation showing the process of seeded amplification during RT-QuIC. Misfolded seeds template an excess of recombinant monomeric α-synuclein which recruits more recombinant protein into growing fibrils during the inter-shake interval. During shaking cycles fibrils are broken apart, exponentially increasing the number of seeds. The reaction is tracked by the β-sheet-binding dye Thioflavin T (ThT). Fluorescence reaches a plateau when all monomeric protein has been consumed.

Medium usually includes the growth supplement B27, containing high concentrations of BSA. This is necessary to maintain the health of the culture but can be removed for short periods without adverse effects to iPSC-DaNs (Baud *et al.*, 2019). The presence of

2% B27 in conditioned media samples for RT-QuIC massively increased lag time, in some cases completely suppressing seeded-aggregation (Fig. 6.3B). This pilot also demonstrated that, like *SNCA*-triplication lines, *SNCA-A53T* media is also capable of seeding aggregation which is particularly interesting given 50% of the α-synuclein these cells express differs in primary sequence to the wildtype recombinant monomer. Fig. 6.3C demonstrates that B27 depletion in the final four days does not increase cytolysis, therefore, B27 was removed going forward.

While 10x conditioned media was used for initial pilots, it was possible that further increasing the concentration would reduce lag time and thus improve the throughput of the assay which typically runs for 5-10 days. However, using 20x conditioned media was not found to provide any meaningful reduction to lag time. Indeed, for the *SNCA*-triplication line trialled, 20x concentration supressed aggregation likely by increasing the concentration of BSA from any residual B27 (Fig. 6.3D). 20x media also necessitated pooling media from 2 wells of cells per line increasing experimental costs, therefore subsequent work used only 10x concentrates.

The optimisation experiments described above were carried out over a period of 18 months during which time spontaneous aggregation of the recombinant monomer in neurobasal media controls became increasingly common until this occurred during every experiment, undermining the validity of results for cell-derived samples. Source of the recombinant monomer is often cited as the cause of spontaneous aggregation (Huang *et al.*, 2024), however in this case the same lot number of commercially produced monomer was used for all replicates (rPeptide, lot r060622AS). Upon thawing and re-suspension, the recombinant protein is subjected to re-monomerisation. Initially, guanidium hydrochloride incubation followed by buffer exchange was highly effective

(Fig. 6.3A), however by December 2023 monomer in the neurobasal media control was routinely found to aggregate with faster kinetics than in cell-derived samples (Fig. 6.3E). In line with ongoing optimisations in the Parkkinen group, heating the monomer for 30 minutes followed by 100 kDa ultrafiltration to remove any aggregates was trialled but still resulted in exponential aggregation in the neurobasal control. Finally, the guanidium chloride treatment was combined with low pass 100 kDa ultrafiltration which prevented aggregation in the neurobasal control and was used for future experiments (Fig. 6.3E).

Despite significant protocol optimisation there was still variation between technical replicates from the same biological sample in one assay. While high technical variability is an innate feature of RT-QuIC assays, I was concerned that such variability may mask a possible disease phenotype. In addition to the stochastic nature of α-synuclein aggregation, it was hypothesised that other secreted proteins in the media may contribute to kinetic variability. Despite the low molecular weight of α-synuclein, its unfolded and disordered conformation in solution results in a much larger hydrodynamic radius and a recombinant protein which runs at ~66 kDa in native PAGE (Dong *et al.*, 2018). As such, it was predicted that unfolded monomeric protein would be retained by a 50 kDa high-pass column as well as by the 10 kDa columns used up to this point, while more of the other proteins in the media would be removed. As hypothesised, concentration with a 50 kDa cut-off column reduced the variability between technical replicates as well as lag time (Fig. 6.3F), however the assay window – defined as the difference in lag time between *SNCA-A53T* lines and healthy controls was also reduced. On balance it was decided to continue with 10 kDa concentration to maximise the assay window, though further experiments to optimise filter size or implement an immunodepletion strategy for the removal of other proteins may further improve the assay.

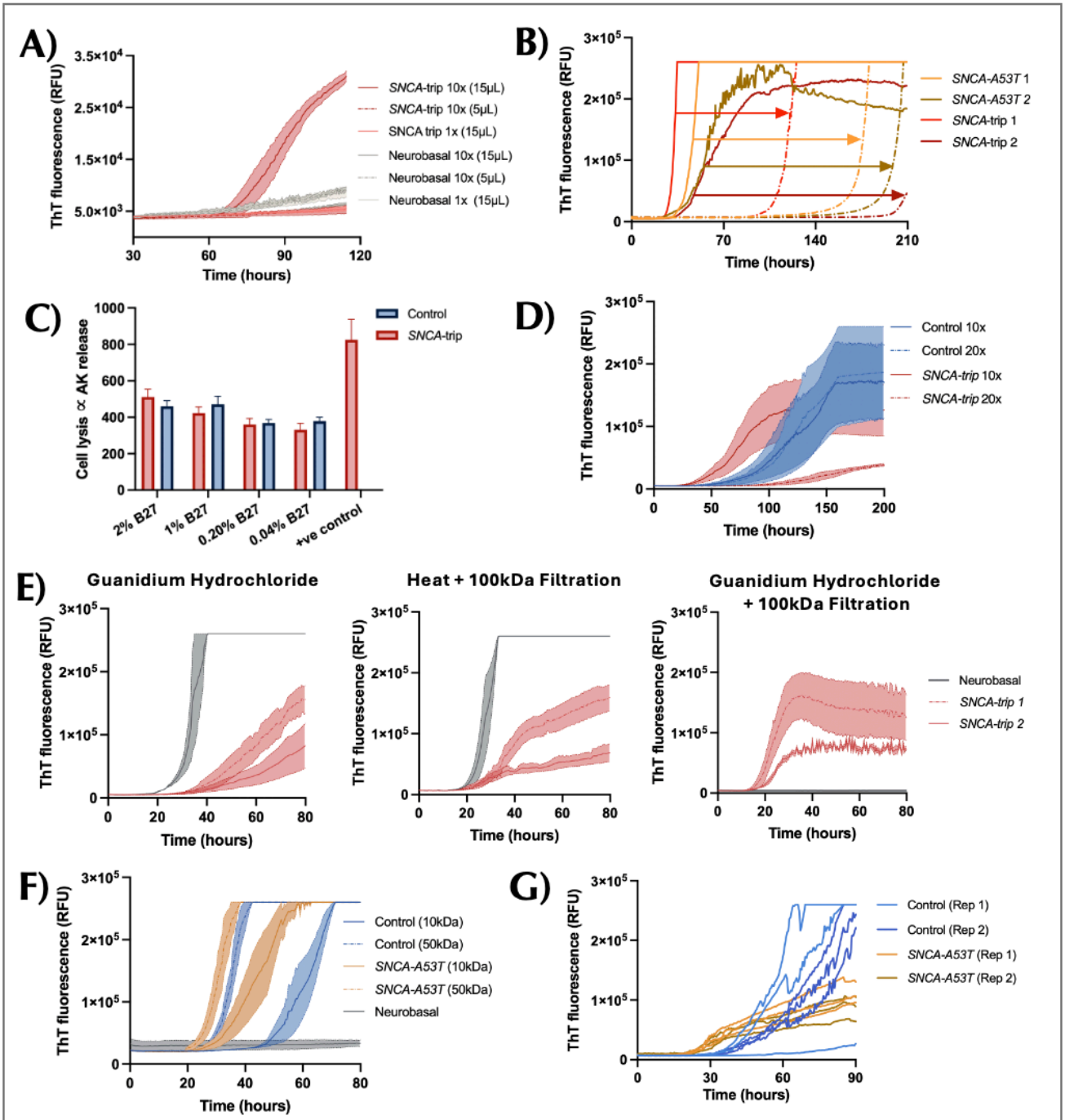

Fig. 6.3 Developing an RT-QuIC assay for iPSC neuron conditioned media.
A) Averaged ThT curves for reactions seeded with 5 or 15 µL of conditioned media from *SNCA*-triplication dopamine neurons or naïve neurobasal. 10x media was concentrated with 10 kDa ultrafiltration columns. **B)** Representative averaged ThT curves for 10x conditioned media from *SNCA*-triplication and *SNCA-A53T* lines cultured in the presence (dotted lines) or absence (solid lines) of B27 (another cell line of each genotype and 2 control lines were also assayed showing the same trend). **C)** Toxilight results measuring adenylate kinase release (luminescence) as a proxy for cytolysis with decreasing B27 concentration. N=2-3 lines per genotype from two independent differentiations. 10 mM caffeine was used as a positive control to tigger stress-induced cell lysis. **D)** Averaged ThT curves for reactions seeded with 10x or 20x conditioned media concentrated with 10 kDa ultrafiltration columns. **E)** Averaged ThT curves for *SNCA*-triplication conditioned media and neurobasal negative controls following 3 different methods of monomer preparation. **F)** Averaged ThT curves for reactions seeded with 15 µL of 10x media concentrated with 10 kDa or 50 kDa ultrafiltration columns. **G)** Representative raw ThT curves for two independent sample preparations replicates per cell line, each assayed in technical triplicate. All data are presented as the mean and S.E.M from three-four technical replicates.

Finally, a limitation of the approach used here was that biological samples are processed separately during the numerous preparation steps (Subchapter 2.8.2), which may introduce additional inter-sample variability, problematic in a quantitative assay. In particular, collecting ultracentrifugation supernatants and using concentration columns may create experimenter-induced variance even with careful technique. To assess the impact of this technical variation, cell lines were grown in duplicate plates and media were harvested and prepared separately from two lines of all three genotypes. Fig. 6.3G shows representative traces from one control and one *SNCA-A53T* line across the two sample preparation replicates. Two-way ANOVA from the three genotypes (6 cell lines) showed a significant effect of cell line identity on lag time ($p_{line\_ID}<0.001$) but no effects of sample preparation replicate or line-replicate interaction ($p_{replicate}= 0.094$, $p_{interaction}=0.171$). Thus, despite the extensive sample manipulations, most of the variability between biological samples is explained by cell line identity making this a valid and robust assay with which to investigate the effect of genotype.

While experiments during assay optimisation hinted that aggregation kinetics for control samples where slower than for PD lines (Fig. 6.3D,F&G) these were clearly underpowered to quantitatively assess a disease phenotype. Use of the optimised protocol demonstrated a statistically significant decrease in lag time for both *SNCA*-triplication and *SNCA-A53T* compared to control (Fig. 6.4A&B). This result is notable not only as the first example of secreted α-synuclein capable of templated aggregation from an iPSC-derived neuron model, but also as evidence that familial PD mutations increase seeding-competent α-synuclein.

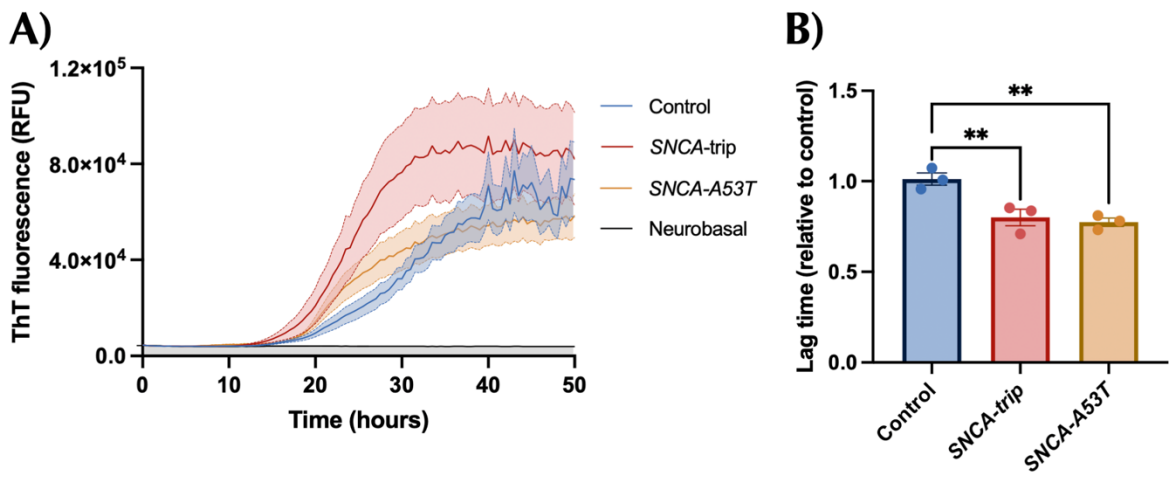

Fig. 6.4 Secretion of seeding-competent α-synuclein is elevated by *SNCA*-mutations.
A) Representative averaged ThT fluorescent curves from Day75 healthy controls, *SNCA* mutant lines and the neurobasal (media) negative control. Data is presented as mean and S.E.M. of three lines from one differentiation. **B)** Quantification of lag phase (the time until fluoresce exceeds 5x the standard deviation of baseline) at Day75. Each data point represents one cell line averaged across two independent differentiations, assayed in quadruplicate. One-way ANOVA with Dunnett's multiple comparisons test shows a significant effect of both PD genotypes. **p<0.01.

Overall, this work establishes a well characterised and robust procedure for the detection of seeding-competent α-synuclein secreted from iPSC-DaNs with optimised sample preparation methods to suit the novel input material. Excitingly, this approach demonstrated a higher seeding capacity of media from neurons with PD mutations suggesting an increase in secretion of α-synuclein capable of templating.

6.3 Intracellular expression of putatively oligomeric α-synuclein

Motivated by the genotype differences in seeding identified with RT-QuIC, I sought to investigate the secreted proteoforms underlying this phenotype. For any proteoform to be secreted by an iPSC-DaN it must be expressed intracellularly. ELISA quantification of serially diluted cell lysates shows that for cells lysed under native conditions (Subchapter 2.4.2.1) the α-synuclein concentration is ~1000-fold higher than that of the corresponding culture media (Fig. 6.5A). It follows that to detect putatively oligomeric/aggregated α-synuclein which is secreted any technique must be readily able to measure the corresponding proteoforms in cell lysates.

Numerous publications have found evidence of triton-X100-insoluble α-synuclein in cell lysates from iPSC-DaNs with a wide range of PD mutations (Tsunemi, Hamada and Krainc, 2014; Chung *et al.*, 2016; A. Ikeda *et al.*, 2019; Cuddy *et al.*, 2019; Oji *et al.*, 2020; Stojkovska *et al.*, 2022; Drobny *et al.*, 2023). Using the Mazzulli group protocol for sequential triton-X100 and SDS extraction (Stojkovska and Mazzulli, 2021), trace quantities of triton-X100-insoluble α-synuclein were identified in cell lysates from control and *SNCA*-triplication neurons but the vast majority was present in the soluble fraction (Fig. 6.5B&C). While the small proportion of triton-X100-insoluble α-synuclein is interesting, the low signal intensity prevents a meaningful genotype comparison and suggests that the concentration of any insoluble α-synuclein in conditioned media would be far below the detection range of this approach.

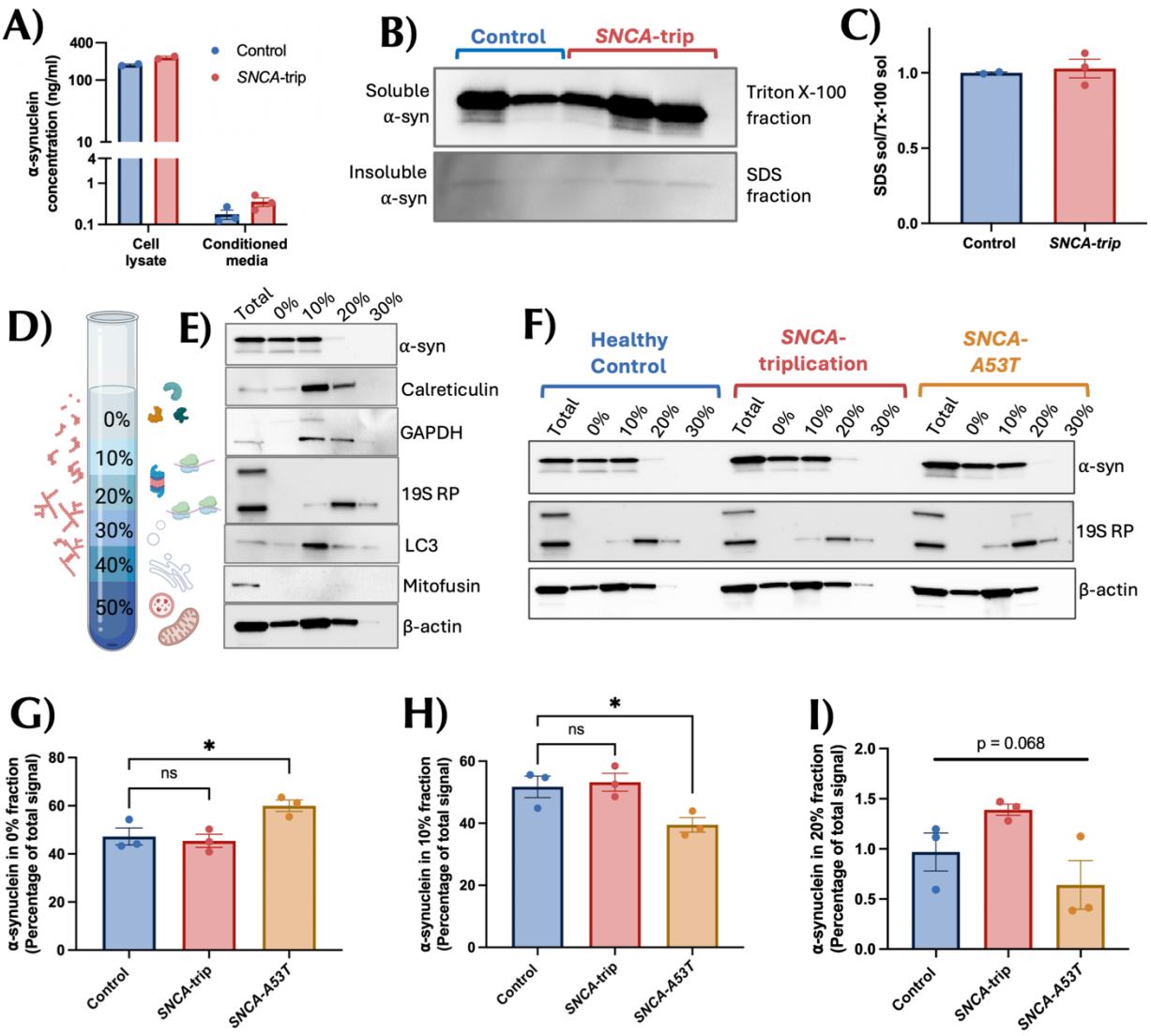

Fig. 6.5 High density α-synuclein expression in dopaminergic neurons.
A) Bio-Techne ELISA quantification of α-synuclein expression in cell lysates and release into conditioned media of healthy control and *SNCA*-triplication neurons at Day60. Cell lysates were diluted 1:30 onto the ELISA plate to be within the range of standards. N=2-3 cell lines per genotype. **B)** Western blots and **C)** Densitometric quantification of triton-X100 soluble and insoluble (SDS soluble) α-synuclein in dopaminergic neurons matured to Day85. N=2-3 cell lines per genotype. **D)** Schematic depicting the predicted sucrose fractions for various organelles and cytosolic components after sucrose density gradient ultracentrifugation. Monomeric α-synuclein and small oligomers are low density while larger aggregates equilibrate at higher sucrose concentrations. **E)** Representative western blots from one of two control cell lines interrogated at Day60 for expression of ER marker calreticulin, cytoplasmic protein GAPDH, the RPT2 subunit of the 19S proteasome regulatory particle, autophagosome/autolysosome marker LC3, mitochondrial marker mitofusin and cytoskeletal component β-actin. **F)** Representative western blot for α-synuclein fractionation in control, *SNCA*-triplication and *SNCA-A53T* neurons. Input samples were pooled by cell line across independent differentiations to achieve sufficient protein concentration over the 2 mL gradient. Densitometric quantification of the proportion of α-synuclein in **G)** the 0% sucrose fraction, **H)** the 10% sucrose fraction and **I)** the 20% sucrose fraction from three cell lines per genotype. One-way ANOVA with Dunnett's multiple comparisons test shows a significant increase in α-synuclein within the 0% fraction in *SNCA-A53T* neurons paired with a decrease in α-synuclein in the 10% fraction, as well as a trending increase in α-synuclein in the 20% fraction in *SNCA*-triplication dopaminergic neurons. N=3 lines per genotype, pooled from 3-4 independent differentiations. *p<0.05

Sucrose density gradient ultracentrifugation can be used to separate low density monomeric α-synuclein from oligomers and fibrillar aggregates (Emin *et al.*, 2022). This approach also fractionates cytoplasmic contents and organelles, providing a degree of subcellular fractionation (Taguchi *et al.*, 2013) – Fig. 6.5D. Using the same protocol as Emin and colleagues[8] the distribution of subcellular markers from iPSC-DaNs was assessed in healthy controls (Fig. 6.5E). This demonstrated that α-synuclein was only present in the 0-20% sucrose fractions which were almost completely devoid of heavy membrane compartments. ER marker calreticulin was also present in the three lowest density fractions while the 19S proteasome regulatory particle (19S RP, RPT2) was absent in the 0% fraction but abundant in the 10, 20 and 30% fractions. Interestingly, the putatively post-translationally modified (higher molecular weight) RPT2 was only present in the total input consistent with the reported ability of PTMs to alter RPT2 subcellular localisation (Kors *et al.*, 2019). LC3 and GAPDH were weakly present in all fractions. Due to its distinctive banding pattern, the 19S RP was selected as a marker of successful fractionation and the experiment was repeated including *SNCA*-mutant PD cell lines.

α-synuclein was found to be most abundant in the 0% and 10% fractions for all three genotypes (Fig. 6.5F). Moreover, the N-terminally truncated band characterised in Chapter 3 was present in all fractions. The proportion of α-synuclein in the 10% sucrose fraction was significantly reduced in *SNCA-A53T* lines compared to healthy controls although there was no change for the *SNCA*-triplications (Fig. 6.5G&H). Conversely, there was a trending increase in the proportion of α-synuclein in the high density 20%

[8]I was a member of this group during my undergraduate degree and worked closely with the first author of this paper on the gradient preparation, ultracentrifugation and subsequent TIRF analysis. As such I am confident that the protocol used here is similar to what Emin and colleagues used to characterise oligomer and aggregate sizes with recombinant α-synuclein.

fraction in *SNCA*-triplication neurons while *SNCA-A53T* did not differ from control. Fractionation markers 19S RP and β-actin did not differ between lines. Reduced α-synuclein in the 10% fraction could indicate fewer intracellular small oligomers in the *SNCA-A53T* line, or this difference could be explained by altered sub-cellular localisation. This confound of interpretation would be absent if assessing the density of free α-synuclein in conditioned media, however the protein input required for this assay (800-1000 µg total protein, 8-10 million dopamine neurons per line) made the technique incompatible with the low α-synuclein concentration in conditioned media, so it was not pursued further.

Despite the low abundance of detergent insoluble α-synuclein (Fig. 6.5B&C), oligomers containing as many as 30+ protomers can remain soluble and detergent labile prior to fibrillar transition (Cremades *et al.*, 2012). This necessitated further study under native conditions, in the absence of detergents. The low isoelectric point of α-synuclein makes it amenable for clear native PAGE (CN-PAGE), where proteins are separated based on their hydrodynamic radius and intrinsic charge. In post-mortem brain tissue this technique demonstrates the presence of low abundance, heat-labile, high molecular weight α-synuclein oligomers with a higher sedimentation coefficient than either recombinant or heat denatured α-synuclein (Gould *et al.*, 2014). As such, CN-PAGE was optimised for α-synuclein oligomer analysis in iPSC-DaNs.

A dominant α-synuclein band from native iPSC-DaN lysates ran at the same position as commercial recombinant protein purified from *E. coli* (Fig. 6.6A), suggesting that most intracellular α-synuclein is monomeric. However, longer exposure of the same CN-PAGE membrane demonstrated the presence of 5 lower bands of fainter intensity. Additionally, there was smeared signal above the monomer position. It was not possible

to run a molecular weight ladder alongside samples to determine the exact masses since commercial native protein ladders are only available for total protein detection (e.g. silver stain and Coomassie blue) and thus unsuitable for western blot. Serial dilution confirmed that the monomer-equivalent band was present in the highest abundance as the signals above and below were lost first (Fig. 6.6B).

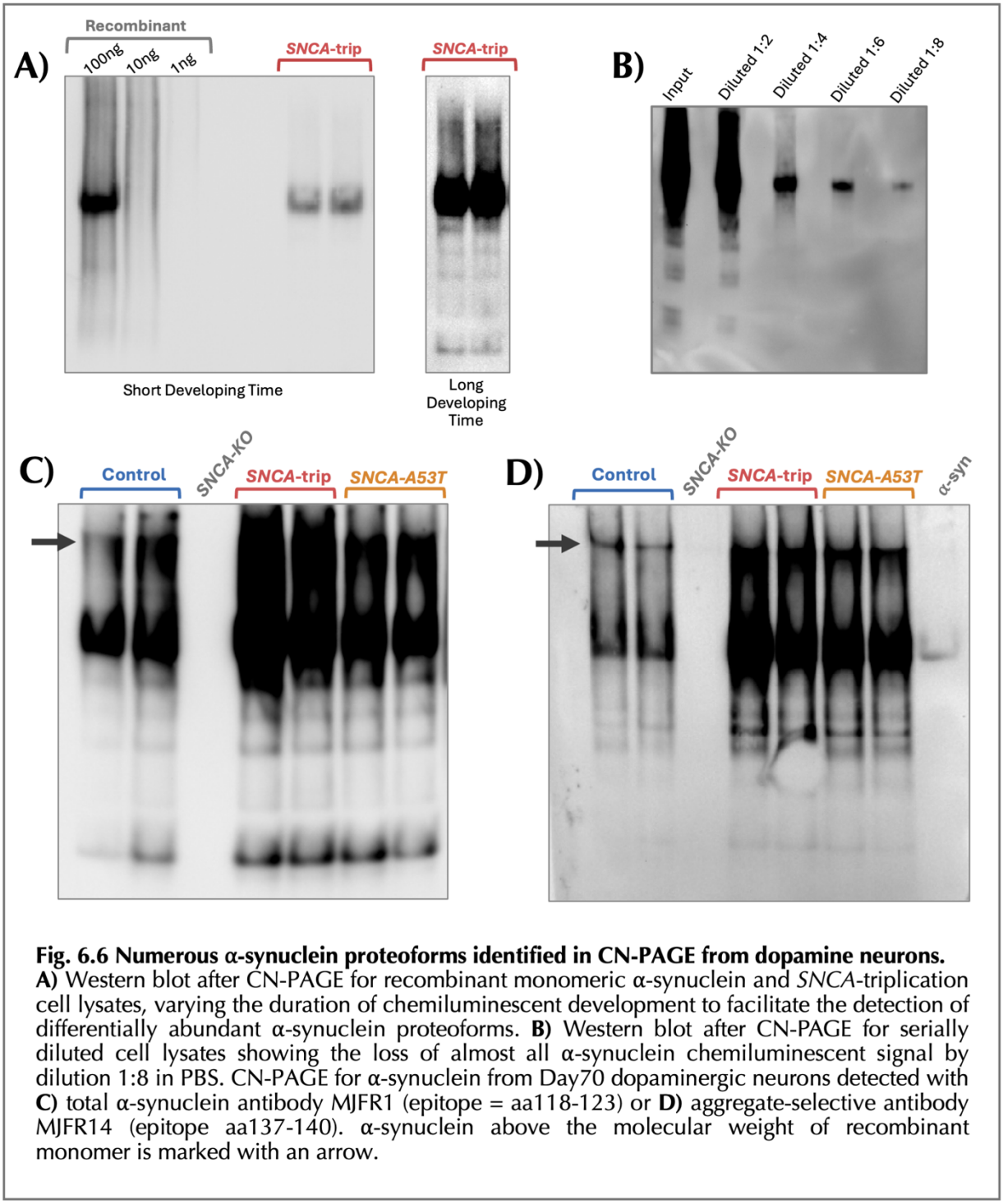

Fig. 6.6 Numerous α-synuclein proteoforms identified in CN-PAGE from dopamine neurons. **A)** Western blot after CN-PAGE for recombinant monomeric α-synuclein and *SNCA*-triplication cell lysates, varying the duration of chemiluminescent development to facilitate the detection of differentially abundant α-synuclein proteoforms. **B)** Western blot after CN-PAGE for serially diluted cell lysates showing the loss of almost all α-synuclein chemiluminescent signal by dilution 1:8 in PBS. CN-PAGE for α-synuclein from Day70 dopaminergic neurons detected with **C)** total α-synuclein antibody MJFR1 (epitope = aa118-123) or **D)** aggregate-selective antibody MJFR14 (epitope aa137-140). α-synuclein above the molecular weight of recombinant monomer is marked with an arrow.

Leveraging this technique to resolve the α-synuclein from healthy controls and *SNCA*-mutant lines demonstrated a further α-synuclein band emerging from the high molecular weight smear with longer chemiluminescent development, which was less intense than the monomer (Fig. 6.6C). This technique is qualitative, so it is not possible to confidently establish whether there was an expression difference of the upper and lower bands between genotypes. However, inclusion of an *SNCA*-knockout out cell line as a control demonstrated that all bands were specific to α-synuclein. Probing the same protein extracts with a reportedly aggregate-selective antibody (MJFR14), detected the monomer and higher band, but some of the lower bands were lost (Fig. 6.6D). MJFR14 also faintly detected recombinant monomeric α-synuclein, raising questions regarding its aggregate specificity.

Given the dependence of CN-PAGE migration on isoelectric point and hydrodynamic radius rather than simply molecular mass the interpretation of the observed banding pattern is non-trivial (Wittig and Schägger, 2008).[9] To better understand the origin of the upper α-synuclein signal (reduced gel shift) as well as the five lower bands (increased gel shift), affinity mapping with various α-synuclein antibodies was used to probe epitope exposure (Fig. 6.7A). Antibodies which bind sequences up to 17 amino acids from the C-terminus detected α-synuclein bands both above and below the position of recombinant monomer. However, 4D6 which binds amino acids 124-134 did not detect lower bands. The epitope of aggregate-selective antibody MJFR14 is 137-140 and this too exhibited markedly reduced detection of α-synuclein bands with the furthest gel shift (Fig. 6.6D). These data suggest that the lower bands could represent C-terminal

[9]To avoid these confounds blue-native PAGE applying a uniform negative charge with Coomassie was also trialled but it was impossible to resolve α-synuclein with this approach in our hands.

truncations of the full-length sequence. High molecular weight α-synuclein oligomers detected in postmortem brain tissue are only stable up to ~55°C (Gould *et al.*, 2014). Boiling cell lysates at 95°C for 10 minutes completely removed the α-synuclein signal above the molecular weight of recombinant monomer (Fig. 6.7B). Interestingly, the signal intensity of the five lower bands was also markedly reduced. This is consistent with previous literature showing that the C-terminally truncated α-synuclein in human red blood cells is heat-labile (Fauvet *et al.*, 2012).

The CN-PAGE findings evidence the presence of heat-labile, high molecular weight α-synuclein in iPSC-DaNs from healthy controls as well as patients with *SNCA*-triplication and *SNCA-A53T* mutations. Moreover, five lower bands were also identified which may be truncations of the C-terminus as they were not detected by C-terminal antibody 4D6. Whilst this approach does not allow quantitive comparison between genotypes, chemiluminescence facilitates enhanced detection of low abundance proteoforms by increasing exposure times and as such is suitable for conditioned media analysis.

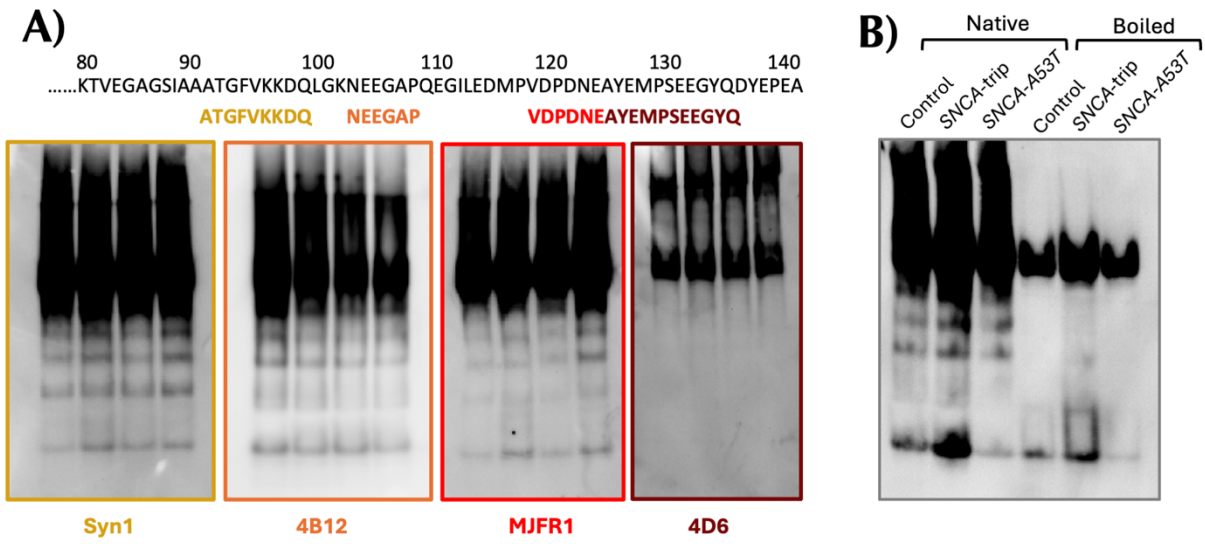

Fig. 6.7 Heat-labile high molecular weight and C-terminally truncated α-synuclein identified by CN-PAGE. **A)** Western blots after CN-PAGE from Day70 neuronal lysates, detecting α-synuclein with four C-terminal antibodies all of which gave no signal in the *SNCA-KO* cell line. Sample order: Control 1, Control 2, Control 3, *SNCA*-triplication. **C)** Western blot after CN-PAGE for native cell lysates maintained on ice or boiled at 95°C for 10 minutes prior to gel loading. α-synuclein was detected with MJFR1.

6.4 Investigating secreted oligomeric α-synuclein

If the high molecular weight, putatively oligomeric, α-synuclein detected with CN-PAGE in cell lysates is secreted into the media, it may underlie the templated misfolding observed in RT-QuIC (Fig. 6.4). Conditioned media was concentrated using 10 kDa ultrafiltration columns and resolved on CN-PAGE, as for cell lysates. The high concentration of BSA from the B27 supplement inhibited gel electrophoresis, but its removal, as for RT-QuIC, permitted detection of α-synuclein with a similar banding pattern to cell lysates (Fig. 6.8A). Whilst the five lower α-synuclein bands were present, the higher molecular weight putatively oligomeric α-synuclein signal was absent from conditioned media blots. This suggests that putatively truncated but not aggregated α-synuclein is released into culture media. However, hydrophobic oligomers/aggregates may preferentially stick to the ultrafiltration devices used to concentrate the media before gel loading, resulting in their apparent absence on the gel.

While the low α-synuclein concentration of conditioned media renders it a more challenging material to work with than cell lysates, media has the advantage that large volumes can be collected through repeated harvesting from the same neurons over time. Column-based techniques are therefore ideal as a large volume of media can be loaded onto the column and then eluted in a much smaller volume. In collaboration with Dr Barnabas Williams in the Draper Group, conditioned media from repeated collection cycles was separated using size-exclusion chromatography (SEC)[10]. α-synuclein was detected in SEC fractions by ELISA which demonstrated its elution between 13.5 and

[10] Our research group does not currently have fluid handling apparatus. On the kind invitation of my college advisor Prof Simon Draper chromatography experiments were carried out using the Draper Group ÄKTA fluid handling apparatus, SEC and C-Tag columns under the supervision and guidance of Barney who also provided valuable input for Eppendorf affinity-purification/enrichment experiments.

15.0 mL which matches the published elution profile for monomeric α-synuclein on the same analytical SEC column (Fauvet *et al.*, 2012; Araki *et al.*, 2016) – Fig. 6.8B. Due to abundance of other proteins in conditioned media the UV trace does not correlate with α-synuclein elution.

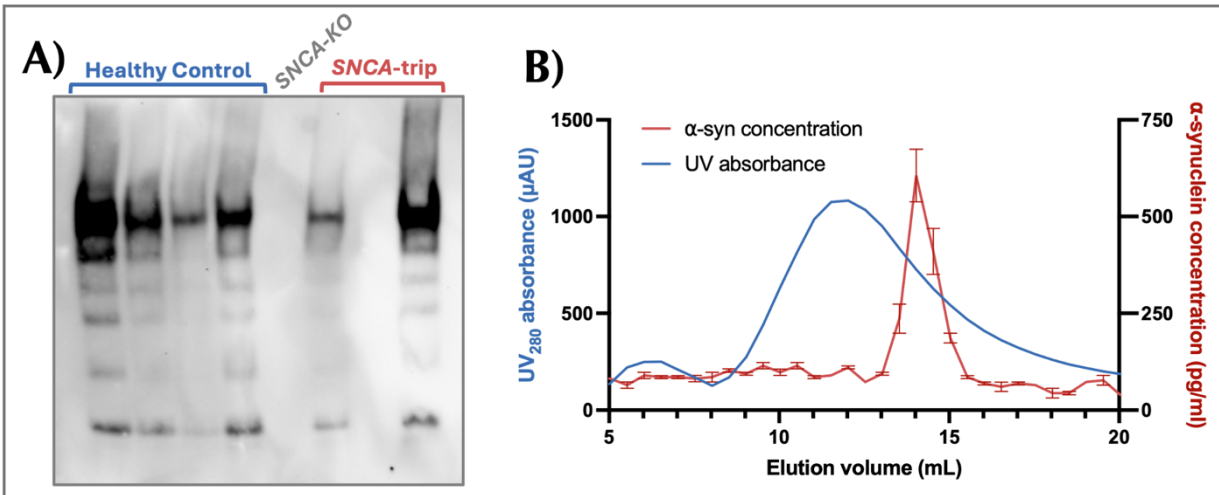

Fig. 6.8 Secreted α-synuclein from patient-derived neurons is predominantly monomeric.
A) Western blots after CN-PAGE from 30x conditioned media harvested from Day70 dopaminergic neurons. N=2-4 lines per genotype. **B)** UV_{280} absorbance trace and corresponding α-synuclein concentrations determined by Bio-Techne ELISA from SEC fractions. 50 mL of unconcentrated conditioned media from *SNCA*-triplication dopamine neurons collected between Day50 and Day75 was loaded onto the column.

Together the CN-PAGE and SEC data suggest that most secreted α-synuclein is monomeric but does not rule out the presence of low abundance oligomers which are below the range of western blot and ELISA detection.

To validate these findings with an orthogonal approach I moved instead to single-molecule techniques. In collaboration with Raman van Wee in the Kukura group we sought to use mass photometry to identify and measure the size of α-synuclein conformers in conditioned media. Mass photometry allows label-free detection of single proteins or protein complexes based on their light scattering properties which are proportional to molecular weight, thereby providing a direct size read-out (Young *et al.*,

2018). Previously, the Kukura group demonstrated that the masses and mobilities of membrane associated proteins can be determined during their lateral diffusion in a supported lipid bilayer (SLB) (Foley *et al.*, 2021). Unpublished, work from the Kukura group has optimised this approach for complex biological samples using additional surface passivation and the introduction of antibodies which induce specific and predictable mass shifts when binding the protein of interest embedded in the SLB (Fig. 6.9A). Antibody-induced contrast enables the detection of small proteins which would otherwise be below the mass range of this technique. Leveraging the intrinsic lipid binding of α-synuclein, and the antibody-conferred specific detection of this approach, we assessed the molecular weight of α-synuclein in conditioned media[11]. Overnight incubation of 20x conditioned media from *SNCA*-triplication neurons with the C-terminal MJFR1 antibody allowed detection of α-synuclein-antibody complexes which were absent in the *SNCA-KO* negative control (Fig. 6.9B&C). Only one mass peak at 212 kDa was detected indicating the absence of a range of differently sized oligomers in the sample. After subtraction of the antibody this corresponds to ~60 kDa which is similar to the mass observed for purified recombinant α-synuclein in the same assay (Fig. 6.9D), but higher than the expected 14.5 kDa. Although it is possible that some α-synuclein in conditioned media samples exists as a trimer/tetramer it is unlikely that this is also true for recombinant control. A single peak at 212 kDa could also be explained if the MJFR1 antibody itself was glycosylated and hence heavier than the expected ~150 kDa.

[11] This work was undertaken as a collaboration between myself and Raman using technology developed by Dr Manish Kushwah, Raman and Prof Philipp Kukura, see section 2.12. I grew the cells and prepared the concentrated media or purified protein samples. Raman prepared the SLBs and optimised the membrane composition and passivation. Data acquisition for biological samples was carried out jointly. Raman performed the data processing and analysis. We contributed equally to experimental design and planning.

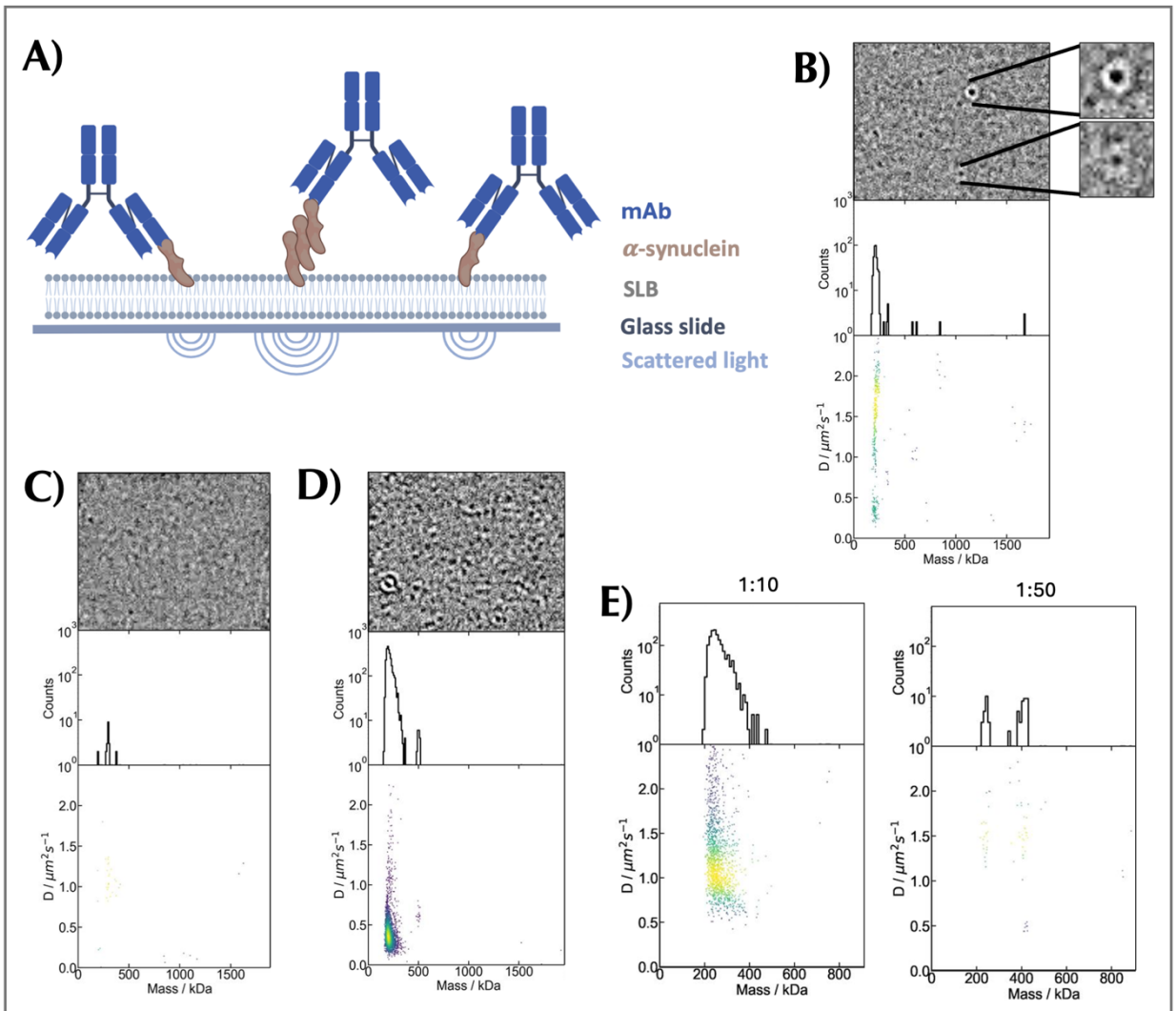

Fig. 6.9 α-synuclein detected in conditioned media with mass photometry.
A) Schematic showing the mass photometry paradigm. α-synuclein binds to the supported lipid bilayer (SLB) on a glass slide and can then be bound by antibodies increasing the contrast to enable detection. **B)** Representative frame from contrast recordings of 20x *SNCA*-triplication conditioned media showing α-synuclein-antibody complexes that appear as black dots in the contrast image. Two zoomed fields of view show examples of large (top) and small (bottom) species. Scatter plots show the mass quantifications of individual binding events plotted against their diffusivity and log histograms represent the projection of counts from the scatter plot. Representative frame from contrast recordings and quantification of mass, diffusivity and counts for **C)** 20x *SNCA-KO* conditioned media and **D)** 100 nM recombinant α-synuclein. **E)** Quantification of mass, diffusivity and counts for detected binding events in *SNCA*-triplication cell lysates diluted 1:10 or 1:50 onto the SLB.

Moreover, the low diffusion coefficients suggest that complexes may have more than one anchor point to the SLB, for example antibodies binding α-synuclein via both Fab regions. Tandem binding to two α-synuclein monomers would also increase the calculated mass of complexes, thus contributing to the unexpectedly high molecular

weight. It is worth noting that recordings were highly variable between experimental replicates. While ~210 kDa complexes were observed in some recordings from control and *SNCA*-triplication conditioned media other technical replicates lacked robust signal.

The assay described here relies on α-synuclein binding to the SLB. However, it is possible that oligomeric α-synuclein rich in β-sheets has lower affinity than monomer for the SLB (Musteikytė *et al.*, 2021). As a positive control for oligomer binding and subsequent detection of oligomer-antibody complexes we sought to investigate α-synuclein in cell lysates where CN-PAGE had already evidenced oligomer existence. Cell lysates are much more complex biological samples than conditioned media. Not only are total protein concentration orders of magnitude higher, but lysates contain a myriad of membrane-associated and integral membrane proteins which would be expected to also bind the SLB. As such, 1:10 dilution of clarified native lysates onto the SLB produced considerable non-specific signal masking detection of α-synuclein-antibody complexes (Fig. 6.9E). However, increasing the dilution factor to reduce non-specific binding also resulted in the loss of α-synuclein detection, suggesting that the requirements of maximal α-synuclein concentration and minimal background could not simultaneously be met with this approach. These results motivated the development of a protocol for low-throughput native purification/enrichment of α-synuclein from iPSC-DaNs.

Existing protocols for purification of α-synuclein from patient samples such as blood or cortical tissue are multi-step, involving a minimum of ion-exchange, hydrophobic interaction and size-exclusion chromatography (Bartels, Choi and Selkoe, 2011; Fauvet *et al.*, 2012; Burré *et al.*, 2013; Luth *et al.*, 2014). However, these protocols require far more protein input than is feasible from iPSC-DaNs due to the sequential losses at each stage. For example, Luth and collages homogenise 20g of cortical tissue prior to protein

extraction which is over three orders of magnitude more input than could be reasonably achieved with stem cells. Thus, it was necessary to optimise a single-step enrichment that both increased the α-synuclein concentration and reduced the concentration of membrane-binding contaminants in the final eluate.

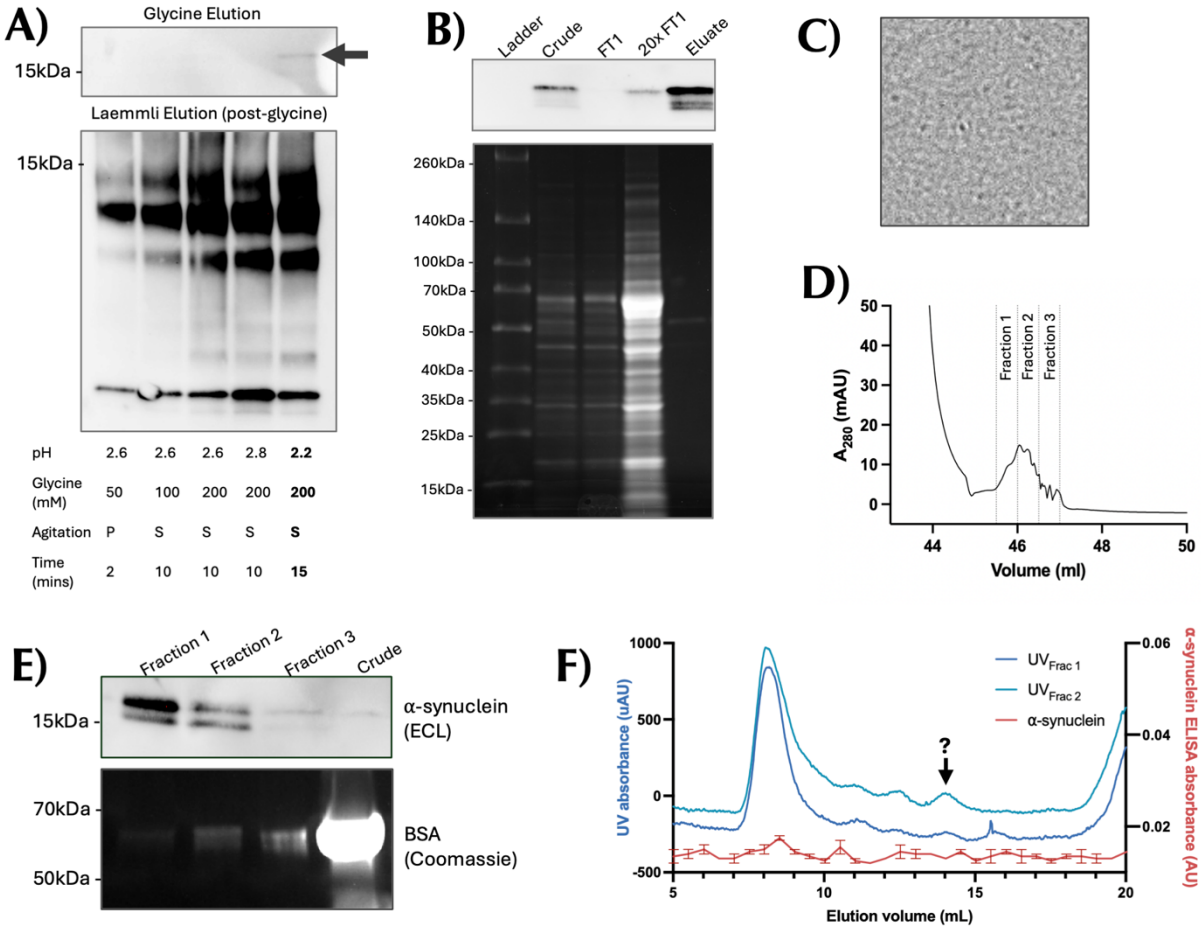

Fig. 6.10 Steps toward native purification of α-synuclein from dopamine neurons.
A) Western blot after SDS-PAGE of immunoprecipitated α-synuclein eluted with 5-200 mM glycine at pH 2.2-2.8 for 2-15 minutes. During elution samples were agitated with either continuous pipetting (P) or shaking at 500 rpm (S). After glycine elution the beads were boiled in Laemmli buffer to elute any remaining α-synuclein. **B)** Western blot and Coomassie staining after SDS-PAGE for the cell lysate (crude), flow through/ first wash (FT1), 20x concentrate of the flow through/ first wash (20x FT1) and the eluted protein from C-tag affinity purification. **C)** Representative frame from contrast recording showing an absence signal for α-synuclein-antibody complexes in SEPEA C-tag eluate. **D)** Representative UV trace during elution for column-based affinity purification of α-synuclein from 100 mL of sequentially collected SNCA-triplication conditioned media using the same C-tag resin. 500 µL α-synuclein-containing fractions were collected. **E)** Western blot and Coomassie staining after SDS-PAGE for eluted fractions showing α-synuclein enrichment and BSA depletion. **F)** SEC UV_{280} absorbance trace and corresponding α-synuclein concentrations determined by ELISA for α-synuclein-containing C-tag fractions. A possible peak for α-synuclein is marked with an arrow although this was below the ELISA detection threshold.

In Chapter 3 α-synuclein immunoprecipitation was used to enrich α-synuclein ahead of mass spectrometry providing a good yield from limited starting material. However, elution involved boiling which would denature any heat-labile oligomers (Gould *et al.*, 2014). Moreover, the immunoprecipitation antibodies were also eluted which may complicate analysis (Fig. 3.9A). To overcome this, antibodies were cross-linked to the protein G beads, all detergents were removed and α-synuclein was eluted under mild conditions with low pH glycine to preserve physiological interactions.[12] However, across a range of conditions the α-synuclein yield was extremely low and mostly remained bound to the beads after elution, making this an inviable strategy (Fig. 6.10A). Commercially available CaptureSelect C-tag resin binds the EPEA sequence which is found at the C-terminus of α-synuclein via high-affinity single domain nanobody NbSyn2. α-synuclein was readily eluted with 2M $MgCl_2$ and pH 2.5 glycine (data not shown) but the condition which gave the least contaminants, as determined by SDS-PAGE and Coomassie staining, was elution with a competing SEPEA peptide (Fig. 6.10B). Although one contaminant was present at ~55 kDa, α-synuclein was clearly enriched compared to input material. The use of a competing peptide in native conditions avoids any potential disruption to oligomers caused by changes in pH and ionic strength. However, there was no signal for α-synuclein-antibody complexes on the SLB when the α-synuclein-enriched C-tag eluate was used for mass photometry (Fig. 6.10C). Whilst surprising, this result indicated that even following enrichment the α-synuclein concentration was still too low for detection with mass photometry.

[12] Low pH citrate, high salt buffers and high pH triethylamine were also trialled but were unable to disrupt the α-synuclein-antibody complexes to elute α-synuclein and are thus not presented.

C-tag resin can also be used for on-column purification making it amenable for purification of α-synuclein from conditioned media (harvested over multiple collections). In two independent replicates a small UV elution peak enabled identification and collection of α-synuclein-containing fractions (Fig. 6.10D&E). Other contaminants, mostly BSA, were depleted but not completely removed (Fig. 6.10E). We considered that SEC as a second step might be able to remove residual contaminants to provide highly pure native α-synuclein which could be concentrated and used for other assays such as CD spectroscopy where α-synuclein monomer and oligomers exhibit distinct spectra (Kaufmann *et al.*, 2016). BSA eluted at ~8.5 mL as previously observed using this column (Martel *et al.*, 2023) – Fig. 6.10F. There was a small UV peak at ~14 mL where α-synuclein was shown to elute previously (Fig. 6.8B), however this did not correspond with α-synuclein ELISA signal (Fig. 6.10F). Other small peaks were also observed in the UV trace but in the absence of ELISA detection it is impossible to conclude whether they were the result of other contaminants or whether they correspond to α-synuclein oligomers. Moreover, if the α-synuclein concentration is too low even for ELISA, there would be insufficient protein for downstream applications. Therefore, the purification of native α-synuclein from lysates and media was not pursued further.

In light of the challenges purifying α-synuclein, I instead piloted another single-molecule technique which should be capable of detecting α-synuclein against a complex background of other proteins. A limitation of the mass photometry approach used above is that monomer is detected as well as any high molecular weight proteoforms. While this is useful for mass estimation, it means that if monomers are present in vast excess the detection oligomers would be precluded. Single Molecule Pull Down (SiMPull) and total internal reflection (TIRF) microscopy is a super-resolution fluorescence imaging

technique, only capable of detecting multimers, oligomers and aggregates (Emin *et al.*, 2022) - Fig. 6.11A. This approach uses the same monoclonal antibody for both capture and detection such that fluorescently labelled detection antibodies are only pulled down to the coverslip when multiple α-synuclein protomers interact exposing a second epitope on the complex. In collaboration with Florence Layburn in the Klenerman Group, concentrated conditioned media samples were assayed using C-terminal antibody Syn211[13]. Robust fluorescent signal was detected in the PFF positive control, but media from *SNCA*-triplication and healthy control neurons lacked fluorescent puncta and resembled the *SNCA*-knockout negative control (Fig. 6.11B), indicating that any oligomers present were below the detection limit.

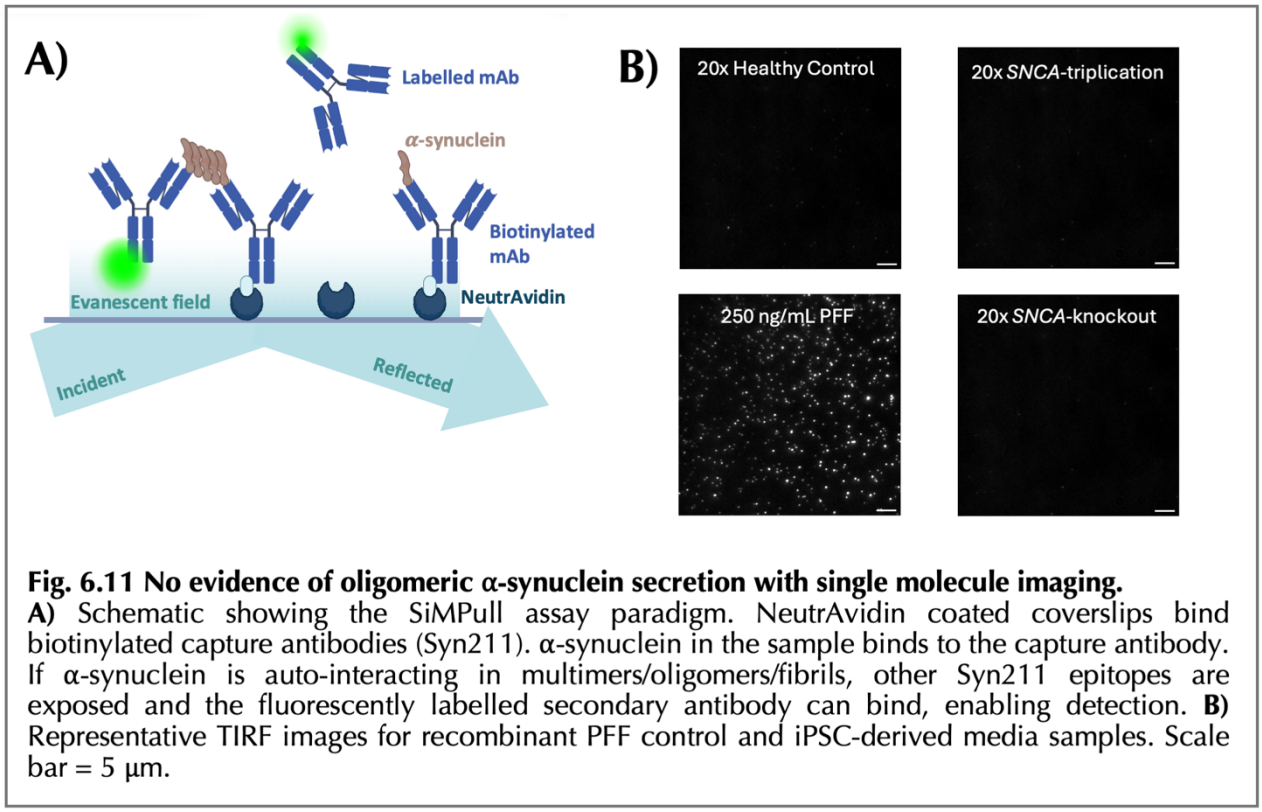

Fig. 6.11 No evidence of oligomeric α-synuclein secretion with single molecule imaging.
A) Schematic showing the SiMPull assay paradigm. NeutrAvidin coated coverslips bind biotinylated capture antibodies (Syn211). α-synuclein in the sample binds to the capture antibody. If α-synuclein is auto-interacting in multimers/oligomers/fibrils, other Syn211 epitopes are exposed and the fluorescently labelled secondary antibody can bind, enabling detection. **B)** Representative TIRF images for recombinant PFF control and iPSC-derived media samples. Scale bar = 5 µm.

[13] This work was undertaken as a collaboration between myself and Florence using published technology from the Klenerman group (University of Cambridge) which is regularly used to assay CSF samples. I grew the cells and prepared the media which was shipped to Cambridge. Florence prepared the coverslips, carried out the immunoassay and did the imaging. We contributed equally to experimental planning carried out over Microsoft Teams.

Together these results suggest that oligomeric/aggregated α-synuclein is not abundantly secreted by iPSC-DaNs in culture. Using four orthogonal approaches monomers but not oligomers were identified in media samples. These data do not rule out the presence of low-concentration α-synuclein oligomers which were below the limit of detection.

6.5 Discussion

Conditioned media from iPSC-DaNs containing secreted α-synuclein templated the misfolding and aggregation of recombinant monomeric protein (Fig. 6.4A&B). This prion-like activity aligns with the consensus that binding of intrinsically disordered monomer to α-synuclein which has already adopted the β-sheet conformation catalyses this misfolding (Li *et al.*, 2022). While it has recently been shown that iPSC-DaNs lacking the PARK2 (parkin) gene express templating-competent species intracellularly (Schmidt *et al.*, 2025), this is – to our knowledge – the first demonstration that seeds are secreted. Media from *SNCA*-triplication or *SNCA-A53T* neurons demonstrated faster aggregation kinetics than media harvested from healthy controls, suggesting a higher concentration of misfolded seeds (Fig. 6.4B).

While the *SNCA*-triplication neurons secrete a higher total amount of α-synuclein into their media this is not the case for the *SNCA-A53T* lines, indicating that proportionally more misfolded seeds are released. Moreover, ~50% of α-synuclein from the *SNCA-A53T* line differs from the recombinant monomer in primary sequence. This suggests that a degree of heterologous seeding takes place, as has been previously reported (Wood *et al.*, 1999). A53T seeds were previously shown to be less efficient at templating of wildtype monomer than an equivalent concentration of wildtype seeds (Sidhu, Segers-Nolten and Subramaniam, 2016). This is despite the reaction kinetics of homologous A53T seeding being considerably faster (Flagmeier *et al.*, 2016). However, it is worth noting that aggregated seeds in these experiments are fibrillar rather than oligomeric. Fibrils exhibit reduced conformational flexibility compared to less structured small oligomers which may hinder cross-seeding since conformational similarity between

monomer and seed is the main driver of seeding efficiency (Sidhu, Segers-Nolten and Subramaniam, 2016). Sidhu and colleagues also observed ultrastructural differences in the fibrils formed by heterologous and homologous seeding reactions. Similarly, the novel RT-FAST assay suggests aggregation seeded by A53T results in larger and more diverse aggregates (Meyer *et al.*, 2022). Since all PD-linked point mutations in *SNCA* alter α-synuclein aggregation kinetics (Flagmeier *et al.*, 2016), future work should leverage the RT-QuIC protocol presented here to assess the seeding capabilities of media from iPSC-DaNs with E46K, A30P and Q51D point mutations, as well as H50Q when such lines have been engineered. It would also be interesting to determine if there is a change in seeding propensity of media from sporadic iPSC lines which lack the strong genetic drivers of disease and better correlate with studies in patient CSF. The effects of seed sequence on fibril architecture (Sidhu, Segers-Nolten and Subramaniam, 2016; Meyer *et al.*, 2022) raise the question of whether there are ultrastructural differences between fibrils produced by RT-QuIC seeded with media from PD or healthy control neurons. Transmission electron microscopy of the RT-QuIC reaction product could be used to answer this question (Lee, Civitelli and Parkkinen, 2024).

Here, lag-time was used to compare reaction kinetics. This parameter was selected because ThT curves for technical replicates of the same sample were found to be most similar in the early part of the reaction. Studies in CSF have investigated other parameters including maximal fluorescence intensity and area under the ThT curve (Poggiolini *et al.*, 2022). Despite altering the plate reader settings to reduce gain, conditioned media samples routinely exceeded the maximum fluorescence threshold of the equipment preventing the accurate computation of these two parameters. Maximal slope was also computed but found to be highly variable between technical replicates, cell lines and

genotypes. Interestingly, the raw data from several reactions showed clear two-part kinetics, with a marked reduction to rate after a rapid initial rise (See *SNCA-A53T* in Fig. 6.3G). Numerous factors could contribute to these observed kinetics including sequestration of recombinant monomer by other proteins in the sample, auto-inhibition of fibrillization above a critical concentration or reaction facilitation by another component of the media (for example a lipid) which is rapidly depleted. While advanced kinetic analysis is beyond the scope of this work, it would be interesting to determine the factors contributing to non-sigmoidal amplification and whether it differs between genotypes.

A key distinction between the RT-QuIC results presented here and published CSF RT-QuIC is that amplification, albeit with a longer lag-time, was also observed in all healthy controls. By contrast in CSF from healthy people there is usually no aggregation within typical assay timeframes of 80-120 hours (Fairfoul *et al.*, 2016; Grossauer *et al.*, 2023). Accordingly, the predictive power of CSF RT-QuIC to distinguish PD patients from controls is usually a binary variable for the presence/absence of aggregation, while comparison of kinetics parameters are correlated with synucleinopathy clinical presentation (Poggiolini *et al.*, 2022; Bräuer *et al.*, 2023; Brockmann *et al.*, 2024). Given the marked reduction in complexity of iPSC-DaN culture compared to aged human brain it would be surprising if dopamine neurons from healthy people secreted seeding-competent α-synuclein in culture but not *in vivo*. It is possible that *in vitro* cells are simply more stressed due to suboptimal culture conditions and may release misfolded α-synuclein seeds through cell lysis. Alternatively, α-synuclein seeds might be secreted into CSF at very low levels in healthy people but another cell type e.g. astrocytes or microglia (absent in iPSC-DaN monoculture) clear them before seeds can amplify, thus

preventing their detection in CSF RT-QuIC. The latter proposal therefore indicates a degree of neuron-extrinsic control of pathology propagation and highlights the need for further work in more translational models. A recent study using novel immuno-infrared sensing to measure α-synuclein folding provides support for the presence of low abundance misfolded seeds in CSF from healthy people. While the abundance of β-sheet α-synuclein was significantly elevated in PD CSF there were multiple control samples with infrared spectra consistent with the presence of β-sheets (Schuler *et al.*, 2025). Hence it is not unreasonable that control iPSC-DaNs could also release misfolded α-synuclein seeds, but at lower levels than the PD lines. As a complimentary approach to examine this hypothesis it would be possible to employ a FRET-based α-synuclein biosensor model to media analysis (Yamasaki *et al.,* 2019). Treating cultures of HEK293T cells expressing α-synuclein-CFP/YFP fusion proteins with conditioned media from PD and healthy control iPSC-DaNs and tracking seeded aggregation in the cells could help to validate whether controls also release α-synuclein seeds as suggested by my RT-QuIC.

To better understand the *SNCA*-triplication and *SNCA-A53T* seeding phenotype I attempted to measure oligomeric and aggregated α-synuclein in conditioned media. The oligomer/aggregate-selective ELISA showed a trending but non-significant increase in both *SNCA*-mutant lines compared to control, with a similar fold change to RT-QuIC lag time (Fig. 6.1F & 6.4B). However, the overall signal was extremely low making it impossible to discount non-specific monomer detection, particularly for the *SNCA*-triplication line where monomer secretion is increased ~1.5-fold (Fig. 6.1E). Separating secreted α-synuclein by hydrodynamic radius under native conditions using CN-PAGE or SEC did not identify any proteoforms larger than α-synuclein monomer (Fig. 6.8A&B). The CN-PAGE from conditioned media did present a faint high molecular weight smear

which was absent in *SNCA-KO* cells that may correlate with ultra-low abundance oligomeric protein, but unlike in cell lysates this did not resolve into a clear band with longer developing times. No oligomer/aggregate signal was detected by SiMPull/TIRF from either healthy control or *SNCA*-triplication conditioned media (Fig. 6.11B). The sensitivity of this technique for α-synuclein in biofluids is thought to be ~150 pg/mL (Saleeb *et al.*, 2023). The concentration of total secreted α-synuclein in patient derived cells measured with this ELISA is ~500 pg/mL (Fig. 4.4H), so even the 20x concentrate would only contain a maximum of ~10 ng/mL α-synuclein, not accounting for loss on concentrator membranes. Hence to be within the detection range of this assay oligomers would need to make up at least ~2 % of the α-synuclein secreted by iPSC-DaNs. ELISAs from CSF suggests that oligomers account for ~9% of total α-synuclein in PD and ~3.5% in controls (Majbour *et al.*, 2016). These values might also be somewhat inflated by low-level detection of monomer in oligomer-selective immunoassays, such that the true prevalence of oligomeric α-synuclein is even lower. Thus, it is unclear whether the SiMPull approach would be able to detect α-synuclein oligomers in iPSC-DaN conditioned media even if they were secreted.

Mass photometry detected a single peak for α-synuclein-antibody complexes in media from *SNCA*-triplication neurons (Fig. 6.9B). If oligomers represent <10% of total α-synuclein as described above in CSF, then we would expect only ~10^1 counts per recording. Moreover, it is very unlikely that all oligomers present would be of the same molecular weight (Zhou and Kurouski, 2020). Hence, an already sub-threshold predicated particle count would be further dispersed across a range of masses so any signal from oligomer-antibody SLB binding would be indistinguishable from noise. The same is true for CN-PAGE where 1:4 dilution of lysate results in loss of the upper band

(Fig. 6.6B) and SEC where 10% of the monomer peak (~60 pg/mL) is well below the noise threshold (Fig. 6.8B). Once again, an oligomer population composed of multiple differently sized proteoforms would push the signal for any single species even further below the detection limit.

From these results we can conclude that although α-synuclein oligomers are clearly not abundant in conditioned media, the assays used here are not sensitive enough to detect oligomers present at or below the fractional concentration measured in CSF (Majbour *et al.*, 2016; Abdi *et al.*, 2021). While it is possible that iPSC-DaNs at Day75 do not secrete oligomeric α-synuclein this is at odds with the RT-QuIC results which indicate the presence of aggregation-prone seeds in culture media. It is possible that another factor secreted by the cells may initiate aggregation in RT-QuIC. However, during the completion of this study the Horrocks lab published complementary data suggesting oligomeric α-synuclein is released, although they were unable to evidence a PD vs control phenotype (Saleeb *et al.*, 2023). Using a dual-colour variant of SiMPull (named STAPull) - which is 3-5 times more sensitive - these authors detected a trending increase in fluorophore colocalization (putative aggregates) in conditioned media from *SNCA*-triplication iPSC-DaNs compared to *SNCA*-knockout controls (Saleeb *et al.*, 2023). Coincident detection events, which indicate the presence of more than one antibody epitope on any given α-synuclein particle (i.e. an oligomer) were ~500 times less common than monomer detection with either fluorophore. These results support my conclusion that secreted oligomers represent a tiny fraction of the total secreted α-synuclein and would be sub-threshold for the techniques I employed to measure them.

The extremely low concentration and consequent challenges in detection of α-synuclein seeds that likely underlie the RT-QuIC phenotype, serve to emphasise the power and

importance of seeding amplification assays. Not only are β-strand proteoforms undetectable with ThT at the start of the RT-QuIC assay but also by a variety of biochemical and biophysical techniques designed for aggregate detection. It is this feature which underscores the power of SAA for diagnostics particularly in prodromal PD. Given the borderline detection using the aggregate-selective ELISA, it would be interesting to try other immuno-enriched techniques that have shown success in patient CSF such as the immuno-infrared spectroscopy mentioned above (Schuler *et al.*, 2025).

In Chapter 3, I identified N-terminally truncated α-synuclein which appeared as lower molecular weight bands in SDS-PAGE (Fig. 3.9). Here, I have identified up to five putatively truncated bands with CN-PAGE (Fig. 6.6, 6.7 & 6.8). These were not detected with antibodies against the most C-terminal epitopes and may represent products of C-terminal truncation (Fauvet *et al.*, 2012). Some additive PTMs also increase the gel shift in CN-PAGE in spite of increasing the molecular weight. For example phosphorylation increases the negative charges on α-synuclein and results in a lower band (Fauvet *et al.*, 2012). While there was little evidence of phospho-α-synuclein in these neurons (Fig. 3.2 & 3.3), it is possible that other modifications, such as methionine oxidation, that increase negative charge may exhibit a similar effect. It is noteworthy that one such site, met-127, falls within the 4D6 epitope and may reduce antibody affinity and subsequent detection.

In addition to the putatively truncated/modified lower bands, heat-labile high molecular weight α-synuclein was identified in cell lysates that was absent/sub-threshold in conditioned media. In some blots this resembled a high molecular weight smear while in others it resolved more clearly into a single band between 480-720 kDa (though the utility of the native protein ladder is questionable since on this scale recombinant monomer ran at ~250 kDa). The Mazzulli lab have also previously identified a single

larger α-synuclein proteoform from cell lysates of iPSC-DaNs, the abundance of which is increased by disease-causing mutations. Using SEC these authors identified a second peak for α-synuclein eluting at ~12.5 mL (100Å) rather than ~16.5 mL (35Å) which was where recombinant monomer eluted from their column (Mazzulli, Zunke, Isacson, *et al.*, 2016; Zunke *et al.*, 2018). Although it is not possible to draw any comparative conclusions regarding the size of oligomers detected by these two complementary techniques it is interesting that these authors also observed only one other dominant α-synuclein population beside from monomer. By contrast, in-cell cross-linking in *SNCA-A53T* or *GBA1-/-* iPSC-DaNs and SDS-PAGE revealed a range of higher molecular weight α-synuclein proteoforms from ~35-100 kDa (Dettmer *et al.*, 2015; Kim *et al.*, 2018). However, it is impossible to be certain that the oligomers they detect are endogenous and not an artifact of the cross-linking process.

Mass photometry for natively extracted α-synuclein from cell lysates would be an ideal approach to better understand the respective sizes of different α-synuclein populations observed on CN-PAGE. This technique should also enable quantitation of relative abundance between PD and control lines. Despite previous success for the detection of spiked recombinant proteins on a background of cell lysates by the Kukura group, it was impossible to detect α-synuclein in iPSC-DaN lysates. Given the importance of transmembrane transport and membrane compartmentalisation to neuronal physiology it is not unlikely that human neurons express more membrane associated proteins than non-neuronal cell types. Indeed, in mouse brain dopamine neurons are enriched in cell surface channels and receptors (Kilfeather *et al.*, 2024). Binding of these molecules to the SLB could explain the non-specific signal which prevented α-synuclein detection in native lysates. The challenges in purifying/enriching α-synuclein for mass photometry

are frustrating, but not unforeseen given the marked down-scaling of input material compared to usual purification methods. Despite western blot detection a Coomassie band could not be detected for eluted α-synuclein from cell lysates or conditioned media, indicating that the concentration was extremely low and unsuitable for mass photometry. In future work SEC could be used to fractionate crude cell lysates, with the same ELISA readout as used for conditioned media. This approach, like that used by Zunke and colleagues, has the potential to provide an orthogonal means of mass estimation for the oligomeric α-synuclein in cell lysates observed by native PAGE, while removing the requirement of purification. Moreover, unlike CN-PAGE, ELISAs are quantitative which would enable a genotype comparison of oligomer abundance.

Our lab and others have used imaging-based assays to evidence intracellular oligomeric/aggregated α-synuclein in iPSC-DaNs (Whiten *et al.*, 2018; Zambon *et al.*, 2019; Virdi *et al.*, 2022). Aggregate puncta measured by super-resolution techniques vary between 25-250 nm with a higher median length in *SNCA*-triplications and *SNCA-A53T* lines (Whiten *et al.*, 2018; Virdi *et al.*, 2022). The most abundant ~75 nm aggregates, if fibrillar in structure, are predicted to be composed of >150 protomers (>2000 kDa), while the largest aggregates would contain >500 protomers (>7000 kDa) (Dearborn *et al.*, 2016). Such large intracellular aggregates are unlikely to be soluble in the detergent-free conditions required for oligomer interrogation on CN-PAGE or by SEC but would be extracted by progressively harsher detergent treatment. Low levels of triton-X100 insoluble α-synuclein were detected here (Fig. 6.5B&C), which is consistent with previous reports from a variety of PD-linked mutations (Chung *et al.*, 2016; Oj *et al.*, 2016; Burbulla *et al.*, 2017; Ryan *et al.*, 2018; Zunke *et al.*, 2018; A. Ikeda *et al.*, 2019; Tsunemi *et al.*, 2019; Drobny *et al.*, 2023). Detergent-insoluble aggregate accumulation

is an aging dependant phenotype and becomes more evident with prolonged time in culture (Tsunemi *et al.*, 2019; Stykel *et al.*, 2021). Previously maturation to Day150 was required to observe a robust disease phenotype possibly explaining the very low signal measured in my experiment (Burbulla *et al.*, 2019).

To our knowledge, this is the first use of a sucrose gradient separation to probe α-synuclein density in iPSC-DaNs. The same approach using brain homogenate from patients with Lewy body dementia detects large α-synuclein aggregates which equilibrate in sucrose fractions up 50% w/v (Kramer and Schulz-Schaeffer, 2007). However, in my experiments α-synuclein was only detected in fractions 0-20% (Fig. 6.5F). This is consistent with iPSC-DaNs modelling an early stage of disease with considerably milder pathology than observed *in vivo*. Atomic force microscopy for *in vitro* aggregated α-synuclein shows that the 10% fraction is predominantly composed of monomeric protein (Emin *et al.*, 2022). Consistent with this finding, the authors could not detect ThT-labelled α-synuclein from the 10% fraction using super-resolution imaging, suggesting that any small oligomers present must either lack β-sheet structure or be below the 20 nm resolution limit. α-synuclein was found to be significantly reduced in the 10% fraction in *SNCA-A53T* triplication lines. It is possible that this is due to a small decrease in oligomer abundance (for example due to the trending increased secretion, Fig. 6.1F). However, it could also be explained by differential interactions with other cytosolic protein due to the point mutation, which might very subtly affect its equilibration density. While the 20% fraction also contains some α-synuclein monomer, ThT imaging shows that β-sheet aggregates are present with lengths 160-220 nm (Emin *et al.*, 2022). A trending increase in the proportion of α-synuclein in the 20% sucrose fraction was observed for *SNCA*-triplication neurons (Fig. 6.5I). While it is possible that

this could also be caused by altered subcellular localisation this is somewhat less likely since *SNCA*-triplication lines express the wildtype α-synuclein sequence. Previous work from our group in the same cell lines demonstrated an increase in oligomeric α-synuclein, as measured by proximity ligation assay, in *SNCA*-triplication but not *SNCA-A53T* iPSC-DaNs compared to controls (Zambon *et al.*, 2019). This technique selectively detects small aggregates rather than larger fibrils (Roberts, Wade-Martins and Alegre-Abarrategui, 2015). Together these data point to a subtle increase in micro-aggregates in our neurons, with predicted sizes that correlate with findings of other groups using DNA-PAINT (Whiten *et al.*, 2018; Virdi *et al.*, 2022).

Overall, the data presented in this chapter validate previous reports that small α-synuclein aggregates are present at low levels in patient-derived iPSC-DaNs and that some of these are detergent insoluble. Furthermore, I show that smaller soluble oligomers of α-synuclein can be identified in native state in the same cells. While I was unable to evidence the secretion of these oligomers directly, I demonstrated that iPSC-DaNs release seeds capable of templated aggregation, a process which amplifies β-sheet conformers bringing them into a measurable concentration range. Crucially, media from neurons carrying *SNCA*-triplication and *SNCA-A53T* mutations demonstrate elevated seeding, suggesting that *SNCA* mutations cause increased secretion of misfolded α-synuclein seeds.

Chapter 7 – General Discussion

In this thesis I have characterised intracellular and secreted proteoforms of α-synuclein in iPSC-derived dopaminergic neurons carrying *SNCA*-triplication, *SNCA-A53T* and *GBA1-N370S* familial mutations. Proteolytically truncated, putatively oligomeric and low levels of alternatively spliced α-synuclein were identified inside neurons, with evidence that truncated proteoforms are also secreted. Total levels of secreted α-synuclein, as well as the seeding capacity of these extracellular forms, were found to differ between PD genotypes and healthy controls. Furthermore, the cellular mechanisms underlying α-synuclein secretion were explored using pharmacology and CRISPRi technology. Secretion was found to be Ca^{2+}-dependant and linked to the endolysosomal system. Synaptotagmin-1, SNAP-23 and GTPases Rab8a and Rab9a were identified as key regulators of this process. Together, these data provide valuable insight to the release and propagation of human α-synuclein which underlie its prion-like behaviour in a highly disease-relevant model.

7.1 iPSC-DaNs as a model of α-synuclein pathology

iPSC-DaNs from patients carrying the *SNCA*-triplication mutation lacked large, phosphorylated aggregates (Figs. 3.2, 3.3). While trace amounts of detergent-insoluble α-synuclein were detected (Fig. 6.5B&C), this was not above the basal level in healthy controls. These findings indicate that iPSC-DaNs model an earlier stage of disease, prior to the accumulation of Lewy pathology observed in human post-mortem brains. Even in the absence of overt aggregate pathology, familial PD mutations were found to perturb α-synuclein homeostasis. Secretion of α-synuclein into the conditioned media was elevated in *SNCA*-triplication and *GBA1-N370S* (but not *SNCA-A53T*) neurons (Figs. 4.1

& 6.1D&E). Extracellular release of α-synuclein can be considered as having a dual role in disease. Secretion reduces the intracellular α-synuclein burden within a single neuron, promoting cell survival but also facilitates prion-like propagation when pathological proteoforms are endocytosed by adjacent cells. This dichotomy is highlighted by the *ATP13A2* mutation which reduces α-synuclein release, for which boosting secretion in iPSC-DaNs promotes α-synuclein clearance and corrects mitochondrial dysfunction (Tsunemi *et al.*, 2019). In PD 50-60% of SNpc neurons are lost before any symptoms are detected, indicating a remarkable capacity of the dopamine system for adaptation (Rinne, 1993). Thus, under an 'altruistic' model, inhibition of α-synuclein secretion from an oligomer/aggregate-containing neuron that prevents the uptake of misfolded seeds by multiple adjacent cells should ultimately be neuroprotective even if at the expense of the α-synuclein-donor neuron. In line with this hypothesis, exposing healthy neurons to secreted α-synuclein from PD lines via co-culturing induces cellular dysfunction including impaired mitochondrial dynamics in the previously healthy cells (Ryan *et al.*, 2018). Moreover, increasing secretion over time (Figs. 4.1A & 6.1D), correlates with previously reported aging-dependent dysfunction (Virdi *et al.*, 2022). Taken together, these data point to elevated α-synuclein secretion in iPSC-derived models as a pathological phenotype.

The secreted α-synuclein from *SNCA*-triplication and *SNCA-A53T* neurons seeded aggregation of recombinant monomer with faster kinetics than controls in RT-QuIC indicating increased abundance, or potency, of seeds (Fig. 6.4). This finding is highly relevant to the wider field as it shows that iPSC-DaN cultures mirror clinical biomarkers. With the increasing interest in CSF SAA for diagnostics and patient stratification, the ability to use native stem-cell derived α-synuclein to better understand reaction kinetics

in vitro cannot be underestimated. Furthermore, using RT-QuIC as a potential readout for drug testing or knockdown/knockout screening in iPSC-derived neuron models could provide an important new angle from which to assess efficacy.

Although it was not possible to identify the proteoforms which contributed to seeding in culture media, truncated and putatively oligomeric α-synuclein were found in iPSC-DaN lysates. N-terminal truncations, confirmed by mass spectrometry, appeared as 2-3 bands on SDS-PAGE of which the uppermost was routinely detected with C-terminal antibodies (Fig. 3.9). This truncation arose in a maturation-dependent manner, was specific to dopamine neurons and did not fractionate to a specific subcellular compartment (Figs. 3.1C, 3.4C&D and 6.5E&F). Moreover, a corresponding band was detected for α-synuclein secreted into culture media (Figs. 4.1C, 6.1C, 6.10E). In the absence of detergents, gel electrophoresis from cell lysates and conditioned media revealed additional low molecular weight proteoforms which may correspond to C-terminal truncations (Figs. 6.6, 6.7 & 6.8A). These were heat labile which may explain their absence in SDS-PAGE where samples are boiled prior to gel loading (Fig. 6.7B). Although α-synuclein is a remarkably heat-stable protein, this stability is almost entirely conferred by the acidic C-terminus, deletion of which causes α-synuclein to aggregate at high temperatures and not be resolved by electrophoresis (Park *et al.*, 2002; Fauvet *et al.*, 2012). Conversely, N-terminal deletions do not influence α-synuclein heat stability (Park *et al.*, 2002). Published reports of C-terminal truncations in post-mortem tissue and animal models typically do not report heating of cell/tissue extracts prior to gel loading, even for electrophoresis under denaturing conditions (Luk *et al.*, 2012; Bhattacharjee *et al.*, 2019; Mahul-Mellier *et al.*, 2025). Moreover, the high isoelectric point of C-terminally truncated α-synuclein results in inefficient gel-to-membrane transfer in classic

tris-glycine buffer (pH 8.3) while carbonate buffer (pH 9.9) more faithfully conserves these low molecular weight proteoforms (Dunn, 1986; Sorrentino and Giasson, 2020). This observation may explain why putative C-terminal truncation products required such long exposure even in native conditions (Fig. 6.6A&B). Characterisation of C-terminal truncations with mass spectrometry would require an alternative approach to the immunoprecipitation, electrophoresis, silver-staining and gel band digest employed in Chapter 3, since efficient dissociation of α-synuclein-antibody complexes required heat denaturation (Fig. 6.10A). With sufficient input material, and silver stain rather than Coomassie detection it is likely that C-Tag purification and SEPEA elution (Fig. 6.10B), would preserve C-terminally truncated α-synuclein for proteomic characterisation.

Both N- and C-terminal truncations of α-synuclein have been shown to affect aggregation *in vitro* and *in vivo*. Products of C-terminal truncation are widely accepted to be more aggregation-prone than the full length sequence, as well as accelerating aggregation of full length α-synuclein when present in mixtures (Sorrentino *et al.*, 2018; Sorrentino and Giasson, 2020). The effects of N-terminal truncation are more nuanced; N-terminally truncated α-synuclein itself exhibits slower aggregation kinetics than the full length sequence (Zibaee *et al.*, 2007; Terada *et al.*, 2018), however in culture cells and mice N-terminal truncations promote the formation of phosphorylated aggregates (Terada *et al.*, 2018; Taguchi, Watanabe and Tanaka, 2025). The N-terminus is essential for the interaction of α-synuclein with lipid membranes and the purportedly anti-aggregatory α-helical conformation which membrane interactions induce (Bartels *et al.*, 2010; Lorenzen *et al.*, 2014; Meade *et al.*, 2023, 2025). Thus, it appears likely that in cellular systems where biological membranes are abundant, the toxicity of N-terminal truncations is mediated by disruption of this stabilising effect. In the context of this

project, the identification of age-dependent, cell-type specific N-terminal truncation products therefore predisposes iPSC-DaNs to time-dependent oligomer formation which may contribute to the cellular phenotypes observed (Zambon *et al.*, 2019; Virdi *et al.*, 2022).

High molecular weight putative oligomers were detected in cell lysates from all genotypes using native PAGE (Figs. 6.6 & 6.7). This technique is qualitative and cannot be used to compare relative abundance between control and *SNCA*-mutant lines, however sucrose density gradient ultracentrifugation demonstrated a trending increase in the abundance of α-synuclein in the 20% fraction for *SNCA*-triplication iPSC-DaNs compared to healthy controls (Fig. 6.5I). As discussed in Chapter 6, previous work characterising α-synuclein proteoforms with super-resolution imaging observed β-sheet-rich oligomers in this fraction (Emin *et al.*, 2022). Together with previous findings, my data support an increased abundance of oligomeric α-synuclein in iPSC-DaNs carrying the *SNCA*-triplication mutation (Mazzulli, Zunke, Tsunemi, *et al.*, 2016; Zambon *et al.*, 2019). It remains to be determined whether abrogating N-terminal α-synuclein truncation with protease inhibitors (as discussed in Chapter 3) would reduce oligomer formation in these neurons.

Overall, I have demonstrated that *SNCA* mutations in iPSC-derived dopamine neurons faithfully recapitulate the early-, but not late-, stage α-synuclein pathology in human patients. α-synuclein is proteolytically truncation and oligomerises intracellularly and then is secreted to the extracellular space (possibly including the export of pathological proteoforms) where it can seed *de novo* aggregation. Crucially, the aggregation propensity of extracellular α-synuclein is increased by familial PD mutations demonstrating the value of iPSC-DaNs as a disease model.

7.2 Mechanisms of α-synuclein secretion from iPSC-DaNs

In line with previous reports, the secretion of free α-synuclein in iPSC-DaNs was found to be dependent on intracellular Ca^{2+} (Emmanouilidou *et al.*, 2010; Zhao *et al.*, 2022; Nakamura *et al.*, 2024) – Fig. 4.6. CRISPRi screening for genetic regulators of α-synuclein secretion identified *SYT1*, encoding Synaptotagmin-1, for which both sgRNAs caused significant reductions to α-synuclein concentration in conditioned media (Fig. 5.9). Synaptotagmin-1 is highly expressed in iPSC-DaNs with no difference between genotypes (Fig. 5.1A), though a recent pre-print suggests it may be downregulated at the mRNA level in PD post-mortem brain but not specifically in SNpc dopaminergic neurons (Cavalcante and Soares-Souza, 2025). Synaptotagmin-1 functions as the major Ca^{2+} sensor for activity-dependent synaptic release of dopamine in SNpc neurons (Banerjee *et al.*, 2020; Delignat-Lavaud *et al.*, 2023). It is also found in the somatodendritic compartment where it acts redundantly with synaptotagmin-7 to facilitate synchronous dopamine release (Hikima *et al.*, 2022; Lebowitz *et al.*, 2022).

During synaptic vesicle release synaptotagmin-1 interacts with a SNARE complex formed of SNAP-25, VAMP2 and syntaxin-1, to confer Ca^{2+} sensitivity to the fusion machinery (Fernández-Chacón *et al.*, 2001; Südhof, 2013). This interaction is mediated by electrostatic interactions between the Ca^{2+}-binding C2B domain of synaptotagmin-1 and acidic residues on syntaxin-1 and SNAP-25 and is thought not to be generalisable to other SNAREs such as SNAP-23 (Chieregatti *et al.*, 2004; Weber *et al.*, 2014; Brewer *et al.*, 2015). As such, a role for synaptotagmin-1 in α-synuclein secretion could indicate synaptic release which would correspond to recent findings suggesting release is reduced by ~20% when firing activity of iPSC-DaNs is prevented (Nuermaimaiti *et al.*, 2025). It is notable however that the effect of *SYT1* knockdown on α-synuclein secretion was

profound, with the *SYT1_1* guide reducing release more than the knockdown of *SNCA* itself (Fig. 5.9). In contrast, neither sgRNA against syntaxin-1A had a significant effect on α-synuclein release (though the knockdown efficiency of the guides was not assessed), which is consistent with previous results (Zhao *et al.*, 2022).

SNAP-25, to which synaptotagmin-1 binds, has also been implicated in the homotypic fusion of endosomes (Sun *et al.*, 2003; Aikawa *et al.*, 2006). Moreover, the syntapotagmin-1 C2B domain can interact with proteins lacking the SNARE motif allowing it to confer Ca^{2+} dependence to other cellular processes such as clathrin mediated endocytosis (in this case through stonin-2 and adaptor protein-2) (Haucke *et al.*, 2000; Jung *et al.*, 2007; Y. Chen *et al.*, 2022). Through coupling to alternative adaptors or involvement in poorly characterised non-synaptic interactions with its cognate SNAREs synaptotagmin-1 may be able to regulate α-synuclein secretion through multiple parallel pathways which would better explain its powerful effect on release than sole reliance on synaptic mechanisms. Importantly, identification of synaptotagmin-1 as a regulator of α-synuclein secretion highlights the importance of carrying out mechanistic studies, in relevant neuronal models since it is not expressed in cell lines such as HEK293T commonly used to investigate α-synuclein release mechanisms (Diril *et al.*, 2006). Future work should repeat the Ca^{2+} chelation experiments (Fig. 4.6A) in *SYT1* knockdown iPSC-DaNs to determine whether the dependence on intracellular Ca^{2+} is lost, thus confirming synaptotagmin-1 as the Ca^{2+} sensor for α-synuclein secretion.

Knockdown of Rab8a and Rab9a were also found to inhibit α-synuclein secretion. Rab GTPases act as switch molecules which regulate intracellular transport, binding to and are central to endosomal and autophagosomal trafficking (Zhang, Jiang and Shi, 2022). Rab8a is widely reported to play a role in the exocytosis of various proteins including

matrix metalloproteases and interleukin-1-β (Bravo-Cordero *et al.*, 2007; Dupont *et al.*, 2011). Rab8a is one of the phosphorylation substrates of leucine-rich repeat kinase 2 (LRRK2), mutations in which are associated with familial PD (Komori and Kuwahara, 2023). Phosphorylation of Rab8a by LRRK2 alters its affinity for effectors such as optineurin and RILPL2 and thus can modulate coupling to downstream pathways (Yu *et al.,* 2018, Waschbüsch *et al.,* 2020). The C-terminus of α-synuclein has been shown to directly bind to the switch region of Rab8a, an interaction which is potentiated by serine-129 phosphorylation (Yin *et al.*, 2014). It is not known whether phosphorylation of Rab8a itself modulates this interaction (Schuelke, Haseeb and Parmar, 2026). Previous studies linking Rab8a to α-synuclein secretion have differed in their findings. CRISPR knockout of *RAB8A* in *NGN2*-induced cortical neurons increased α-synuclein levels in culture media measured by dot-blot (Mamais *et al.*, 2024). However, in SH-SY5Y cells *RAB8A* knockdown dramatically supressed α-synuclein secretion and crucially, by measuring lactate dehydrogenase in conditioned media, these authors ruled out changes in passive α-synuclein release through cell lysis (Nakamura *et al.*, 2024; Sawai, Nakamura and Arawaka, 2025). Furthermore, overexpression of *RAB8A* in PC12 cells significantly increases α-synuclein secretion (Ejlerskov *et al.*, 2013).

These dichotomous results may be explained by the involvement of Rab8a in two (or more) distinct release pathways. Where α-synuclein secretion was reduced by *RAB8A* knockdown studies found that secretion was from the autophagy-lysosome pathway, and as such, levels of the lysosomal hydrolase cathepsin B in culture media were also reduced by *RAB8A* deficiency (Ejlerskov *et al.*, 2013; Nakamura *et al.*, 2024; Sawai, Nakamura and Arawaka, 2025). Rab8a also regulates unconventional protein secretion from the recycling endosome in collaboration with Rab11a, though the effect

directionality of Rab8a depletion on substrate release is less clear (Henry and Sheff, 2008; X. Li *et al.*, 2024). In this pathway knockdown of *RAB11A* results in the accumulation of proteins for secretion in enlarged and distorted Rab8a positive vesicles (X. Li *et al.*, 2024). Coupling to recycling vs autophagy pathways is modulated by phosphorylation and is therefore influenced by familial PD gain-of-function LRRK2 mutations (Mamais *et al.,* 2021). Given that there was no effect of the *RAB11A_2* guide which reduced target mRNA expression by 50% in iPSC-DaNs (Figs. 5.9 & 5.10A), it seems likely that the effect of *RAB8A* knockdown in this study is through impaired trafficking of autolysosomes and lysosomes toward the plasma membrane.

Other than co-localisation in the late endosome Rab9a has not previously been linked to α-synuclein secretion (Xu *et al.*, 2018). This GTPase is thought to function in trafficking between the endolysosomal system and the trans-Golgi network including the delivery of membrane vesicles for autophagosome expansion and the trafficking of lysosomal hydrolase enzymes (Kucera, Bakke and Progida, 2016). To our knowledge Rab9a has not previously been linked directly to exocytotic pathways, however if α-synuclein secretion proceeds in part by a mechanism involving the autophagy-lysosome pathway, as suggested by *RAB8A*, then it stands to reason that impairing autophagosome formation with *RAB9A* knockdown could decrease α-synuclein release (Nishida *et al.*, 2009). It is important for future work to quantify autophagic flux and lysosome function in the case of both knockdowns as well as to determine whether the secretion of lysosome markers is altered. Identification of both Rab proteins underscores the importance of using a genetic approach to investigate α-synuclein secretion mechanisms as there are currently no specific small molecule inhibitors for either of these proteins.

SNAP-23 is the dominant Qbc-SNARE for endosomal and lysosomal fusion with the plasma membrane and has been consistently linked to α-synuclein secretion making it an encouraging, if unsurprising, hit (Fontaine *et al.*, 2016; Dingjan *et al.*, 2018; Xie *et al.*, 2022; Zhao *et al.*, 2022; Sawai, Nakamura and Arawaka, 2025). SNAP-23 can interact with a variety of Qa- and R-SNAREs including VAMP7 which was also identified as a possible hit (Fig. 5.10C). While SNAP-23 identification confirms involvement of unconventional endosomal secretion, it does not confirm which upstream pathways have trafficked α-synuclein into this compartment. SNAP-23-mediated secretion of free α-synuclein can be categorised as the plasma membrane fusion of either autophagosomes/autolysosomes/lysosomes which have accumulated α-synuclein through macro- or chaperone-mediated autophagy or late-endosomes which have accumulated α-synuclein through MAPS. Quercetin, which was previously reported as a potent inhibitor of the essential MAPS chaperone DNAJC5, reduced α-synuclein secretion from healthy control and PD iPSC-DaNs (Fig. 4.3). However, the *DNAJC5_1* sgRNA had no effect on α-synuclein secretion despite decreasing target expression by ~70% (Fig. 5.9, 5.10B). By contrast in differentiated SH-SY5Y cells a similar level of knockdown, achieved with shRNA, decreased α-synuclein release more than 4-fold (Wu, Sirkis and Schekman, 2022). It is worth noting that for the two other key MAPS regulators included in the screen, RT-qPCR results for knockdown efficiency were inconclusive, so it is not possible to reliably interpret the effects of sgRNAs on α-synuclein secretion (Fig. 5.10A).

Two plausible hypotheses reconcile pharmacology and genetic data regarding DNAJC5. MAPS selectively secretes misfolded proteins (Lee *et al.*, 2016), for α-synuclein this likely corresponds to small oligomers containing β-strand α-synuclein. While the presence of

putative oligomers was evidenced in neurons matured to Day70 with the Kriks protocol (Fig. 6.5F, 6.6 & 6.7), I did not investigate whether *NGN2* iPSC-DaNs also express high molecular weight α-synuclein. If *NGN2* iPSC-DaNs at Day36 only express correctly folded monomeric α-synuclein then it follows that DNAJC5 depletion would have negligible effects. In either cell model, the low abundance of putatively misfolded α-synuclein, against a background majority of correctly folded monomeric α-synuclein would make changes in this activity of the MAPS pathway challenging to detect with a total α-synuclein ELISA. In future, assessing the effect of *DNAJC5* knockdown on RT-QuIC lag time could provide a more sensitive readout for release of misfolded protein. Alternatively, given its polypharmacology, the effects of quercetin on α-synuclein release may be mediated through a different pathway, for example it is widely recognised to stimulate autophagy which may promote α-synuclein degradation and reduce release (Mundo Rivera *et al.*, 2024). Independent of why *DNAJC5* knockdown does not alter release in *NGN2* iPSC-DaNs it indicates that the effect of *SNAP23* knockdown must be mediated through pathways involving the exocytosis of vesicles from the autophagy-lysosome pathway rather than the late endosome. Furthermore, in previous reports SNAP-23-mediated secretory autophagy was found to be Ca^{2+}-dependant and co-regulated by Rab8a suggesting that all identified hits cluster in one pathway indicative of autophagosome/lysosome fusion with the plasma membrane even in the absence of lysosomal stressors (Nakamura *et al.*, 2024; Sawai, Nakamura and Arawaka, 2025).

Reducing *ATG5* expression by ~50% did not significantly reduce α-synuclein secretion (Fig. 5.9 & 5.10B). While at first it is challenging to rationalise these findings with a release mechanism reliant on autophagosome formation, it should be noted that the form of macroautophagy stimulated by Rab9a is independent of Atg5 (Nishida *et al.*, 2009).

Overall, the integration of genetic and pharmacological data suggests that under quiescent conditions the secretion of free α-synuclein from iPSC-DaNs is through Ca^{2+}-dependent release of autophagic (and possibly to a lesser extent synaptic) vesicles. I therefore hypothesise that following uptake into Rab9-positive autophagosomes, α-synuclein is trafficked by Rab8a to the plasma membrane where SNAP-23 and VAMP7 facilitate Ca^{2+}-dependent fusion. It is unclear whether autophagosomes fuse with lysosomes during this trajectory, thus being released as autolysosomes containing lysosomal proteases. Given that disruption of degradative lysosomal function, either with mutant GCase or chloroquine (Fig. 4.1 & 4.2E-G) boost α-synuclein release (Fig. 4.1 & 4.2E-G), I posit that secreted vesicles represent a population of mature autophagosomes just prior to lysosome fusion. As such drugs that impair autophagosome-lysosome fusion would increase the size of this vesicle pool and facilitate release as observed for bafilomycin A1 and chloroquine (Fernandes *et al.*, 2016) – Fig. 4.2E-G. While not mechanistically definitive, the work presented here provides a strong basis for more targeted future experiments to assess how molecules involved in autophagosome maturation regulate α-synuclein release. Moreover, the screen has identified previously unknown targets such as Rab9a of potential interest for therapeutic manipulation.

7.3 Technical challenges: Applying biophysics to cell biology systems

This project demonstrated that iPSC-DaNs express putatively pathological proteoforms of α-synuclein which differ in (at least) primary and quaternary structure from the α-synuclein produced in bacterial or mammalian expression systems (Bartels, Choi and Selkoe, 2011; Fauvet *et al.*, 2012). However, characterising proteoforms in low

availability cell-derived samples where technical and financial limitations prevent scale-up, represented a major challenge. Broadly, the issues we experienced pertained either to sample complexity and the requirement of purification or total sample concentration.

The complexity of cytosolic mixtures generated from neuronal cell lysis necessitated purification/enrichment, however despite numerous attempts at optimisation the α-synuclein concentration of eluates was too low for both intact mass spectrometry and mass photometry. Indeed, the only biophysical technique which generated successful results was proteomic mass spectrometry which did not require preservation of native conformations and thus facilitated more efficient electrophoretic purification. An alternative approach is to directly characterise these molecules within their cellular environment, where the concentration is considerably higher, using single molecule imaging approaches such as AD-PAINT (relying on DNA aptamer) for aggregate detection (Whiten *et al.*, 2018; Virdi *et al.*, 2022). While powerful, this technique doesn't allow α-synuclein and β-amyloid aggregates to be distinguished and is not suitable for analysis of the smallest oligomers.

Challenges of sample complexity can be reduced by studying α-synuclein in conditioned media which contains many fewer proteins, however, in our hands sample concentration was too low to investigate oligomeric proteoforms with mass photometry or SiMPull. It is however worth noting that we were able to detect a single α-synuclein population with mass photometry, which was absent in media from *SNCA*-knockout neurons, and which already represents considerable sensitivity improvement. Using single-molecule fluorescence approaches this difference between *SNCA*-knockout and *SNCA*-triplication has been reported previously (Saleeb *et al.*, 2023), but no publications to date have been able to discriminate PD and control genotypes. It appears that current techniques do not

have the power to decern the subtle differences caused by familial mutations when working close to or at their limits of detection.

Considerably more success has been had with the detection and characterisation of β-amyloid from the conditioned media of iPSC-derived neuronal models. A SiMPull variant that uses the 6E10 β-amyloid antibody has recently evidenced an increase in number and median size of soluble aggregates in the conditioned media of trisomy 21 iPSC-derived organoids (Fertan *et al.*, 2024). These and other authors have also been able to achieve sub-diffraction limit morphology characterisation with DNA-PAINT variants demonstrating that β-amyloid aggregate size segregates with disease genotype (Whiten *et al.*, 2020; Fertan *et al.*, 2024). It is unclear whether this is simply due to higher concentration of secreted amyloid, since not only do clinical studies in CSF differ regarding which biomarker is more abundant but more importantly the use of different iPSC-derived neuronal cell types and culture paradigms hinders comparison (Kang, 2013; Vergallo *et al.*, 2018). Antibody affinity for the target molecule also plays a crucial role in defining the detection range. For SiMPull which requires α-synuclein-antibody complexes to remain intact throughout imaging (in contrast to the transient binding in DNA-PAINT), it is possible that using a higher affinity α-synuclein antibody may improve detection at low concentrations. Anecdotally, MJFR1 proved the highest affinity antibody I worked with in this project, however in the absence of published dissociation constants it is not possible to conclude whether it would be a better than Syn211.

While single-molecule fluorescence imaging approaches remain the best characterised methods for the detection of aggregation prone proteins in biofluids (Yang, Perrett and Wu, 2021), other platforms are emerging which may be able to detect α-synuclein proteoforms in iPSC-derived conditioned media samples. For example, combining

oligomer-selective DNA carriers with unprocessed CSF samples has recently demonstrated significantly elevated levels of sub-20 nm oligomeric α-synuclein in PD patients using nano-pore sensing (Liu *et al.*, 2023). Moreover, integration of two-colour coincident detection (as for STAPull discussed in Chapter 6) with in-solution monitoring using microfluidics enabled >30-fold improvement in detection limit through reduction of non-specific antibody adsorption to coverslips (Chappard *et al.*, 2023). Integrating these kinds of technical advances with increasingly high-throughput iPSC-derived neuron models, e.g. *NGN2* neurons with faster differentiation timelines, will likely enable characterisation of proteoforms which evaded detection in this project. Such insights will be essential to develop an understanding of the effects of manipulations to cellular function, for example with preclinical therapeutics, on the proteoforms and pathogenicity of α-synuclein secreted.

7.4 Conclusion

This thesis set out to characterise the proteoforms of α-synuclein expressed and secreted by iPSC-DaNs from familial PD patients. I have demonstrated that, in the absence of extrinsic insult, α-synuclein does not bear the additive PTMs observed in post-mortem brain but is truncated at the N-terminus in an ageing-dependent manner. This truncation appears to be specific to dopamine neurons and may reflect a low molecular weight proteoform identified in post-mortem tissue from vulnerable brain regions. Other heat-labile truncation products were also identified which appear to represent truncations to the C-terminus of α-synuclein. I demonstrated the presence of high molecular weight putatively aggregated/oligomeric α-synuclein in iPSC-DaNs and provide suggestive evidence that these proteoforms may be more abundant in patient-derived neurons that

have triplication of the *SNCA* locus. Having optimised a seeding amplification assay to amplify putatively misfolded oligomeric seeds I demonstrated that the α-synuclein secreted by *SNCA*-mutant iPSC-DaNs exhibits elevated templating capacity compared to α-synuclein in conditioned media from controls. Interrogating secretion mechanisms suggests a central role of autophagy in α-synuclein release from iPSC-DaNs. Moreover, through CRISPR interference I identify four key regulatory genes; *SYT1, SNAP-23*, *RAB8A* and *RAB9A* that map to a pathway of Ca^{2+}-dependent fusion of α-synuclein-containing autophagosomes with the plasma membrane.

Overall, this thesis demonstrates the value of iPSC-derived dopaminergic models to further our understanding of the prion-like propagation of α-synuclein which occurs when seeding-competent proteoforms are secreted. In PD the spread of α-synuclein seeds contributes significantly to the progression of pathology and dysfunction, as such reliable *in vitro* models could play an essential role in the development of a long-awaited disease-modifying therapy.

References

Abdelmotilib, H. *et al.* (2017) 'α-Synuclein fibril-induced inclusion spread in rats and mice correlates with dopaminergic Neurodegeneration', *Neurobiology of Disease*, 105, pp. 84–98. Available at: https://doi.org/10.1016/j.nbd.2017.05.014.

Abdi, I.Y. *et al.* (2021) 'Preanalytical Stability of CSF Total and Oligomeric Alpha-Synuclein', *Frontiers in Aging Neuroscience*, 13, p. 638718. Available at: https://doi.org/10.3389/fnagi.2021.638718.

Abeliovich, A. *et al.* (2000) 'Mice Lacking α-Synuclein Display Functional Deficits in the Nigrostriatal Dopamine System', *Neuron*, 25(1), pp. 239–252. Available at: https://doi.org/10.1016/S0896-6273(00)80886-7.

Abeywardana, T. and Pratt, M.R. (2015) 'Extent of Inhibition of α-Synuclein Aggregation in Vitro by SUMOylation Is Conjugation Site- and SUMO Isoform-Selective', *Biochemistry*, 54(4), pp. 959–961. Available at: https://doi.org/10.1021/bi501512m.

Abounit, S. *et al.* (2016) 'Tunneling nanotubes spread fibrillar α-synuclein by intercellular trafficking of lysosomes', *The EMBO Journal*, 35(19), pp. 2120–2138. Available at: https://doi.org/10.15252/embj.201593411.

Adav, S.S. and Sze, S.K. (2020) 'Hypoxia-Induced Degenerative Protein Modifications Associated with Aging and Age-Associated Disorders', *Aging and Disease*, 11(2), p. 341. Available at: https://doi.org/10.14336/AD.2019.0604.

Agarwal, A. *et al.* (2024) 'VAMP2 regulates phase separation of α-synuclein', *Nature Cell Biology*, 26(8), pp. 1296–1308. Available at: https://doi.org/10.1038/s41556-024-01451-6.

Agarwal, D. *et al.* (2020) 'A single-cell atlas of the human substantia nigra reveals cell-specific pathways associated with neurological disorders', *Nature Communications*, 11(1), p. 4183. Available at: https://doi.org/10.1038/s41467-020-17876-0.

Aikawa, Y. *et al.* (2006) 'A Second SNARE Role for Exocytic SNAP25 in Endosome Fusion', *Molecular Biology of the Cell*, 17(5), pp. 2113–2124. Available at: https://doi.org/10.1091/mbc.e06-01-0074.

Alvarez-Erviti, L. *et al.* (2011) 'Lysosomal dysfunction increases exosome-mediated alpha-synuclein release and transmission', *Neurobiology of Disease*, 42(3), pp. 360–367. Available at: https://doi.org/10.1016/j.nbd.2011.01.029.

Anagnostou, D. *et al.* (2023) 'Assessment of Aggregated and Exosome-Associated α-Synuclein in Brain Tissue and Cerebrospinal Fluid Using Specific Immunoassays', *Diagnostics*, 13(13), p. 2192. Available at: https://doi.org/10.3390/diagnostics13132192.

Anderson, J.P. *et al.* (2006) 'Phosphorylation of Ser-129 Is the Dominant Pathological Modification of α-Synuclein in Familial and Sporadic Lewy Body Disease', *Journal of Biological Chemistry*, 281(40), pp. 29739–29752. Available at: https://doi.org/10.1074/jbc.M600933200.

Anheim, M. *et al.* (2012) 'Penetrance of Parkinson disease in glucocerebrosidase gene mutation carriers', *Neurology*, 78(6), pp. 417–420. Available at: https://doi.org/10.1212/WNL.0b013e318245f476.

Aniszewska, A. *et al.* (2022) 'Modeling Parkinson's disease-related symptoms in alpha-synuclein overexpressing mice', *Brain and Behavior*, 12(7), p. e2628. Available at: https://doi.org/10.1002/brb3.2628.

Antonin, W. (2000) 'A SNARE complex mediating fusion of late endosomes defines conserved properties of SNARE structure and function', *The EMBO Journal*, 19(23), pp. 6453–6464. Available at: https://doi.org/10.1093/emboj/19.23.6453.

Antonschmidt, L. *et al.* (2022) 'The clinical drug candidate anle138b binds in a cavity of lipidic α-synuclein fibrils'. Edmond. Available at: https://doi.org/10.17617/3.9C6TEW.

Anwar, S. *et al.* (2011) 'Functional Alterations to the Nigrostriatal System in Mice Lacking All Three Members of the Synuclein Family', *The Journal of Neuroscience*, 31(20), pp. 7264–7274. Available at: https://doi.org/10.1523/JNEUROSCI.6194-10.2011.

Araki, K. *et al.* (2016) 'A small-angle X-ray scattering study of alpha-synuclein from human red blood cells', *Scientific Reports*, 6(1), p. 30473. Available at: https://doi.org/10.1038/srep30473.

Araki, K. *et al.* (2018) 'The localization of α-synuclein in the process of differentiation of human erythroid cells', *International Journal of Hematology*, 108(2), pp. 130–138. Available at: https://doi.org/10.1007/s12185-018-2457-8.

Arena, G. *et al.* (2024) 'Polygenic Risk Scores Validated in Patient-Derived Cells Stratify for Mitochondrial Subtypes of Parkinson's Disease', *Annals of Neurology*, 96(1), pp. 133–149. Available at: https://doi.org/10.1002/ana.26949.

Back, M.J. *et al.* (2018) 'Activation of neutral sphingomyelinase 2 by starvation induces cell-protective autophagy via an increase in Golgi-localized ceramide', *Cell Death & Disease*, 9(6), p. 670. Available at: https://doi.org/10.1038/s41419-018-0709-4.

Bae, E.-J. *et al.* (2014) 'Glucocerebrosidase depletion enhances cell-to-cell transmission of α-synuclein', *Nature Communications*, 5(1), p. 4755. Available at: https://doi.org/10.1038/ncomms5755.

Bandres-Ciga, S. *et al.* (2020) 'Genetics of Parkinson's disease: An introspection of its journey towards precision medicine', *Neurobiology of Disease*, 137, p. 104782. Available at: https://doi.org/10.1016/j.nbd.2020.104782.

Banerjee, A. *et al.* (2020) 'Synaptotagmin-1 is the Ca2+ sensor for fast striatal dopamine release', *eLife*, 9, p. e58359. Available at: https://doi.org/10.7554/eLife.58359.

Bar, H. and Zweifach, A. (2020) 'Z' Does Not Need to Be > 0.5', *Slas Discovery*, 25(9), p. 1000. Available at: https://doi.org/10.1177/2472555220942764.

Barbour, R. *et al.* (2008) 'Red Blood Cells Are the Major Source of Alpha-Synuclein in Blood', *Neurodegenerative Diseases*, 5(2), pp. 55–59. Available at: https://doi.org/10.1159/000112832.

Barbuti, P. *et al.* (2020) 'Using High-Content Screening to Generate Single-Cell Gene-Corrected Patient-Derived iPS Clones Reveals Excess Alpha-Synuclein with Familial Parkinson's Disease Point Mutation A30P', *Cells*, 9(9), p. 2065. Available at: https://doi.org/10.3390/cells9092065.

Bartels, T. *et al.* (2010) 'The N-Terminus of the Intrinsically Disordered Protein α-Synuclein Triggers Membrane Binding and Helix Folding', *Biophysical Journal*, 99(7), pp. 2116–2124. Available at: https://doi.org/10.1016/j.bpj.2010.06.035.

Bartels, T., Choi, J.G. and Selkoe, D.J. (2011) 'α-Synuclein occurs physiologically as a helically folded tetramer that resists aggregation', *Nature*, 477(7362), pp. 107–110. Available at: https://doi.org/10.1038/nature10324.

Baud, A. *et al.* (2019) 'An Optimized Method for the Proteomic Analysis of Low Volumes of Cell Culture Media and the Secretome: The Application and the Demonstration of Altered Protein Expression in iPSC-Derived Neuronal Cell Lines from Parkinson's Disease Patients', *Journal of Proteome Research*, 18(3), pp. 1198–1207. Available at: https://doi.org/10.1021/acs.jproteome.8b00831.

Beccano-Kelly, D.A. *et al.* (2023) 'Calcium dysregulation combined with mitochondrial failure and electrophysiological maturity converge in Parkinson's iPSC-dopamine neurons', *iScience*, 26(7), p. 107044. Available at: https://doi.org/10.1016/j.isci.2023.107044.

Bell, R. *et al.* (2022) 'N-Terminal Acetylation of α-Synuclein Slows down Its Aggregation Process and Alters the Morphology of the Resulting Aggregates', *Biochemistry*, 61(17), pp. 1743–1756. Available at: https://doi.org/10.1021/acs.biochem.2c00104.

Bengoa-Vergniory, N. *et al.* (2020) 'CLR01 protects dopaminergic neurons in vitro and in mouse models of Parkinson's disease', *Nature Communications*, 11(1), p. 4885. Available at: https://doi.org/10.1038/s41467-020-18689-x.

Bentley-DeSousa, A., Clegg, D. and Ferguson, S.M. (2025) 'LRRK2, lysosome damage, and Parkinson's disease', *Current Opinion in Cell Biology*, 93, p. 102482. Available at: https://doi.org/10.1016/j.ceb.2025.102482.

Berninger, B. *et al.* (2007) 'Functional Properties of Neurons Derived from In Vitro Reprogrammed Postnatal Astroglia', *Journal of Neuroscience*, 27(32), pp. 8654–8664. Available at: https://doi.org/10.1523/JNEUROSCI.1615-07.2007.

Bettinger, J.Q. *et al.* (2019) 'Quantitative Analysis of in Vivo Methionine Oxidation of the Human Proteome', *Journal of Proteome Research* [Preprint]. Available at: https://doi.org/10.1021/acs.jproteome.9b00505.

Beyer, K. *et al.* (2008) 'Differential expression of alpha-synuclein, parkin, and synphilin-1 isoforms in Lewy body disease', *neurogenetics*, 9(3), pp. 163–172. Available at: https://doi.org/10.1007/s10048-008-0124-6.

Beyer, K. and Ariza, A. (2013) 'Alpha-Synuclein Posttranslational Modification and Alternative Splicing as a Trigger for Neurodegeneration', *Molecular Neurobiology*, 47(2), pp. 509–524. Available at: https://doi.org/10.1007/s12035-012-8330-5.

Bhattacharjee, P. *et al.* (2019) 'Mass Spectrometric Analysis of Lewy Body-Enriched α-Synuclein in Parkinson's Disease', *Journal of Proteome Research*, 18(5), pp. 2109–2120. Available at: https://doi.org/10.1021/acs.jproteome.8b00982.

Bhattacharya, S. *et al.* (2024) 'Conformational Selection of α-Synuclein Tetramers at Biological Interfaces', *Journal of Chemical Information and Modeling*, 64(20), pp. 8010–8023. Available at: https://doi.org/10.1021/acs.jcim.4c01459.

Binolfi, A. *et al.* (2016) 'Intracellular repair of oxidation-damaged α-synuclein fails to target C-terminal modification sites', *Nature Communications*, 7(1), p. 10251. Available at: https://doi.org/10.1038/ncomms10251.

Binolfi, A., Theillet, F.-X. and Selenko, P. (2012) 'Bacterial in-cell NMR of human α-synuclein: a disordered monomer by nature?', *Biochemical Society Transactions*, 40(5), pp. 950–954. Available at: https://doi.org/10.1042/BST20120096.

Bisaglia, M. *et al.* (2014) 'Are dopamine derivatives implicated in the pathogenesis of Parkinson's disease?', *Ageing Research Reviews*, 13, pp. 107–114. Available at: https://doi.org/10.1016/j.arr.2013.12.009.

Blauwendraat, C., Nalls, M.A. and Singleton, A.B. (2020) 'The genetic architecture of Parkinson's disease', *The Lancet Neurology*, 19(2), pp. 170–178. Available at: https://doi.org/10.1016/S1474-4422(19)30287-X.

Bloem, B.R., Okun, M.S. and Klein, C. (2021) 'Parkinson's disease', *The Lancet*, 397(10291), pp. 2284–2303. Available at: https://doi.org/10.1016/S0140-6736(21)00218-X.

Bono, K. *et al.* (2020) 'Endosomal dysfunction in iPSC-derived neural cells from Parkinson's disease patients with VPS35 D620N', *Molecular Brain*, 13(1), pp. 1–15. Available at: https://doi.org/10.1186/s13041-020-00675-5.

Borghammer, P. *et al.* (2021) 'Neuropathological evidence of body-first vs. brain-first Lewy body disease', *Neurobiology of Disease*, 161, p. 105557. Available at: https://doi.org/10.1016/j.nbd.2021.105557.

Bougea, A. (2024) 'Seeding Aggregation Assays in Lewy Bodies Disorders: A Narrative State-of-the-Art Review', *International Journal of Molecular Sciences*, 25(19), p. 10783. Available at: https://doi.org/10.3390/ijms251910783.

Braak, H. *et al.* (2003) 'Staging of brain pathology related to sporadic Parkinson's disease', *Neurobiology of Aging*, 24(2), pp. 197–211. Available at: https://doi.org/10.1016/S0197-4580(02)00065-9.

Brahic, M. *et al.* (2016) 'Axonal transport and secretion of fibrillar forms of α-synuclein, Aβ42 peptide and HTTExon 1', *Acta Neuropathologica*, 131(4), pp. 539–548. Available at: https://doi.org/10.1007/s00401-016-1538-0.

Brahmachari, S. *et al.* (2016) 'Activation of tyrosine kinase c-Abl contributes to α-synuclein–induced neurodegeneration', *Journal of Clinical Investigation*, 126(8), pp. 2970–2988. Available at: https://doi.org/10.1172/JCI85456.

Bräuer, S. *et al.* (2023) 'Kinetic parameters of alpha-synuclein seed amplification assay correlate with cognitive impairment in patients with Lewy body disorders', *Acta Neuropathologica Communications*, 11(1), p. 162. Available at: https://doi.org/10.1186/s40478-023-01653-3.

Bravo-Cordero, J.J. *et al.* (2007) 'MT1-MMP proinvasive activity is regulated by a novel Rab8-dependent exocytic pathway', *The EMBO Journal*, 26(6), pp. 1499–1510. Available at: https://doi.org/10.1038/sj.emboj.7601606.

Brazdis, R.-M. *et al.* (2020) 'Demonstration of brain region-specific neuronal vulnerability in human iPSC-based model of familial Parkinson's disease', *Human Molecular Genetics*, 29(7), pp. 1180–1191. Available at: https://doi.org/10.1093/hmg/ddaa039.

Bressan, E. *et al.* (2023) 'The Foundational Data Initiative for Parkinson Disease: Enabling efficient translation from genetic maps to mechanism', *Cell Genomics*, 3(3), p. 100261. Available at: https://doi.org/10.1016/j.xgen.2023.100261.

Brewer, K.D. *et al.* (2015) 'Dynamic binding mode of a Synaptotagmin-1–SNARE complex in solution', *Nature Structural & Molecular Biology*, 22(7), pp. 555–564. Available at: https://doi.org/10.1038/nsmb.3035.

Brochner, B.V. *et al.* (2025) 'Single-vesicle Tracking of α-Synuclein Oligomers Reveals Pore Formation by a Three-Stage Model', *ACS Nano*, 19(36), pp. 32108–32122. Available at: https://doi.org/10.1021/acsnano.5c04005.

Brockmann, K. *et al.* (2024) 'CSF α-synuclein seed amplification kinetic profiles are associated with cognitive decline in Parkinson's disease', *npj Parkinson's Disease*, 10(1), p. 24. Available at: https://doi.org/10.1038/s41531-023-00627-5.

Bsoul, R. *et al.* (2025) 'Accurate detection of pathologic α-synuclein in CSF, skin, olfactory mucosa, and urine with a uniform seeding amplification assay', *Acta Neuropathologica Communications*, 13(1), p. 113. Available at: https://doi.org/10.1186/s40478-025-02034-8.

Buell, A.K. *et al.* (2014) 'Solution conditions determine the relative importance of nucleation and growth processes in α-synuclein aggregation', *Proceedings of the National Academy of Sciences*, 111(21), pp. 7671–7676. Available at: https://doi.org/10.1073/pnas.1315346111.

Burai, R. *et al.* (2015) 'Elucidating the Role of Site-Specific Nitration of α-Synuclein in the Pathogenesis of Parkinson's Disease via Protein Semisynthesis and Mutagenesis', *Journal of the American Chemical Society*, 137(15), pp. 5041–5052. Available at: https://doi.org/10.1021/ja5131726.

Buratta, S. *et al.* (2020) 'Lysosomal Exocytosis, Exosome Release and Secretory Autophagy: The Autophagic- and Endo-Lysosomal Systems Go Extracellular', *International Journal of Molecular Sciences*, 21(7), p. 2576. Available at: https://doi.org/10.3390/ijms21072576.

Burbulla, L.F. *et al.* (2017) 'Dopamine oxidation mediates mitochondrial and lysosomal dysfunction in Parkinson's disease', *Science* [Preprint]. Available at: https://doi.org/10.1126/science.aam9080.

Burbulla, L.F. *et al.* (2019) 'A modulator of wild-type glucocerebrosidase improves pathogenic phenotypes in dopaminergic neuronal models of Parkinson's disease', *Science Translational Medicine* [Preprint]. Available at: https://doi.org/10.1126/scitranslmed.aau6870.

Burré, J. *et al.* (2010) 'α-Synuclein Promotes SNARE-Complex Assembly in Vivo and in Vitro', *Science* [Preprint]. Available at: https://doi.org/10.1126/science.1195227.

Burré, J. *et al.* (2013) 'Properties of native brain α-synuclein', *Nature*, 498(7453), pp. E4–E6. Available at: https://doi.org/10.1038/nature12125.

Busch, D.J. *et al.* (2014) 'Acute increase of α-synuclein inhibits synaptic vesicle recycling evoked during intense stimulation', *Molecular Biology of the Cell*. Edited by S. Lemmon, 25(24), pp. 3926–3941. Available at: https://doi.org/10.1091/mbc.e14-02-0708.

Bussell, R. and Eliezer, D. (2003) 'A Structural and Functional Role for 11-mer Repeats in α-Synuclein and Other Exchangeable Lipid Binding Proteins', *Journal of Molecular Biology*, 329(4), pp. 763–778. Available at: https://doi.org/10.1016/S0022-2836(03)00520-5.

Calabresi, P. *et al.* (2023) 'Advances in understanding the function of alpha-synuclein: implications for Parkinson's disease', *Brain*, 146(9), pp. 3587–3597. Available at: https://doi.org/10.1093/brain/awad150.

Carling, P.J. *et al.* (2020) 'Deep phenotyping of peripheral tissue facilitates mechanistic disease stratification in sporadic Parkinson's disease', *Progress in Neurobiology*, 187, p. 101772. Available at: https://doi.org/10.1016/j.pneurobio.2020.101772.

Carling, P.J. *et al.* (2022) 'Multiparameter phenotypic screening for endogenous TFEB and TFE3 translocation identifies novel chemical series modulating lysosome function', *Autophagy* [Preprint]. Available at: https://www.tandfonline.com/doi/abs/10.1080/15548627.2022.2095834 (Accessed: 13 August 2022).

Carmo-Gonçalves, P. *et al.* (2018) 'Exploring the role of methionine residues on the oligomerization and neurotoxic properties of DOPAL-modified α-synuclein', *Biochemical and Biophysical Research Communications*, 505(1), pp. 295–301. Available at: https://doi.org/10.1016/j.bbrc.2018.09.111.

Cavalcante, G.C. and Soares-Souza, G.B. (2025) 'Downregulation of the Ca2+ sensor Synaptotagmin-1 (SYT1) in Parkinson's Disease: Insights from Gene Expression Profiling'. bioRxiv, p. 2025.09.12.675906. Available at: https://doi.org/10.1101/2025.09.12.675906.

Cerri, S. *et al.* (2021) 'GBA Mutations Influence the Release and Pathological Effects of Small Extracellular Vesicles from Fibroblasts of Patients with Parkinson's Disease', *International Journal of Molecular Sciences*, 22(4), p. 2215. Available at: https://doi.org/10.3390/ijms22042215.

Chakraborty, R. *et al.* (2023) 'Tunnelling nanotubes between neuronal and microglial cells allow bi-directional transfer of α-Synuclein and mitochondria', *Cell Death & Disease*, 14(5), p. 329. Available at: https://doi.org/10.1038/s41419-023-05835-8.

Chambers, S.M. *et al.* (2009) 'Highly efficient neural conversion of human ES and iPS cells by dual inhibition of SMAD signaling', *Nature Biotechnology*, 27(3), pp. 275–280. Available at: https://doi.org/10.1038/nbt.1529.

Chan, C.S., Gertler, T.S. and Surmeier, D.J. (2010) 'A molecular basis for the increased vulnerability of substantia nigra dopamine neurons in aging and Parkinson's disease', *Movement Disorders*, 25(S1), pp. S63–S70. Available at: https://doi.org/10.1002/mds.22801.

Chappard, A. *et al.* (2023) 'Single-Molecule Two-Color Coincidence Detection of Unlabeled alpha-Synuclein Aggregates', *Angewandte Chemie International Edition*, 62(15), p. e202216771. Available at: https://doi.org/10.1002/anie.202216771.

Chartier-Harlin, M.-C. *et al.* (2004) 'α-synuclein locus duplication as a cause of familial Parkinson's disease', *The Lancet*, 364(9440), pp. 1167–1169. Available at: https://doi.org/10.1016/S0140-6736(04)17103-1.

Chavarría, C. *et al.* (2024) 'Revisiting the role of 3-nitrotyrosine residues in the formation of alpha-synuclein oligomers and fibrils', *Archives of Biochemistry and Biophysics*, 752, p. 109858. Available at: https://doi.org/10.1016/j.abb.2023.109858.

Chen, K. *et al.* (2022) 'LRP1 is a neuronal receptor for α-synuclein uptake and spread', *Molecular Neurodegeneration*, 17(1), p. 57. Available at: https://doi.org/10.1186/s13024-022-00560-w.

Chen, S.W. *et al.* (2015) 'Structural characterization of toxic oligomers that are kinetically trapped during α-synuclein fibril formation', *Proceedings of the National Academy of Sciences*, 112(16). Available at: https://doi.org/10.1073/pnas.1421204112.

Chen, V. *et al.* (2020) 'The mechanistic role of alpha-synuclein in the nucleus: impaired nuclear function caused by familial Parkinson's disease SNCA mutations', *Human Molecular Genetics*, 29(18), pp. 3107–3121. Available at: https://doi.org/10.1093/hmg/ddaa183.

Chen, Y. *et al.* (2019) 'Engineering synucleinopathy-resistant human dopaminergic neurons by CRISPR-mediated deletion of the SNCA gene', *European Journal of Neuroscience*, 49(4), pp. 510–524. Available at: https://doi.org/10.1111/ejn.14286.

Chen, Y. *et al.* (2022) 'Synaptotagmin-1 is a bidirectional Ca2+ sensor for neuronal endocytosis', *Proceedings of the National Academy of Sciences*, 119(20), p. e2111051119. Available at: https://doi.org/10.1073/pnas.2111051119.

Chieregatti, E. *et al.* (2004) 'SNAP-23 Functions in Docking/Fusion of Granules at Low Ca^{2+}', *Molecular Biology of the Cell*, 15(4), pp. 1918–1930. Available at: https://doi.org/10.1091/mbc.e03-09-0684.

Chiu, C.-C. *et al.* (2016) 'Increased Rab35 expression is a potential biomarker and implicated in the pathogenesis of Parkinson's disease', *Oncotarget*, 7(34), p. 54215. Available at: https://doi.org/10.18632/oncotarget.11090.

Choi, B.-K. *et al.* (2013) 'Large α-synuclein oligomers inhibit neuronal SNARE-mediated vesicle docking', *Proceedings of the National Academy of Sciences*, 110(10), pp. 4087–4092. Available at: https://doi.org/10.1073/pnas.1218424110.

Choi, M.L. *et al.* (2022) 'Pathological structural conversion of α-synuclein at the mitochondria induces neuronal toxicity', *Nature Neuroscience*, 25(9), pp. 1134–1148. Available at: https://doi.org/10.1038/s41593-022-01140-3.

Chu, Y. *et al.* (2019) 'Intrastriatal alpha-synuclein fibrils in monkeys: spreading, imaging and neuropathological changes', *Brain*, 142(11), pp. 3565–3579. Available at: https://doi.org/10.1093/brain/awz296.

Chung, S.Y. *et al.* (2016) 'Parkin and PINK1 Patient iPSC-Derived Midbrain Dopamine Neurons Exhibit Mitochondrial Dysfunction and α-Synuclein Accumulation', *Stem Cell Reports*, 7(4), pp. 664–677. Available at: https://doi.org/10.1016/j.stemcr.2016.08.012.

Chutna, O. *et al.* (2014) 'The small GTPase Rab11 co-localizes with α-synuclein in intracellular inclusions and modulates its aggregation, secretion and toxicity', *Human Molecular Genetics*, 23(25), pp. 6732–6745. Available at: https://doi.org/10.1093/hmg/ddu391.

Coelho-Cerqueira, E., de Araújo Correia Campos, C. and Follmer, C. (2019) 'Formation of large oligomers of DOPAL-modified α-synuclein is modulated by the oxidation of methionine residues located at C-terminal domain', *Biochemical and Biophysical Research Communications*, 509(2), pp. 367–372. Available at: https://doi.org/10.1016/j.bbrc.2018.12.128.

Colla, E. *et al.* (2012) 'Accumulation of Toxic α-Synuclein Oligomer within Endoplasmic Reticulum Occurs in α-Synucleinopathy In Vivo', *Journal of Neuroscience*, 32(10), pp. 3301–3305. Available at: https://doi.org/10.1523/JNEUROSCI.5368-11.2012.

Corenblum, M. *et al.* (2023) 'Parallel neurodegenerative phenotypes in sporadic Parkinson's disease fibroblasts and midbrain dopamine neurons', *Progress in Neurobiology*, 229, p. 102501. Available at: https://doi.org/10.1016/j.pneurobio.2023.102501.

Courte, J. *et al.* (2023) 'Synapses do not facilitate prion-like transfer of alpha-synuclein: a quantitative study in reconstructed unidirectional neural networks', *Cellular and Molecular Life Sciences*, 80(10), p. 284. Available at: https://doi.org/10.1007/s00018-023-04915-4.

Credle, J.J. *et al.* (2015) 'α-Synuclein-mediated inhibition of ATF6 processing into COPII vesicles disrupts UPR signaling in Parkinson's disease', *Neurobiology of Disease*, 76, pp. 112–125. Available at: https://doi.org/10.1016/j.nbd.2015.02.005.

Cremades, N. *et al.* (2012) 'Direct Observation of the Interconversion of Normal and Toxic Forms of α-Synuclein', *Cell*, 149(5), pp. 1048–1059. Available at: https://doi.org/10.1016/j.cell.2012.03.037.

Cuddy, L.K. *et al.* (2019) 'Stress-Induced Cellular Clearance Is Mediated by the SNARE Protein ykt6 and Disrupted by α-Synuclein', *Neuron*, 104(5), pp. 869-884.e11. Available at: https://doi.org/10.1016/j.neuron.2019.09.001.

Dada, S.T. *et al.* (2023) 'Spontaneous nucleation and fast aggregate-dependent proliferation of α-synuclein aggregates within liquid condensates at neutral pH', *Proceedings of the National Academy of Sciences*, 120(9), p. e2208792120. Available at: https://doi.org/10.1073/pnas.2208792120.

Danielson, S.R. *et al.* (2009) 'Preferentially Increased Nitration of α-Synuclein at Tyrosine-39 in a Cellular Oxidative Model of Parkinson's Disease', *Analytical Chemistry*, 81(18), pp. 7823–7828. Available at: https://doi.org/10.1021/ac901176t.

Danzer, K.M. *et al.* (2011) 'Heat-shock protein 70 modulates toxic extracellular α-synuclein oligomers and rescues trans-synaptic toxicity', *The FASEB Journal*, 25(1), pp. 326–336. Available at: https://doi.org/10.1096/fj.10-164624.

Danzer, K.M. *et al.* (2012) 'Exosomal cell-to-cell transmission of alpha synuclein oligomers', *Molecular Neurodegeneration*, 7(1), pp. 1–18. Available at: https://doi.org/10.1186/1750-1326-7-42.

De Boni, L. *et al.* (2022) 'Brain region-specific susceptibility of Lewy body pathology in synucleinopathies is governed by α-synuclein conformations', *Acta Neuropathologica*, 143(4), pp. 453–469. Available at: https://doi.org/10.1007/s00401-022-02406-7.

De Boni, L. *et al.* (2024) 'Aggregation-resistant alpha-synuclein tetramers are reduced in the blood of Parkinson's patients', *EMBO Molecular Medicine*, 16(7), pp. 1657–1674. Available at: https://doi.org/10.1038/s44321-024-00083-5.

Dearborn, A.D. *et al.* (2016) 'α-Synuclein Amyloid Fibrils with Two Entwined, Asymmetrically Associated Protofibrils', *Journal of Biological Chemistry*, 291(5), pp. 2310–2318. Available at: https://doi.org/10.1074/jbc.M115.698787.

Del Rey, N.L.-G. *et al.* (2024) 'Calbindin and Girk2/Aldh1a1 define resilient vs vulnerable dopaminergic neurons in a primate Parkinson's disease model', *npj Parkinson's Disease*, 10(1), p. 165. Available at: https://doi.org/10.1038/s41531-024-00777-0.

Delenclos, M. *et al.* (2017) 'Investigation of Endocytic Pathways for the Internalization of Exosome-Associated Oligomeric Alpha-Synuclein', *Frontiers in Neuroscience*, 11, p. 252923. Available at: https://doi.org/10.3389/fnins.2017.00172.

Delignat-Lavaud, B. *et al.* (2023) 'Synaptotagmin-1-dependent phasic axonal dopamine release is dispensable for basic motor behaviors in mice', *Nature Communications*, 14(1), p. 4120. Available at: https://doi.org/10.1038/s41467-023-39805-7.

Deng, J. *et al.* (2017) 'Neurons Export Extracellular Vesicles Enriched in Cysteine String Protein and Misfolded Protein Cargo', *Scientific Reports*, 7(1), pp. 1–12. Available at: https://doi.org/10.1038/s41598-017-01115-6.

Dettmer, U. *et al.* (2013) 'In Vivo Cross-linking Reveals Principally Oligomeric Forms of α-Synuclein and β-Synuclein in Neurons and Non-neural Cells', *Journal of Biological Chemistry*, 288(9), pp. 6371–6385. Available at: https://doi.org/10.1074/jbc.M112.403311.

Dettmer, U. *et al.* (2015) 'Parkinson-causing α-synuclein missense mutations shift native tetramers to monomers as a mechanism for disease initiation', *Nature Communications*, 6(1), pp. 1–16. Available at: https://doi.org/10.1038/ncomms8314.

Devine, M.J. *et al.* (2011) 'Parkinson's disease induced pluripotent stem cells with triplication of the α-synuclein locus', *Nature Communications*, 2(1), pp. 1–10. Available at: https://doi.org/10.1038/ncomms1453.

Dhanve, P. *et al.* (2023) 'Ambroxol: A potential therapeutics against neurodegeneration', *Health Sciences Review*, 7, p. 100096. Available at: https://doi.org/10.1016/j.hsr.2023.100096.

Diao, J. *et al.* (2013) 'Native α-synuclein induces clustering of synaptic-vesicle mimics via binding to phospholipids and synaptobrevin-2/VAMP2', *eLife*, 2, p. e00592. Available at: https://doi.org/10.7554/eLife.00592.

Dikiy, I. *et al.* (2016) 'Semisynthetic and in Vitro Phosphorylation of Alpha-Synuclein at Y39 Promotes Functional Partly Helical Membrane-Bound States Resembling Those Induced by PD Mutations', *ACS Chemical Biology*, 11(9), pp. 2428–2437. Available at: https://doi.org/10.1021/acschembio.6b00539.

Dilsizoglu Senol, A. *et al.* (2019) 'Effect of tolytoxin on tunneling nanotube formation and function', *Scientific Reports*, 9(1), pp. 1–15. Available at: https://doi.org/10.1038/s41598-019-42161-6.

Dimos, J.T. *et al.* (2008) 'Induced Pluripotent Stem Cells Generated from Patients with ALS Can Be Differentiated into Motor Neurons', *Science*, 321(5893), pp. 1218–1221. Available at: https://doi.org/10.1126/science.1158799.

Dingjan, I. *et al.* (2018) 'Endosomal and Phagosomal SNAREs', *Physiological Reviews* [Preprint]. Available at: https://doi.org/10.1152/physrev.00037.2017.

Diril, M.K. *et al.* (2006) 'Stonin 2 Is an AP-2-Dependent Endocytic Sorting Adaptor for Synaptotagmin Internalization and Recycling', *Developmental Cell*, 10(2), pp. 233–244. Available at: https://doi.org/10.1016/j.devcel.2005.12.011.

Do, Q.B. *et al.* (2024) 'Early deficits in an in vitro striatal microcircuit model carrying the Parkinson's GBA-N370S mutation', *NPJ Parkinson's Disease*, 10, p. 82. Available at: https://doi.org/10.1038/s41531-024-00694-2.

Dong, C. *et al.* (2018) 'Structural characteristics and membrane interactions of tandem α-synuclein oligomers', *Scientific Reports*, 8(1), p. 6755. Available at: https://doi.org/10.1038/s41598-018-25133-0.

Dorsey, E.R. and Bloem, B.R. (2024) 'Parkinson's Disease Is Predominantly an Environmental Disease', *Journal of Parkinson's Disease*, 14(3), p. 451. Available at: https://doi.org/10.3233/JPD-230357.

Doyle, L. and Wang, M. (2019) 'Overview of Extracellular Vesicles, Their Origin, Composition, Purpose, and Methods for Exosome Isolation and Analysis', *Cells*, 8(7), p. 727. Available at: https://doi.org/10.3390/cells8070727.

Drobny, A. *et al.* (2023) 'Reciprocal effects of alpha-synuclein aggregation and lysosomal homeostasis in synucleinopathy models', *Translational Neurodegeneration*, 12(1), pp. 1–21. Available at: https://doi.org/10.1186/s40035-023-00363-z.

Dunn, S.D. (1986) 'Effects of the modification of transfer buffer composition and the renaturation of proteins in gels on the recognition of proteins on western blots by monoclonal antibodies', *Analytical Biochemistry*, 157(1), pp. 144–153. Available at: https://doi.org/10.1016/0003-2697(86)90207-1.

Dupont, N. *et al.* (2011) 'Autophagy-based unconventional secretory pathway for extracellular delivery of IL-1β', *The EMBO journal*, 30(23), pp. 4701–4711. Available at: https://doi.org/10.1038/emboj.2011.398.

Dusonchet, J. *et al.* (2011) 'A Rat Model of Progressive Nigral Neurodegeneration Induced by the Parkinson's Disease-Associated G2019S Mutation in LRRK2', *The Journal of Neuroscience*, 31(3), p. 907. Available at: https://doi.org/10.1523/JNEUROSCI.5092-10.2011.

Dutta, S. *et al.* (2023) 'Development of a Novel Electrochemiluminescence ELISA for Quantification of α-Synuclein Phosphorylated at Ser^{129} in Biological Samples', *ACS Chemical Neuroscience*, 14(7), pp. 1238–1248. Available at: https://doi.org/10.1021/acschemneuro.2c00676.

Eijsvogel, P. *et al.* (2024) 'Target engagement and immunogenicity of an active immunotherapeutic targeting pathological α-synuclein: a phase 1 placebo-controlled trial', *Nature Medicine*, 30(9), pp. 2631–2640. Available at: https://doi.org/10.1038/s41591-024-03101-8.

Ejlerskov, P. *et al.* (2013) 'Tubulin Polymerization-promoting Protein (TPPP/p25α) Promotes Unconventional Secretion of α-Synuclein through Exophagy by Impairing Autophagosome-Lysosome Fusion *', *Journal of Biological Chemistry*, 288(24), pp. 17313–17335. Available at: https://doi.org/10.1074/jbc.M112.401174.

Emin, D. *et al.* (2022) 'Small soluble α-synuclein aggregates are the toxic species in Parkinson's disease', *Nature Communications*, 13(1), p. 5512. Available at: https://doi.org/10.1038/s41467-022-33252-6.

Emmanouilidou, E. *et al.* (2010) 'Cell-Produced α-Synuclein Is Secreted in a Calcium-Dependent Manner by Exosomes and Impacts Neuronal Survival', *The Journal of Neuroscience*, 30(20), p. 6838. Available at: https://doi.org/10.1523/JNEUROSCI.5699-09.2010.

Eslamboli, A. *et al.* (2007) 'Long-term consequences of human alpha-synuclein overexpression in the primate ventral midbrain', *Brain*, 130(3), pp. 799–815. Available at: https://doi.org/10.1093/brain/awl382.

Evans, J.R. *et al.* (2024) 'The diversity of SNCA transcripts in neurons, and its impact on antisense oligonucleotide therapeutics', *bioRxiv*, p. 2024.05.30.596437. Available at: https://doi.org/10.1101/2024.05.30.596437.

Fairfoul, G. *et al.* (2016) 'Alpha-synuclein RT-QuIC in the CSF of patients with alpha-synucleinopathies', *Annals of Clinical and Translational Neurology*, 3(10), pp. 812–818. Available at: https://doi.org/10.1002/acn3.338.

Fares, M.-B. *et al.* (2014) 'The novel Parkinson's disease linked mutation G51D attenuates in vitro aggregation and membrane binding of -synuclein, and enhances its secretion and nuclear localization in cells', *Human Molecular Genetics*, 23(17), pp. 4491–4509. Available at: https://doi.org/10.1093/hmg/ddu165.

Fauvet, B. *et al.* (2012) 'α-Synuclein in Central Nervous System and from Erythrocytes, Mammalian Cells, and Escherichia coli Exists Predominantly as Disordered Monomer *', *Journal of Biological Chemistry*, 287(19), pp. 15345–15364. Available at: https://doi.org/10.1074/jbc.M111.318949.

Fellner, L. *et al.* (2021) 'Autophagy in α-Synucleinopathies—An Overstrained System', *Cells*, 10(11), p. 3143. Available at: https://doi.org/10.3390/cells10113143.

Fernandes Gomes, B. *et al.* (2023) 'α-Synuclein seed amplification assay as a diagnostic tool for parkinsonian disorders', *Parkinsonism & Related Disorders*, 117, p. 105807. Available at: https://doi.org/10.1016/j.parkreldis.2023.105807.

Fernandes, H.J.R. *et al.* (2016) 'ER Stress and Autophagic Perturbations Lead to Elevated Extracellular α-Synuclein in GBA-N370S Parkinson's iPSC-Derived Dopamine Neurons', *Stem Cell Reports*, 6(3), pp. 342–356. Available at: https://doi.org/10.1016/j.stemcr.2016.01.013.

Fernández-Chacón, R. *et al.* (2001) 'Synaptotagmin I functions as a calcium regulator of release probability', *Nature*, 410(6824), pp. 41–49. Available at: https://doi.org/10.1038/35065004.

Fernández-Chacón, R. *et al.* (2004) 'The Synaptic Vesicle Protein CSPα Prevents Presynaptic Degeneration', *Neuron*, 42(2), pp. 237–251. Available at: https://doi.org/10.1016/S0896-6273(04)00190-4.

Fernandopulle, M.S. *et al.* (2018) 'Transcription-factor mediated differentiation of human iPSCs into neurons', *Current protocols in cell biology*, 79(1), p. e51. Available at: https://doi.org/10.1002/cpcb.51.

Fertan, E. *et al.* (2024) 'Cerebral organoids with chromosome 21 trisomy secrete Alzheimer's disease-related soluble aggregates detectable by single-molecule-fluorescence and super-resolution microscopy', *Molecular Psychiatry*, 29(2), pp. 369–386. Available at: https://doi.org/10.1038/s41380-023-02333-3.

Fertan, E. *et al.* (2025) 'Super-resolution microscopy of nanoscopic alpha-synuclein aggregates in brain samples indicates a subset of cells have disrupted protein homeostasis prior to Lewy body formation in Parkinson's disease'. Neuroscience. Available at: https://doi.org/10.1101/2025.09.16.676632.

Fiorenzano, A. *et al.* (2021) 'Single-cell transcriptomics captures features of human midbrain development and dopamine neuron diversity in brain organoids', *Nature Communications*, 12(1), p. 7302. Available at: https://doi.org/10.1038/s41467-021-27464-5.

Flagmeier, P. *et al.* (2016) 'Mutations associated with familial Parkinson's disease alter the initiation and amplification steps of α-synuclein aggregation', *Proceedings of the National Academy of Sciences*, 113(37), pp. 10328–10333. Available at: https://doi.org/10.1073/pnas.1604645113.

Foley, E.D.B. *et al.* (2021) 'Mass photometry enables label-free tracking and mass measurement of single proteins on lipid bilayers', *Nature Methods*, 18(10), pp. 1247–1252. Available at: https://doi.org/10.1038/s41592-021-01261-w.

Fontaine, S.N. *et al.* (2016) 'DnaJ/Hsc70 chaperone complexes control the extracellular release of neurodegenerative-associated proteins', *The EMBO Journal*, 35(14), pp. 1537–1549. Available at: https://doi.org/10.15252/embj.201593489.

Førland, M.G. *et al.* (2020) 'The value of cerebrospinal fluid α-synuclein and the tau/α-synuclein ratio for diagnosis of neurodegenerative disorders with Lewy pathology', *European Journal of Neurology*, 27(1), pp. 43–50. Available at: https://doi.org/10.1111/ene.14032.

Fox, M.A. and Umemori, H. (2006) 'Seeking long-term relationship: axon and target communicate to organize synaptic differentiation', *Journal of Neurochemistry*, 97(5), pp. 1215–1231. Available at: https://doi.org/10.1111/j.1471-4159.2006.03834.x.

Frank-Cannon, T.C. *et al.* (2008) 'Parkin Deficiency Increases Vulnerability to Inflammation-Related Nigral Degeneration', *The Journal of Neuroscience*, 28(43), pp. 10825–10834. Available at: https://doi.org/10.1523/JNEUROSCI.3001-08.2008.

Franks, S.N.J., Heon-Roberts, R. and Ryan, B.J. (2024) 'CRISPRi: a way to integrate iPSC-derived neuronal models', *Biochemical Society Transactions*, 52(2), pp. 539–551. Available at: https://doi.org/10.1042/BST20230190.

Freund, T.F., Powell, J.F. and Smith, A.D. (1984) 'Tyrosine hydroxylase-immunoreactive boutons in synaptic contact with identified striatonigral neurons, with particular reference to dendritic spines', *Neuroscience*, 13(4), pp. 1189–1215. Available at: https://doi.org/10.1016/0306-4522(84)90294-X.

Fukuda, M. (2013) 'The Role of Synaptotagmin and Synaptotagmin-Like Protein (Slp) in Regulated Exocytosis', in *Madame Curie Bioscience Database [Internet]*. Landes Bioscience. Available at: https://www.ncbi.nlm.nih.gov/books/NBK6281/ (Accessed: 10 November 2025).

Fusco, G. *et al.* (2014) 'Direct observation of the three regions in α-synuclein that determine its membrane-bound behaviour', *Nature Communications*, 5(1), p. 3827. Available at: https://doi.org/10.1038/ncomms4827.

Fussi, N. *et al.* (2018) 'Exosomal secretion of α-synuclein as protective mechanism after upstream blockage of macroautophagy', *Cell Death & Disease*, 9(7). Available at: https://doi.org/10.1038/s41419-018-0816-2.

Gadhavi, J. *et al.* (2025) 'Carbamylation Promotes Sequence-Specific Amyloidogenesis in the α-Synuclein KTKEGV Repeat Motifs', *ACS Chemical Neuroscience*, 16(19), pp. 3861–3872. Available at: https://doi.org/10.1021/acschemneuro.5c00561.

Galichet, C., Guillemot, F. and Parras, C.M. (2008) 'Neurogenin 2 has an essential role in development of the dentate gyrus', *Development*, 135(11), pp. 2031–2041. Available at: https://doi.org/10.1242/dev.015115.

Gámez-Valero, A. and Beyer, K. (2018) 'Alternative Splicing of Alpha- and Beta-Synuclein Genes Plays Differential Roles in Synucleinopathies', *Genes*, 9(2), p. 63. Available at: https://doi.org/10.3390/genes9020063.

Georgiou, N. *et al.* (2023) 'Quercetin: A Potential Polydynamic Drug', *Molecules*, 28(24), p. 8141. Available at: https://doi.org/10.3390/molecules28248141.

Ghanem, S.S. *et al.* (2022) 'α-Synuclein phosphorylation at serine 129 occurs after initial protein deposition and inhibits seeded fibril formation and toxicity', *Proceedings of the National Academy of Sciences*, 119(15), p. e2109617119. Available at: https://doi.org/10.1073/pnas.2109617119.

Ghosh, D. *et al.* (2014) 'The Newly Discovered Parkinson's Disease Associated Finnish Mutation (A53E) Attenuates α-Synuclein Aggregation and Membrane Binding', *Biochemistry*, 53(41), pp. 6419–6421. Available at: https://doi.org/10.1021/bi5010365.

Giasson, B.I. *et al.* (2000) 'Oxidative Damage Linked to Neurodegeneration by Selective α-Synuclein Nitration in Synucleinopathy Lesions', *Science*, 290(5493), pp. 985–989. Available at: https://doi.org/10.1126/science.290.5493.985.

Giasson, B.I. *et al.* (2001) 'A Hydrophobic Stretch of 12 Amino Acid Residues in the Middle of α-Synuclein Is Essential for Filament Assembly', *Journal of Biological Chemistry*, 276(4), pp. 2380–2386. Available at: https://doi.org/10.1074/jbc.M008919200.

Gilbert, L.A. *et al.* (2013) 'CRISPR-Mediated Modular RNA-Guided Regulation of Transcription in Eukaryotes', *Cell*, 154(2), pp. 442–451. Available at: https://doi.org/10.1016/j.cell.2013.06.044.

Glaser, C.B. *et al.* (2005) 'Methionine oxidation, α-synuclein and Parkinson's disease', *Biochimica et Biophysica Acta (BBA) - Proteins and Proteomics*, 1703(2), pp. 157–169. Available at: https://doi.org/10.1016/j.bbapap.2004.10.008.

Gonçalves, S.A. *et al.* (2016) 'shRNA-Based Screen Identifies Endocytic Recycling Pathway Components That Act as Genetic Modifiers of Alpha-Synuclein Aggregation, Secretion and Toxicity', *PLOS Genetics*, 12(4), p. e1005995. Available at: https://doi.org/10.1371/journal.pgen.1005995.

Gorisse, L. *et al.* (2016) 'Protein carbamylation is a hallmark of aging', *Proceedings of the National Academy of Sciences*, 113(5), pp. 1191–1196. Available at: https://doi.org/10.1073/pnas.1517096113.

Gould, N. *et al.* (2014) 'Evidence of Native α-Synuclein Conformers in the Human Brain', *Journal of Biological Chemistry*, 289(11), pp. 7929–7934. Available at: https://doi.org/10.1074/jbc.C113.538249.

Greenbaum, E.A. *et al.* (2005) 'The E46K Mutation in α-Synuclein Increases Amyloid Fibril Formation', *Journal of Biological Chemistry*, 280(9), pp. 7800–7807. Available at: https://doi.org/10.1074/jbc.M411638200.

Greten-Harrison, B. *et al.* (2010) 'αβγ-Synuclein triple knockout mice reveal age-dependent neuronal dysfunction', *Proceedings of the National Academy of Sciences*, 107(45), pp. 19573–19578. Available at: https://doi.org/10.1073/pnas.1005005107.

Grey, M. *et al.* (2015) 'Acceleration of α-Synuclein Aggregation by Exosomes *', *Journal of Biological Chemistry*, 290(5), pp. 2969–2982. Available at: https://doi.org/10.1074/jbc.M114.585703.

Grossauer, A. *et al.* (2023) 'α-Synuclein Seed Amplification Assays in the Diagnosis of Synucleinopathies Using Cerebrospinal Fluid—A Systematic Review and Meta-Analysis', *Movement Disorders Clinical Practice*, 10(5), pp. 737–747. Available at: https://doi.org/10.1002/mdc3.13710.

Grudina, C. *et al.* (2019) 'Human NPCs can degrade α–syn fibrils and transfer them preferentially in a cell contact-dependent manner possibly through TNT-like structures', *Neurobiology of Disease*, 132, p. 104609. Available at: https://doi.org/10.1016/j.nbd.2019.104609.

Guerrero-Ferreira, R. *et al.* (2018) *Cryo-EM structure of alpha-synuclein fibrils*, *eLife*. eLife Sciences Publications Limited. Available at: https://doi.org/10.7554/eLife.36402.

Guerrero-Ferreira, R. *et al.* (2019) 'Two new polymorphic structures of human full-length alpha-synuclein fibrils solved by cryo-electron microscopy', *eLife*, 8, p. e48907. Available at: https://doi.org/10.7554/eLife.48907.

Gustafsson, G. *et al.* (2018) 'Secretion and Uptake of α-Synuclein Via Extracellular Vesicles in Cultured Cells', *Cellular and Molecular Neurobiology*, 38(8), pp. 1539–1550. Available at: https://doi.org/10.1007/s10571-018-0622-5.

Guzman, J.N. *et al.* (2010) 'Oxidant stress evoked by pacemaking in dopaminergic neurons is attenuated by DJ-1', *Nature*, 468(7324), pp. 696–700. Available at: https://doi.org/10.1038/nature09536.

Harraz, M.M. *et al.* (2021) 'Cocaine-induced locomotor stimulation involves autophagic degradation of the dopamine transporter', *Molecular Psychiatry*, 26(2), pp. 370–382. Available at: https://doi.org/10.1038/s41380-020-00978-y.

Hartfield, E.M. *et al.* (2014) 'Physiological Characterisation of Human iPS-Derived Dopaminergic Neurons', *PLoS ONE*. Edited by P. Lewis, 9(2), p. e87388. Available at: https://doi.org/10.1371/journal.pone.0087388.

Hasan, S. *et al.* (2023) 'Multi-modal proteomic characterization of lysosomal function and proteostasis in progranulin-deficient neurons', *Molecular Neurodegeneration*, 18(1), p. 87. Available at: https://doi.org/10.1186/s13024-023-00673-w.

Hasegawa, T. *et al.* (2011) 'The AAA-ATPase VPS4 Regulates Extracellular Secretion and Lysosomal Targeting of α-Synuclein', *PLoS ONE*. Edited by W. Smith, 6(12), p. e29460. Available at: https://doi.org/10.1371/journal.pone.0029460.

Hasibeder, A. *et al.* (2015) 'Evaluation and Validation of the Detection of soluble Triggering Receptor Expressed on Myeloid Cells 1 by Enzyme-linked immunosorbent Assay', *Scientific Reports*, 5(1), p. 15381. Available at: https://doi.org/10.1038/srep15381.

Hass, E.W. *et al.* (2021) 'Disease-, region- and cell type specific diversity of α-synuclein carboxy terminal truncations in synucleinopathies', *Acta Neuropathologica Communications*, 9(1), p. 146. Available at: https://doi.org/10.1186/s40478-021-01242-2.

Hassanin, E. *et al.* (2025) 'Penetrance of Parkinson's disease in GBA1 carriers depends on variant severity and polygenic background', *npj Parkinson's Disease*, 11(1), p. 162. Available at: https://doi.org/10.1038/s41531-025-00997-y.

Hatano, T. *et al.* (2024) 'α-Synuclein: A Promising Biomarker for Parkinson's Disease and Related Disorders', *Journal of Movement Disorders*, 17(2), pp. 127–137. Available at: https://doi.org/10.14802/jmd.24075.

Haucke, V. *et al.* (2000) 'Dual interaction of synaptotagmin with μ2- and α-adaptin facilitates clathrin-coated pit nucleation', *The EMBO Journal*, 19(22), pp. 6011–6019. Available at: https://doi.org/10.1093/emboj/19.22.6011.

Hay, J.C. (2007) 'Calcium: a fundamental regulator of intracellular membrane fusion?', *EMBO reports*, 8(3), pp. 236–240. Available at: https://doi.org/10.1038/sj.embor.7400921.

Heinrich, C. *et al.* (2010) 'Directing Astroglia from the Cerebral Cortex into Subtype Specific Functional Neurons', *PLoS Biology*. Edited by R.D.G. McKay, 8(5), p. e1000373. Available at: https://doi.org/10.1371/journal.pbio.1000373.

Heinzel, S. *et al.* (2019) 'Update of the MDS research criteria for prodromal Parkinson's disease', *Movement Disorders*, 34(10), pp. 1464–1470. Available at: https://doi.org/10.1002/mds.27802.

Heman-Ackah, S.M. *et al.* (2017) 'Alpha-synuclein induces the unfolded protein response in Parkinson's disease SNCA triplication iPSC-derived neurons', *Human Molecular Genetics*, 26(22), pp. 4441–4450. Available at: https://doi.org/10.1093/hmg/ddx331.

Henry, L. and Sheff, D.R. (2008) 'Rab8 Regulates Basolateral Secretory, But Not Recycling, Traffic at the Recycling Endosome', *Molecular Biology of the Cell*, 19(5), pp. 2059–2068. Available at: https://doi.org/10.1091/mbc.e07-09-0902.

Hikima, T. *et al.* (2022) 'Synaptotagmins 1 and 7 Play Complementary Roles in Somatodendritic Dopamine Release', *Journal of Neuroscience*, 42(19), pp. 3919–3930. Available at: https://doi.org/10.1523/JNEUROSCI.2416-21.2022.

Hoffmann, A.-C. *et al.* (2019) 'Extracellular aggregated alpha synuclein primarily triggers lysosomal dysfunction in neural cells prevented by trehalose', *Scientific Reports*, 9(1), p. 544. Available at: https://doi.org/10.1038/s41598-018-35811-8.

Horlbeck, M.A. *et al.* (2016) 'Compact and highly active next-generation libraries for CRISPR-mediated gene repression and activation', *eLife*, 5, p. e19760. Available at: https://doi.org/10.7554/eLife.19760.

Horne, R.I. *et al.* (2023) 'Secondary Processes Dominate the Quiescent, Spontaneous Aggregation of α-Synuclein at Physiological pH with Sodium Salts', *ACS Chemical Neuroscience*, 14(17), pp. 3125–3131. Available at: https://doi.org/10.1021/acschemneuro.3c00282.

Hu, J. *et al.* (2024) 'Phosphorylation and O-GlcNAcylation at the same α-synuclein site generate distinct fibril structures', *Nature Communications*, 15(1), p. 2677. Available at: https://doi.org/10.1038/s41467-024-46898-1.

Huang, J. *et al.* (2024) 'Pathological α-synuclein detected by real-time quaking-induced conversion in synucleinopathies', *Experimental Gerontology*, 187, p. 112366. Available at: https://doi.org/10.1016/j.exger.2024.112366.

Huh, C.J. *et al.* (2016) *Maintenance of age in human neurons generated by microRNA-based neuronal conversion of fibroblasts*, *eLife*. eLife Sciences Publications Limited. Available at: https://doi.org/10.7554/eLife.18648.

Huh, Y.E. *et al.* (2023) 'GBA1 Variants and Parkinson's Disease: Paving the Way for Targeted Therapy', *Journal of Movement Disorders*, 16(3), pp. 261–278. Available at: https://doi.org/10.14802/jmd.23023.

Hulme, A.J. *et al.* (2020) 'Molecular and Functional Characterization of Neurogenin-2 Induced Human Sensory Neurons', *Frontiers in Cellular Neuroscience*, 14, p. 600895. Available at: https://doi.org/10.3389/fncel.2020.600895.

Hulme, A.J. *et al.* (2021) 'Making neurons, made easy: The use of Neurogenin-2 in neuronal differentiation', *Stem Cell Reports*, 17(1), pp. 14–34. Available at: https://doi.org/10.1016/j.stemcr.2021.11.015.

Hutchison, R.M. *et al.* (2024) 'Cinpanemab in Early Parkinson Disease', *Neurology*, 102(5), p. e209137. Available at: https://doi.org/10.1212/WNL.0000000000209137.

Iannielli, A. *et al.* (2022) 'Modeling native and seeded Synuclein aggregation and related cellular dysfunctions in dopaminergic neurons derived by a new set of isogenic iPSC lines with SNCA multiplications', *Cell Death & Disease*, 13(10), pp. 1–16. Available at: https://doi.org/10.1038/s41419-022-05330-6.

Ikeda, A. *et al.* (2019) 'Mutations in CHCHD2 cause α-synuclein aggregation', *Human Molecular Genetics*, 28(23), pp. 3895–3911. Available at: https://doi.org/10.1093/hmg/ddz241.

Ikeda, K. *et al.* (2019) 'Dopamine Transporter Imaging in Parkinson Disease: Progressive Changes and Therapeutic Modification after Anti-parkinsonian Medications', *Internal Medicine*, 58(12), pp. 1665–1672. Available at: https://doi.org/10.2169/internalmedicine.2489-18.

Ilijic, E., Guzman, J.N. and Surmeier, D.J. (2011) 'The L-type channel antagonist isradipine is neuroprotective in a mouse model of Parkinson's disease', *Neurobiology of Disease*, 43(2), pp. 364–371. Available at: https://doi.org/10.1016/j.nbd.2011.04.007.

Iljina, M. *et al.* (2016) 'Kinetic model of the aggregation of alpha-synuclein provides insights into prion-like spreading', *Proceedings of the National Academy of Sciences*, 113(9). Available at: https://doi.org/10.1073/pnas.1524128113.

Ingelsson, M. (2016) 'Alpha-Synuclein Oligomers—Neurotoxic Molecules in Parkinson's Disease and Other Lewy Body Disorders', *Frontiers in Neuroscience*, 10. Available at: https://doi.org/10.3389/fnins.2016.00408.

Inglis, K.J. *et al.* (2009) 'Polo-like Kinase 2 (PLK2) Phosphorylates α-Synuclein at Serine 129 in Central Nervous System', *Journal of Biological Chemistry*, 284(5), pp. 2598–2602. Available at: https://doi.org/10.1074/jbc.C800206200.

Inoue, S. *et al.* (2023) 'CRISPR-Cas9-Edited *SNCA* Knockout Human Induced Pluripotent Stem Cell-Derived Dopaminergic Neurons and Their Vulnerability to Neurotoxicity', *Biological and Pharmaceutical Bulletin*, 46(3), pp. 517–522. Available at: https://doi.org/10.1248/bpb.b22-00839.

Itahana, Y., Yeh, E.T.H. and Zhang, Y. (2006) 'Nucleocytoplasmic shuttling modulates activity and ubiquitination-dependent turnover of SUMO-specific protease 2', *Molecular and Cellular Biology*, 26(12), pp. 4675–4689. Available at: https://doi.org/10.1128/MCB.01830-05.

Itakura, E., Kishi-Itakura, C. and Mizushima, N. (2012) 'The Hairpin-type Tail-Anchored SNARE Syntaxin 17 Targets to Autophagosomes for Fusion with Endosomes/Lysosomes', *Cell*, 151(6), pp. 1256–1269. Available at: https://doi.org/10.1016/j.cell.2012.11.001.

Ivey, P.-M.E. *et al.* (2025) 'Mechanisms of Alpha-Synuclein-Seeded Aggregation in Neurons Revealed by Fluorescence Lifetime Imaging', *ACS Chemical Neuroscience*, 16(11), pp. 2128–2140. Available at: https://doi.org/10.1021/acschemneuro.5c00236.

Iwata, A. *et al.* (2003) 'Alpha-synuclein degradation by serine protease neurosin: implication for pathogenesis of synucleinopathies', *Human Molecular Genetics*, 12(20), pp. 2625–2635. Available at: https://doi.org/10.1093/hmg/ddg283.

Iyer, A. *et al.* (2017) 'C-Terminal Truncated α-Synuclein Fibrils Contain Strongly Twisted β-Sheets', *Journal of the American Chemical Society*, 139(43), pp. 15392–15400. Available at: https://doi.org/10.1021/jacs.7b07403.

Jacquemyn, J. *et al.* (2025) 'Glucosylceramide induced ectosomes propagate pathogenic α-synuclein in Parkinson's disease'. Available at: https://doi.org/10.1101/2025.02.14.638390.

Janeczek, P. *et al.* (2015) 'Differential expression of α-synuclein splice variants in the brain of alcohol misusers: Influence of genotype', *Drug and Alcohol Dependence*, 155, pp. 284–292. Available at: https://doi.org/10.1016/j.drugalcdep.2015.05.045.

Janezic, S. *et al.* (2013) 'Deficits in dopaminergic transmission precede neuron loss and dysfunction in a new Parkinson model', *Proceedings of the National Academy of Sciences*, 110(42). Available at: https://doi.org/10.1073/pnas.1309143110.

Jang, A. *et al.* (2010) 'Non-classical exocytosis of α-synuclein is sensitive to folding states and promoted under stress conditions', *Journal of Neurochemistry*, 113(5), pp. 1263–1274. Available at: https://doi.org/10.1111/j.1471-4159.2010.06695.x.

Jin, J. *et al.* (2017) 'Accelerating the clinical development of protein-based vaccines for malaria by efficient purification using a four amino acid C-terminal "C-tag"', *International Journal for Parasitology*, 47(7), pp. 435–446. Available at: https://doi.org/10.1016/j.ijpara.2016.12.001.

Jung, N. *et al.* (2007) 'Molecular basis of synaptic vesicle cargo recognition by the endocytic sorting adaptor stonin 2', *Journal of Cell Biology*, 179(7), pp. 1497–1510. Available at: https://doi.org/10.1083/jcb.200708107.

Jy, S. *et al.* (2001) 'Induction of neuronal cell death by Rab5A-dependent endocytosis of alpha-synuclein', *The Journal of biological chemistry*, 276(29). Available at: https://doi.org/10.1074/jbc.M101318200.

Kakuda, K. *et al.* (2024) 'Lysophagy protects against propagation of α-synuclein aggregation through ruptured lysosomal vesicles', *Proceedings of the National Academy of Sciences*, 121(1), p. e2312306120. Available at: https://doi.org/10.1073/pnas.2312306120.

Kamath, T. *et al.* (2022) 'Single-cell genomic profiling of human dopamine neurons identifies a population that selectively degenerates in Parkinson's disease', *Nature Neuroscience*, 25(5), pp. 588–595. Available at: https://doi.org/10.1038/s41593-022-01061-1.

Kang, J.-H. (2013) 'Association of Cerebrospinal Fluid β-Amyloid 1-42, T-tau, P-tau$_{181}$, and α-Synuclein Levels With Clinical Features of Drug-Naive Patients With Early Parkinson Disease', *JAMA Neurology* [Preprint]. Available at: https://doi.org/10.1001/jamaneurol.2013.3861.

Kang, L. *et al.* (2012) 'N-terminal acetylation of α-synuclein induces increased transient helical propensity and decreased aggregation rates in the intrinsically disordered monomer', *Protein Science*, 21(7), pp. 911–917. Available at: https://doi.org/10.1002/pro.2088.

Karampetsou, M. *et al.* (2020) 'Intrastriatal Administration of Exosome-Associated Pathological Alpha-Synuclein Is Not Sufficient by Itself to Cause Pathology Transmission', *Frontiers in Neuroscience*, 14, p. 246. Available at: https://doi.org/10.3389/fnins.2020.00246.

Katz, D.M. *et al.* (1983) 'Expression of catecholaminergic characteristics by primary sensory neurons in the normal adult rat in vivo.', *Proceedings of the National Academy of Sciences*, 80(11), pp. 3526–3530. Available at: https://doi.org/10.1073/pnas.80.11.3526.

Kaufmann, T.J. *et al.* (2016) 'Intracellular soluble α-synuclein oligomers reduce pyramidal cell excitability', *The Journal of Physiology*, 594(10), pp. 2751–2772. Available at: https://doi.org/10.1113/JP271968.

Kellie, J.F. *et al.* (2014) 'Quantitative Measurement of Intact Alpha-Synuclein Proteoforms from Post-Mortem Control and Parkinson's Disease Brain Tissue by Intact Protein Mass Spectrometry', *Scientific Reports*, 4(1), p. 5797. Available at: https://doi.org/10.1038/srep05797.

Kilfeather, P. *et al.* (2024) 'Single-cell spatial transcriptomic and translatomic profiling of dopaminergic neurons in health, aging, and disease', *Cell Reports*, 43(3), p. 113784. Available at: https://doi.org/10.1016/j.celrep.2024.113784.

Killinger, B.A. *et al.* (2018) 'The vermiform appendix impacts the risk of developing Parkinson's disease', *Science Translational Medicine*, 10(465), p. eaar5280. Available at: https://doi.org/10.1126/scitranslmed.aar5280.

Kim, M.S. *et al.* (2023) 'Advanced human iPSC-based preclinical model for Parkinson's disease with optogenetic alpha-synuclein aggregation', *Cell Stem Cell*, 30(7), pp. 973-986.e11. Available at: https://doi.org/10.1016/j.stem.2023.05.015.

Kim, S. *et al.* (2018) 'GBA1 deficiency negatively affects physiological α-synuclein tetramers and related multimers', *Proceedings of the National Academy of Sciences*, 115(4), pp. 798–803. Available at: https://doi.org/10.1073/pnas.1700465115.

Kim, T.Y. and Lee, B.D. (2025) 'Current therapeutic strategies in Parkinson's disease: Future perspectives', *Molecules and Cells*, 48(11), p. 100274. Available at: https://doi.org/10.1016/j.mocell.2025.100274.

Kirik, D. *et al.* (2002) 'Parkinson-Like Neurodegeneration Induced by Targeted Overexpression of α-Synuclein in the Nigrostriatal System', *Journal of Neuroscience*, 22(7), pp. 2780–2791. Available at: https://doi.org/10.1523/JNEUROSCI.22-07-02780.2002.

Klein, C. and Westenberger, A. (2012) 'Genetics of Parkinson's Disease', *Cold Spring Harbor Perspectives in Medicine*, 2(1), p. a008888. Available at: https://doi.org/10.1101/cshperspect.a008888.

Kleinknecht, A. *et al.* (2016) 'C-Terminal Tyrosine Residue Modifications Modulate the Protective Phosphorylation of Serine 129 of α-Synuclein in a Yeast Model of Parkinson's Disease', *PLOS Genetics*. Edited by B. Lu, 12(6), p. e1006098. Available at: https://doi.org/10.1371/journal.pgen.1006098.

Knott, G.J. and Doudna, J.A. (2018) 'CRISPR-Cas guides the future of genetic engineering', *Science (New York, N.Y.)*, 361(6405), p. 866. Available at: https://doi.org/10.1126/science.aat5011.

Komori, T. and Kuwahara, T. (2023) 'An Update on the Interplay between LRRK2, Rab GTPases and Parkinson's Disease', Biomolecules, 13(11), p. 1645. Available at: https://doi.org/10.3390/biom13111645.

Korczyn, A.D. and Hassin-Baer, S. (2015) 'Can the disease course in Parkinson's disease be slowed?', *BMC Medicine*, 13(1), pp. 295, s12916-015-0534–x. Available at: https://doi.org/10.1186/s12916-015-0534-x.

Kordower, J.H. *et al.* (2008) 'Lewy body–like pathology in long-term embryonic nigral transplants in Parkinson's disease', *Nature Medicine*, 14(5), pp. 504–506. Available at: https://doi.org/10.1038/nm1747.

Kors, S. *et al.* (2019) 'Regulation of Proteasome Activity by (Post-)transcriptional Mechanisms', *Frontiers in Molecular Biosciences*, 6, p. 48. Available at: https://doi.org/10.3389/fmolb.2019.00048.

Koukouraki, P. and Doxakis, E. (2016) 'Constitutive translation of human α-synuclein is mediated by the 5′-untranslated region', *Open Biology*, 6(4), p. 160022. Available at: https://doi.org/10.1098/rsob.160022.

Kouroupi, G. *et al.* (2017) 'Defective synaptic connectivity and axonal neuropathology in a human iPSC-based model of familial Parkinson's disease', *Proceedings of the National Academy of Sciences*, 114(18), pp. E3679–E3688. Available at: https://doi.org/10.1073/pnas.1617259114.

Kramer, M.L. and Schulz-Schaeffer, W.J. (2007) 'Presynaptic α-Synuclein Aggregates, Not Lewy Bodies, Cause Neurodegeneration in Dementia with Lewy Bodies', *The Journal of Neuroscience*, 27(6), pp. 1405–1410. Available at: https://doi.org/10.1523/JNEUROSCI.4564-06.2007.

Kriks, S. *et al.* (2011) 'Dopamine neurons derived from human ES cells efficiently engraft in animal models of Parkinson's disease', *Nature*, 480(7378), pp. 547–551. Available at: https://doi.org/10.1038/nature10648.

Krokhin, O.V. *et al.* (2006) 'Deamidation of -Asn-Gly- Sequences during Sample Preparation for Proteomics: Consequences for MALDI and HPLC-MALDI Analysis', *Analytical Chemistry*, 78(18), pp. 6645–6650. Available at: https://doi.org/10.1021/ac061017o.

Krüger, R. *et al.* (1998) 'AlaSOPro mutation in the gene encoding α-synuclein in Parkinson's disease', *Nature Genetics*, 18(2), pp. 106–108. Available at: https://doi.org/10.1038/ng0298-106.

Kucera, A., Bakke, O. and Progida, C. (2016) 'The multiple roles of Rab9 in the endolysosomal system', *Communicative & Integrative Biology*, 9(4), p. e1204498. Available at: https://doi.org/10.1080/19420889.2016.1204498.

Kumar, M. and Feldman, R.A. (2025) 'Inhibition or genetic reduction of ASAH1/acid ceramidase restore α-synuclein clearance in mutant GBA1 dopamine neurons from Parkinson's patients', *Human Molecular Genetics*, 34(24), pp. 2075–2087. Available at: https://doi.org/10.1093/hmg/ddaf166.

Kunadt, M. *et al.* (2015) 'Extracellular vesicle sorting of α-Synuclein is regulated by sumoylation', *Acta Neuropathologica*, 129(5), pp. 695–713. Available at: https://doi.org/10.1007/s00401-015-1408-1.

Lang, C. *et al.* (2019) 'Single-Cell Sequencing of iPSC-Dopamine Neurons Reconstructs Disease Progression and Identifies HDAC4 as a Regulator of Parkinson Cell Phenotypes', *Cell Stem Cell*, 24(1), pp. 93-106.e6. Available at: https://doi.org/10.1016/j.stem.2018.10.023.

Laperle, A.H. *et al.* (2020) 'iPSC modeling of young-onset Parkinson's disease reveals a molecular signature of disease and novel therapeutic candidates', *Nature Medicine*, 26(2), pp. 289–299. Available at: https://doi.org/10.1038/s41591-019-0739-1.

Lashuel, H.A. *et al.* (2022) 'Revisiting the specificity and ability of phospho-S129 antibodies to capture alpha-synuclein biochemical and pathological diversity', *npj Parkinson's Disease*, 8(1), pp. 1–19. Available at: https://doi.org/10.1038/s41531-022-00388-7.

Lautenschläger, J. *et al.* (2018) 'C-terminal calcium binding of α-synuclein modulates synaptic vesicle interaction', *Nature Communications*, 9(1), p. 712. Available at: https://doi.org/10.1038/s41467-018-03111-4.

Lawton, M. *et al.* (2018) 'Developing and validating Parkinson's disease subtypes and their motor and cognitive progression', *Journal of Neurology, Neurosurgery & Psychiatry*, 89(12), pp. 1279–1287. Available at: https://doi.org/10.1136/jnnp-2018-318337.

Lázaro, D.F. *et al.* (2014) 'Systematic Comparison of the Effects of Alpha-synuclein Mutations on Its Oligomerization and Aggregation', *PLoS Genetics*. Edited by D. Kaganovich, 10(11), p. e1004741. Available at: https://doi.org/10.1371/journal.pgen.1004741.

Lebowitz, J.J. *et al.* (2022) 'Synaptotagmin-1 is a Ca2+ sensor for somatodendritic dopamine release', *Cell reports*, 42(1), p. 111915. Available at: https://doi.org/10.1016/j.celrep.2022.111915.

Lebowitz, J.J. *et al.* (2024) 'Synaptotagmin-7 Counteracts Short-Term Depression during Phasic Dopamine Release', *eNeuro*, 11(3), p. ENEURO.0501. Available at: https://doi.org/10.1523/ENEURO.0501-23.2024.

Lee, B.R. and Kamitani, T. (2011) 'Improved Immunodetection of Endogenous α-Synuclein', *PLoS ONE*. Edited by M.B. Feany, 6(8), p. e23939. Available at: https://doi.org/10.1371/journal.pone.0023939.

Lee, H.-J. *et al.* (2011) 'Enzyme-linked immunosorbent assays for alpha-synuclein with species and multimeric state specificities', *Journal of Neuroscience Methods*, 199(2), pp. 249–257. Available at: https://doi.org/10.1016/j.jneumeth.2011.05.020.

Lee, H.-J. *et al.* (2013) 'Autophagic failure promotes the exocytosis and intercellular transfer of α-synuclein', *Experimental & Molecular Medicine*, 45(5), pp. e22–e22. Available at: https://doi.org/10.1038/emm.2013.45.

Lee, H.-J., Patel, S. and Lee, S.-J. (2005) 'Intravesicular Localization and Exocytosis of α-Synuclein and its Aggregates', *Journal of Neuroscience*, 25(25), pp. 6016–6024. Available at: https://doi.org/10.1523/JNEUROSCI.0692-05.2005.

Lee, J. *et al.* (2018) 'Secretion of misfolded cytosolic proteins from mammalian cells is independent of chaperone-mediated autophagy', *Journal of Biological Chemistry*, 293(37), pp. 14359–14370. Available at: https://doi.org/10.1074/jbc.RA118.003660.

Lee, J. *et al.* (2023) 'Abnormal triaging of misfolded proteins by adult neuronal ceroid lipofuscinosis-associated DNAJC5/CSPα mutants causes lipofuscin accumulation', *Autophagy*, 19(1), pp. 204–223. Available at: https://doi.org/10.1080/15548627.2022.2065618.

Lee, J.-E. *et al.* (2018) 'Mapping Surface Hydrophobicity of α-Synuclein Oligomers at the Nanoscale', *Nano Letters*, 18(12), pp. 7494–7501. Available at: https://doi.org/10.1021/acs.nanolett.8b02916.

Lee, J.-G. *et al.* (2016) 'Unconventional secretion of misfolded proteins promotes adaptation to proteasome dysfunction in mammalian cells', *Nature Cell Biology*, 18(7), pp. 765–776. Available at: https://doi.org/10.1038/ncb3372.

Lee, S.S., Civitelli, L. and Parkkinen, L. (2024) 'Brain-derived and in vitro-seeded alpha-synuclein fibrils exhibit distinct biophysical profiles'. Available at: https://doi.org/10.7554/eLife.92775.2.

Lesage, S. *et al.* (2013) 'G51D α-synuclein mutation causes a novel Parkinsonian–pyramidal syndrome', *Annals of Neurology*, 73(4), pp. 459–471. Available at: https://doi.org/10.1002/ana.23894.

Levine, P.M. *et al.* (2019) 'α-Synuclein O-GlcNAcylation alters aggregation and toxicity, revealing certain residues as potential inhibitors of Parkinson's disease', *Proceedings of the National Academy of Sciences*, 116(5), pp. 1511–1519. Available at: https://doi.org/10.1073/pnas.1808845116.

Lewkowich, I.P., Campbell, J.D. and HayGlass, K.T. (2001) 'Comparison of chemiluminescent assays and colorimetric ELISAs for quantification of murine IL-12, human IL-4 and murine IL-4: chemiluminescent substrates provide markedly enhanced sensitivity', *Journal of Immunological Methods*, 247(1–2), pp. 111–118. Available at: https://doi.org/10.1016/S0022-1759(00)00306-9.

Li, B. *et al.* (2018) 'Cryo-EM of full-length α-synuclein reveals fibril polymorphs with a common structural kernel', *Nature Communications*, 9(1), p. 3609. Available at: https://doi.org/10.1038/s41467-018-05971-2.

Li, J. *et al.* (2022) 'Clinical application of prion-like seeding in α-synucleinopathies: Early and non-invasive diagnosis and therapeutic development', *Frontiers in Molecular Neuroscience*, 15, p. 975619. Available at: https://doi.org/10.3389/fnmol.2022.975619.

Li, J.-Y. *et al.* (2008) 'Lewy bodies in grafted neurons in subjects with Parkinson's disease suggest host-to-graft disease propagation', *Nature Medicine*, 14(5), pp. 501–503. Available at: https://doi.org/10.1038/nm1746.

Li, M. *et al.* (2024) 'QuICSeedR: an R package for analyzing fluorophore-assisted seed amplification assay data', *Bioinformatics*. Edited by J. Cheng, 41(1), p. btae752. Available at: https://doi.org/10.1093/bioinformatics/btae752.

Li, W. *et al.* (2005) 'Aggregation promoting C-terminal truncation of α-synuclein is a normal cellular process and is enhanced by the familial Parkinson's disease-linked mutations', *Proceedings of the National Academy of Sciences*, 102(6), pp. 2162–2167. Available at: https://doi.org/10.1073/pnas.0406976102.

Li, X. *et al.* (2024) 'Coordination of RAB-8 and RAB-11 during unconventional protein secretion', *Journal of Cell Biology*, 223(2), p. e202306107. Available at: https://doi.org/10.1083/jcb.202306107.

Lin, L. *et al.* (2016) 'Molecular Features Underlying Neurodegeneration Identified through In Vitro Modeling of Genetically Diverse Parkinson's Disease Patients', *Cell Reports*, 15(11), pp. 2411–2426. Available at: https://doi.org/10.1016/j.celrep.2016.05.022.

Liu, J. *et al.* (2009) 'Rab11a and HSP90 Regulate Recycling of Extracellular α-Synuclein', *Journal of Neuroscience*, 29(5), pp. 1480–1485. Available at: https://doi.org/10.1523/JNEUROSCI.6202-08.2009.

Liu, S. *et al.* (2004) 'α-Synuclein produces a long-lasting increase in neurotransmitter release', *The EMBO Journal* [Preprint]. Available at: https://doi.org/10.1038/sj.emboj.7600451.

Liu, Y. *et al.* (2023) 'Single-Molecule Detection of α-Synuclein Oligomers in Parkinson's Disease Patients Using Nanopores', *ACS Nano*, 17(22), pp. 22999–23009. Available at: https://doi.org/10.1021/acsnano.3c08456.

Lobanova, E. *et al.* (2022) 'Imaging protein aggregates in the serum and cerebrospinal fluid in Parkinson's disease', *Brain*, 145(2), pp. 632–643. Available at: https://doi.org/10.1093/brain/awab306.

Lokappa, S.B. and Ulmer, T.S. (2011) 'α-Synuclein Populates Both Elongated and Broken Helix States on Small Unilamellar Vesicles', *Journal of Biological Chemistry*, 286(24), pp. 21450–21457. Available at: https://doi.org/10.1074/jbc.M111.224055.

Lorenzen, N. *et al.* (2014) 'The N-terminus of α-synuclein is essential for both monomeric and oligomeric interactions with membranes', *FEBS Letters*, 588(3), pp. 497–502. Available at: https://doi.org/10.1016/j.febslet.2013.12.015.

Lou, X. *et al.* (2017) 'α-Synuclein may cross-bridge v-SNARE and acidic phospholipids to facilitate SNARE-dependent vesicle docking', *Biochemical Journal*, 474(12), pp. 2039–2049. Available at: https://doi.org/10.1042/BCJ20170200.

Lövestam, S. *et al.* (2021) 'Seeded assembly *in vitro* does not replicate the structures of α-synuclein filaments from multiple system atrophy', *FEBS Open Bio*, 11(4), pp. 999–1013. Available at: https://doi.org/10.1002/2211-5463.13110.

Lucken-Ardjomande Häsler, S. *et al.* (2020) 'GRAF2, WDR44, and MICAL1 mediate Rab8/10/11–dependent export of E-cadherin, MMP14, and CFTR ΔF508', *Journal of Cell Biology*, 219(5), p. e201811014. Available at: https://doi.org/10.1083/jcb.201811014.

Ludtmann, M.H.R. *et al.* (2018) 'α-synuclein oligomers interact with ATP synthase and open the permeability transition pore in Parkinson's disease', *Nature Communications*, 9(1), p. 2293. Available at: https://doi.org/10.1038/s41467-018-04422-2.

Luk, K.C. *et al.* (2012) 'Pathological α-Synuclein Transmission Initiates Parkinson-like Neurodegeneration in Nontransgenic Mice', *Science*, 338(6109), pp. 949–953. Available at: https://doi.org/10.1126/science.1227157.

Luo, F. *et al.* (2020) 'Developmental deficits and early signs of neurodegeneration revealed by PD patient derived dopamine neurons', *Stem Cell Research*, 49, p. 102027. Available at: https://doi.org/10.1016/j.scr.2020.102027.

Luth, E.S. *et al.* (2014) 'Soluble, Prefibrillar α-Synuclein Oligomers Promote Complex I-dependent, Ca2+-induced Mitochondrial Dysfunction', *Journal of Biological Chemistry*, 289(31), pp. 21490–21507. Available at: https://doi.org/10.1074/jbc.M113.545749.

Magalhaes, J. *et al.* (2018a) 'Effects of ambroxol on the autophagy-lysosome pathway and mitochondria in primary cortical neurons', *Scientific Reports*, 8(1), pp. 1–12. Available at: https://doi.org/10.1038/s41598-018-19479-8.

Magalhaes, J. *et al.* (2018b) 'Effects of ambroxol on the autophagy-lysosome pathway and mitochondria in primary cortical neurons', *Scientific Reports*, 8(1), pp. 1–12. Available at: https://doi.org/10.1038/s41598-018-19479-8.

Mahul-Mellier, A.-L. *et al.* (2025) 'Differential role of C-terminal truncations on alpha-synuclein pathology and Lewy body formation', *npj Parkinson's Disease*, 11(1), p. 261. Available at: https://doi.org/10.1038/s41531-025-01084-y.

Majbour, N.K. *et al.* (2016) 'Oligomeric and phosphorylated alpha-synuclein as potential CSF biomarkers for Parkinson's disease', *Molecular Neurodegeneration*, 11(1), p. 7. Available at: https://doi.org/10.1186/s13024-016-0072-9.

Maltsev, A.S., Ying, J. and Bax, A. (2012) 'Impact of N-Terminal Acetylation of α-Synuclein on Its Random Coil and Lipid Binding Properties', *Biochemistry*, 51(25), pp. 5004–5013. Available at: https://doi.org/10.1021/bi300642h.

Mamais, A. et al. (2021) 'Mutations in LRRK2 linked to Parkinson disease sequester Rab8a to damaged lysosomes and regulate transferrin-mediated iron uptake in microglia', PLOS Biology, 19(12), p. e3001480. Available at: https://doi.org/10.1371/journal.pbio.3001480.

Mamais, A. *et al.* (2024) 'The LRRK2 kinase substrates RAB8a and RAB10 contribute complementary but distinct disease-relevant phenotypes in human neurons', *Stem Cell Reports*, 19(2), pp. 163–173. Available at: https://doi.org/10.1016/j.stemcr.2024.01.001.

Mandegar, M.A. *et al.* (2016) 'CRISPR Interference Efficiently Induces Specific and Reversible Gene Silencing in Human iPSCs', *Cell Stem Cell*, 18(4), pp. 541–553. Available at: https://doi.org/10.1016/j.stem.2016.01.022.

Mandler, M. *et al.* (2014) 'Next-generation active immunization approach for synucleinopathies: implications for Parkinson's disease clinical trials', *Acta Neuropathologica*, 127(6), pp. 861–879. Available at: https://doi.org/10.1007/s00401-014-1256-4.

Manzanza, N. de O., Sedlackova, L. and Kalaria, R.N. (2021) 'Alpha-Synuclein Post-translational Modifications: Implications for Pathogenesis of Lewy Body Disorders', *Frontiers in Aging Neuroscience*, 13, p. 690293. Available at: https://doi.org/10.3389/fnagi.2021.690293.

Mao, X. *et al.* (2016) 'Pathological α-synuclein transmission initiated by binding lymphocyte-activation gene 3', *Science*, 353(6307), p. aah3374. Available at: https://doi.org/10.1126/science.aah3374.

Marotta, N.P. *et al.* (2015) 'O-GlcNAc modification blocks the aggregation and toxicity of the protein α-synuclein associated with Parkinson's disease', *Nature Chemistry*, 7(11), pp. 913–920. Available at: https://doi.org/10.1038/nchem.2361.

Martel, A. *et al.* (2023) 'Upgraded D22 SEC–SANS setup dedicated to the biology community', *Journal of Applied Crystallography*, 56(4), pp. 994–1001. Available at: https://doi.org/10.1107/S1600576723004119.

Marton, R.M. and Ioannidis, J.P.A. (2019) 'A Comprehensive Analysis of Protocols for Deriving Dopaminergic Neurons from Human Pluripotent Stem Cells', *Stem Cells Translational Medicine*, 8(4), pp. 366–374. Available at: https://doi.org/10.1002/sctm.18-0088.

Masuda-Suzukake, M. *et al.* (2013) 'Prion-like spreading of pathological α-synuclein in brain', *Brain*, 136(4), pp. 1128–1138. Available at: https://doi.org/10.1093/brain/awt037.

Matsuda, W. *et al.* (2009) 'Single Nigrostriatal Dopaminergic Neurons Form Widely Spread and Highly Dense Axonal Arborizations in the Neostriatum', *Journal of Neuroscience*, 29(2), pp. 444–453. Available at: https://doi.org/10.1523/JNEUROSCI.4029-08.2009.

Matsui, Hideaki *et al.* (2023) 'Phosphorylation of α-synuclein at T64 results in distinct oligomers and exerts toxicity in models of Parkinson's disease', *Proceedings of the National Academy of Sciences*, 120(23), p. e2214652120. Available at: https://doi.org/10.1073/pnas.2214652120.

Mavroeidi, P. *et al.* (2022) 'Exosomes in Alpha-Synucleinopathies: Propagators of Pathology or Potential Candidates for Nanotherapeutics?', *Biomolecules*, 12(7), p. 957. Available at: https://doi.org/10.3390/biom12070957.

Mazzulli, J.R. *et al.* (2011) 'Gaucher Disease Glucocerebrosidase and α-Synuclein Form a Bidirectional Pathogenic Loop in Synucleinopathies', *Cell*, 146(1), pp. 37–52. Available at: https://doi.org/10.1016/j.cell.2011.06.001.

Mazzulli, J.R., Zunke, F., Tsunemi, T., *et al.* (2016) 'Activation of β-Glucocerebrosidase Reduces Pathological α-Synuclein and Restores Lysosomal Function in Parkinson's Patient Midbrain Neurons', *Journal of Neuroscience*, 36(29), pp. 7693–7706. Available at: https://doi.org/10.1523/JNEUROSCI.0628-16.2016.

Mazzulli, J.R., Zunke, F., Isacson, O., *et al.* (2016) 'α-Synuclein–induced lysosomal dysfunction occurs through disruptions in protein trafficking in human midbrain synucleinopathy models', *Proceedings of the National Academy of Sciences*, 113(7), pp. 1931–1936. Available at: https://doi.org/10.1073/pnas.1520335113.

McCormack, A.L., Mak, S.K. and Di Monte, D.A. (2012) 'Increased α-synuclein phosphorylation and nitration in the aging primate substantia nigra', *Cell Death & Disease*, 3(5), pp. e315–e315. Available at: https://doi.org/10.1038/cddis.2012.50.

McGlinchey, R.P. *et al.* (2019) 'C-terminal α-synuclein truncations are linked to cysteine cathepsin activity in Parkinson's disease', *Journal of Biological Chemistry*, 294(25), pp. 9973–9984. Available at: https://doi.org/10.1074/jbc.RA119.008930.

McGlinchey, R.P. *et al.* (2021) 'The N terminus of α-synuclein dictates fibril formation', *Proceedings of the National Academy of Sciences*, 118(35), p. e2023487118. Available at: https://doi.org/10.1073/pnas.2023487118.

McGuinness, W. *et al.* (2025) 'TFEB and TFE3 have cell-type specific expression in the brain and divergent roles in neurons', *bioRxiv*, p. 2025.04.22.649949. Available at: https://doi.org/10.1101/2025.04.22.649949.

McLean, J.R. *et al.* (2011) 'Transcript expression levels of full-length alpha-synuclein and its three alternatively spliced variants in Parkinson's disease brain regions and in a transgenic mouse model of alpha-synuclein overexpression', *Molecular and Cellular Neurosciences*, 49(2), p. 230. Available at: https://doi.org/10.1016/j.mcn.2011.11.006.

McTiernan, N., Kjosås, I. and Arnesen, T. (2025) 'Illuminating the impact of N-terminal acetylation: from protein to physiology', *Nature Communications*, 16(1), pp. 1–15. Available at: https://doi.org/10.1038/s41467-025-55960-5.

Meade, R.M. *et al.* (2023) 'An N-terminal alpha-synuclein fragment binds lipid vesicles to modulate lipid-induced aggregation', *Cell Reports Physical Science*, 4(9), p. 101563. Available at: https://doi.org/10.1016/j.xcrp.2023.101563.

Meade, R.M. *et al.* (2025) 'Stabilizing a Native Fold of Alpha-Synuclein with Short Helix-Constrained Peptides', *JACS Au*, 5(9), pp. 4321–4336. Available at: https://doi.org/10.1021/jacsau.5c00694.

Meier, F. *et al.* (2012) 'Semisynthetic, Site-Specific Ubiquitin Modification of α-Synuclein Reveals Differential Effects on Aggregation', *Journal of the American Chemical Society*, 134(12), pp. 5468–5471. Available at: https://doi.org/10.1021/ja300094r.

Meyer, N. *et al.* (2022) 'Real-Time Fast Amyloid Seeding and Translocation of α-Synuclein with a Nanopipette', *ACS Central Science*, 8(4), pp. 441–448. Available at: https://doi.org/10.1021/acscentsci.1c01404.

Miao, Y. *et al.* (2025) 'Modulation of O-GlcNAc cycling influences α-synuclein amplification, degradation, and associated neuroinflammatory pathology', *Molecular Neurodegeneration*, 20(1), p. 113. Available at: https://doi.org/10.1186/s13024-025-00904-2.

Miller, J.D. *et al.* (2013) 'Human iPSC-Based Modeling of Late-Onset Disease via Progerin-Induced Aging', *Cell Stem Cell*, 13(6), pp. 691–705. Available at: https://doi.org/10.1016/j.stem.2013.11.006.

Minakaki, G. *et al.* (2018) 'Autophagy inhibition promotes SNCA/alpha-synuclein release and transfer via extracellular vesicles with a hybrid autophagosome-exosome-like phenotype', *Autophagy* [Preprint]. Available at: https://www.tandfonline.com/doi/abs/10.1080/15548627.2017.1395992 (Accessed: 10 October 2021).

Mingo, Y.B., Escobar Galvis, M.L. and Henderson, M.X. (2025) 'α-Synuclein pathology and mitochondrial dysfunction: Toxic partners in Parkinson's disease', *Neurobiology of Disease*, 209, p. 106889. Available at: https://doi.org/10.1016/j.nbd.2025.106889.

Mishizen-Eberz, A.J. *et al.* (2005) 'Cleavage of α-Synuclein by Calpain: Potential Role in Degradation of Fibrillized and Nitrated Species of α-Synuclein', *Biochemistry*, 44(21), pp. 7818–7829. Available at: https://doi.org/10.1021/bi047846q.

Mohamed, N.-V. *et al.* (2021) 'Midbrain organoids with an *SNCA* gene triplication model key features of synucleinopathy', *Brain Communications*, 3(4), p. fcab223. Available at: https://doi.org/10.1093/braincomms/fcab223.

Mollenhauer, B. *et al.* (2011) 'α-Synuclein and tau concentrations in cerebrospinal fluid of patients presenting with parkinsonism: a cohort study', *The Lancet Neurology*, 10(3), pp. 230–240. Available at: https://doi.org/10.1016/S1474-4422(11)70014-X.

Mollenhauer, B. *et al.* (2012) 'α-Synuclein in human cerebrospinal fluid is principally derived from neurons of the central nervous system', *Journal of Neural Transmission*, 119(7), pp. 739–746. Available at: https://doi.org/10.1007/s00702-012-0784-0.

Mollenhauer, B. (2014) 'Quantification of α-synuclein in cerebrospinal fluid: How ideal is this biomarker for Parkinson's disease?', *Parkinsonism & Related Disorders*, 20, pp. S76–S79. Available at: https://doi.org/10.1016/S1353-8020(13)70020-8.

Moreau, K. *et al.* (2011) 'Autophagosome Precursor Maturation Requires Homotypic Fusion', *Cell*, 146(2), pp. 303–317. Available at: https://doi.org/10.1016/j.cell.2011.06.023.

Mubariz, F. *et al.* (2023) 'Deregulation of mTORC1-TFEB axis in human iPSC model of GBA1-associated Parkinson's disease', *Frontiers in Neuroscience*, 17, p. 1152503. Available at: https://doi.org/10.3389/fnins.2023.1152503.

Mundo Rivera, V.M. *et al.* (2024) 'Natural Autophagy Activators to Fight Age-Related Diseases', *Cells*, 13(19), p. 1611. Available at: https://doi.org/10.3390/cells13191611.

Musteikytė, G. *et al.* (2021) 'Interactions of α-synuclein oligomers with lipid membranes', *Biochimica et Biophysica Acta (BBA) - Biomembranes*, 1863(4), p. 183536. Available at: https://doi.org/10.1016/j.bbamem.2020.183536.

Nakai, M. *et al.* (2007) 'Expression of α-synuclein, a presynaptic protein implicated in Parkinson's disease, in erythropoietic lineage', *Biochemical and Biophysical Research Communications*, 358(1), pp. 104–110. Available at: https://doi.org/10.1016/j.bbrc.2007.04.108.

Nakamura, Y. *et al.* (2024) 'Neuronal activity promotes secretory autophagy for the extracellular release of α-synuclein', *Journal of Biological Chemistry*, 300(7), p. 107419. Available at: https://doi.org/10.1016/j.jbc.2024.107419.

Nalls, M.A. *et al.* (2019) 'Identification of novel risk loci, causal insights, and heritable risk for Parkinson's disease: a meta-analysis of genome-wide association studies', *The Lancet Neurology*, 18(12), pp. 1091–1102. Available at: https://doi.org/10.1016/S1474-4422(19)30320-5.

Nayak, A. and Müller, S. (2014) 'SUMO-specific proteases/isopeptidases: SENPs and beyond', *Genome Biology*, 15(7), p. 422. Available at: https://doi.org/10.1186/s13059-014-0422-2.

Neely, M.D. *et al.* (2017) 'From the Cover: Manganese and Rotenone-Induced Oxidative Stress Signatures Differ in iPSC-Derived Human Dopamine Neurons', *Toxicological sciences*, 159(2), pp. 366–379. Available at: https://doi.org/10.1093/toxsci/kfx145.

Negro, A. *et al.* (2002) 'Multiple phosphorylation of α-synuclein by protein tyrosine kinase Syk prevents eosin-induced aggregation', *The FASEB Journal*, 16(2), pp. 1–22. Available at: https://doi.org/10.1096/fj.01-0517fje.

Ngolab, J. *et al.* (2017) 'Brain-derived exosomes from dementia with Lewy bodies propagate α-synuclein pathology', *Acta Neuropathologica Communications*, 5(1), pp. 1–10. Available at: https://doi.org/10.1186/s40478-017-0445-5.

Nguyen, H.N. *et al.* (2011) 'LRRK2 Mutant iPSC-Derived DA Neurons Demonstrate Increased Susceptibility to Oxidative Stress', *Cell Stem Cell*, 8(3), pp. 267–280. Available at: https://doi.org/10.1016/j.stem.2011.01.013.

Nimmo, J.T. *et al.* (2020) 'Novel antibodies detect additional α-synuclein pathology in synucleinopathies: potential development for immunotherapy', *Alzheimer's Research & Therapy*, 12(1), p. 159. Available at: https://doi.org/10.1186/s13195-020-00727-x.

Nimmo, J.T. *et al.* (2022) 'Immunisation with UB-312 in the Thy1SNCA mouse prevents motor performance deficits and oligomeric α-synuclein accumulation in the brain and gut', *Acta Neuropathologica*, 143(1), pp. 55–73. Available at: https://doi.org/10.1007/s00401-021-02381-5.

Nishida, Y. *et al.* (2009) 'Discovery of Atg5/Atg7-independent alternative macroautophagy', *Nature*, 461(7264), pp. 654–658. Available at: https://doi.org/10.1038/nature08455.

Nuber, S. *et al.* (2018) 'Abrogating Native α-Synuclein Tetramers in Mice Causes a L-DOPA-Responsive Motor Syndrome Closely Resembling Parkinson's Disease', *Neuron*, 100(1), pp. 75-90.e5. Available at: https://doi.org/10.1016/j.neuron.2018.09.014.

Nuermaimaiti, M. *et al.* (2025) 'Human induced pluripotent stem cell-derived dopaminergic neurons release alpha-synuclein through neuronal activity', *Neuroscience Research*, 212, pp. 105–114. Available at: https://doi.org/10.1016/j.neures.2024.11.007.

Oh, C. *et al.* (2022) 'S-Nitrosylation of p62 Inhibits Autophagic Flux to Promote α-Synuclein Secretion and Spread in Parkinson's Disease and Lewy Body Dementia', *Journal of Neuroscience*, 42(14), pp. 3011–3024. Available at: https://doi.org/10.1523/JNEUROSCI.1508-21.2022.

Ohgita, T. *et al.* (2022) 'Mechanisms of enhanced aggregation and fibril formation of Parkinson's disease-related variants of α-synuclein', *Scientific Reports*, 12(1), p. 6770. Available at: https://doi.org/10.1038/s41598-022-10789-6.

Öhrfelt, A. *et al.* (2011) 'Identification of Novel α-Synuclein Isoforms in Human Brain Tissue by using an Online NanoLC-ESI-FTICR-MS Method', *Neurochemical Research*, 36(11), pp. 2029–2042. Available at: https://doi.org/10.1007/s11064-011-0527-x.

Oj, R. *et al.* (2016) 'A predictive computational framework for direct reprogramming between human cell types', *Nature genetics*, 48(3). Available at: https://doi.org/10.1038/ng.3487.

Oji, Y. *et al.* (2020) 'Variants in saposin D domain of prosaposin gene linked to Parkinson's disease', *Brain*, 143(4), pp. 1190–1205. Available at: https://doi.org/10.1093/brain/awaa064.

Okarmus, J. *et al.* (2020) 'Lysosomal perturbations in human dopaminergic neurons derived from induced pluripotent stem cells with PARK2 mutation', *Scientific Reports*, 10(1), p. 10278. Available at: https://doi.org/10.1038/s41598-020-67091-6.

Okuzumi, A. *et al.* (2018) 'Rapid dissemination of alpha-synuclein seeds through neural circuits in an in-vivo prion-like seeding experiment', *Acta Neuropathologica Communications*, 6(1), p. 96. Available at: https://doi.org/10.1186/s40478-018-0587-0.

Oliveira, L.M.A. *et al.* (2015) 'Elevated α-synuclein caused by SNCA gene triplication impairs neuronal differentiation and maturation in Parkinson's patient-derived induced pluripotent stem cells', *Cell Death & Disease*, 6(11), pp. e1994–e1994. Available at: https://doi.org/10.1038/cddis.2015.318.

O'Sullivan, M.J. and Lindsay, A.J. (2020) 'The Endosomal Recycling Pathway—At the Crossroads of the Cell', *International Journal of Molecular Sciences*, 21(17), p. 6074. Available at: https://doi.org/10.3390/ijms21176074.

Outeiro, T.F. and Koss, D.J. (2025) 'Nuclear Alpha-Synuclein: Mechanisms and Implications for Synucleinopathies', *Movement Disorders*, p. mds.70138. Available at: https://doi.org/10.1002/mds.70138.

Ovesný, M. *et al.* (2014) 'ThunderSTORM: a comprehensive ImageJ plug-in for PALM and STORM data analysis and super-resolution imaging', *Bioinformatics*, 30(16), pp. 2389–2390. Available at: https://doi.org/10.1093/bioinformatics/btu202.

Pacelli, C. *et al.* (2015) 'Elevated Mitochondrial Bioenergetics and Axonal Arborization Size Are Key Contributors to the Vulnerability of Dopamine Neurons', *Current Biology*, 25(18), pp. 2349–2360. Available at: https://doi.org/10.1016/j.cub.2015.07.050.

Pagano, G. *et al.* (2016) 'Age at onset and Parkinson disease phenotype', *Neurology*, 86(15), pp. 1400–1407. Available at: https://doi.org/10.1212/WNL.0000000000002461.

Pagano, G. *et al.* (2022) 'Trial of Prasinezumab in Early-Stage Parkinson's Disease', *New England Journal of Medicine*, 387(5), pp. 421–432. Available at: https://doi.org/10.1056/NEJMoa2202867.

Pagano, G. *et al.* (2024) 'Prasinezumab slows motor progression in rapidly progressing early-stage Parkinson's disease', *Nature Medicine*, 30(4), pp. 1096–1103. Available at: https://doi.org/10.1038/s41591-024-02886-y.

Paleologou, K.E. *et al.* (2008) 'Phosphorylation at Ser-129 but Not the Phosphomimics S129E/D Inhibits the Fibrillation of α-Synuclein*', *Journal of Biological Chemistry*, 283(24), pp. 16895–16905. Available at: https://doi.org/10.1074/jbc.M800747200.

Paleologou, K.E. *et al.* (2010) 'Phosphorylation at S87 Is Enhanced in Synucleinopathies, Inhibits α-Synuclein Oligomerization, and Influences Synuclein-Membrane Interactions', *The Journal of Neuroscience*, 30(9), pp. 3184–3198. Available at: https://doi.org/10.1523/JNEUROSCI.5922-09.2010.

Park, M.J. *et al.* (2011) 'Elevated Levels of α-Synuclein Oligomer in the Cerebrospinal Fluid of Drug-Naïve Patients with Parkinson's Disease', *Journal of Clinical Neurology*, 7(4), p. 215. Available at: https://doi.org/10.3988/jcn.2011.7.4.215.

Park, S.M. *et al.* (2002) 'Stress-Induced Aggregation Profiles of GST–α-Synuclein Fusion Proteins: Role of the C-Terminal Acidic Tail of α-Synuclein in Protein Thermosolubility and Stability', *Biochemistry*, 41(12), pp. 4137–4146. Available at: https://doi.org/10.1021/bi015961k.

Parra-Rivas, L.A. *et al.* (2023) 'Serine-129 phosphorylation of α-synuclein is an activity-dependent trigger for physiologic protein-protein interactions and synaptic function', *Neuron*, 111(24), pp. 4006-4023.e10. Available at: https://doi.org/10.1016/j.neuron.2023.11.020.

Patro, R. *et al.* (2017) 'Salmon provides fast and bias-aware quantification of transcript expression', *Nature Methods*, 14(4), pp. 417–419. Available at: https://doi.org/10.1038/nmeth.4197.

Perfeito, R. *et al.* (2014) 'Linking alpha-synuclein phosphorylation to reactive oxygen species formation and mitochondrial dysfunction in SH-SY5Y cells', *Molecular and Cellular Neuroscience*, 62, pp. 51–59. Available at: https://doi.org/10.1016/j.mcn.2014.08.002.

Periñán, M.T. *et al.* (2022) 'Effect Modification between Genes and Environment and Parkinson's Disease Risk', *Annals of Neurology*, 92(5), pp. 715–724. Available at: https://doi.org/10.1002/ana.26467.

Perrier, A.L. *et al.* (2004) 'Derivation of midbrain dopamine neurons from human embryonic stem cells', *Proceedings of the National Academy of Sciences*, 101(34), pp. 12543–12548. Available at: https://doi.org/10.1073/pnas.0404700101.

Pertea, M. *et al.* (2015) 'StringTie enables improved reconstruction of a transcriptome from RNA-seq reads', *Nature Biotechnology*, 33(3), pp. 290–295. Available at: https://doi.org/10.1038/nbt.3122.

Pitcairn, C. *et al.* (2023) 'Impaired Autophagic-Lysosomal Fusion in Parkinson's Patient Midbrain Neurons Occurs through Loss of ykt6 and Is Rescued by Farnesyltransferase Inhibition', *Journal of Neuroscience*, 43(14), pp. 2615–2629. Available at: https://doi.org/10.1523/JNEUROSCI.0610-22.2023.

Plotegher, N. *et al.* (2017) 'DOPAL derived alpha-synuclein oligomers impair synaptic vesicles physiological function', *Scientific Reports*, 7(1), p. 40699. Available at: https://doi.org/10.1038/srep40699.

Poehler, A.-M. *et al.* (2014) 'Autophagy modulates SNCA/α-synuclein release, thereby generating a hostile microenvironment', *Autophagy*, 10(12), pp. 2171–2192. Available at: https://doi.org/10.4161/auto.36436.

Poewe, W. *et al.* (2017) 'Parkinson disease', *Nature Reviews Disease Primers*, 3(1), p. 17013. Available at: https://doi.org/10.1038/nrdp.2017.13.

Poggiolini, I. *et al.* (2022) 'Diagnostic value of cerebrospinal fluid alpha-synuclein seed quantification in synucleinopathies', *Brain*, 145(2), pp. 584–595. Available at: https://doi.org/10.1093/brain/awab431.

Polymeropoulos, M.H. *et al.* (1997) 'Mutation in the α-Synuclein Gene Identified in Families with Parkinson's Disease', *Science* [Preprint]. Available at: https://doi.org/10.1126/science.276.5321.2045.

Pons, M.-L. *et al.* (2022) 'Proteomics Challenges for the Assessment of Synuclein Proteoforms as Clinical Biomarkers in Parkinson's Disease', *Frontiers in Aging Neuroscience*, 14, p. 818606. Available at: https://doi.org/10.3389/fnagi.2022.818606.

Pringsheim, T. *et al.* (2014) 'The prevalence of Parkinson's disease: A systematic review and meta-analysis', *Movement Disorders*, 29(13), pp. 1583–1590. Available at: https://doi.org/10.1002/mds.25945.

Prots, I. *et al.* (2018) 'α-Synuclein oligomers induce early axonal dysfunction in human iPSC-based models of synucleinopathies', *Proceedings of the National Academy of Sciences*, 115(30), pp. 7813–7818. Available at: https://doi.org/10.1073/pnas.1713129115.

Proukakis, C. *et al.* (2013) 'A novel α-synuclein missense mutation in Parkinson disease', *Neurology*, 80(11), p. 1062. Available at: https://doi.org/10.1212/WNL.0b013e31828727ba.

Pujols, J. *et al.* (2018) 'Small molecule inhibits α-synuclein aggregation, disrupts amyloid fibrils, and prevents degeneration of dopaminergic neurons', *Proceedings of the National Academy of Sciences of the United States of America*, 115(41), p. 10481. Available at: https://doi.org/10.1073/pnas.1804198115.

Puspita, L., Deline, M. and Shim, J. (2025) 'Dual SMAD inhibition as a versatile platform in human pluripotent stem cell–based regenerative medicine and disease modeling', *Molecules and Cells*, 48(11), p. 100284. Available at: https://doi.org/10.1016/j.mocell.2025.100284.

Raghavan, A. *et al.* (2024) 'Astroglia proliferate upon the biogenesis of tunneling nanotubes via α-synuclein dependent transient nuclear translocation of focal adhesion kinase', *iScience*, 27(8), p. 110565. Available at: https://doi.org/10.1016/j.isci.2024.110565.

Ramalingam, N., Jin, S.-X., *et al.* (2023) 'Dynamic physiological α-synuclein S129 phosphorylation is driven by neuronal activity', *npj Parkinson's Disease*, 9(1), p. 4. Available at: https://doi.org/10.1038/s41531-023-00444-w.

Ramalingam, N., Brontesi, L., *et al.* (2023) 'Dynamic reversibility of α-synuclein serine-129 phosphorylation is impaired in synucleinopathy models', *EMBO reports*, 24(12), p. e57145. Available at: https://doi.org/10.15252/embr.202357145.

Rao, S.K. *et al.* (2004) 'Identification of SNAREs Involved in Synaptotagmin VII-regulated Lysosomal Exocytosis', *Journal of Biological Chemistry*, 279(19), pp. 20471–20479. Available at: https://doi.org/10.1074/jbc.M400798200.

Ray, S. *et al.* (2020) 'α-Synuclein aggregation nucleates through liquid–liquid phase separation', *Nature Chemistry*, 12(8), pp. 705–716. Available at: https://doi.org/10.1038/s41557-020-0465-9.

Recasens, A. *et al.* (2014) 'Lewy body extracts from Parkinson disease brains trigger α-synuclein pathology and neurodegeneration in mice and monkeys', *Annals of Neurology*, 75(3), pp. 351–362. Available at: https://doi.org/10.1002/ana.24066.

Reimer, L. *et al.* (2022) 'Protein kinase R dependent phosphorylation of α-synuclein regulates its membrane binding and aggregation', *PNAS Nexus*. Edited by A. Abramov, 1(5), p. pgac259. Available at: https://doi.org/10.1093/pnasnexus/pgac259.

Resh, M.D. (2006) 'Use of analogs and inhibitors to study the functional significance of protein palmitoylation', *Methods*, 40(2), pp. 191–197. Available at: https://doi.org/10.1016/j.ymeth.2006.04.013.

Reumann, D. *et al.* (2023) 'In vitro modeling of the human dopaminergic system using spatially arranged ventral midbrain–striatum–cortex assembloids', *Nature Methods*, 20(12), pp. 2034–2047. Available at: https://doi.org/10.1038/s41592-023-02080-x.

Riederer, P. *et al.* (2025) 'Levodopa treatment: impacts and mechanisms throughout Parkinson's disease progression', *Journal of Neural Transmission*, 132(6), pp. 743–779. Available at: https://doi.org/10.1007/s00702-025-02893-4.

Rinne, J.O. (1993) 'Nigral degeneration in parkinson's disease', *Movement Disorders*, 8(S1), pp. S31–S35. Available at: https://doi.org/10.1002/mds.870080507.

Roberts, R.F., Wade-Martins, R. and Alegre-Abarrategui, J. (2015) 'Direct visualization of alpha-synuclein oligomers reveals previously undetected pathology in Parkinson's disease brain', *Brain*, 138(6), pp. 1642–1657. Available at: https://doi.org/10.1093/brain/awv040.

Rodger, A.T., ALNasser, M. and Carter, W.G. (2023) 'Are Therapies That Target α-Synuclein Effective at Halting Parkinson's Disease Progression? A Systematic Review', *International Journal of Molecular Sciences*, 24(13), p. 11022. Available at: https://doi.org/10.3390/ijms241311022.

Röntgen, A. *et al.* (2024) 'Modulation of α-synuclein in vitro aggregation kinetics by its alternative splice isoforms', *Proceedings of the National Academy of Sciences*, 121(7), p. e2313465121. Available at: https://doi.org/10.1073/pnas.2313465121.

Röntgen, A. *et al.* (2025) 'Aggregation of α-synuclein splice isoforms through a phase separation pathway', *Science Advances*, 11(16), p. eadq5396. Available at: https://doi.org/10.1126/sciadv.adq5396.

Rostami, J. *et al.* (2017) 'Human Astrocytes Transfer Aggregated Alpha-Synuclein via Tunneling Nanotubes', *The Journal of Neuroscience*, 37(49), pp. 11835–11853. Available at: https://doi.org/10.1523/JNEUROSCI.0983-17.2017.

Rott, R. *et al.* (2017) 'SUMOylation and ubiquitination reciprocally regulate α-synuclein degradation and pathological aggregation', *Proceedings of the National Academy of Sciences*, 114(50), pp. 13176–13181. Available at: https://doi.org/10.1073/pnas.1704351114.

Rovere, M. *et al.* (2018) 'Refolding of helical soluble α-synuclein through transient interaction with lipid interfaces', *FEBS Letters*, 592(9), pp. 1464–1472. Available at: https://doi.org/10.1002/1873-3468.13047.

Ruf, V.C. *et al.* (2019) 'Different Effects of α-Synuclein Mutants on Lipid Binding and Aggregation Detected by Single Molecule Fluorescence Spectroscopy and ThT Fluorescence-Based Measurements', *ACS Chemical Neuroscience*, 10(3), pp. 1649–1659. Available at: https://doi.org/10.1021/acschemneuro.8b00579.

Rutherford, N.J. *et al.* (2014) 'Divergent effects of the H50Q and G51D *SNCA* mutations on the aggregation of α-synuclein', *Journal of Neurochemistry*, 131(6), pp. 859–867. Available at: https://doi.org/10.1111/jnc.12806.

Ryan, S.D. *et al.* (2013) 'Isogenic Human iPSC Parkinson's Model Shows Nitrosative Stress-Induced Dysfunction in MEF2-PGC1α Transcription', *Cell*, 155(6), pp. 1351–1364. Available at: https://doi.org/10.1016/j.cell.2013.11.009.

Ryan, T. *et al.* (2018) 'Cardiolipin exposure on the outer mitochondrial membrane modulates α-synuclein', *Nature Communications*, 9(1), pp. 1–17. Available at: https://doi.org/10.1038/s41467-018-03241-9.

Rydbirk, R. et al. (2016) 'Assessment of brain reference genes for RT-qPCR studies in neurodegenerative diseases', Scientific Reports, 6(1), p. 37116. Available at: https://doi.org/10.1038/srep37116.

Sacino, A.N. *et al.* (2014) 'Intramuscular injection of α-synuclein induces CNS α-synuclein pathology and a rapid-onset motor phenotype in transgenic mice', *Proceedings of the National Academy of Sciences*, 111(29), pp. 10732–10737. Available at: https://doi.org/10.1073/pnas.1321785111.

Saleeb, R.S. *et al.* (2023) 'Two-color coincidence single-molecule pulldown for the specific detection of disease-associated protein aggregates', *Science Advances*, 9(46), p. eadi7359. Available at: https://doi.org/10.1126/sciadv.adi7359.

Sánchez-Danés, A. *et al.* (2012) 'Disease-specific phenotypes in dopamine neurons from human iPS-based models of genetic and sporadic Parkinson's disease', *EMBO Molecular Medicine* [Preprint]. Available at: https://doi.org/10.1002/emmm.201200215.

Sano, K. *et al.* (2021) 'Tyrosine 136 phosphorylation of α-synuclein aggregates in the Lewy body dementia brain: involvement of serine 129 phosphorylation by casein kinase 2', *Acta Neuropathologica Communications*, 9(1), p. 182. Available at: https://doi.org/10.1186/s40478-021-01281-9.

Santhosh Kumar, S. *et al.* (2024) 'Sequential CRISPR screening reveals partial NatB inhibition as a strategy to mitigate alpha-synuclein levels in human neurons', *Science Advances*, 10(6), p. eadj4767. Available at: https://doi.org/10.1126/sciadv.adj4767.

Sanyal, A. *et al.* (2020) 'LRRK2 Kinase Inhibition Rescues Deficits in Lysosome Function Due to Heterozygous GBA1 Expression in Human iPSC-Derived Neurons', *Frontiers in Neuroscience*, 14, p. 531923. Available at: https://doi.org/10.3389/fnins.2020.00442.

Sarchione, A. *et al.* (2021) 'Alpha-Synuclein and Lipids: The Elephant in the Room?', *Cells*, 10(9). Available at: https://doi.org/10.3390/cells10092452.

Sasaki, A. *et al.* (2015) 'Sensitive western blotting for detection of endogenous Ser129-phosphorylated α-synuclein in intracellular and extracellular spaces', *Scientific Reports*, 5(1), p. 14211. Available at: https://doi.org/10.1038/srep14211.

Sawai, T., Nakamura, Y. and Arawaka, S. (2025) 'Secretory autophagy mediates lysosomal and autophagic degradation for α-synuclein proteostasis', *Journal of Biological Chemistry*, 301(8), p. 110474. Available at: https://doi.org/10.1016/j.jbc.2025.110474.

Schaser, A.J. *et al.* (2020) 'Trans-synaptic and retrograde axonal spread of Lewy pathology following pre-formed fibril injection in an in vivo A53T alpha-synuclein mouse model of synucleinopathy', *Acta Neuropathologica Communications*, 8(1), p. 150. Available at: https://doi.org/10.1186/s40478-020-01026-0.

Scheiblich, H. *et al.* (2024) 'Microglia rescue neurons from aggregate-induced neuronal dysfunction and death through tunneling nanotubes', *Neuron*, 112(18), pp. 3106-3125.e8. Available at: https://doi.org/10.1016/j.neuron.2024.06.029.

Scheper, W. and Hoozemans, J.J.M. (2013) 'A new PERKspective on neurodegeneration', *Science Translational Medicine*, 5(206), p. 206fs37. Available at: https://doi.org/10.1126/scitranslmed.3007641.

Schmidt, S.I. *et al.* (2025) 'Formation of seeding-competent α-synuclein aggregates in parkin-deficient iPSC-derived human neurons', *npj Parkinson's Disease*, 11(1), p. 180. Available at: https://doi.org/10.1038/s41531-025-01038-4.

Scholz, K. *et al.* (2025) 'Rab27b Promotes Lysosomal Function and Alpha-Synuclein Clearance in Neurons', *The Journal of Neuroscience*, 45(14), p. e1579242025. Available at: https://doi.org/10.1523/JNEUROSCI.1579-24.2025.

Schöndorf, D.C. *et al.* (2014) 'iPSC-derived neurons from GBA1-associated Parkinson's disease patients show autophagic defects and impaired calcium homeostasis', *Nature Communications*, 5(1), pp. 1–17. Available at: https://doi.org/10.1038/ncomms5028.

Schuelke, S., Haseeb, S. and Parmar, M.S. (2026) 'Rab8a dysregulation in Parkinson's disease: A convergence of genetic and molecular pathologies', Molecular Biology Reports, 53(1), p. 443. Available at: https://doi.org/10.1007/s11033-026-11567-7.

Schuler, M. *et al.* (2025) 'Alpha-synuclein misfolding as fluid biomarker for Parkinson's disease measured with the iRS platform', *EMBO Molecular Medicine*, 17(6), pp. 1203–1221. Available at: https://doi.org/10.1038/s44321-025-00229-z.

Schweighauser, M. *et al.* (2020) 'Structures of α-synuclein filaments from multiple system atrophy', *Nature*, 585(7825), pp. 464–469. Available at: https://doi.org/10.1038/s41586-020-2317-6.

Senol, A.D. *et al.* (2021) 'α-Synuclein fibrils subvert lysosome structure and function for the propagation of protein misfolding between cells through tunneling nanotubes', *PLOS Biology*, 19(7), p. e3001287. Available at: https://doi.org/10.1371/journal.pbio.3001287.

Shahnawaz, M. *et al.* (2020) 'Discriminating α-synuclein strains in Parkinson's disease and multiple system atrophy', *Nature*, 578(7794), pp. 273–277. Available at: https://doi.org/10.1038/s41586-020-1984-7.

Shaltouki, A. *et al.* (2015) 'Mitochondrial Alterations by PARKIN in Dopaminergic Neurons Using PARK2 Patient-Specific and PARK2 Knockout Isogenic iPSC Lines', *Stem Cell Reports*, 4(5), pp. 847–859. Available at: https://doi.org/10.1016/j.stemcr.2015.02.019.

Shearer, L.J., Petersen, N.O. and Woodside, M.T. (2021) 'Internalization of α-synuclein oligomers into SH-SY5Y cells', *Biophysical Journal*, 120(5), pp. 877–885. Available at: https://doi.org/10.1016/j.bpj.2020.12.031.

Sheta, R. *et al.* (2022) 'Combining NGN2 programming and dopaminergic patterning for a rapid and efficient generation of hiPSC-derived midbrain neurons', *Scientific Reports*, 12(1), p. 17176. Available at: https://doi.org/10.1038/s41598-022-22158-4.

Sheta, R. *et al.* (2023) 'Optimized protocol for the generation of functional human induced-pluripotent-stem-cell-derived dopaminergic neurons', *STAR Protocols*, 4(3), p. 102486. Available at: https://doi.org/10.1016/j.xpro.2023.102486.

Shippey, L.E. *et al.* (2022) 'Propagation of Parkinson's disease by extracellular vesicle production and secretion', *Biochemical Society Transactions*, 50(5), pp. 1303–1314. Available at: https://doi.org/10.1042/BST20220204.

Siddiqi, F.H. *et al.* (2019) 'Felodipine induces autophagy in mouse brains with pharmacokinetics amenable to repurposing', *Nature Communications*, 10(1), pp. 1–14. Available at: https://doi.org/10.1038/s41467-019-09494-2.

Sidhu, A., Segers-Nolten, I. and Subramaniam, V. (2016) 'Conformational Compatibility Is Essential for Heterologous Aggregation of α-Synuclein', *ACS Chemical Neuroscience*, 7(6), pp. 719–727. Available at: https://doi.org/10.1021/acschemneuro.5b00322.

Singleton, A.B. *et al.* (2003) 'α-Synuclein Locus Triplication Causes Parkinson's Disease', *Science*, 302(5646), pp. 841–841. Available at: https://doi.org/10.1126/science.1090278.

Sinha, S. *et al.* (2011) 'Lysine-Specific Molecular Tweezers Are Broad-Spectrum Inhibitors of Assembly and Toxicity of Amyloid Proteins', *Journal of the American Chemical Society*, 133(42), pp. 16958–16969. Available at: https://doi.org/10.1021/ja206279b.

Smith, D.K. *et al.* (2016) 'Small Molecules Modulate Chromatin Accessibility to Promote NEUROG2-Mediated Fibroblast-to-Neuron Reprogramming', *Stem Cell Reports*, 7(5), pp. 955–969. Available at: https://doi.org/10.1016/j.stemcr.2016.09.013.

Smith, L. and Schapira, A.H.V. (2022) 'GBA Variants and Parkinson Disease: Mechanisms and Treatments', *Cells*, 11(8), p. 1261. Available at: https://doi.org/10.3390/cells11081261.

Solana-Manrique, C. *et al.* (2025) 'Two- and Three-Dimensional In Vitro Models of Parkinson's and Alzheimer's Diseases: State-of-the-Art and Applications', *International Journal of Molecular Sciences*, 26(2), p. 620. Available at: https://doi.org/10.3390/ijms26020620.

Soldner, F. *et al.* (2011) 'Generation of Isogenic Pluripotent Stem Cells Differing Exclusively at Two Early Onset Parkinson Point Mutations', *Cell*, 146(2), pp. 318–331. Available at: https://doi.org/10.1016/j.cell.2011.06.019.

Somayaji, M. *et al.* (2020) 'A dual role for α-synuclein in facilitation and depression of dopamine release from substantia nigra neurons in vivo', *Proceedings of the National Academy of Sciences*, 117(51), pp. 32701–32710. Available at: https://doi.org/10.1073/pnas.2013652117.

Sorrentino, Z.A. *et al.* (2018) 'Physiological C-terminal truncation of α-synuclein potentiates the prion-like formation of pathological inclusions', *Journal of Biological Chemistry*, 293(49), pp. 18914–18932. Available at: https://doi.org/10.1074/jbc.RA118.005603.

Sorrentino, Z.A. and Giasson, B.I. (2020) 'The emerging role of α-synuclein truncation in aggregation and disease', *Journal of Biological Chemistry*, 295(30), pp. 10224–10244. Available at: https://doi.org/10.1074/jbc.REV120.011743.

Spencer, B. *et al.* (2016) 'α-Synuclein interferes with the ESCRT-III complex contributing to the pathogenesis of Lewy body disease', *Human Molecular Genetics*, 25(6), pp. 1100–1115. Available at: https://doi.org/10.1093/hmg/ddv633.

Spillantini, M.G. *et al.* (1997) 'α-Synuclein in Lewy bodies', *Nature*, 388(6645), pp. 839–840. Available at: https://doi.org/10.1038/42166.

Stark, G.R., Stein, W.H. and Moore, S. (1960) 'Reactions of the Cyanate Present in Aqueous Urea with Amino Acids and Proteins', *Journal of Biological Chemistry*, 235(11), pp. 3177–3181. Available at: https://doi.org/10.1016/S0021-9258(20)81332-5.

Stojkovska, I. *et al.* (2022) 'Rescue of α-synuclein aggregation in Parkinson's patient neurons by synergistic enhancement of ER proteostasis and protein trafficking', *Neuron*, 110(3), pp. 436-451.e11. Available at: https://doi.org/10.1016/j.neuron.2021.10.032.

Stojkovska, I. and Mazzulli, J.R. (2021) 'Detection of pathological alpha-synuclein aggregates in human iPSC-derived neurons and tissue', *STAR Protocols*, 2(1), p. 100372. Available at: https://doi.org/10.1016/j.xpro.2021.100372.

Strohäker, T. *et al.* (2019) 'Structural heterogeneity of α-synuclein fibrils amplified from patient brain extracts', *Nature Communications*, 10(1), p. 5535. Available at: https://doi.org/10.1038/s41467-019-13564-w.

Stuendl, A. *et al.* (2016) 'Induction of α-synuclein aggregate formation by CSF exosomes from patients with Parkinson's disease and dementia with Lewy bodies', *Brain*, 139(2), pp. 481–494. Available at: https://doi.org/10.1093/brain/awv346.

Stykel, M.G. *et al.* (2021) 'α-Synuclein mutation impairs processing of endomembrane compartments and promotes exocytosis and seeding of α-synuclein pathology', *Cell Reports*, 35(6), p. 109099. Available at: https://doi.org/10.1016/j.celrep.2021.109099.

Südhof, T.C. (2013) 'Neurotransmitter Release: The Last Millisecond in the Life of a Synaptic Vesicle', *Neuron*, 80(3), p. 10.1016/j.neuron.2013.10.022. Available at: https://doi.org/10.1016/j.neuron.2013.10.022.

Sulzer, D. and Surmeier, D.J. (2012) 'Neuronal vulnerability, pathogenesis and Parkinson's disease', *Movement disorders : official journal of the Movement Disorder Society*, 28(1), p. 41. Available at: https://doi.org/10.1002/mds.25095.

Sun, W. *et al.* (2003) 'Hrs regulates early endosome fusion by inhibiting formation of an endosomal SNARE complex', *Journal of Cell Biology*, 162(1), pp. 125–137. Available at: https://doi.org/10.1083/jcb.200302083.

Surmeier, D.J. *et al.* (2022) 'Re-Analysis of the STEADY-PD II Trial—Evidence for Slowing the Progression of Parkinson's Disease', *Movement Disorders*, 37(2), pp. 334–342. Available at: https://doi.org/10.1002/mds.28850.

Surmeier, D.J., Obeso, J.A. and Halliday, G.M. (2017) 'Selective neuronal vulnerability in Parkinson disease', *Nature Reviews Neuroscience*, 18(2), pp. 101–113. Available at: https://doi.org/10.1038/nrn.2016.178.

Suthar, S.K. and Lee, S.-Y. (2023) 'Truncation or proteolysis of α-synuclein in Parkinsonism', *Ageing Research Reviews*, 90, p. 101978. Available at: https://doi.org/10.1016/j.arr.2023.101978.

Taguchi, K., Watanabe, Y. and Tanaka, M. (2025) 'SENP2-based N-terminal truncation of α-synuclein in Lewy pathology propagation', *iScience*, 28(2), p. 111935. Available at: https://doi.org/10.1016/j.isci.2025.111935.

Taguchi, Y. *et al.* (2013) 'Critical Significance of the Region between Helix 1 and 2 for Efficient Dominant-Negative Inhibition by Conversion-Incompetent Prion Protein', *PLoS Pathogens*. Edited by J. Bartz, 9(6), p. e1003466. Available at: https://doi.org/10.1371/journal.ppat.1003466.

Takahashi, K. and Yamanaka, S. (2006) 'Induction of Pluripotent Stem Cells from Mouse Embryonic and Adult Fibroblast Cultures by Defined Factors', *Cell*, 126(4), pp. 663–676. Available at: https://doi.org/10.1016/j.cell.2006.07.024.

Takahashi, M. *et al.* (2007) 'Oxidative stress-induced phosphorylation, degradation and aggregation of α-synuclein are linked to upregulated CK2 and cathepsin D', *European Journal of Neuroscience*, 26(4), pp. 863–874. Available at: https://doi.org/10.1111/j.1460-9568.2007.05736.x.

Tang, Q. *et al.* (2021) 'Alpha-Synuclein defects autophagy by impairing SNAP29-mediated autophagosome-lysosome fusion', *Cell Death & Disease*, 12(10), p. 854. Available at: https://doi.org/10.1038/s41419-021-04138-0.

Tanik, S.A. *et al.* (2013) 'Lewy Body-like α-Synuclein Aggregates Resist Degradation and Impair Macroautophagy', *The Journal of Biological Chemistry*, 288(21), pp. 15194–15210. Available at: https://doi.org/10.1074/jbc.M113.457408.

Tanner, C.M. *et al.* (2011) 'Rotenone, Paraquat, and Parkinson's Disease', *Environmental Health Perspectives*, 119(6), pp. 866–872. Available at: https://doi.org/10.1289/ehp.1002839.

Tanner, C.M. and Ostrem, J.L. (2024) 'Parkinson's Disease', *New England Journal of Medicine*. Edited by A.H. Ropper, 391(5), pp. 442–452. Available at: https://doi.org/10.1056/NEJMra2401857.

Tanudjojo, B. *et al.* (2021) 'Phenotypic manifestation of α-synuclein strains derived from Parkinson's disease and multiple system atrophy in human dopaminergic neurons', *Nature Communications*, 12(1), pp. 1–16. Available at: https://doi.org/10.1038/s41467-021-23682-z.

Terada, M. *et al.* (2018) 'The effect of truncation on prion-like properties of α-synuclein', *Journal of Biological Chemistry*, 293(36), pp. 13910–13920. Available at: https://doi.org/10.1074/jbc.RA118.001862.

The Parkinson Study Group STEADY-PD III Investigators (2020) 'Isradipine Versus Placebo in Early Parkinson Disease', *Annals of Internal Medicine*, 172(9), pp. 591–598. Available at: https://doi.org/10.7326/M19-2534.

Theillet, F.-X. *et al.* (2016) 'Structural disorder of monomeric α-synuclein persists in mammalian cells', *Nature*, 530(7588), pp. 45–50. Available at: https://doi.org/10.1038/nature16531.

Thibaudeau, T.A., Anderson, R.T. and Smith, D.M. (2018) 'A common mechanism of proteasome impairment by neurodegenerative disease-associated oligomers', *Nature Communications*, 9(1), p. 1097. Available at: https://doi.org/10.1038/s41467-018-03509-0.

Tian, R. *et al.* (2019) 'CRISPR Interference-Based Platform for Multimodal Genetic Screens in Human iPSC-Derived Neurons', *Neuron*, 104(2), pp. 239-255.e12. Available at: https://doi.org/10.1016/j.neuron.2019.07.014.

Tong, J. *et al.* (2011) 'Distribution of vesicular monoamine transporter 2 protein in human brain: implications for brain imaging studies', *Journal of Cerebral Blood Flow & Metabolism*, 31(10), p. 2065. Available at: https://doi.org/10.1038/jcbfm.2011.63.

Trexler, A.J. and Rhoades, E. (2012) 'N-terminal acetylation is critical for forming α-helical oligomer of α-synuclein', *Protein Science*, 21(5), pp. 601–605. Available at: https://doi.org/10.1002/pro.2056.

Tseng, E. *et al.* (2019) 'The Landscape of SNCA Transcripts Across Synucleinopathies: New Insights From Long Reads Sequencing Analysis', *Frontiers in Genetics*, 10, p. 584. Available at: https://doi.org/10.3389/fgene.2019.00584.

Tsunemi, T. *et al.* (2019) 'Increased Lysosomal Exocytosis Induced by Lysosomal Ca2+ Channel Agonists Protects Human Dopaminergic Neurons from α-Synuclein Toxicity', *Journal of Neuroscience*, 39(29), pp. 5760–5772. Available at: https://doi.org/10.1523/JNEUROSCI.3085-18.2019.

Tsunemi, T., Hamada, K. and Krainc, D. (2014) 'ATP13A2/PARK9 Regulates Secretion of Exosomes and α-Synuclein', *Journal of Neuroscience*, 34(46), pp. 15281–15287. Available at: https://doi.org/10.1523/JNEUROSCI.1629-14.2014.

Uemura, N. *et al.* (2023) 'α-Synuclein aggregates amplified from patient-derived Lewy bodies recapitulate Lewy body diseases in mice', *Nature Communications*, 14(1), p. 6892. Available at: https://doi.org/10.1038/s41467-023-42705-5.

Ulmer, T.S. *et al.* (2005) 'Structure and Dynamics of Micelle-bound Human α-Synuclein', *Journal of Biological Chemistry*, 280(10), pp. 9595–9603. Available at: https://doi.org/10.1074/jbc.M411805200.

Underwood, R. *et al.* (2020) 'The GTPase Rab27b regulates the release, autophagic clearance, and toxicity of α-synuclein', *Journal of Biological Chemistry*, 295(23), pp. 8005–8016. Available at: https://doi.org/10.1074/jbc.RA120.013337.

Valenzuela, M.M.A. *et al.* (2015) 'Exosomes Secreted from Human Cancer Cell Lines Contain Inhibitors of Apoptosis (IAP)', *Cancer Microenvironment*, 8(2), p. 65. Available at: https://doi.org/10.1007/s12307-015-0167-9.

Vamvaca, K., Lansbury Jr., P.T. and Stefanis, L. (2011) 'N-terminal deletion does not affect α-synuclein membrane binding, self-association and toxicity in human neuroblastoma cells, unlike yeast', *Journal of Neurochemistry*, 119(2), pp. 389–397. Available at: https://doi.org/10.1111/j.1471-4159.2011.07431.x.

Van Den Eeden, S.K. (2003) 'Incidence of Parkinson's Disease: Variation by Age, Gender, and Race/Ethnicity', *American Journal of Epidemiology*, 157(>11), pp. 1015–1022. Available at: https://doi.org/10.1093/aje/kwg068.

Van der Perren, A. *et al.* (2020) 'The structural differences between patient-derived α-synuclein strains dictate characteristics of Parkinson's disease, multiple system atrophy and dementia with Lewy bodies', *Acta Neuropathologica*, 139(6), pp. 977–1000. Available at: https://doi.org/10.1007/s00401-020-02157-3.

Van Der Wateren, I.M. *et al.* (2018) 'C-terminal truncation of α-synuclein promotes amyloid fibril amplification at physiological pH', *Chemical Science*, 9(25), pp. 5506–5516. Available at: https://doi.org/10.1039/C8SC01109E.

Vasili, E. *et al.* (2025) 'Glycation of alpha-synuclein enhances aggregation and neuroinflammatory responses', *npj Parkinson's Disease*, 11(1), p. 307. Available at: https://doi.org/10.1038/s41531-025-01159-w.

Vergallo, A. *et al.* (2018) 'Association of cerebrospinal fluid α-synuclein with total and phospho-tau$_{181}$ protein concentrations and brain amyloid load in cognitively normal subjective memory complainers stratified by Alzheimer's disease biomarkers', *Alzheimer's & Dementia*, 14(12), pp. 1623–1631. Available at: https://doi.org/10.1016/j.jalz.2018.06.3053.

Vicente Miranda, H. *et al.* (2017) 'Glycation potentiates α-synuclein-associated neurodegeneration in synucleinopathies', *Brain*, 140(5), pp. 1399–1419. Available at: https://doi.org/10.1093/brain/awx056.

Vijayan, R. *et al.* (2016) 'Structural insights into the polypharmacological activity of quercetin on serine/threonine kinases', *Drug Design, Development and Therapy*, Volume 10, pp. 3109–3123. Available at: https://doi.org/10.2147/DDDT.S118423.

Virdi, G.S. *et al.* (2022) 'Protein aggregation and calcium dysregulation are hallmarks of familial Parkinson's disease in midbrain dopaminergic neurons', *npj Parkinson's Disease*, 8(1), p. 162. Available at: https://doi.org/10.1038/s41531-022-00423-7.

Volc, D. *et al.* (2020) 'Safety and immunogenicity of the α-synuclein active immunotherapeutic PD01A in patients with Parkinson's disease: a randomised, single-blinded, phase 1 trial', *The Lancet. Neurology*, 19(7), pp. 591–600. Available at: https://doi.org/10.1016/S1474-4422(20)30136-8.

Volles, M.J. *et al.* (2001) 'Vesicle Permeabilization by Protofibrillar α-Synuclein: Implications for the Pathogenesis and Treatment of Parkinson's Disease', *Biochemistry*, 40(26), pp. 7812–7819. Available at: https://doi.org/10.1021/bi0102398.

Volpicelli-Daley, L.A., Luk, K.C. and Lee, V.M.-Y. (2014) 'Addition of exogenous α-Synuclein Pre-formed fibrils to Primary Neuronal Cultures to seed recruitment of endogenous α-Synuclein to Lewy body and Lewy Neurite-like aggregates', *Nature protocols*, 9(9), p. 2135. Available at: https://doi.org/10.1038/nprot.2014.143.

Vroman, R. *et al.* (2025) 'A high-fidelity microfluidic platform reveals retrograde propagation as the main mechanism of α-Synuclein spread in human neurons', *npj Parkinson's Disease*, 11(1), p. 80. Available at: https://doi.org/10.1038/s41531-025-00936-x.

Wang, B. *et al.* (2018) '14-3-3 Proteins Reduce Cell-to-Cell Transfer and Propagation of Pathogenic α-Synuclein', *Journal of Neuroscience*, 38(38), pp. 8211–8232. Available at: https://doi.org/10.1523/JNEUROSCI.1134-18.2018.

Wang, C. *et al.* (2017) 'Scalable Production of iPSC-Derived Human Neurons to Identify Tau-Lowering Compounds by High-Content Screening', *Stem Cell Reports*, 9(4), pp. 1221–1233. Available at: https://doi.org/10.1016/j.stemcr.2017.08.019.

Wang, H. *et al.* (2023) 'C/EBPβ/AEP is age-dependently activated in Parkinson's disease and mediates α-synuclein in the gut and brain', *npj Parkinson's Disease*, 9(1), p. 1. Available at: https://doi.org/10.1038/s41531-022-00430-8.

Wang, L. *et al.* (2024) 'Mono-UFMylation promotes misfolding-associated secretion of α-synuclein', *Science Advances*, 10(11), p. eadk2542. Available at: https://doi.org/10.1126/sciadv.adk2542.

Wang, W. *et al.* (2011) 'A soluble α-synuclein construct forms a dynamic tetramer', *Proceedings of the National Academy of Sciences*, 108(43), pp. 17797–17802. Available at: https://doi.org/10.1073/pnas.1113260108.

Wang, Y. *et al.* (2012) 'Phosphorylated α-Synuclein in Parkinson's Disease', *Science Translational Medicine*, 4(121). Available at: https://doi.org/10.1126/scitranslmed.3002566.

Wang, Z. *et al.* (2010) 'Enrichment and Site Mapping of *O*-Linked *N*-Acetylglucosamine by a Combination of Chemical/Enzymatic Tagging, Photochemical Cleavage, and Electron Transfer Dissociation Mass Spectrometry*', *Molecular & Cellular Proteomics*, 9(1), pp. 153–160. Available at: https://doi.org/10.1074/mcp.M900268-MCP200.

Wang, Z. *et al.* (2023) 'Polypharmacology of ambroxol in the treatment of COVID-19', *Bioscience Reports*, 43(2). Available at: https://doi.org/10.1042/BSR20221927.

Waschbüsch, D. et al. (2020) 'Structural Basis for Rab8a Recruitment of RILPL2 via LRRK2 Phosphorylation of Switch 2', Structure, 28(4), pp. 406-417.e6. Available at: https://doi.org/10.1016/j.str.2020.01.005.

Waxman, E.A. and Giasson, B.I. (2008) 'Specificity and Regulation of Casein Kinase/Mediated Phosphorylation of α-Synuclein', *Journal of neuropathology and experimental neurology*, 67(5), p. 402. Available at: https://doi.org/10.1097/NEN.0b013e3186fc995.

Weber, J.P. *et al.* (2014) 'Synaptotagmin-7 Is an Asynchronous Calcium Sensor for Synaptic Transmission in Neurons Expressing SNAP-23', *PLoS ONE*. Edited by J.D. Spafford, 9(11), p. e114033. Available at: https://doi.org/10.1371/journal.pone.0114033.

Weihofen, A. *et al.* (2019) 'Development of an aggregate-selective, human-derived α-synuclein antibody BIIB054 that ameliorates disease phenotypes in Parkinson's disease models', *Neurobiology of Disease*, 124, pp. 276–288. Available at: https://doi.org/10.1016/j.nbd.2018.10.016.

Whiten, D.R. *et al.* (2018) 'Nanoscopic Characterisation of Individual Endogenous Protein Aggregates in Human Neuronal Cells', *ChemBioChem*, 19(19), pp. 2033–2038. Available at: https://doi.org/10.1002/cbic.201800209.

Whiten, D.R. *et al.* (2020) 'Tumour necrosis factor induces increased production of extracellular amyloid-β- and α-synuclein-containing aggregates by human Alzheimer's disease neurons', *Brain Communications*, 2(2), p. fcaa146. Available at: https://doi.org/10.1093/braincomms/fcaa146.

Williams, A. *et al.* (2008) 'Novel targets for Huntington's disease in an mTOR-independent autophagy pathway', *Nature Chemical Biology*, 4(5), pp. 295–305. Available at: https://doi.org/10.1038/nchembio.79.

Wiseman, J.A. *et al.* (2024) 'Aggregate-prone brain regions in Parkinson's disease are rich in unique N-terminus α-synuclein conformers with high proteolysis susceptibility', *npj Parkinson's Disease*, 10(1), p. 1. Available at: https://doi.org/10.1038/s41531-023-00614-w.

Wiseman, J.A., Reddy, K. and Dieriks, B.V. (2025) 'From onset to advancement: the temporal spectrum of α-synuclein in synucleinopathies', *Ageing Research Reviews*, 104, p. 102640. Available at: https://doi.org/10.1016/j.arr.2024.102640.

Wittig, I. and Schägger, H. (2008) 'Features and applications of blue-native and clear-native electrophoresis', *PROTEOMICS*, 8(19), pp. 3974–3990. Available at: https://doi.org/10.1002/pmic.200800017.

Wood, S.J. *et al.* (1999) 'α-Synuclein Fibrillogenesis Is Nucleation-dependent', *Journal of Biological Chemistry*, 274(28), pp. 19509–19512. Available at: https://doi.org/10.1074/jbc.274.28.19509.

Woodard, C.M. *et al.* (2014) 'iPSC-Derived Dopamine Neurons Reveal Differences between Monozygotic Twins Discordant for Parkinson's Disease', *Cell Reports*, 9(4), pp. 1173–1182. Available at: https://doi.org/10.1016/j.celrep.2014.10.023.

Wooten, G.F. (2004) 'Are men at greater risk for Parkinson's disease than women?', *Journal of Neurology, Neurosurgery & Psychiatry*, 75(4), pp. 637–639. Available at: https://doi.org/10.1136/jnnp.2003.020982.

Wrasidlo, W. *et al.* (2016) 'A de novo compound targeting α-synuclein improves deficits in models of Parkinson's disease', *Brain*, 139(12), pp. 3217–3236. Available at: https://doi.org/10.1093/brain/aww238.

Wright Willis, A. *et al*. (2010) 'Geographic and Ethnic Variation in Parkinson Disease: A Population-Based Study of US Medicare Beneficiaries', *Neuroepidemiology*, 34(3), pp. 143–151. Available at: https://doi.org/10.1159/000275491.

Wu, J. *et al*. (2007) 'ATF6α Optimizes Long-Term Endoplasmic Reticulum Function to Protect Cells from Chronic Stress', *Developmental Cell*, 13(3), pp. 351–364. Available at: https://doi.org/10.1016/j.devcel.2007.07.005.

Wu, K.-M. *et al*. (2025) 'Neuronal FAM171A2 mediates α-synuclein fibril uptake and drives Parkinson's disease', *Science*, 387(6736), pp. 892–900. Available at: https://doi.org/10.1126/science.adp3645.

Wu, S. and Schekman, R.W. (2024) 'Intercellular transmission of alpha-synuclein', *Frontiers in Molecular Neuroscience*, 17, p. 1470171. Available at: https://doi.org/10.3389/fnmol.2024.1470171.

Wu, S., Sirkis, D.W. and Schekman, R. (2022) *Unconventional secretion of α-synuclein mediated by palmitoylated DNAJC5 oligomers*. preprint. Biochemistry. Available at: https://doi.org/10.1101/2022.01.27.477991.

Xiao, W. *et al*. (2014) 'Late stages of hematopoiesis and B cell lymphopoiesis are regulated by α-synuclein, a key player in Parkinson's disease', *Immunobiology*, 219(11), pp. 836–844. Available at: https://doi.org/10.1016/j.imbio.2014.07.014.

Xie, Y.X. *et al*. (2022) 'Lysosomal exocytosis releases pathogenic α-synuclein species from neurons in synucleinopathy models', *Nature Communications*, 13(1), pp. 1–16. Available at: https://doi.org/10.1038/s41467-022-32625-1.

Xu, C.K. *et al*. (2024) 'α-Synuclein oligomers form by secondary nucleation', *Nature Communications*, 15(1), p. 7083. Available at: https://doi.org/10.1038/s41467-024-50692-4.

Xu, F. *et al*. (2010) 'Quercetin Targets Cysteine String Protein (CSPα) and Impairs Synaptic Transmission', *PLOS ONE*, 5(6), p. e11045. Available at: https://doi.org/10.1371/journal.pone.0011045.

Xu, Y. *et al*. (2018) 'DNAJC5 facilitates USP19-dependent unconventional secretion of misfolded cytosolic proteins', *Cell Discovery*, 4(1), pp. 1–18. Available at: https://doi.org/10.1038/s41421-018-0012-7.

Yahalom, G. et al. (2020) 'Age at Onset of Parkinson's Disease Among Ashkenazi Jewish Patients: Contribution of Environmental Factors, LRRK2 p.G2019S and GBA p.N370S Mutations', Journal of Parkinson's Disease, 10(3), pp. 1123–1132. Available at: https://doi.org/10.3233/JPD-191829.

Yamada, K. and Iwatsubo, T. (2018) 'Extracellular α-synuclein levels are regulated by neuronal activity', *Molecular Neurodegeneration*, 13(1), pp. 1–8. Available at: https://doi.org/10.1186/s13024-018-0241-0.

Yamamori, H. *et al*. (2007) 'Tau in cerebrospinal fluid: A sensitive sandwich enzyme-linked immunosorbent assay using tyramide signal amplification', *Neuroscience Letters*, 418(2), pp. 186–189. Available at: https://doi.org/10.1016/j.neulet.2007.03.022.

Yamasaki, T.R. et al. (2019) 'Parkinson's disease and multiple system atrophy have distinct α-synuclein seed characteristics', The Journal of Biological Chemistry, 294(3), pp. 1045–1058. Available at: https://doi.org/10.1074/jbc.RA118.004471.

Yan, Q. *et al*. (2004) 'Ca2+ and N-Ethylmaleimide-sensitive Factor Differentially Regulate Disassembly of SNARE Complexes on Early Endosomes', *Journal of Biological Chemistry*, 279(18), pp. 18270–18276. Available at: https://doi.org/10.1074/jbc.M400093200.

Yan, S. *et al*. (2025) 'Single extracellular vesicle detection assay identifies membrane-associated α-synuclein as an early-stage biomarker in Parkinson's disease', *Cell Reports Medicine*, 6(3), p. 101999. Available at: https://doi.org/10.1016/j.xcrm.2025.101999.

Yang, J., Perrett, S. and Wu, S. (2021) 'Single Molecule Characterization of Amyloid Oligomers', *Molecules*, 26(4), p. 948. Available at: https://doi.org/10.3390/molecules26040948.

Yang, S. *et al*. (2020) 'Glucocerebrosidase activity, cathepsin D and monomeric α-synuclein interactions in a stem cell derived neuronal model of a PD associated GBA1 mutation', *Neurobiology of Disease*, 134, p. 104620. Available at: https://doi.org/10.1016/j.nbd.2019.104620.

Yang, S.-Y. *et al*. (2017) 'A Human Neural Crest Stem Cell-Derived Dopaminergic Neuronal Model Recapitulates Biochemical Abnormalities in GBA1 Mutation Carriers', *Stem Cell Reports*, 8(3), pp. 728–742. Available at: https://doi.org/10.1016/j.stemcr.2017.01.011.

Yang, Y. *et al*. (2017) 'Secretory carrier membrane protein 5 is an autophagy inhibitor that promotes the secretion of α-synuclein via exosome', *PLOS ONE*, 12(7), p. e0180892. Available at: https://doi.org/10.1371/journal.pone.0180892.

Yin, G. *et al*. (2014) 'α-Synuclein interacts with the switch region of Rab8a in a Ser129 phosphorylation-dependent manner', *Neurobiology of Disease*, 70, pp. 149–161. Available at: https://doi.org/10.1016/j.nbd.2014.06.018.

Young, G. *et al*. (2018) 'Quantitative mass imaging of single molecules', *Science (New York, N.Y.)*, 360(6387), p. 423. Available at: https://doi.org/10.1126/science.aar5839.

Young, J.E., Martinez, R.A. and La Spada, A.R. (2009) 'Nutrient Deprivation Induces Neuronal Autophagy and Implicates Reduced Insulin Signaling in Neuroprotective Autophagy Activation', *Journal of Biological Chemistry*, 284(4), pp. 2363–2373. Available at: https://doi.org/10.1074/jbc.M806088200.

Yu, M. et al. (2018) 'LRRK2 mediated Rab8a phosphorylation promotes lipid storage', Lipids in Health and Disease, 17(1), p. 34. Available at: https://doi.org/10.1186/s12944-018-0684-x.

Yu, L.-R. and Veenstra, T.D. (2021) 'Characterization of Phosphorylated Proteins Using Mass Spectrometry', *Current Protein & Peptide Science*, 22(2), pp. 148–157. Available at: https://doi.org/10.2174/1389203721999201123200439.

Yuan, Y. *et al.* (2008) 'Overexpressed Alpha-Synuclein Regulated the Nuclear Factor-kappaB Signal Pathway', *Cellular and Molecular Neurobiology*, 28(1), pp. 21–33. Available at: https://doi.org/10.1007/s10571-007-9185-6.

Zambon, F. *et al.* (2019) 'Cellular α-synuclein pathology is associated with bioenergetic dysfunction in Parkinson's iPSC-derived dopamine neurons', *Human Molecular Genetics*, 28(12), pp. 2001–2013. Available at: https://doi.org/10.1093/hmg/ddz038.

Zarranz, J.J. *et al.* (2004) 'The new mutation, E46K, of α-synuclein causes parkinson and Lewy body dementia', *Annals of Neurology*, 55(2), pp. 164–173. Available at: https://doi.org/10.1002/ana.10795.

Zhang, J., Jiang, Z. and Shi, A. (2022) 'Rab GTPases: The principal players in crafting the regulatory landscape of endosomal trafficking', *Computational and Structural Biotechnology Journal*, 20, pp. 4464–4472. Available at: https://doi.org/10.1016/j.csbj.2022.08.016.

Zhang, J., Li, X. and Li, J.-D. (2019) 'The Roles of Post-translational Modifications on α-Synuclein in the Pathogenesis of Parkinson's Diseases', *Frontiers in Neuroscience*, 13. Available at: https://doi.org/10.3389/fnins.2019.00381.

Zhang, J.-H., Chung, T.D.Y. and Oldenburg, K.R. (1999) 'A Simple Statistical Parameter for Use in Evaluation and Validation of High Throughput Screening Assays', *SLAS Discovery*, 4(2), pp. 67–73. Available at: https://doi.org/10.1177/108705719900400206.

Zhang, N.-Y., Tang, Z. and Liu, C.-W. (2008) 'α-Synuclein Protofibrils Inhibit 26 S Proteasome-mediated Protein Degradation', *Journal of Biological Chemistry*, 283(29), pp. 20288–20298. Available at: https://doi.org/10.1074/jbc.M710560200.

Zhang, P. *et al.* (2020) 'Translation of the intrinsically disordered protein α-synuclein is inhibited by a small molecule targeting its structured mRNA', *Proceedings of the National Academy of Sciences*, 117(3), pp. 1457–1467. Available at: https://doi.org/10.1073/pnas.1905057117.

Zhang, Y. *et al.* (2013) 'Rapid Single-Step Induction of Functional Neurons from Human Pluripotent Stem Cells', *Neuron*, 78(5), pp. 785–798. Available at: https://doi.org/10.1016/j.neuron.2013.05.029.

Zhang, Z. *et al.* (2014) 'Cleavage of tau by asparagine endopeptidase mediates the neurofibrillary pathology in Alzheimer's disease', *Nature Medicine*, 20(11), pp. 1254–1262. Available at: https://doi.org/10.1038/nm.3700.

Zhang, Zhentao *et al.* (2017) 'Asparagine endopeptidase cleaves α-synuclein and mediates pathologic activities in Parkinson's disease', *Nature Structural & Molecular Biology*, 24(8), pp. 632–642. Available at: https://doi.org/10.1038/nsmb.3433.

Zhao, K. *et al.* (2020) 'Parkinson's disease-related phosphorylation at Tyr39 rearranges α-synuclein amyloid fibril structure revealed by cryo-EM', *Proceedings of the National Academy of Sciences*, 117(33), pp. 20305–20315. Available at: https://doi.org/10.1073/pnas.1922741117.

Zhao, N. *et al.* (2023) 'The α-Synuclein Monomer May Have Different Misfolding Mechanisms in the Induction of α-Synuclein Fibrils with Different Polymorphs', *Biomolecules*, 13(4), p. 682. Available at: https://doi.org/10.3390/biom13040682.

Zhao, X. *et al.* (2022) 'SNARE Proteins Mediate α-Synuclein Secretion via Multiple Vesicular Pathways', *Molecular Neurobiology*, 59(1), pp. 405–419. Available at: https://doi.org/10.1007/s12035-021-02599-0.

Zhou, J. *et al.* (2011) 'Changes in the solubility and phosphorylation of α-synuclein over the course of Parkinson's disease', *Acta Neuropathologica*, 121(6), pp. 695–704. Available at: https://doi.org/10.1007/s00401-011-0815-1.

Zhou, L. and Kurouski, D. (2020) 'Structural Characterization of Individual α-Synuclein Oligomers Formed at Different Stages of Protein Aggregation by Atomic Force Microscopy-Infrared Spectroscopy', *Analytical Chemistry*, 92(10), pp. 6806–6810. Available at: https://doi.org/10.1021/acs.analchem.0c00593.

Zibaee, S. *et al.* (2007) 'Sequence Determinants for Amyloid Fibrillogenesis of Human α-Synuclein', *Journal of Molecular Biology*, 374(2), pp. 454–464. Available at: https://doi.org/10.1016/j.jmb.2007.09.039.

Zubkova, E. *et al.* (2024) 'Autophagy-Dependent Secretion: Crosstalk between Autophagy and Exosome Biogenesis', *Current Issues in Molecular Biology*, 46(3), pp. 2209–2235. Available at: https://doi.org/10.3390/cimb46030142.

Zunke, F. *et al.* (2018) 'Reversible Conformational Conversion of α-Synuclein into Toxic Assemblies by Glucosylceramide', *Neuron*, 97(1), pp. 92-107.e10. Available at: https://doi.org/10.1016/j.neuron.2017.12.012.